AN INTEGRATED APPROACH TO PREDICT ETTRINGITE FORMATION IN SULFATE SOILS AND IDENTIFYING SULFATE DAMAGE ALONG SH 130

A Thesis

by

SACHIN KUNAGALLI NATARAJAN

Submitted to the Office of Graduate Studies of
Texas A&M University
in partial fulfillment of the requirements for the degree of

MASTER OF SCIENCE

December 2004

Major Subject: Civil Engineering

AN INTEGRATED APPROACH TO PREDICT ETTRINGITE FORMATION IN SULFATE SOILS AND IDENTIFYING SULFATE DAMAGE ALONG SH 130

A Thesis

by

SACHIN KUNAGALLI NATARAJAN

Submitted to Texas A&M University
in partial fulfillment of the requirements
for the degree of

MASTER OF SCIENCE

Approved as to style and content by:

Dallas N. Little (Chair of Committee)	Robert L. Lytton (Member)
Bruce E. Herbert (Member)	Paul Roschke (Head of Department)

December 2004

Major Subject: Civil Engineering

ABSTRACT

An Integrated Approach to Predict Ettringite Formation in Sulfate Soils and Identifying Sulfate Damage Along SH 130.

(December 2004)

Sachin Kunagalli Natarajan, B.E., University of Mysore, Mysore, India

Chair of Advisory Committee: Dr. Dallas N. Little

Expansive soils are treated with anhydrous or hydrated lime. The use of calcium-based stabilizers such as calcium oxide (lime) in sulfate-bearing clay soils has historically led to distress due to the formation of an expansive mineral called ettringite and possibly another such mineral, thaumasite. Predicting the precipitation of these minerals is a complex problem related not only to soil composition but also construction methods, availability of water, ion migration, and whether the expansive mineral growth can be accommodated by the void structure in the surrounding soil. In trying to control the damage associated with such occurrences, engineers have attempted to determine a threshold value of soluble sulfates, a quantity that is relatively easy and quick to measure, at which significant ettringite growth and, therefore, structural distress occurs. Unfortunately, experience alone and "rules-of-thumb" based on experience are not sufficient to deal with this complex issue. This thesis describes how thermodynamic geochemical models of lime-treated soil can be used as a first step toward establishing problematic threshold levels of soluble sulfates for a specific soil. A foundation for the model development is presented, and two different soils are compared to illustrate their very different sensitivities to ettringite growth upon the addition of hydrated lime.

Various soil series along the route of SH 130 between Austin and San Antonio have been identified to contain soluble sulfate that may pose a problem for soil stabilization using lime and cement. Since the model predicts ettringite growth based upon site-specific properties, this thesis also shows how the model can be used to assess the potential amelioration effects of soluble silica.

Research was conducted at the Texas Transportation Institute to develop a methodology for identifying areas which are susceptible for ettringite formation. The proposed methodology uses a magnetometer to quickly screen large areas for high sulfate. Application of GIS to identify ettringite formation using soils, topographical, and geological maps is also illustrated in this thesis.

DEDICATION

I dedicate this work to my parents, Padma Natarajan and K.S. Natarajan, for their support in reaching my goal and all through my life. It is to them I owe all my accomplishments. I would also like to dedicate my work to my brother, Sunil Kunagalli, and sister-in-law, Ramya Sunil, for their moral support. The extreme interest taken by my mother has made me see this great day. Thank you, mom.

ACKNOWLEDGEMENTS

I would like to thank my advisor, Dr. Little. It has been an honor and great pleasure working with Dr Little. He has been a true mentor, both personally and academically. He had great confidence in my abilities. His willingness to share his knowledge resulted in a great learning experience. The monetary and academic support I received from Dr. Little throughout the graduate studies is invaluable. Hats off to this great person without whose support I would not have achieved this success.

I would like to thank Dr. Lytton and Dr. Herbert and for their valuable suggestions and comments throughout the period of this research. I greatly appreciate the support and guidance received from both of them.

I would like to thank Lone Star Infrastructure (LSI) for supporting this research. The experience I gained doing the research is invaluable. I would like to thank Mr. David Taylor, Mr. Sid Ibrahim, Mr. Terry Oliver, Mr. Danny Rains, and Mr. Steve Hinton of LSI who helped in achieving success at various stages of the project. I would like to acknowledge Mr. Eric Berger of Chemical Lime Company and Mr. Scot Gordon of CTL Thompson for their support during the research. I would also like to thank Chris Markley and Li-Jung Quo for carrying out the chemical analysis (Table 16 through 19). Special thanks to the technicians in the McNew Lab for their support throughout the testing period at TTI. Thank you all for your help.

Last but not least, I would like to thank all my friends and relatives: Vijaya Shreedhar, H.P.Shreedhar, and my cousin, Mithun, for their confidence in achieving my goals. Lastly, I would like to thank my family for all the support I received throughout my life. Thank you one and all.

TABLE OF CONTENTS

Page

CHAPTER Page

LIST OF TABLES

LIST OF FIGURES

FIGURE Page

CHAPTER I

INTRODUCTION

1.1 HISTORICAL BACKGROUND

The addition of lime to clayey soil increases the strength and decreases the soil swell potential. The amount by which the swell potential decreases and density increases is debatable. "The increase in strength has been used to justify decrease in structural section and reduction in plasticity index has been used to extend the life expectancy of structure built over expansive clay soils" [*1*]. The reduction in maximum dry density is 3 to 5 pounds per cubic foot and increase in optimum moisture content (OMC) is 2 to 4 percent [*2*]. But other researchers have found that the density reduction may be as much as 13 percent and the increase in OMC may be as much as 14.6 percent with addition of lime to medium plasticity clay and thus these numbers may be on the order of 15 percent and 29 percent, respectively, for highly expansive soils [*3*].

Lime added to soil decreases plasticity and increases stability. However, the use of lime in sulfate bearing clay can lead to the development of minerals like ettringite and thaumasite both hydrous sulfate minerals. Ettringite ($Ca_6(Al(OH)_6)2(SO_4)_3 \cdot 26H_2O$), has been implicated in the sulfate attack on cement and concrete, as well as stabilized soils [*4, 5, 6*].

General information regarding ettringite is provided in Table 1 [*7*].

The style and format of this thesis follows that of *Transportation Research Record.*

Table 1 Ettringite fact sheet [*7*]

General Ettringite Information

Chemical Formula:	$Ca_6Al_2(SO_4)_3(OH)_{12}{\cdot}26(H_2O)$
Composition:	Molecular Weight = 1,255.11 gm Calcium 19.16 % Ca 26.81 % CaO Aluminum 4.30 % Al 8.12 % Al_2O_3 Hydrogen 5.14 % H 45.93 % H_2O Sulfur 7.66 % S 19.14 % SO_3 Oxygen 63.74 % O 100.00 % 100.00 % = TOTAL OXIDE
Empirical Formula:	$Ca_6Al_2(SO_4)_3(OH)_{12}{\cdot}26(H_2O)$
Locality:	Ettringer Bellerberg, Ettringen, Mayen, Eifel, Rheinland-Pfalz, Germany Location Data.
Name Origin:	Named for the locality
Synonym:	ICSD 16045 PDF 41-1451

Ettringite Crystallography

Axial Ratios:	a:c = 1:0.95458
Cell Dimensions:	a = 22.46, c = 21.44, Z = 8; V = 9,366.45 Den(Calc)= 1.78
Crystal System:	**Hexagonal - Dihexagonal Dipyramidal**H-M Symbol (6/m 2/m 2/m) Space Group: P 6_3/mmc
X Ray Diffraction:	By Intensity(I/I_o): 9.65(1), 5.58(0.8), 3.21(0.6),

Physical Properties of Ettringite

Cleavage:	[1010] Perfect
Color:	Colorless, White.
Density:	1.8
Diaphaneity:	Transparent
Habit:	Acicular - Occurs as needle-like crystals.
Hardness:	2-2.5 - Gypsum-Finger Nail
Luminescence:	Non-fluorescent.
Luster:	Vitreous (Glassy)
Magnetism:	Nonmagnetic

Table 1 continued

Streak:	white

Optical Properties of Ettringite

Gladstone-Dale:	
	CI $_{meas}$= -0.014 (Superior) - where the CI = (1-K_{PDmeas}/K_C) CI $_{calc}$= -0.026 (Excellent) - where the CI = (1-K_{PDcalc}/K_C) K_{PDcalc}= 0.2699,K_{PDmeas}= 0.2669,K_C= 0.2632
Optical Data:	Uniaxial (-), e=1.47, w=1.491, bire=0.0210.

Calculated Properties of Ettringite

Electron Density:	**$\rho_{electron}$=1.89 gm/cc** note: $\rho_{Ettringite}$ =1.80 gm/cc.
Photoelectric:	**$PE_{Ettringite}$ = 2.97** barns/electron **U=$PE_{Ettringite}$ x $\rho_{electron}$= 5.60** barns/cc.
Radioactivity:	**GRapi = 0** (Gamma Ray American Petroleum Institute Units) Ettringite is **Not Radioactive**

1.2 SIGNIFICANCE OF THE PROBLEM

Ettringite is a hydrous calcium alumino-sulfate mineral that precipitates in environments with high pH and high sulfate activity [8]. Ettringite often forms when a calcium-based stabilizer is added to sulfate-bearing clay soils [9*, 10, 11, 12*]. Ettringite, which tends to form very small (μm), fibrous crystals [13], damages the soil structure through mineral expansion during its precipitation [*9*]. To make the matter even more complex, a second mineral, thaumasite may develop through the isostructural transformation of ettringite at temperatures below about 15^{o}C in the presence of soluble silica and carbonate. The result of the formation of ettringite can be considerable expansion, while the formation of thaumasite will result in a loss of strength and is normally preceded by the formation of ettringite [*4, 6, 14, 15, 16*].

The amount of damage due to ettringite formation depends on a number of factors including: (i) the thermodynamic favorability of ettringite precipitation in specific soils, (ii) the quantity of limiting reactants that stoichiometrically control the mass of ettringite formed, (iii) the migration of water, sulfate and other ions that support continued ettringite nucleation, (iv) the strength of the pozzolanic or cementitious matrix, and (v) the spatial arrangement of the ettringite crystals in the soil matrix. Ettringite can grow in void spaces that accommodate their growth without substantial expansion or within a dense matrix such that the soil matrix cannot accommodate the crystal growth.

The solubility of ettringite can be written as:

$$Ca_6(Al(OH)_6)2(SO_4)_3{\cdot}26H_2O \Leftrightarrow 6Ca^{2+} + 2Al(OH)^{4-} + 3SO_4^{2-} + 4OH^- + 26H_2O$$

Ettringite precipitates in highly alkaline solutions with high activities of Ca, SO_4^{2-} and Al. Additional geochemical factors that control the growth of ettringite are

temperature and dissolved CO_2 and H_2O activities [*17*]. The precipitation-dissolution of ettringite is fast and it reaches steady state in approximately 150 hours at a pH of 11.5 [*17*]. As discussed earlier, the main idea of resorting to lime stabilization is to reduce the cost of pavement construction on soft, clay soils and to provide a working table for construction equipment during wet weather. But the adverse reactions between added lime and sulfates present in the soil lead to expansive mineral formation which increases the cost in turn. Lime stabilization of soil reduces the cost of construction significantly but the cost of repair because of the damage caused due to expansive mineral growth is much more than the cost of lime stabilization.

1.3 OBJECTIVE OF THE STUDY

Lonestar Infrastructure (LSI) is coordinating the design and building of a toll road between Seguin, Texas, east of San Antonio along IH-10, and Georgetown, Texas, east of Austin. This toll road is intended to by-pass a congested portion of one of the nation's most heavily truck-trafficked highways. The preliminary design for SH-130 is a continually reinforced Portland cement concrete mainline with asphalt concrete frontage roads along the 94-mile corridor. Because of the expansive clay soils in the corridor, chemical stabilization of the subgrade soils is necessary both as a construction expedient and to provide structural support for the asphalt pavements.

The soils along the SH 130 corridor have high contents of amorphous silica and clay minerals, major sources of Si and Al, carbonate, providing both Ca and CO_3^{2-}, and sulfur bearing minerals. The two major geologic sources of SO_4^{2-} in the SH 130 corridor are sediments that contain significant pyrite (FeS_2), especially those deposited in near-shore environments, such as marls, shales or carbonates that contain high levels of clay

minerals, and sediments that contain significant evaporite deposits. The sulfur in pyrite is oxidized to SO_4^{2-}, while evaporates contain significant amounts of gypsum (Ca SO_4) and other sulfate-containing minerals that release sulfate through dissolution.

In order to minimize the risk of sulfate-induced heave in lime and cement-treated subgrade soils along the SH 130 corridor, a research project conducted by Texas Transportation Institute (TTI) at Texas A&M University established a protocol to:

1. Screen for potentially problematic soils based on GIS mapping of the corridor, which accounts for geology, pedology, and topography;
2. Establish spatial heterogeneity of sulfate levels through the characterization of terrain conductivity using electromagnetics (EM31, Geonic Ltd.), and
3. Evaluate the risk of swelling based on thermodynamic modeling and stoichiometric analysis of the lime-treated soils.

One objective of this paper is to compare thermodynamic model predictions of ettringite formation in lime-treated soils to current understanding based upon engineering practice and experience.

1.4 PREVIOUS STUDIES

Pavement failures due to ettringite formation have been noted in the literature and have grown in number since Mitchell's classic 1986 paper [9] regarding the Stewart avenue failure. His study demonstrated that the pavement failure was caused due to growth of ettringite and thaumasite. But the study did not address where the problem can occur, how it occurs, and what causes ettringite formation. These questions were later addressed by Hunter [*18*]. He conducted a detailed study to explain the geochemistry of lime

induced heave in sulfate bearing clay soils and defined the explanation for the physio/chemical mechanism by which expansive minerals like ettringite and thaumasite cause damage to the pavements. Figure 1 and Figure 2 illustrate the severity of damage due to ettringite formation.

The solubility thermodynamics of ettringite revealed that ettringite probably forms first and in the presence of carbonate and at temperature below 15°C converts to Thaumasite [*18*]. Early attempts at predicting ettringite and thaumasite formation used geochemical models based upon thermodynamics [*19,20*]. In his 1989 Ph.D. dissertation, Dal Hunter [*18*] assessed the relative stability of ettringite to other sulfate minerals prone to develop in sulfate-bearing clay soils stabilized with calcium oxide (CaO) or calcium hydroxide ($Ca(OH)_2$). Some of the highlights of Hunter's findings are:

1. Slight increases in the activity of calcium, a rise in the pH, or an increase in the activity of aluminum favors the precipitation of ettringite in sulfate-bearing clay soil amended with lime.
2. The stability field of ettringite increased as the activity of aluminum increased, and the activity of aluminum increased from approximately 10^{-6} to 10^{-3} when lime and adequate water was added to the soil system.
3. An increase in the activity of calcium and/or sulfate drives the reaction into the stability field of ettringite.

Although most of Hunter's research simulated the Stewart Avenue soils (Las Vegas, NV) with simple geochemical models of only three minerals: gypsum, ettringite, and portlandite ($Ca(OH)_2$); his results were very instructive. Hunter [*18*] predicted, for his simplified system and at a pH of about 12.3, that ettringite was thermodynamically more

Figure 1 Illustration of sulfate-induced damage

Figure 2 Illustration of sulfate-induced damage

stable than gypsum at soluble sulfate contents as low as 15 parts per million (ppm).

However, Hunter [*18*] raised his estimates of the amount of soluble sulfates needed to cause damage based on swell observations. Using stoichiometrics, he correlated observed swell with the mass of material, sulfate, calcium oxide, aluminum, and water required to support the observed volume increase. He adjusted the total volume increase, based on observed swell and density measurements, to account for volume change due to crystal growth as well as the concomitant void development associated with the growing minerals. Based on his observations from soils at Stewart Avenue, Hunter suggested a threshold limit of 5,000 ppm for soluble sulfates for damage by ettringite formation in flexible pavements. This accounts for the fact that some of the swell due to mineral growth can be accommodated in the void structure of the soil.

The aforementioned studies provided the base for our studies to develop phase diagrams, varying calcium, alumina, pH and sulfate. The primary objective is to demonstrate that these phase diagrams can be used to predict the stability of ettringite in the field using chemical analysis. The phase diagrams were validated by adding lime to soil from project site along US 290 and US 79. Differential Scanning Calorimetry (DSC) and X-Ray Diffraction (XRD) were run to prove the presence of ettringite in the samples if any.

The use of magnetometer to quickly screen large areas for the presence of sulfate was also studied. Chemical Lime Company (CLC) had sponsored research in the City of Frisco, Texas, to assess the potential of using electrical conductivity to screen for soluble sulfates. CLC worked with Professor Tom Petry of the University of Missouri-Rolla and Professor Dallas Little of Texas A&M in assessing this methodology. The basis of this

approach was work done in the mid-1990s by Professor Robert L. Lytton [*21*] at Texas A&M that demonstrated that electrical conductivity can be used to screen for salt contents and to rapidly screen for the presence of sulfates. CLC worked with Professor Little and the Soil Science Department at Texas A&M to identify a list of potential, commercially available electrical conductivity measuring devices. These were ultimately evaluated in a controlled study in Frisco, Texas, under the direction of Professor Petry and Mr. Eric Berger of CLC. The results of this study revealed that the EM 38 Magnetometer is the most effective device based on test repeatability, ability to detect threshold sulfate contents, and efficiency of testing over a large area.

Finally, based on knowledge of the soils, topological, and geological maps of the area, it is possible to predict areas where the probability of ettringite formation is high. This report includes the methodology to predict heaving potential areas (due to ettringite formation). Geographic Information Systems (GIS) is the most efficient tool that can be used to predict heaving potential areas as GIS software has the capability to analyze multi layered maps. The analysis with GIS becomes much easier because, geological, topological, and soils maps can be superimposed. The data regarding the type of soil, geology of the bed rock and topography can be obtained rapidly. The complete thought process is discussed in detail in chapter III.

CHAPTER II

LIME STABILIZATION OF CLAY

2.1 BACKGROUND

Lime (CaO or $Ca(OH)_2$) has been used for several decades to stabilize soil subgrade. With the addition of lime to soil, the swelling decreases and strength increases. The series of reactions taking place between lime and clay after addition of lime to the soil system is discussed in detail by Little [*2*]. Various mechanisms involved in lime stabilization and the necessity for stabilizing the soil is also explained. Lime should be considered for all soils exceeding PI of 10 and percentage of soil passing number 200 sieve exceeding 25 [*2*]. Hydrated high calcium lime, monohydrated dolomitic lime, calcitic quicklime and dolomitic quicklime are the types of lime used for soil stabilization. With the addition of lime to a clay-water system, calcium replaces most of the cations present at the clay surface which is explained by the Lyotropic series; higher valence cations replace lower valence cations. With the decrease in thickness of the adsorbed water layer, attraction between the particles increases and is known as Flocculation/Agglomeration. As a result, the soil becomes more workable, possesses higher aggregate shear strength, and internal friction of agglomerates also increases. Immediate strength gain can be observed in soil stabilized with lime [*22*] as shown in Figure 3. Apart from immediate short term strength gain, there is long term strength gain also, which is dependent on the mineralogical properties and soil conditions. The pozzolanically active soil reacts with lime to form a cemented matrix among soil particles. Pozzolanic strength development is time dependent. With the addition of lime pH of the soil system increases. At very high pH silica and alumina solubilizes as demonstrated in Figure 4. Eades and Grim adopted this

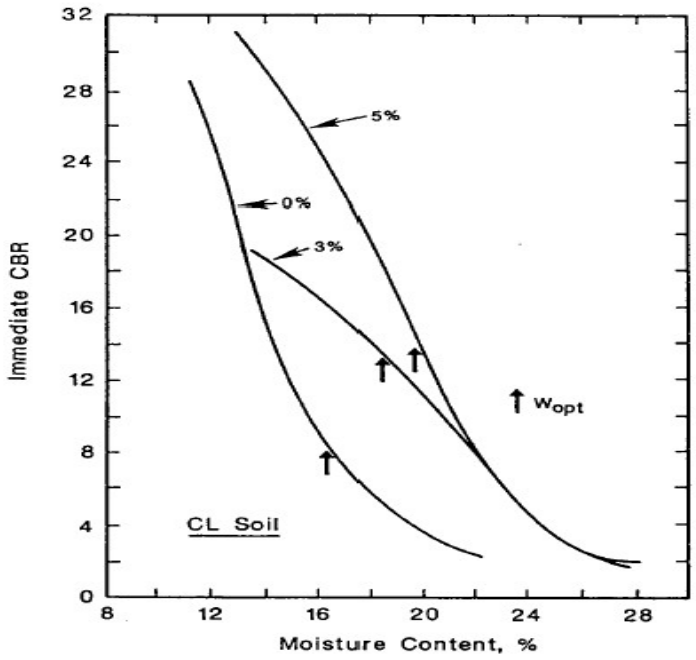

Figure 3 Immediate shear strength gain in soil stabilized with lime (after Thompson, 1976) [*1*]

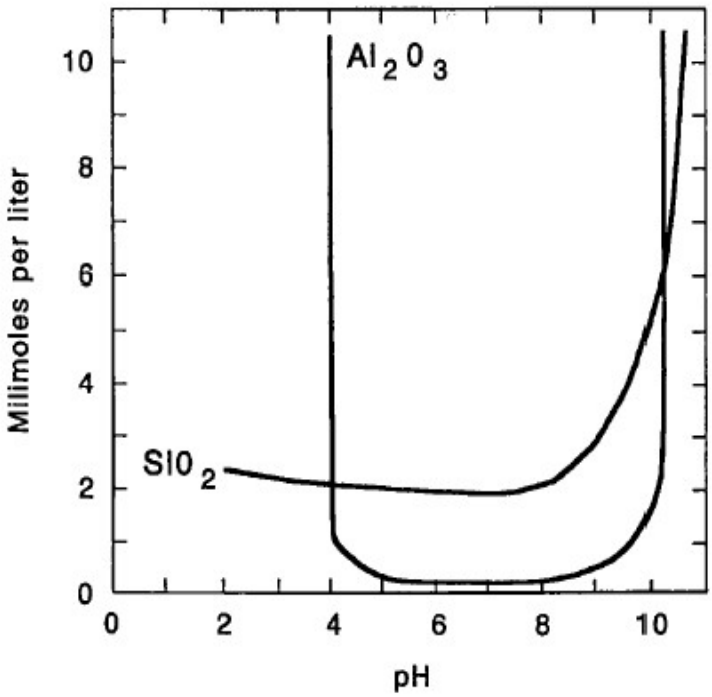

Figure 4 Solubility curves of silica and alumina at high pH environment (After Keller, 1964) [*1*]

increase in pH phenomenon in their design procedure for lime-soil mixtures.

2.2 LIME SOIL REACTION

With the aforementioned literature as the background, the mechanism of lime soil reaction can be explained as follows. Lime soil reaction occurs in four different stages

- Cation exchange
- Flocculation/Agglomeration
- Carbonation, and
- Pozzolanic Reaction

Eades and Grim documented changes in clay with the addition of lime, using X-ray diffraction (XRD) and Differential Thermal Analysis (DTA). “Little (1991) used the XRD analysis to demonstrate the mineralogical change that occurs at the clay surface upon the addition of lime. The XRD spectrum is used to identify clay minerals as a function of the angle of reflection of the X-ray beam” [*2*].This is demonstrated in Figure 5.

2.3 THE PROBLEM OF SULFATE BEARING CLAY SOIL

When lime is added to soil, pozzolanic reactions take place to form Calcium Silicate Hydrate (CSH) and Calcium Aluminate Hydrate (CAH). But when soluble sulfate is present in the soil in high concentrations; it reacts with calcium from lime and alumina from soil to form calcium-aluminate-sulfate-hydrate (CAŚH). If the concentration of sulfate is not very high, then monosulfoaluminate may instead form. The growth of calcium-aluminate-sulfate-hydrate is harmful because of the high volume expansion. The formation of secondary minerals occurs at high potential pressure of approximately 241 Mpa. Ettringite has a low specific gravity of 1.7+, 80% of the atoms in this mineral

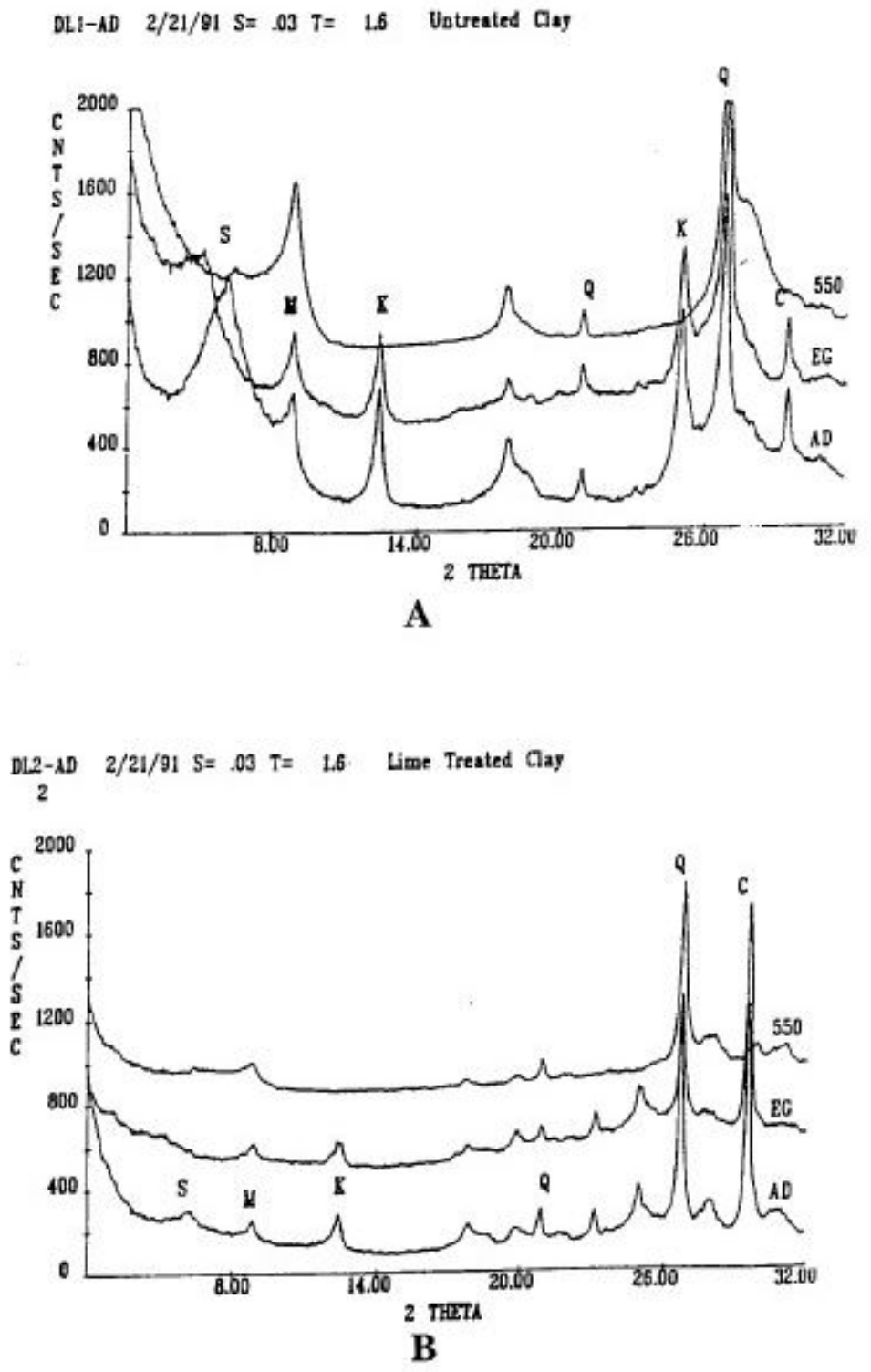

Figure 5 X-Ray diffraction pattern used to prove the reactions occurring between lime and clay surface. In (A) the XRD spectra of the natural soil produces an intense smectite peaks while the peak essentially diminishes upon lime treatment (B). (Reprinted with permission from [*2*].)

is either water or hydroxide which accounts for low specific gravity.

The sulfate minerals are in low concentrations in surface soils and rocks. Gypsum is a major source of sulfate that causes sulfate-induced heave in lime treated soils. Gypsum is present in soils developed in the montmorillonitic Eagle Ford shales group. It is the most common sulfate mineral found in sedimentary rocks. "The pyrite-bearing Eagle Ford shale contains gypsum produced by reaction of calcium carbonate in the shale with acid sulfate from oxidation weathering of pyrite (FeS_2). Eagle Ford soils do not always produce sulfate-induced heave everywhere that road base has been lime-treated, but the problem is observed most frequently where roads follow streams, or run across low-lying areas or hillside slopes" [*23*]. Iron sulfide polymorphs, pyrite and marcasite are very common in sedimentary rocks, as accessory minerals in igneous rocks, and in contact and regional metamorphic rocks [*24*]. According to Krauskopf [*25*] pyrite oxidation, which is bacterially catalyzed, produces the insoluble iron oxides hematite or goethite and sulfuric acid. There are several forms of sulfate but the most common ones found in Texas are pyrite and marcasite.

This report discusses the use of a magnetometer to screen large areas for the presence of sulfates. The basic principle of the magnetometer is to measure the electrical conductivity of the soil based on a magnetic field generated by the dipoles of the magnetometer. This is discussed in detail in chapter IV.

Sulfate problems have been identified in several parts of United States and across the world. The concern for sulfate problems in stabilized soil has increased among the researchers. Sulfate problems have been identified by the Texas Department of Transportation in several parts of Texas. One such example was along US 67 near

Waxahachie where heaving was observed in the pavement and was attributed to the formation of Ettringite. Another typical example of heaving due to Ettringite formation was the classic example of failure in parking lot and the pavements in Las Vegas, Nevada. Stewarts Avenue and Owens Avenue heaved as much as 12 inches and 8 inches, respectively, two years after construction [*18*]. The failure of these pavements received national attention when Mitchell discussed in the annual Terzaghi Lecture [9]. The failure was attributed to the formation of ettringite and thaumasite. Concrete deterioration due to the formation of ettringite has been recognized for many years [*26*]. "Conversations with the state of Texas Highway Department (Gerald Peck, personal communication, 1983) revealed the occurrence of lime induced heave on US Highway 10 between Amarillo and Fort Worth, in 1975. Damage was blamed on the growth of gypsum and it was stated that it was an occasional problem where lime reacted with sulfate in the native soils. Maximum heave was on the order of half inch" [*18*]. Heaving of Interstate 70 in Grand County of eastern Utah was documented by Utah Department of Transportation, distress along US Highway 41 in Davidson and Sumner Counties documented by the Tennessee Department of Transportation are several other cases of sulfate induced heave in lime-treated soils. Sulfate induced heave has been observed in Australia, Europe and the United Arab Emirates. Researchers including Lambe, Michales and Moh (1960) [*27*], and Ladd, Moh and Lambe (1960) [*28*], Hollis and Fawcett (1966) [*29*] concluded that small amounts of sulfates increase the strength of the soil in certain soil types. However, in 1974 the California Division of Highways stated that sulfates can be detrimental to lime treated soils as they enhance swelling.

CHAPTER III

FIELD SITE

3.1 INTRODUCTION

SH 130 passes through four counties; Williamson, Travis, Caldwell, and Guadalupe. This research focused on finding areas of high sulfate concentration and problematic areas where heaving is presumed to occur due to the formation of ettringite. Two sites were selected for this study. Preliminary testing results from CTL Thompson were used to identify the areas of interest. The first site was near US 290. This site was known to contain high sulfate contents. A grid of 100m by 200m was set up along the proposed SH 130 corridor. The distance between intermediate points were 50m. Three different locations B1, C3 and C5 were selected for depth analysis. A trench was dug to a depth of 10ft and conductivity readings at each 12 inch increment were noted. The second site selected was along US 79. This site was believed to be very low in sulfates. A grid of 100m by 150 m was established. Intermediate points at every 50m were selected for analysis. The depth analysis was limited to 4ft because of the low conductivity. The latitude and longitude of all the locations both along US 290 and US 79 were noted down to represent the site in GIS.

3.2 GEOLOGY, SOILS, AND TOPOGRAPHY

As mentioned earlier, the 94 mile corridor passes through four counties. The geology, soils and topography is considerably different in these counties. As such the parameters will be explained individually according to the counties.

In Williamson County the corridor passes through three different soil map units, Branyon-Houston Black-Burleson, Austin-Houston Black-Castephen, and Oakalla-

Sunev. Branyon-Houston Black-Burleson soils are formed from clayey alluvium and marine clays and shales; on ancient stream terraces and uplands. The soil is calcareous, moderately alkaline, and has a high shrink-swell potential. Austin-Houston Black-Castephen is formed in marine chalk, marl, shale, and clays: on uplands. Oakalla-Sunev soils are calcareous, loamy soils formed in alluvium: on bottom lands and stream terraces. Even this soil is high in lime content and is moderately alkaline throughout.

In Travis County, the soil units are Houston Black-Heiden, Burleson-Wilson, Ferris-Heiden, Bergstrom-Norwood, Travis-Chaney, and Lewisville-Patrick. A few drawbacks of these soil units are high shrink-swell, corrosivity, and low permeability. Good care is required when laying underground pipelines as risk of corrosion is very high in these types of soil units.

In Caldwell County; Heiden-Houston Black, Branyon-Lewisville, and Trinity association are the units through which the corridor pass. In this County the soils are calcareous. Some of the problems of these soil units are low permeability, high shrink-swell, and high corrosivity. As such extra caution is required in construction of roads and buildings. The areas of the Trinity association are frequently flooded.

Crockett-Demona-Windthorst, Branyon-Barbarosa-Lewisville, Houston Black-Heiden, Sunev-Seguin, and Austin-Eddy soil units are of concern. The units are well drained, loamy to sandy soils on uplands. The shrink-swell potential of the soils of these units is high. These soils are best suited for irrigation. Also some areas are sources of gravel. The Sunev-Seguin areas are frequented with flooding and in such cases the limitations are severe because the depth of chalk is shallow.

The county soil survey report lists that Ferris, Heiden, and Houston Black found

in the region have common characteristics like montmorillonitic, calcareous, high shrink swell, low strength, low permeability, moderate alkalinity and high corrosivity. The survey reports gypsum in AC and C horizon of Ferris and Heiden soils.

3.3 APPLICATIONS OF GIS

GIS maps can be adapted to determine heaving potential areas based on geology, soils, and topography. GIS power lies in its ability to visually present spatial data within a geographic reference, analyze patterns that could not have been seen without GIS assistance, and reveal hidden trends and distributions. Arc View 8.3, Geographic Information System (GIS) software can be used to create dynamic maps by adding multi-layered data. Existing databases for soils, geology, and topography can be accessed to supply spatial records that can be used to display multi-layered maps. Heaving due to the growth of the expansive mineral ettringite can be predicted using multi-layered GIS maps. GIS provides the ability to analyze multi layer maps of geology, soils, and topography, which make it possible to predict heaving potential.

Ettringite, calcium aluminate sulfate hydrate (CASH), requires sufficient concentrations of calcium, alumina, and sulfate and abundant water to form. In the field, the areas prone to form ettringite can be predicted using GIS. Calcium is provided to the system by added lime used to stabilize the soil. Clay minerals normally provide an ample amount of alumina. As such, the sulfate and amount of water are the only other variables that dictate ettringite formation in the field. The presence of sulfates can be predicted from the geology of the bed rock and the type of soil. The available water can be predicted from topography. In the past, determining heave sensitive (due to ettringite formation) areas based on geology, soils and topography was a cumbersome process.

With advancing technology and the availability of a sophisticated software like Arc View GIS, the process is simplified and more direct.

The geology maps of Williamson, Travis, Caldwell, and Guadalupe counties are accessed from the Texas Natural Resources Information System (TNRIS) [*30*]. This is represented in Figure 6. The data set for each of the rock types includes field ID (FID), area (ft^2), perimeter (ft), rock description, etc. The table does not provide sulfate content. An additional table that identified the possibility of sulfate in particular rock types was developed and spatially joined to the existing table. This is represented in Table 2. This provides a new layer for geology for the four counties and sulfate content of any location in any of the four counties.

The soils maps of the four counties are accessed from the Soil Survey Geographic Database (SSURGO). The soils data was accessed from the county soil survey [*53, 54, 55, 56*] and spatially joined to the existing table and saved as a layer file. This was done on all four counties and saved as a new layer file. The soils maps for each of the counties are represented in Figure 7, Figure 8, Figure 9, and Figure 10. Sulfate, soil swell, and permeability are shown in Table 3, Table 4, Table 5, and Table 6. The new layer map of soils provides the ability to identify high sulfate areas. The area field represents the area

of a particular soil series in square feet. MUSYM represents the soil series based on the county soil survey report. Sulfates, soil swell, and permeability indicate the severity; nonetheless it does not give the actual concentration of sulfate in the soil series. Sulfate concentration shows the severity of an area to heave due to the growth of ettringite. Soil swell and permeability indirectly indicate the clay content which is a measure of the amount of alumina and water needed for the formation of ettringite.

The third layer is the baseline of SH 130. The baseline or the centerline of SH 130 lies in two different co-ordinate systems. In Williamson County the base line falls in NAD 1983 StatePlane Texas South Central FIPS 4204 (Feet) where as in Travis County the co-ordinate system is in NAD 1983 StatePlane Texas Central FIPS 4203 (Feet). The co-ordinates for the base line were provided by Lone Star Infrastructure. Our sampling locations along US 290 and US 79 are in NAD 1983 UTM Zone 14 co-ordinate system. The baseline of SH 130 along with existing roads is shown is Figure 11.

Finally, in order to analyze the topography of the area, aerial photographs are overlapped on the existing 3 layer maps. The aerial photos are downloaded from TNRIS [*30*] for topographical analysis.

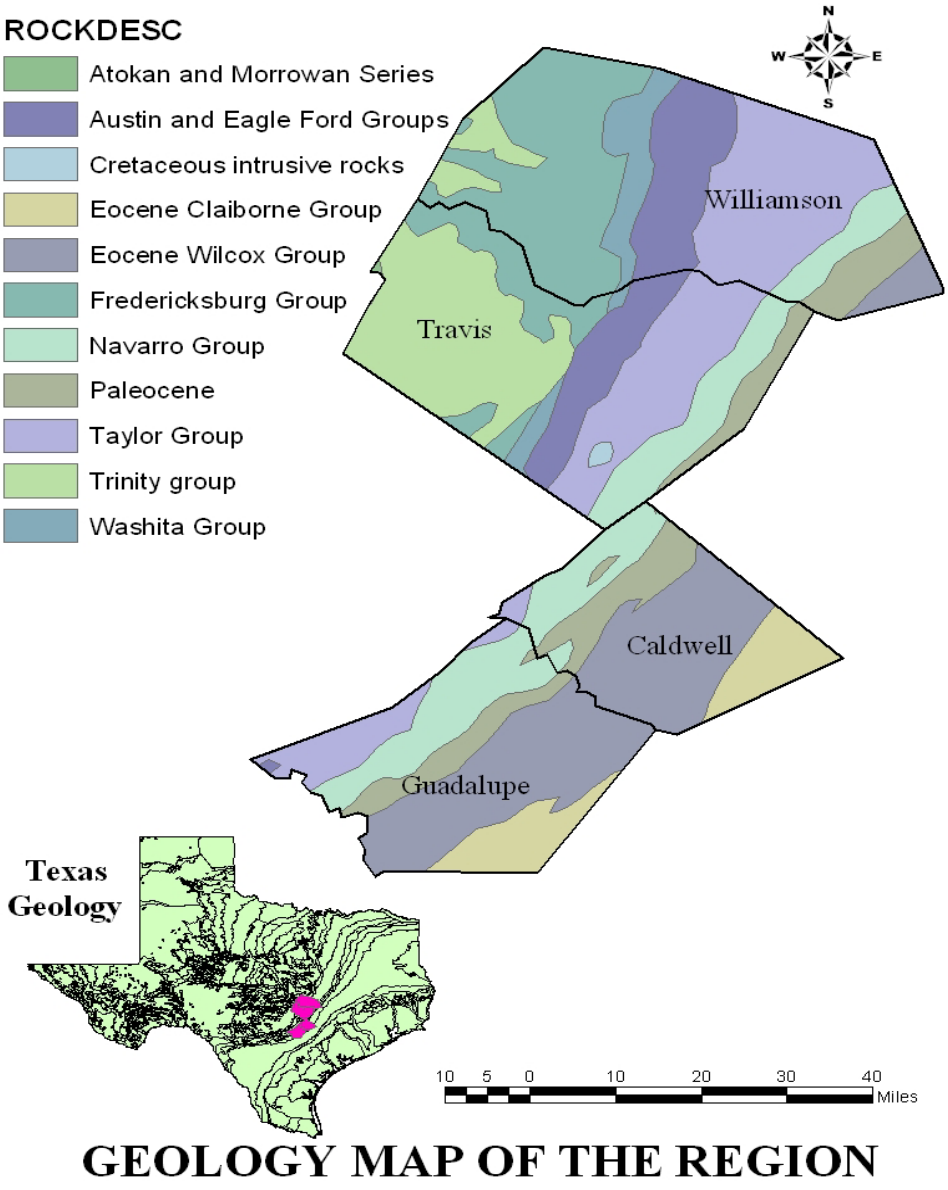

Figure 6 Geology map [*30*]

Table 2 Attribute table for geology

AREA	UNIT	ROCKDESC	COMMENTS
6.551	Te2	Eocene Claiborne Group	Sediments primarily consists of sandstones, conglomerates, clays and shales.
0.001	uK2	Austin and Eagle Ford Groups	Includes Pepper Shale,Cloice Shale,Bouldin Flags,& South Bosque Marl members.Likely to contain high levels of pyrite
1.453	uK3	Taylor Group	Marine calcareous clay.Likely to contain high levels of pyrite
6.551	Te2	Eocene Claiborne Group	Sediments primarily consists of sandstones, conglomerates, clays and shales.
1.453	uK3	Taylor Group	Marine calcareous clay.Likely to contain high levels of pyrite
0.001	Tx	Paleocene	Highly glauconitic sands and sandy clays
1.560	Te1	Eocene Wilcox Group	Primarily composed of mud with various amounts of sand and lignite.
1.560	Te1	Eocene Wilcox Group	Primarily composed of mud with various amounts of sand and lignite.
0.753	Tx	Paleocene	Highly glauconitic sands and sandy clays
0.753	Tx	Paleocene	Highly glauconitic sands and sandy clays
0.001	Ki	Cretaceous intrusive rocks	Sulfate: No-data
0.008	lK2	Fredericksburg Group	Sulfate: No-data
0.081	lK2	Fredericksburg Group	Sulfate: No-data
0.026	lK3	Washita Group	Sulfate: No-data
0.018	PP1	Atokan and Morrowan Series	No-data
0.018	PP1	Atokan and Morrowan Series	No-Data
1.560	Te1	Eocene Wilcox Group	Primarily composed of mud with various amounts of sand and lignite.
1.019	lK1	Trinity group	Include interfingering carbonates deposited in a variety of near-shore environments and softer limestones
0.753	Tx	Paleocene	Highly glauconitic sands and sandy clays
0.753	uK4	Navarro Group	Marine marl and carbonaceous shale
0.008	lK1	Trinity group	Include interfingering carbonates deposited in a variety of near-shore environments and softer limestones
0.646	lK2	Fredericksburg Group	Sulfate: No-data
0.023	lK1	Trinity group	Include interfingering carbonates deposited in a variety of near-shore environments and softer limestones
1.453	uK3	Taylor Group	Marine calcareous clay.Likely to contain high levels of pyrite
1.327	uK2	Austin and Eagle Ford Groups	Includes Pepper Shale,Cloice Shale,Bouldin Flags,& South Bosque Marl members.Likely to contain high levels of pyrite
0.945	lK3	Washita Group	Sulfate: No-data
0.646	lK2	Fredericksburg Group	Sulfate: No-data

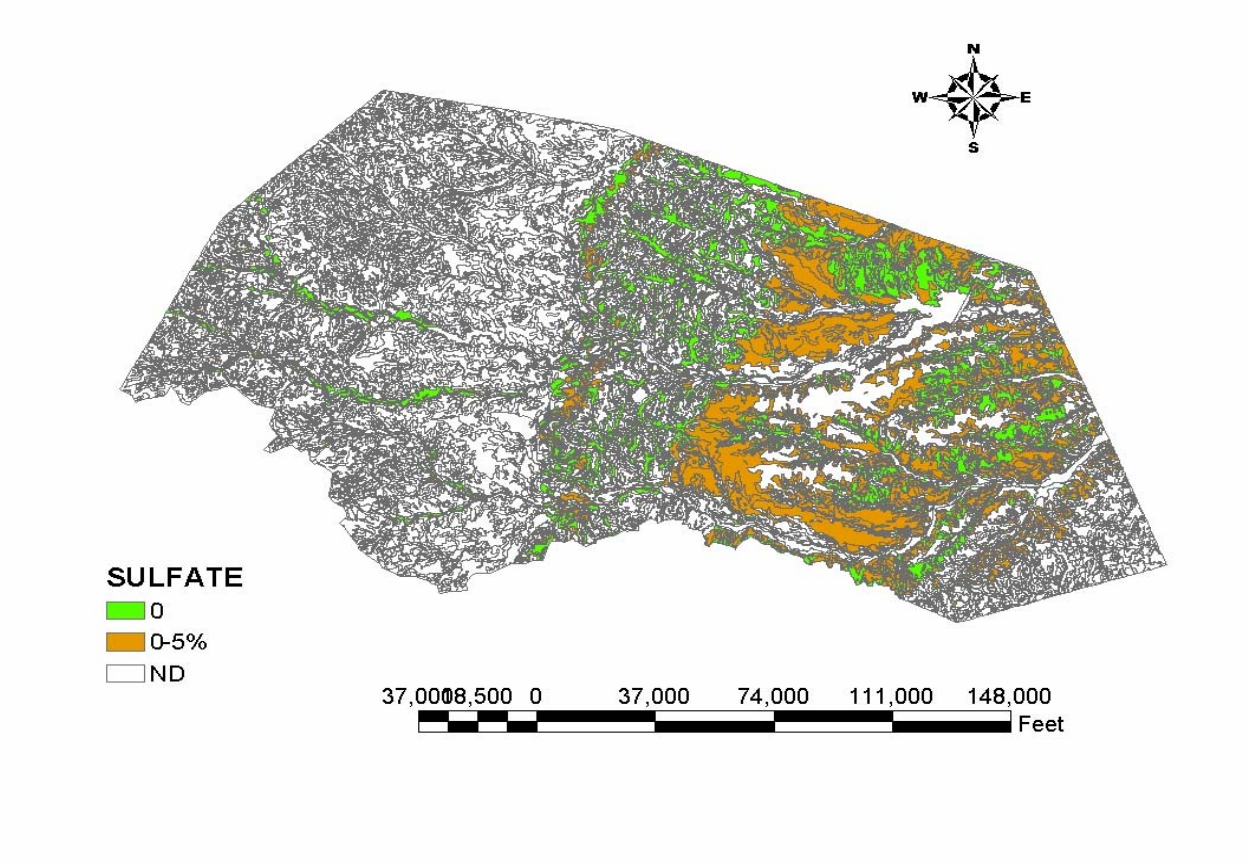

Figure 7 Soils map of Williamson County [*30*]

Table 3 Attribute table for Williamson soil [*53*]

MUSYM	SULFATE	SHRINK SWELL	PERMEABILITY
HuB	0	very high	very slow
HeC2	0-5%	very high	slow
DnB	ND	high	slow
HsE	0-5%	very high	very slow
CfB	ND	very high	moderate
HeB	0-5%	very high	slow
FaB	ND	very high	moderate
HeB	0-5%	very high	slow
FhE	0-5%	very high	very slow
HeB	0-5%	very high	slow
HuB	0	very high	very slow
HeB	0-5%	very high	slow
HsE	0-5%	very high	very slow
AuB	ND	moderate	moderately slow
HuA	0	very high	moderate
HeC2	0-5%	very high	slow
HuA	0	very high	moderate
HuB	0	very high	very slow
DnB	ND	high	slow
HeC2	0-5%	very high	slow
HuB	0	very high	very slow
HuC2	0	very high	very slow
HuB	0	very high	very slow
HeB	0-5%	very high	slow
HuB	0	very high	very slow
HuB	0	very high	very slow
HuA	0	very high	moderate
HuA	0	very high	moderate
HuB	0	very high	very slow
HuC2	0	very high	very slow
HeC2	0-5%	very high	slow
HuC2	0	very high	very slow
AwC2	ND	high	moderate
HuA	0	very high	moderate

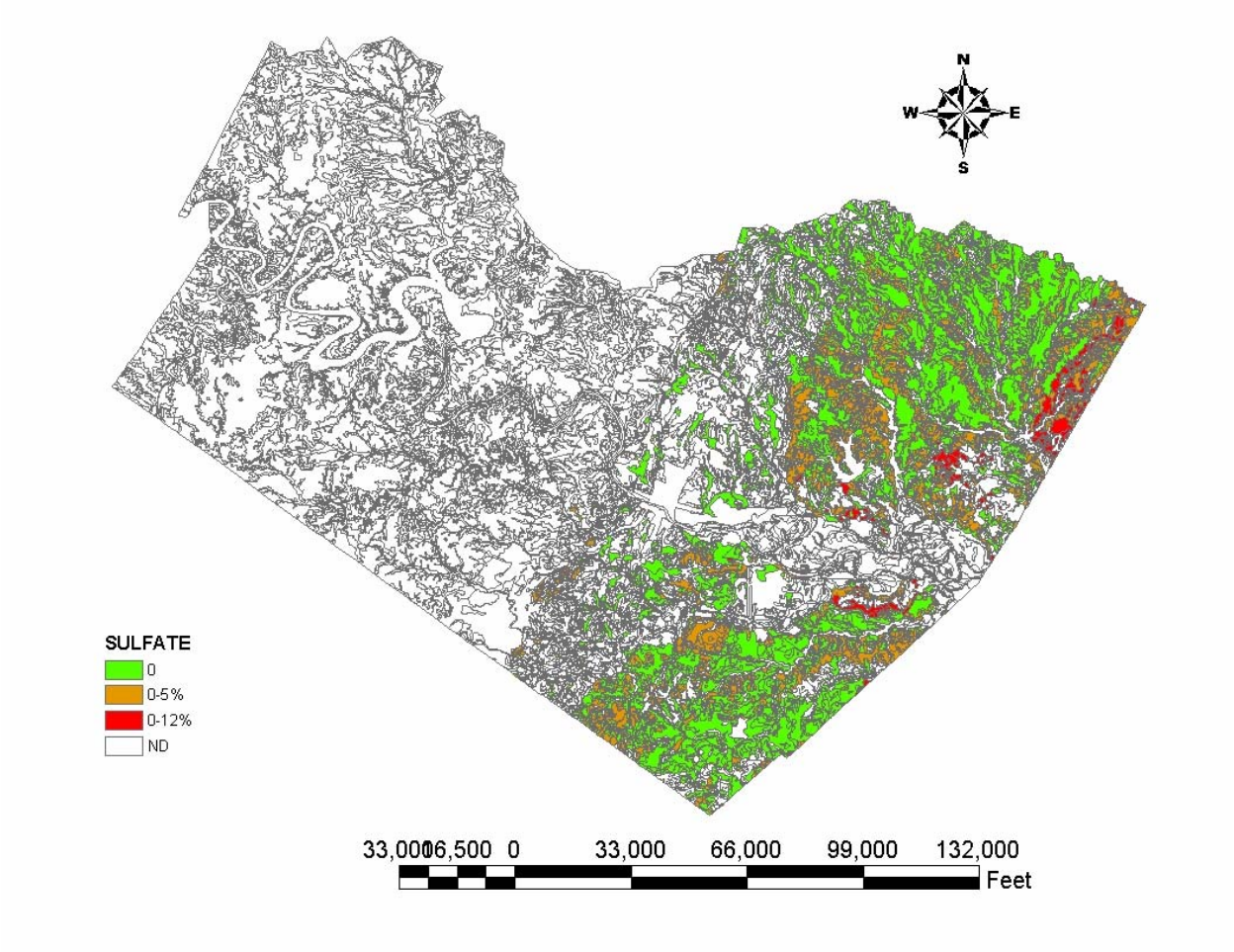

Figure 8 Soils map of Travis County [*30*]

Table 4 Attribute table for Travis soil [*54*]

MUSYM	SULFATE	SHRINK SWELL	PERMEABILITY
HnC2	0	high	very slow
HnC2	0	high	very slow
HnC2	0	high	very slow
HeD2	0-5%	very high	very slow
HeD2	0-5%	very high	very slow
HeD2	0-5%	very high	very slow
HnA	0	high	very slow
HnB	0	high	very slow
HnC2	0	high	very slow
HeD2	0-5%	very high	very slow
HeD2	0-5%	very high	very slow
HnB	0	high	very slow
HeC2	0-5%	very high	slow
HeD2	0-5%	very high	very slow
HeD2	0-5%	very high	very slow
HeC2	0-5%	very high	slow
HeC2	0-5%	very high	slow
HeC2	0-5%	very high	slow
HeD2	0-5%	very high	very slow
FhF3	0-5%	high	very slow
HeD2	0-5%	very high	very slow
HeC2	0-5%	very high	slow
WlB	0-12%	high	very slow
WlB	0-12%	high	very slow
FhF3	0-5%	high	very slow
HeD2	0-5%	very high	very slow
WlA	0-12%	high	very slow
WlA	0-12%	high	very slow
HnB	0	high	very slow
WlB	0-12%	high	very slow
HeC2	0-5%	very high	slow
HeC2	0-5%	very high	slow
HeC2	0-5%	very high	slow
HnB	0	high	very slow
HeD2	0-5%	very high	very slow
Md	ND	ND	ND
HeD2	0-5%	very high	very slow
WlA	0-12%	high	very slow
FhF3	0-5%	high	very slow
FhF3	0-5%	high	very slow
HeD2	0-5%	very high	very slow
FhF3	0-5%	high	very slow

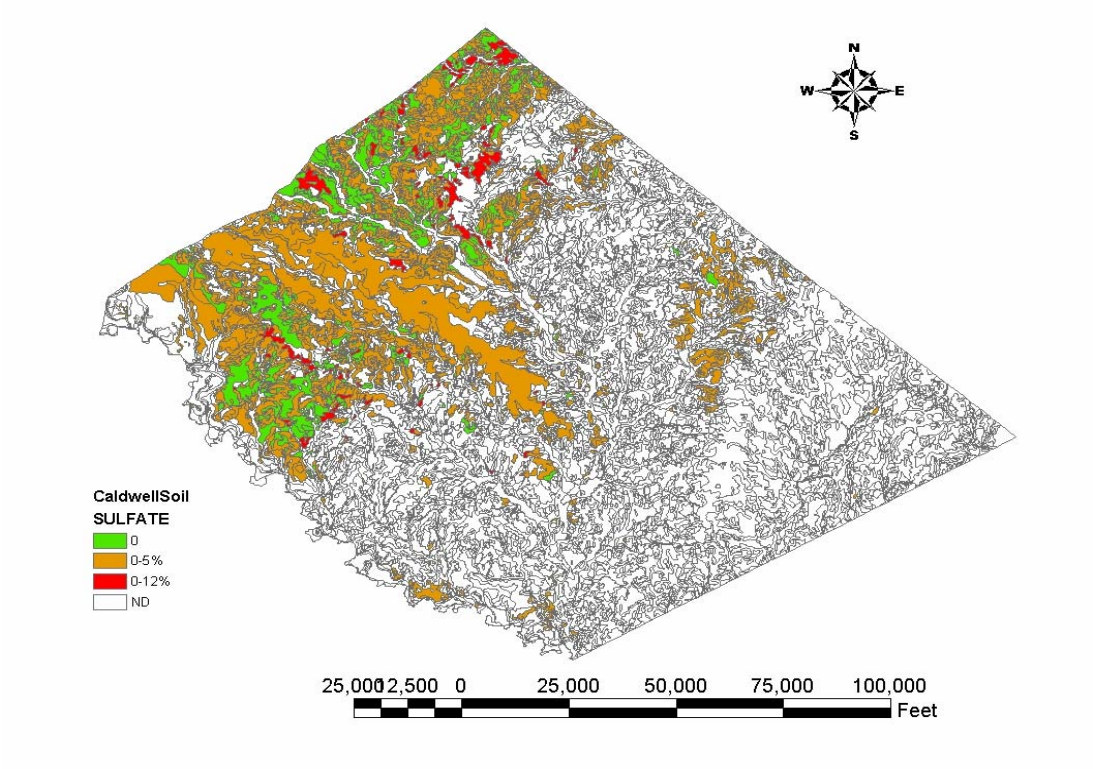

Figure 9 Soils map of Caldwell County [*30*]

Table 5 Attribute table for Caldwell soil [*55*]

MUSYM	SULFATE	SOIL SWELL	PERMEABILITY
WgC	0-12%	high	very slow
HoB	0	very high	very slow
HeC2	0-5%	very high	slow
HeD2	0-5%	very high	very slow
HeB	0-5%	very high	slow
HeC2	0-5%	very high	slow
HoC2	0	very high	very slow
HeD2	0-5%	very high	very slow
HeC2	0-5%	very high	slow
HeB	0-5%	very high	slow
HgD	0-5%	very high	very slow
WgC	0-12%	high	very slow
HhF3	0-5%	very high	very slow
HhF3	0-5%	very high	very slow
Ts	ND	very high	flooding
HhF3	0-5%	very high	very slow
HpD	0	very high	very slow
HeC2	0-5%	very high	slow
HeD2	0-5%	very high	very slow
HeB	0-5%	very high	slow
HhF3	0-5%	very high	very slow
HhF3	0-5%	very high	very slow
WgC	0-12%	high	very slow
WgC	0-12%	high	very slow
HpD	0	very high	very slow
HgD	0-5%	very high	very slow
HeD2	0-5%	very high	very slow
HoC2	0	very high	very slow
WgC	0-12%	high	very slow
HpD	0	very high	very slow
HoB	0	very high	very slow
BuB	ND	high	very slow
HhF3	0-5%	very high	very slow
BuB	ND	high	very slow
WgC	0-12%	high	very slow
WgC	0-12%	high	very slow
HhF3	0-5%	very high	very slow
HoB	0	very high	very slow
HoB	0	very high	very slow
HhF3	0-5%	very high	very slow
HpD	0	very high	very slow
WgC	0-12%	high	very slow

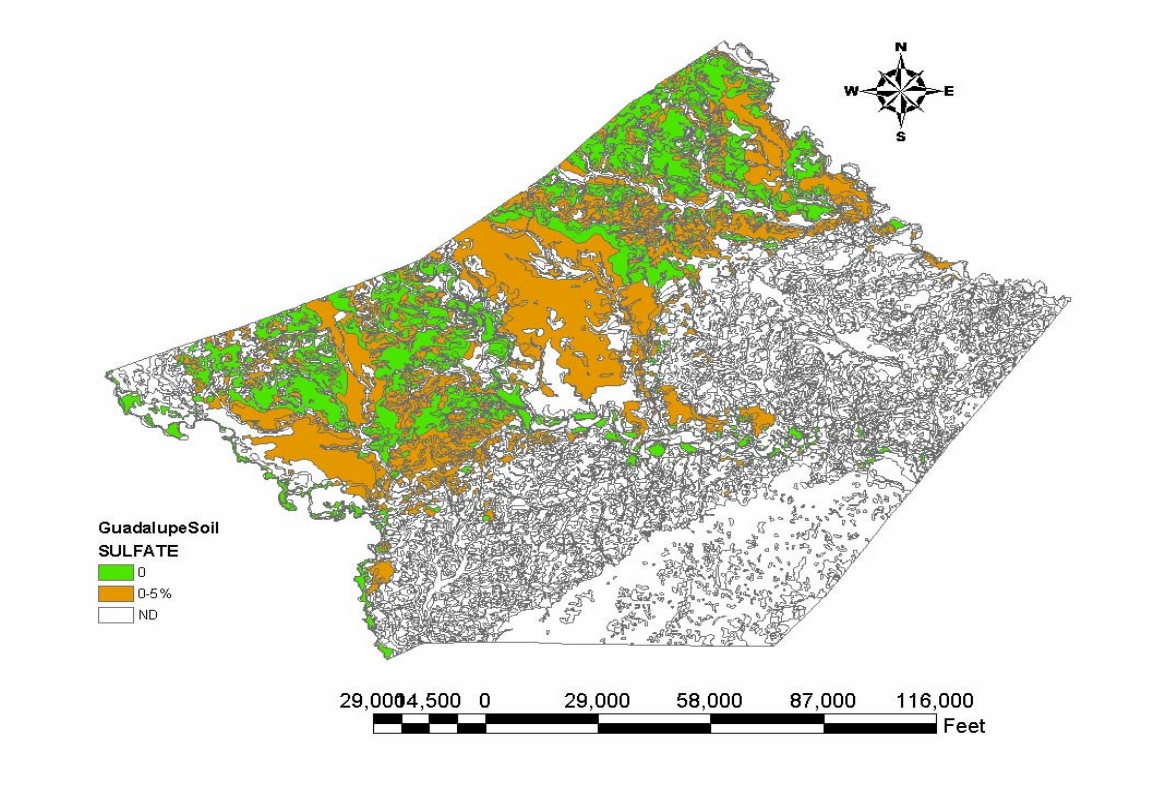

Figure 10 Soils map of Guadalupe County [*30*]

Table 6 Attribute table for Guadalupe soil [*56*]

MUSYM	SULFATE	SOIL SWELL	PERMEABILITY
BrA	0-5%	very high	very slow
BrB	0-5%	very high	moderate
FhF3	0-5%	high	very slow
HpB	0	very high	very slow
HeD3	0-5%	very high	very slow
HoA	0	very high	very slow
SuC3	0	moderate	moderate
HeC3	0-5%	very high	slow
BrA	0-5%	very high	very slow
HeD3	0-5%	very high	very slow
HeC3	0-5%	very high	slow
HeC3	0-5%	very high	slow
HpC	0	very high	very slow
HeD3	0-5%	very high	very slow
AuB	ND	moderate	moderately slow
HpC	0	very high	very slow
HpC	0	very high	very slow
HeC	0-5%	very high	slow
HeB	0-5%	very high	slow
AlC3	ND	high	moderate
HoB	0	very high	very slow
BrA	0-5%	very high	very slow
HeC3	0-5%	very high	slow
FhF3	0-5%	high	very slow
HpB	0	very high	very slow
HeC	0-5%	very high	slow
BaB	ND	slight	slow
HpB	0	very high	very slow
Tr	ND	very high	flooding
HeD3	0-5%	very high	very slow
HeC	0-5%	very high	slow
HpC	0	very high	very slow
FhF3	0-5%	high	very slow
HeB	0-5%	very high	slow
HpC	0	very high	very slow
HpC	0	very high	very slow
Tw	ND	high	slow & flooding
HoA	0	very high	very slow
HpC	0	very high	very slow
HoB	0	very high	very slow
HpC	0	very high	very slow

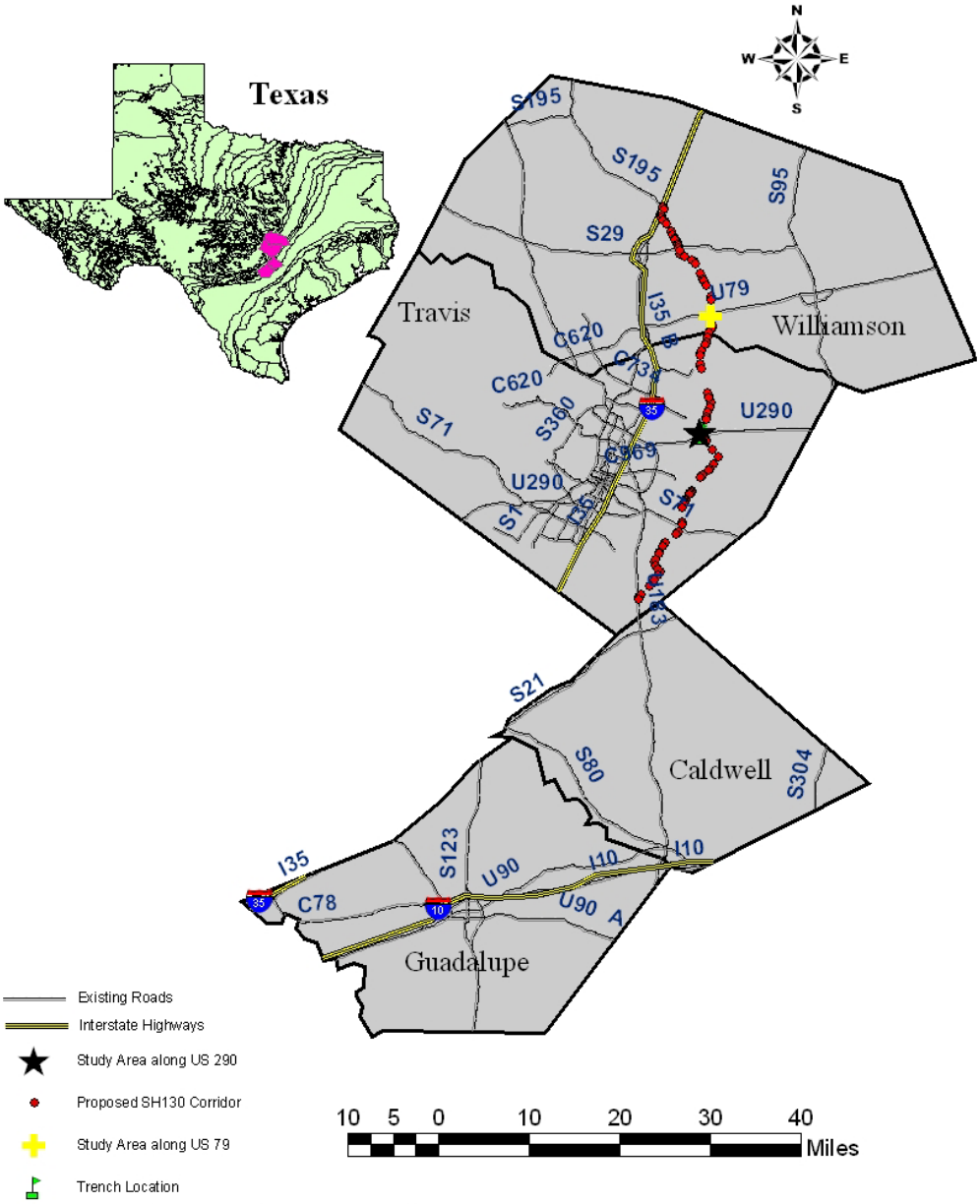

State Highway 130 with Existing Roads

Figure 11 State Highway 130 with existing roads [*30*]

Heave potential due to formation of ettringite is predicted based on the following methodology. The methodology is illustrated with respect to our project sampling location along US 290.

1. The first step is to determine whether the bed rock contains sulfate. The geology of the bed rock is instituted by accessing the recently developed database of geology. The important information about a particular location is displayed in a table. The comment section gives the information regarding sulfates. The bed rock for the location along US 290 as identified by the map is the Taylor group. This is illustrated in Figure 12. The comment on this bed rock confirms that the Taylor group is likely to contain high levels of pyrite.
2. The next step is to determine if the soils formed on these bed rocks also contain sulfates. This is achieved by collecting soil data in the GIS data base. The 100ft × 250ft grid marked along the proposed corridor spreads into two soil series both of which contain high levels of sulfate. The sulfate content identified for this location varies from 0 to 5 %, Figure 13.
3. The preliminary investigation regarding bed rock and soil provided evidence for the presence of sulfate in the location; the next step is to look in to the topography of the area. The topography of the location is an important criterion because, lower elevations are more susceptible to deposition of sulfates during runoff. During the runoff, much of the soluble salts will be washed and transported to lower elevation points along with water. When water dries up, salts are deposited, leading to excessive salt concentration at lower altitudes. Consequently such spots become more susceptible to ettringite formation. Therefore, aerial photos of the

location were analyzed to approximate surface water movement after precipitation. A digital elevation model (DEM) of the area was analyzed to evaluate topography. The DEM serves as a cross reference for the aerial photographs in order to analyze the topography. The topographic map of the location along US 290 reveals that it is a low lying area. This is represented in Figure 14. The red area in Figure 14 indicates higher elevation and green indicates low lying areas. The change in intensity of color indicates change of slope. Steady color indicates flat terrain.

4. The aforementioned analysis indicates that the location along US 290 is susceptible for ettringite formation. But, it should be kept in mind that GIS maps are not an accurate measurement to determine whether ettringite is definitely going to form or not. This is because sulfates contents are approximated and are determined by bed rock and the soil series. It is not an exact value of the amount of sulfate present in a location. However, the GIS map can fairly eliminate the areas where possibility of heaving is less based on geology and soil association.

The main idea behind developing the GIS maps for the corridor is to eliminate the traditional method of testing the soil at frequent intervals. The new method devised for Lone Star Infrastructure through this research at Texas Transportation Institute allows predicting problematic areas very efficiently at less cost. Millions of dollars of investigation costs can be saved by the use of this map as it limits field testing. Field testing can be limited to places where geology predicts sulfates in the bed rock as well as in soils and the topography identifies low lying areas. GIS aids in reducing the areas for screening but with the use of magnetometers, the areas can further be

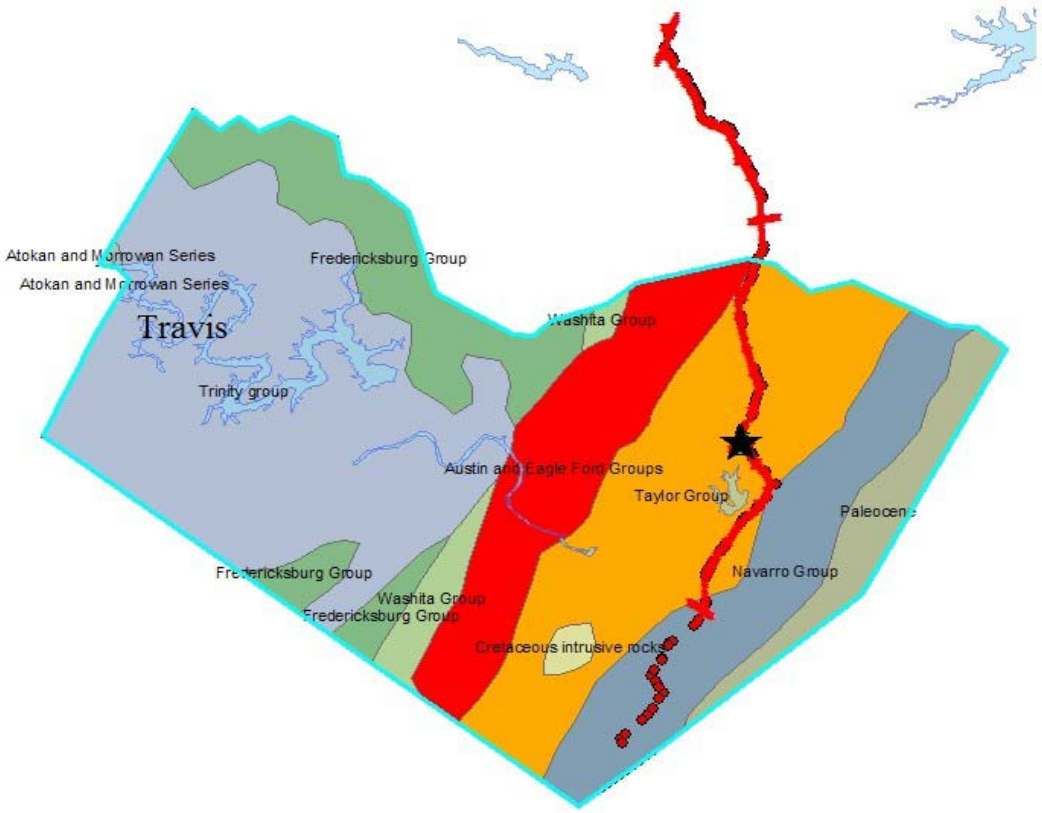

Figure 12 Geology of the location along US 290 [*30*]

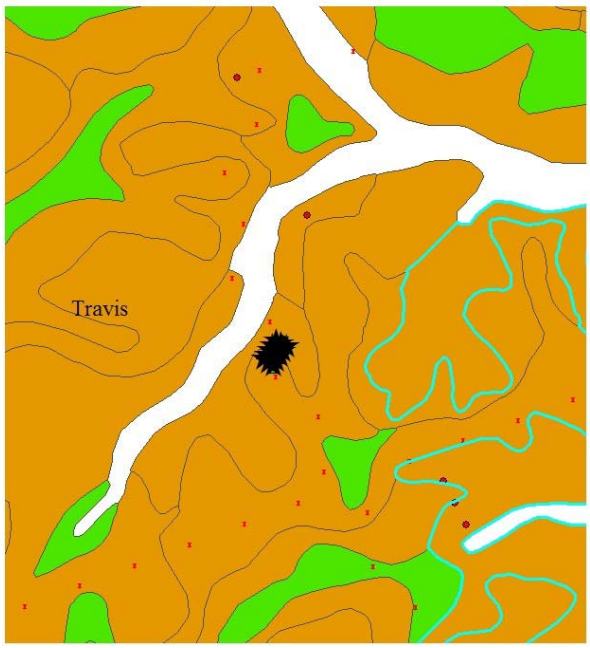

Figure 13 Soils map of the location along US 290 [*30*]

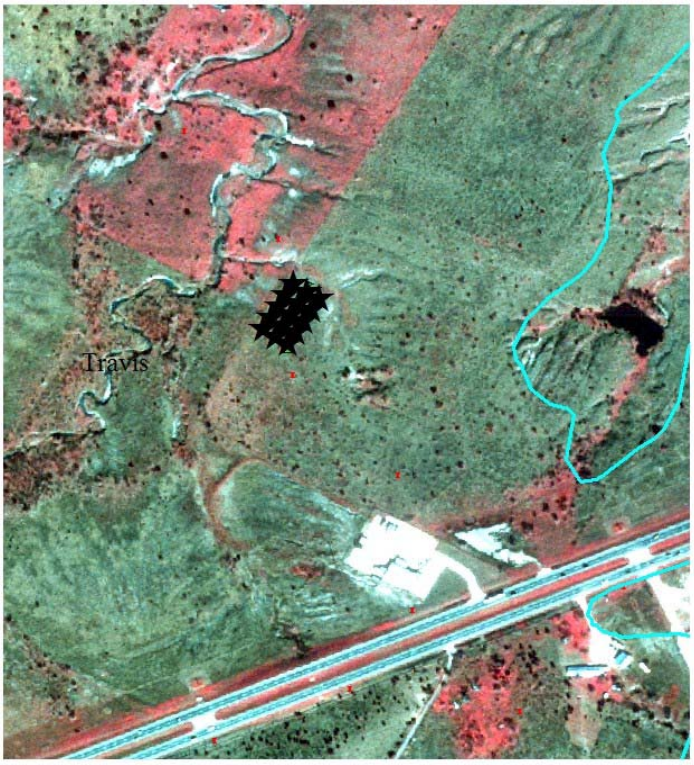

Figure 14 Topography map of location along US 290 [*30*]

refined.

Hence, with these two techniques, chemical analysis and development of stability models are limited to very few areas which in turn reduce time and resources. The operation and utility of the magnetometer is discussed in detail in the following chapter.

CHAPTER IV

MAGNETOMETER

4.1 INTRODUCTION

Electrical conductivity (EC) is a soil property that can be measured rapidly across a large area. The quick determination of electrical conductivity of the soil makes it a crucial component when information is needed in an area with limited resource input. “Bulk soil EC has been successfully related to soil salinity (Rooney et al., 1998), water storage, water content, organic matter, and texture” [*31*]. Sulfate, one of the main components for ettringite formation can be determined in the field using magnetometer at relatively high frequency. The EM 38 instrument can be used to determine the threshold level of sulfates in the field. The EM 38 is easily portable and has demonstrated the ability to detect threshold level of soluble sulfates that have been empirically related to distress potential.

Chemical Lime Company (CLC) sponsored research in the City of Frisco, Texas, to assess the potential of using electrical conductivity to screen for soluble sulfates. CLC worked with Professor Tom Petry of the University of Missouri-Rolla and Professor Dallas Little of Texas A&M in assessing this methodology. The basis of this approach was work done in the mid-1990s by Professor Robert L. Lytton [*21*] at Texas A&M that demonstrated that electrical conductivity can be used to screen for salt contents and to rapidly screen for the presence of sulfates. CLC worked with Professor Little and the Soil Science Department at Texas A&M to identify a list of potential, commercially available electrical conductivity measuring devices. These were ultimately evaluated in a controlled study in Frisco, Texas, under the direction of Professor Petry and Mr. Eric Berger of CLC. The results of this study were that the EM 38 Magnetometer was the

most effective device of the three based on test repeatability, ability to detect threshold sulfate contents, and efficiency of testing over a large area.

The most impressive attribute of the EM 38 is its ability to detect electrical conductivities (approximately 300 mS/m) in field tests that are consistent with threshold levels of soluble sulfates that correspond to sulfate-induced damage (approximately 3,000 to 5,000 ppm –Figure 15). The magnetometer, Figure 16, is used to measure sulfate contents in the direction perpendicular to the long axis of the instrument, which means that it can canvass an area about 1 meter wide and 1.5 meter deep. The readings are not time dependent; therefore, readings can be taken as fast as the magnetometer can be practically moved over the area of evaluation. With this property in mind, the magnetometer can be adapted to an "all terrain" vehicle to accommodate rapid testing.

4.2 OPERATION

The EM38 is a light weight instrument about one meter long. The EM38 device has a transmitting and a receiving coil. The transmitting coil generates a secondary magnetic field that varies in strength with depth of soil, known as electromagnetic induction. The transmitter coil applies an alternating current through the soil that creates a magnetic field that is time dependent. This in turn creates eddy currents that flow through the conductor (soil). The receiver coil senses both primary and secondary magnetic fields. The ratio of the relative strengths of the secondary and primary magnetic field represents the bulk electrical conductivity of the soil. Amplitude and phase change measurements between the two fields can define the electrical properties of the conductor and geometry of the field [*32*]. This is illustrated in Figure 17. The conductivity readings obtained in milliSeimens/meter is the apparent conductivity. The EM38 averages the values to a

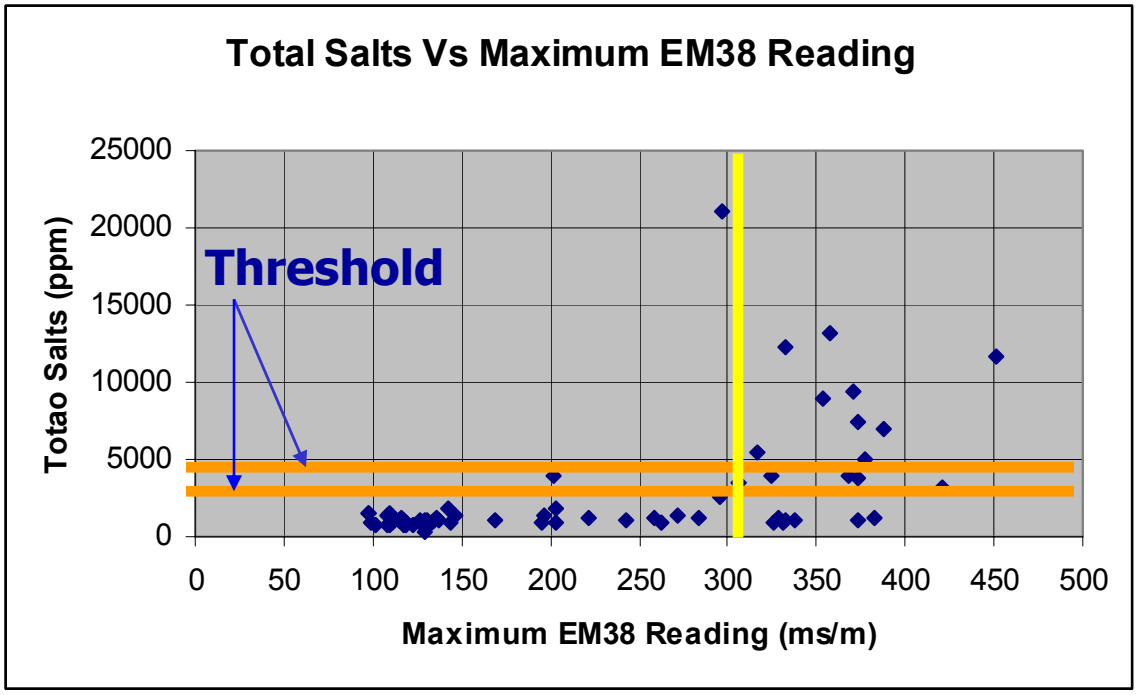

Figure 15 Threshold level of soluble sulfates corresponding to sulfate-induced damage

Figure 16 The EM 38 Conductivity Meter

depth of 1.5m. The depth of penetration of the EM38 in the horizontal dipole mode is 0.75m and 1.5m in the vertical dipole mode. Horizontal and vertical dipole measurements are read on the digital meters located on the top and side of the EM38. Continuous or station measurements can also be taken from a standing position using the optional carrying handle with trigger and cable for connection to the DL720 data logger. In this mode of operation 3000 data points can easily be obtained in one hour. "Soil bulk electrical conductivity is affected by a number of properties of the soil - clay content / cation exchange capacity, water content, and the concentration of salt in the soil and bulk density/porosity. The bulk electrical conductivity readings are directly and positively related to each of soil clay content, soil salt content and soil water content. So that light textured, non-saline, well-drained soils will give relatively low EM readings whilst heavy textured, saline, poorly drained soils will give relatively high readings (Geoff Beecher, et. al, 2003)" [*33*].

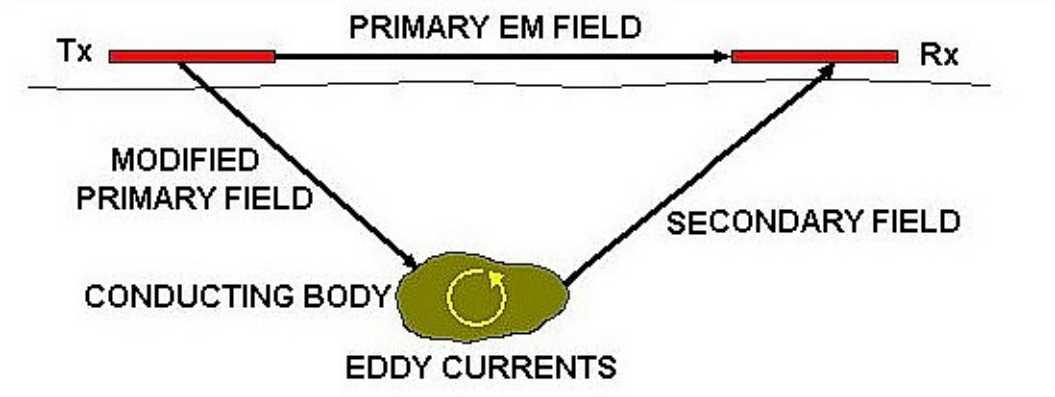

Figure 17 The working principle of EM 38 (After Keary and Brooks, 1991)

4.3 CONDUCTIVITY DETERMINATION USING EM38

With the aforementioned principles of operation of the EM38 instrument as background, the conductivity meter (EM38) was used in the field to quickly scan the areas for sulfates. Two areas were selected for screening based on the GIS analysis. The areas are selected such that one was rich in sulfates and the other very low in sulfates. Based on the analysis using GIS, the potential for ettringite formation is high along US 290 and very low along US 79. The EM38 conductivity meter was calibrated every time before scanning the areas for sulfates. Although calibrating the instrument at such high frequency is not required, it was calibrated to avoid any erroneous readings. The calibrating procedure is explained in Appendix A. After calibrating, the EM38 was held on the surface of the ground at a height of 2 to 3 cms and the conductivity readings were noted since the data logger was not used. Three different locations were selected where a trench was dug and conductivity was measured using the EM38 up to a depth of 10ft. The objective of going to a depth of 10ft was to observe the pattern of conductivity with depth. The conductivity reading at every 1ft depth was recorded. Table 7, Table 8, and Table 9 show the conductivity of the area at three different locations B1, C3, and C5 along US 290 and

Table 7 Conductivity along US 290 (boring location B1)

Sample Location	GIS Location Northing	Easting	Depth	EM 38 Reading ms/m
B 1	3357760	635274.7	6in	298
	3357760	635274.7	12in	305
	3357760	635274.7	2ft	365
	3357760	635274.7	3ft	475
	3357760	635274.7	5ft	550
	3357760	635274.7	6ft	683
	3357760	635274.7	7.5ft	731
	3357760	635274.7	10ft	620

Table 8 Conductivity along US 290 (boring location C3)

Sample Location	GIS Location Northing	Easting	Depth	EM 38 Reading ms/m
C 3	3357725	635272.2	1ft	181
	3357725	635272.2	2ft	216
	3357725	635272.2	3ft	266
	3357725	635272.2	4ft	345
	3357725	635272.2	5ft	463
	3357725	635272.2	7ft	542
	3357725	635272.2	9ft	663

Table 9 Conductivity along US 290 (boring location C5)

Sample Location	GIS Northing	Location Easting	Depth	EM 38 Reading (ms/m)
	3357698	635256.3	1ft	149
	3357698	635256.3	2ft	198
	3357698	635256.3	3ft	238
C 5	3357698	635256.3	4ft	300
	3357698	635256.3	5ft	424
	3357698	635256.3	8ft	540
	3357698	635256.3	10ft	481

Table 10 Conductivity along US 79

Sampling Location	GIS Northing	Location Easting	Surface Reading (ms/m)		4ft Deep Reading (ms/m)	
			EM 31	EM 38	EM 31	EM 38
A1	3378614	636567.5	41	114.0	88	133.5
A2	3378629	636571.5	40	112.1	80	122.1
A3	3378644	636575.5	42	112.1	77	127.4
A4	3378658	636579.2	42	112.2	81	124.1
B1	3378609	636582.4	34	109.0	73	127.9
B2	3378624	636586.7	37	108.5	62	119.7
B3	3378639	636590.2	40	112.6	72	123.2
B4	3378654	636593.9	43	113.5	70	128.6
C1	3378604	636596.4	34	110.0	78	123.7
C2	3378620	636601.3	38	113.6	71	125.4
C3	3378634	636605	41	115.1	74	130.6
C4	3378648	636608.9	48	117.8	73	133.0

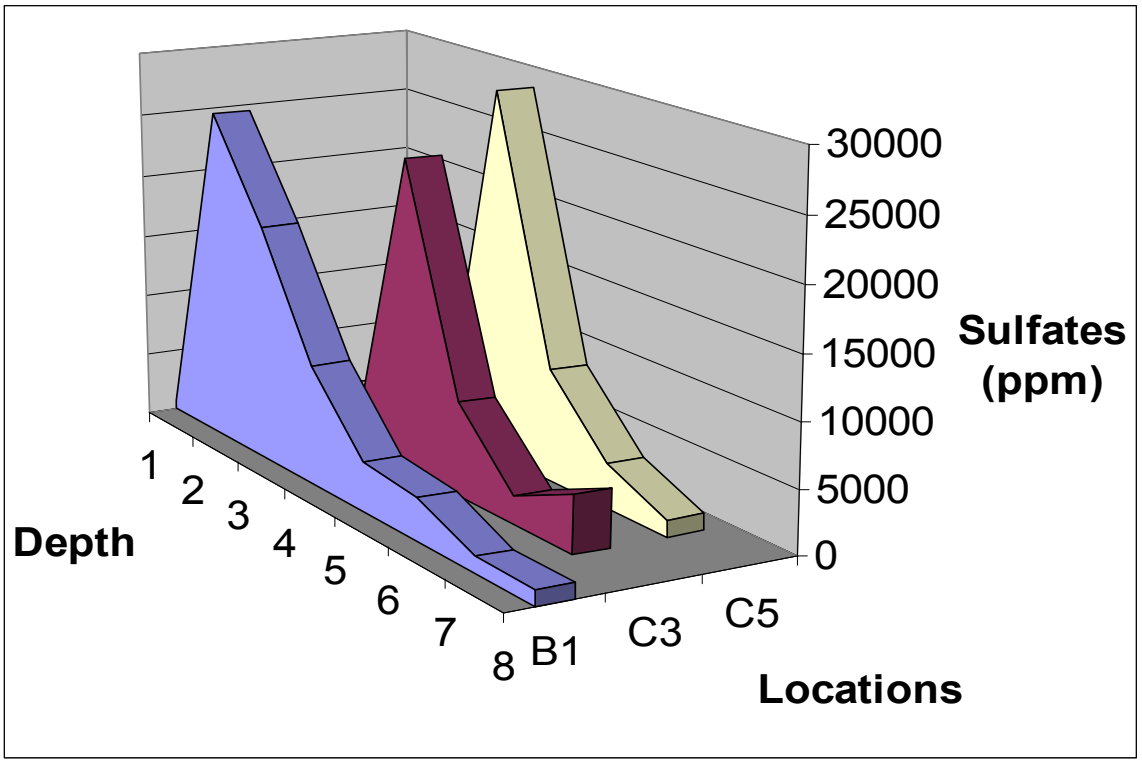

Figure 18 Variation of sulfate along slope of the surface

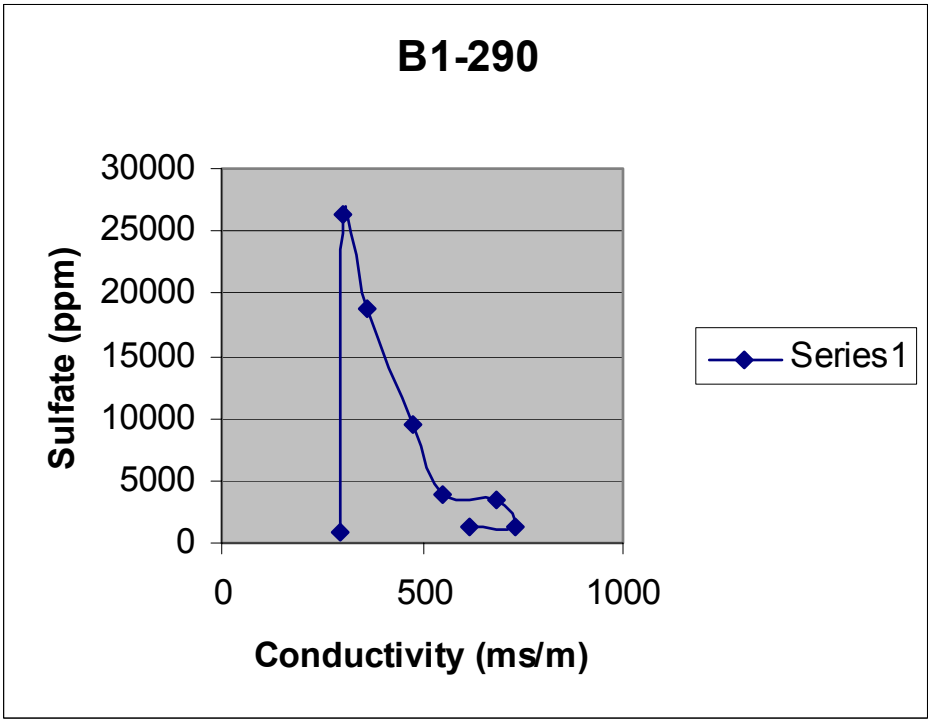

Figure 19 Variation of sulfate with depth at B1 location

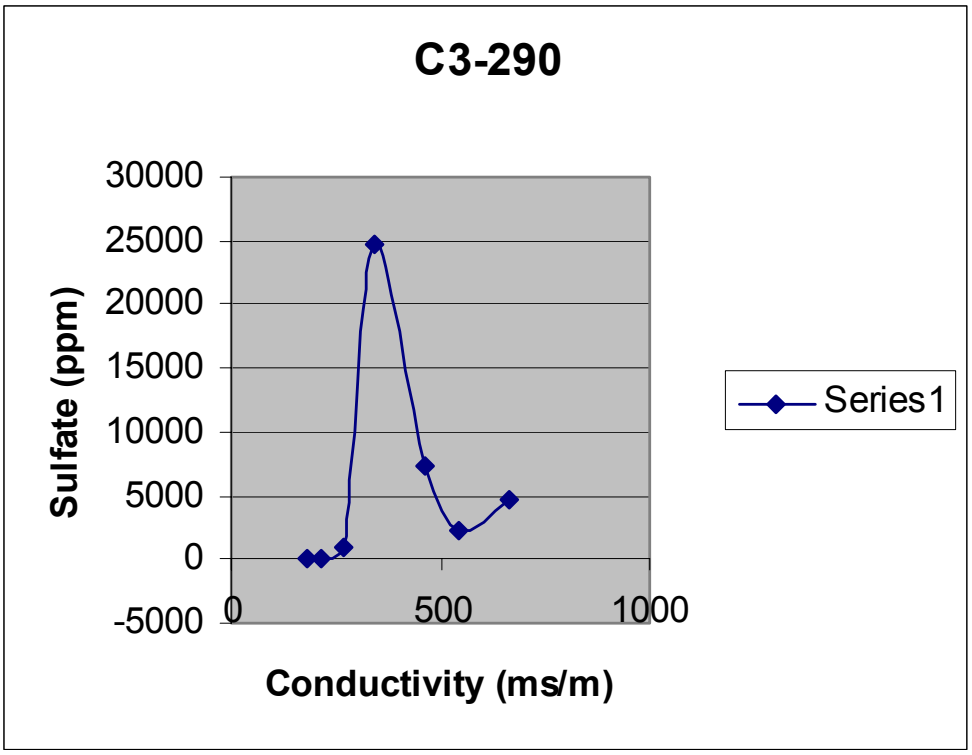

Figure 20 Variation of sulfate with depth at C3 location

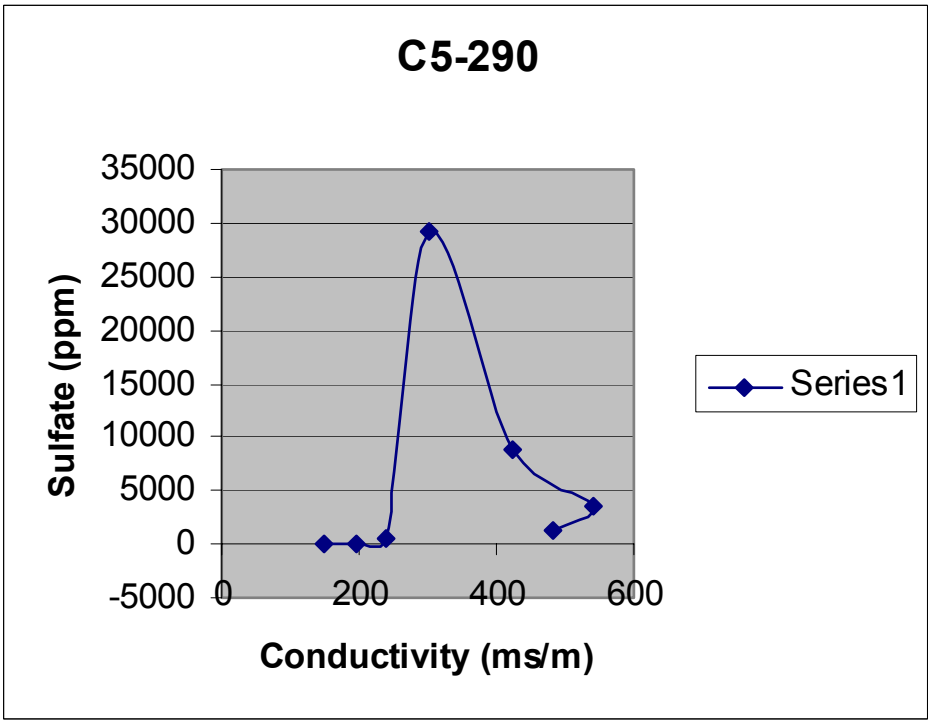

Figure 21 Variation of sulfate with depth at C5 location

Table 10 shows conductivity along US 79. Soil samples were collected at every foot depth to analyze for sulfates and mineralogy.

Figure 18, Figure 19, Figure 20, and Figure 21 show the variation of sulfate with depth. Note that the concentration of sulfates increases with depth and then decreases after reaching a maximum value. This can be attributed to the fact that ground water might have carried sulfate and deposited it at shallow depths. Also the surface runoff after precipitation may carry soluble salts on the surface and deposit in low lying areas. This is clearly visible in Figure 18. B1 is a low lying area compared to C3 and C5. Location C5 is at very high elevation. The concentration of sulfate at shallow depths in C5 is lower compared to B1. This is evident in Figure 19, Figure 20, and Figure 21. From the tables it is also evident that the sulfate concentrations are increasing with decrease in elevation. The raison d'être; the horizontal dipole readings interfered with the vertical dipole readings. The walls of the trench were less than 0.75 m apart, which is the range of the magnetometer in horizontal direction. As such, the conductivity measured in the trench did not indicate the actual conductivity. The results clearly indicate that magnetometers should never be used in a trench. But if conductivity measurements are needed at depths, then care should be taken to see that the trench is wide enough (greater than 0.75m) to eliminate horizontal and vertical dipole interference. Based on the results of magnetometer, soil samples are collected for laboratory analysis to determine the chemistry of the natural soil.

CHAPTER V

SOIL CHARACTERIZATION

5.1 INTRODUCTION

Soil samples were collected along the proposed route. The soils are characterized based on results by CTL Thompson and soil survey report. Sieve analysis, moisture content, atterberg limits, unconfined compressive strength, swell, sulfates, and soil classification were considered in characterizing the soils. The concentrations of calcium, silica, alumina, sulfate, and moisture content were determined for the soil along US 290 and US 79. These results were used to develop the stability models for the soil at our project site. Stability models were validated by mixing the soil with 5% lime at 3% to 4% over optimum moisture and cured for 28 days at different temperature conditions. Before mixing the soil with lime, the concentration of sulfate was determined. Differential Scanning Calorimetry testing was conducted to quantify the amount of ettringite in the prepared samples.

5.2 SULFATE EXTRACTION

It has been proven that different water: soil ratios yield different sulfate levels because of the difference in solubility properties of sulfate compounds [34]. As a result 10:1 water: soil ratio was adopted to determine the concentration of sulfates in the soil. The Texas Department of Transportation (Tex-620-J) utilizes 30g of soil in 300 ml of deionized water. Petry (1994) tested replicates of gypsum rich soils from Cedar Hill State Park. 1:1 extraction was performed in water at different pH levels, and the sulfate level obtained indicated that pH has a strong influence on the solubility of gypsum [35]. The procedure to find the amount of sulfates is explained as follows.

1. Representative soil is taken, air-dried to facilitate screening and passed through the No 4 sieve. Only the material passing No 4 is used in testing.
2. The soil is then completely dried in an oven at $230^0 \pm 9^0$ F for 15 hours.
3. 75g (dry basis) representative soil sample is weighed and placed in 1000ml plastic bottle.
4. 750ml of deionozed (DI) water is added and bottle is sealed. Sample is shaken for 30 min using mechanical shaker (200 rpm), or by hand every 15 min for 1 hour.
5. It is then allowed to stand for 1 hour.
6. About 30 ml of the liquid from above the soil sediment is transferred into the three centrifuge tubes.
7. Suspended solids are centrifuged out at 1200 rpm for 15 min.
8. The content of all three tubes is emptied into a 50 ml beaker.
9. 0.5ml of content is immediately pipetted off (automatic pipette) of the extract into a tube. And then diluted with 4.5 ml of DI water.
10. Last step is to determine the sulfate concentration in the solution by ion chromatography (Dionex System)

The concentration is expressed in ppm. The sulfate concentration along with moisture content and total soluble salts is shown in Table 11, Table 12, and Table 13 for US 290. Table 14 shows sulfate, moisture content, and total soluble salts along US 79. This value is used as one of the input to develop the stability models.

Table 11 Sulfate, moisture content, and total soluble salts (boring location B1- US 290)

Sample Location	GIS Northing	Location Easting	Depth	Moisture Content (%)	Sulfate Content (ppm)	Total Soluble Salts (ppm)
B 1	3357760	635274.7	6in	24.1	773	935
	3357760	635274.7	12in	24.7	26262	27267
	3357760	635274.7	2ft	24.3	18700	19978
	3357760	635274.7	3ft	26.4	9404	9435
	3357760	635274.7	5ft	27.8	3965	4400
	3357760	635274.7	6ft	25.1	3373	3594
	3357760	635274.7	7.5ft	25.8	1255	1444
	3357760	635274.7	10ft	23.9	1190	1362

Table 12 Sulfate, moisture content, and total soluble salts (boring location C3- US 290)

Sample Location	GIS Northing	Location Easting	Depth	Moisture Content (%)	Sulfate Content (ppm)	Total Soluble Salts (ppm)
C 3	3357725	635272.2	1ft	26.3	0	141
	3357725	635272.2	2ft	20.4	0	107
	3357725	635272.2	3ft	19.7	946	1337
	3357725	635272.2	4ft	18.6	24674	25998
	3357725	635272.2	5ft	22.0	7409	8119
	3357725	635272.2	7ft	24.5	2247	2946
	3357725	635272.2	9ft	25.8	4579	5087

Table 13 Sulfate, moisture content, and total soluble salts (boring location C5- US 290)

Location	GIS Northing	Location Easting	Depth	Moisture Content (%)	Sulfate content (ppm)	Total Soluble Salts (ppm)
	3357698	635256.3	1ft	27.2	0	109
	3357698	635256.3	2ft	20.1	0	159
	3357698	635256.3	3ft	20.8	594	867
C 5	3357698	635256.3	4ft	20.0	29189	30343
	3357698	635256.3	5ft	23.5	8841	9337
	3357698	635256.3	8ft	24.9	3473	3981
	3357698	635256.3	10ft	21.6	1309	1681

Table 14 Sulfate, moisture content, and total soluble salts (boring location US 79)

Location	GIS Northing	Location Easting	Moisture Content (%)	Sulfate Content (ppm)	Total Soluble Salts (ppm)
A1	3378614	636567.5	24.2	0	109
A2	3378629	636571.5	23.8	0	108
A3	3378644	636575.5	23.5	0	103
A4	3378658	636579.2	24.1	0	109
B1	3378609	636582.4	22.6	0	110
B2	3378624	636586.7	25.4	0	109
B3	3378639	636590.2	23.1	0	102
B4	3378654	636593.9	22.3	0	104
C1	3378604	636596.4	23.6	0	103
C2	3378620	636601.3	22.0	0	103
C3	3378634	636605	21.3	0	102
C4	3378648	636608.9	24.7	0	108

In Table 11, Table 12, Table 13, and Table 14 the northing and easting for each of the location indicate the GIS location. These locations are used in representing the site in GIS and to analyze the geology of the bed rock and soil association. The concentration of sulfates determined above is used in the initial speciation modeling to determine the activity of sulfate and other ions. The background and crucial steps involved in determining the activity of ions is discussed in detail below.

5.3 DEVELOPMENT OF PHASE DIAGRAMS

The solubility thermodynamics of ettringite divulge that ettringite in all probability forms first and in the presence of carbonate and at temperature below 15^{o}C converts to Thaumasite [*18*]. Dr Hunter developed diagrams of ettringite relative to portlandite and gypsum. Stability diagrams were developed based on equilibrium and thermodynamic values of minerals, like portlandite and gypsum.

The aforementioned studies provided the base for this study. The crucial objective of the research is to demonstrate that phase diagrams can be used to predict the stability of a mineral in the field based on chemical analysis.

A model is a tool used to predict reality using certain inputs. The model is not useful until it predicts reality to certain degree of accuracy. A geochemical model is a tool to predict equilibrium states of the minerals based on thermodynamics using chemical analysis data. Hunter [*18*] created plots of stability of ettringite relative to portlandite and gypsum. The stability of ettringite was calculated based on respective equilibrium reactions. The plots were developed to study the variation in stability fields of ettringite with variation in sulfate, calcium, or aluminum. This seems to be a simple and reliable approach when it is known for sure that ettringite forms in the system and

how its stability is affected with variation in calcium, sulfate, or aluminum. But the degree of complexity increases concerning new minerals that might precipitate in the system. Therefore geochemical models are used to determine the stability of minerals based on thermodynamics. The engineering experience and "rules of thumb" can help to predict potential ettringite formation, but quantitative estimates are needed for precise estimation. Precipitation-dissolution of ettringite in soils and sediments can be predicted using thermodynamics [*20, 36*].

The validation of geochemical model is necessary to support engineering decisions that are based on model results [*38, 39*]. The important factors that influence the validity of the phase diagrams are: quality of the thermodynamic database; the soil characterization data; validity of the activity coefficient models as a function of the system ionic strength. Since the kinetics of ettringite and associated calcium and sulfate mineral formation is relatively rapid, the assumption of local equilibrium is likely to be appropriate in most cases [*17, 40, 41*]. This may not be true for many associated minerals that contain aluminum and silica; therefore evaluation of the appropriate aluminum and silicate phases needs to be included in the model. A pressing need is to predict ettringite formation based on geochemical processes besides precipitation-dissolution for a range of soils.

The hypothesis of this research is that the stability or phase diagram can be used to identify the thermodynamically stable phases that will develop when calcium oxide, hydrated lime, or other calcium containing cementitious or pozzolanic stabilizers are added to sulfate-bearing clays. Furthermore, the stability model or phase diagram is useful in that it may help define a site-specific threshold level where soluble sulfates

become problematic because significant levels of expansive minerals develop at the threshold level. The hypothesis is that different soils have different threshold levels of soluble sulfates; and, therefore, phase diagrams can be used to define this threshold level and thus help define the specification level.

An additional hypothesis is that the stability of a phase diagram can be used to assess the impact of additives to the soil system being evaluated. For example, a long standing approach to mitigate sulfate reactions in lime stabilized soils is to add pozzolans such as fly ash, ground, granulated blast furnace slag [*42*], or other forms of soluble silica. The fundamental premise is that the soluble silica will force the reaction into some other stability field other than ettringite and prevent deleterious expansion. The stability model would thus become a valuable assessment tool or virtual experiment to assess the impact of a selected type and amount of additive.

Petry [*11*] correctly points out that a major problem preventing a clear identification of a threshold soluble sulfate level above which damage can be expected is the method of partitioning soluble sulfates from the soil. Since sulfate has a finite solubility, the amount of sulfates partitioned depends on the amount of water used to partition. Petry suggests a 10:1 water-to-soil solution to partition. Based on this approach, which is now routinely used in Texas Method Tex 620-J, Petry suggests that sulfate levels above about 2,000 ppm or 0.2 percent have the potential to induce damage due to swelling, and that sulfate levels above about 10,000 ppm or 1 percent induce severe damage. Hunter [*18*] also suggested a 10,000 ppm threshold as a standard for severe distress potential, but warns that much lower soluble sulfate levels can lead to severe damage, especially when one considers an open system where sulfate ions can migrate to

ettringite nucleation sites and "feed" the growth of this potentially expansive mineral.

Mitchell and Dermatas [*43*] identified soluble sulfate contents as low as 3,000 ppm that lead to the formation of ettringite, and this is supported by Perrin's [*44*] study of swelling soils in the Joe Pool Lake areas south of Fort Worth, Texas, in the Eagle Ford formation. Laboratory work by McCallister and Tidwell [*45*] identified levels of risk based on soluble sulfate content. They suggested that sulfate levels between 100 to 5,000 ppm pose a low to moderate threat; levels between 5,000 ppm and 12,000 ppm pose a moderate to serious threat, and levels above 12,000 ppm pose a very high risk of damage. Little, et al., [*46*] suggested similar levels based on field observations and laboratory testing. Rollings et al. [*47*] provides an extensive review of the literature regarding risk and measured levels of soluble sulfates, and their work was used as a key document in this review of procedures. Harris et al. [*12*] substantiated a threshold level of soluble sulfates related to significant distress based on extensive laboratory testing. They also identified that the fineness of the sulfates affects the reactivity of the sulfates and hence the potential for damage and must be considered.

In 2002, Orange County, California [*48*] evaluated the impact of soluble sulfates on swell potential in three soils from the area. Sulfate levels of 0, 5,000, 8,000, and 14,000 ppm (plus or minus 500 ppm) were collected and tested from each soil type with 4 percent CaO and 4 percent CaO plus 8 percent fly ash. None of the soils with soluble sulfate levels below 14,000 ppm exhibited significant swell during a 60-day period. The pH levels of these soils dropped below 10 during the period of testing, which may indicate that a strong pozzolanic reaction used up the reagents before or instead of forming ettringite.

During the construction of the Denver International Airport, CTL/Thompson, Inc., [*49*] the Quality Assurance Manager for geotechnical operations, tested approximately 40 samples of lime treated claystone soils. They initially used a threshold soluble sulfate level of 3,000 ppm, but based on the testing felt confident to raise the allowable sulfate content to 8,000 ppm. However a close look at the CTL/Thompson data revealed that below about 3,000 ppm swell was essentially non-existent and a small rise in swell began at about 3,000 ppm.

Clearly, the threshold level associated with damage is a variable "call" when based on experience. Some of this variation is due to the definition of distress (e.g., level of swell associated with damage, whether based on lab or field evidence, duration of evaluation, etc.). However, it is probable that a significant portion of the variability is due to soil chemistry, ion activity, and thus the impact of the level of sulfates at which ettringite formation is thermodynamically favorable in the soil-lime mixture. Based on experience, one sees a general trend that soils that are highly pozzolanically reactive, e.g., Orange County, California, soils require greater levels of soluble sulfates to trigger ettringite grow compared to less reactive clays.

The most challenging task in developing a model is to conceptualize the system. The system can either be a closed one or open system. The imperative part of the model is an equilibrium system which remains in sort of chemical equilibrium. "The equilibrium system contains an aqueous fluid and optionally one or more minerals. The temperature and composition of the equilibrium system are known at the beginning of the model, which allows the systems' equilibrium state to be calculated." [*50*]. The only types of equilibrium that can exist are complete equilibrium, metastable equilibrium, or partial

equilibrium.

To illustrate the utility of the stability models to differentiate sensitivity to ettringite formation in lime-treated soils based on sulfate content, consider two different soils. The first is a soil from Frisco, Texas. This soil comes from an area notorious for damage due to ettringite formation in lime-treated soils in the region. This soil comes from the Eagle Ford formation, which is described by Burkhart et al [*23*] to be highly susceptible to ettringite precipitation due to high pyritic content, and pedological effects that promote high sulfate levels. The second soil is from a location along the SH 130 corridor near the intersection of Parmer Lane and US 290 in Austin. Pertinent properties of both soils are described in Table 15. The SH 130 soil comes from the Taylor formation and contains variable levels of soluble sulfates. While damage due to ettringite formation is documented in this area, it is much less common than in the Eagle Ford formation.

Two very different approaches were used to develop stability models for the soil systems studied: a reaction path approach and a predominance approach. In the former, the reactive ions were extracted at a pH of 7 and then reactive minerals were selected based on the chemical analysis of the soil in question. The minerals selected (based on experience) as reactive were allowed to react to completion. This is a very conservative approach. The second approach, predominance, considers the aqueous chemistry of the system. The first step is to extract the ions in a pH 12 environment, since this environment exists when lime is added. We assumed that we were able to quantify all ion concentrations in the extract. In this approach a selected percentage of lime, CaO, was allowed to react in this aqueous environment to completion of the reaction. The major limitation of this method is the possibility that minerals may precipitate from solution

Table 15 Comparison of Frisco (Eagle Ford Formation) and Parmer-US 290 (Taylor Formation) soils

	Eagle Ford Formation	Taylor Formation
Geology	Tan to brown in color. montmorillonitic shale with high shrink-swell potential	Tan to brown in color. High shrink-swell potential
Mineralogy	38 - 88% clay About 50% clay are smectites High swell potential, compressibility, and creep deformation	40 - 60% clay Smectites, mica, kaolinite, calcite High swell potential
Atterberg Limits	LL = 39 - 140 PI = 16 - 113 CaCo3 = 2 - 39% Water Content = 4 - 25%	LL = 30 - 120 PI = 10 - 100 CaCo3 = ~50% Water Content = 18 - 28%
Unified Classification	Inorganic clay with high plasticity (CH)	Clayey Sand (SC), Fat Clay (CH), Lean Clay (CL)
Chemical Analysis	Magnesium = 53 mg/kg (*) Potassium = 158 mg/kg (*) Aluminum = 5 mg/kg (*) Calcium = 3640 mg/kg (*) Sulfate = 35000 mg/kg Silicon = 33 mg/kg (*) Iron = 5 mg/kg (*) Chloride = 18 mg/kg (*)	Magnesium = 30 mg/kg Potassium = 50 mg/kg Aluminum = 3 mg/kg Calcium = 100 mg/kg Sulfate = 30000 mg/kg Silicon = 55 mg/kg Iron = 10 mg/kg Chloride = 50 mg/kg

Note: Chemical Analysis: Left column results (*) obtained by C. Markley and L. J. Quo, Department of Geology and Geophysics, Texas A&M University, and used with permission.

before these measurements can be made or that the time is not sufficient to allow complete reaction. The major limitation of the reaction path model is that it is not likely that selected reactive minerals will completely react. Thus, the reaction path method is probably overly conservative.

At this point, the author believes that the predominance method best simulates actual conditions. The author has observed that stability models based on the predominance approach demonstrate that as soluble sulfate content is reduced, the ettringite stability field is diminished and that as the level of soluble silica increases, the ettringite stability field is diminished. These observations are very important because one expects a threshold level of sulfates to be required to trigger ettringite formation, and it is known form experience that adding sources of soluble silica can interrupt the formation of ettringite. The initial equilibrium of the system is found by chemical analysis of the soil. The concentration of ions in mg/kg of calcium, magnesium, potassium, iron, alumina, silica, and sulfate are determined using the chemical analysis.

Table 16, Table 17, Table 18 shows the initial chemistry of the soil along US 290 and Table 19 for US 79 at pH extract of 12. Initial model parameters used in the development of the thermodynamic models are presented in Table 20. This is used in the model as the initial system. This system is then allowed to react with 5% lime. The "React" [*50*] runs the simulation to calculate the activity coefficients of all the ions based on the thermodynamic data. The activity coefficients are calculated based on the Debye-Hückel equation. The Debye-Hückel equation is the result of the analysis conducted by Robinson and Stokes [*51*] in 1968 to calculate the activity coefficient of ions.

Table 16 Chemical analysis of US 290 soil (location B1)

		Extracted at pH 12 (mg/kg)						
Location	**Depth**	**Mg**	**K**	**Ca**	**Fe**	**Al**	**SO4**	**Si**
B 1	6in	1.540	41.130	2.680	78.800	80.900	427.20	72.135
		47.523	54.338	1.868	120.099	178.510	551.52	
	12in	1.540	38.340	416.500	0.160	0.180	3387.20	23.424
		17.420	54.700	492.500	0.220	0.980	3211.20	
	2ft	12.471	54.099	634.945	0.218	0.969	4520.97	21.041
		21.960	54.700	638.000	0.220	0.980	4699.20	
	3ft	21.664	54.458	151.327	0.219	0.976	4025.31	26.886
		27.906	54.458	113.794	0.219	0.976	3451.86	
	5ft	10.517	54.579	1.876	0.220	0.978	1112.73	50.532
		15.334	54.218	1.863	0.218	4.024	1549.43	
	6ft	27.670	54.700	1.880	29.460	73.300	571.20	61.390
		22.710	54.579	1.876	10.337	36.838	553.97	
	7.5ft	12.210	54.700	1.880	0.220	0.980	539.20	50.645
		21.870	54.700	1.880	12.280	38.660	491.20	
	10ft	13.500	54.700	1.880	0.220	2.750	475.20	52.794
		13.520	54.700	1.880	0.220	3.450	491.20	

Table 17 Chemical analysis of US 290 soil (location C3)

		Extracted at pH 12 (mg/kg)						
Location	**Depth**	**Mg**	**K**	**Ca**	**Fe**	**Al**	**SO4**	**Si**
C 3	1ft	15.890	42.550	2.680	112.900	149.500	427.20	47.063
		55.852	54.458	1.872	127.235	223.009	409.38	
	2ft	143.700	54.700	35.230	396.200	842.000	971.20	90.759
		127.732	54.458	20.350	325.653	703.872	887.26	
	3ft	8.950	54.579	1.876	0.220	3.353	346.43	63.398
		72.261	54.822	1.884	171.982	313.697	604.54	
	4ft	64.800	352.700	7600.000	0.220	0.980	7067.20	29.155
		61.500	332.700	8500.000	0.220	0.980	6811.20	
	5ft	14.787	54.579	1.876	0.220	0.978	2964.61	69.116
		13.500	54.338	1.868	0.219	0.974	2109.14	
	7ft	11.180	54.700	1.880	0.220	0.980	1147.20	92.908
		12.750	54.700	1.880	0.220	0.980	955.20	
	9ft	30.750	54.700	1.880	44.850	92.400	699.20	60.673
		22.730	54.700	1.880	18.790	48.320	683.20	

Table 18 Chemical analysis of US 290 soil (location C5)

		Extracted at pH 12 (mg/kg)						
Location	**Depth**	**Mg**	**K**	**Ca**	**Fe**	**Al**	**SO4**	**Si**
C 5	1ft	20.220	54.700	1.880	25.880	55.900	171.20	41.332
		21.677	54.218	1.863	22.371	49.857	153.83	
	2ft	97.022	54.099	4.322	251.110	515.275	612.40	42.295
		82.500	54.700	1.880	200.100	392.400	555.20	
	3ft	183.485	54.458	48.196	513.717	1203.650	1173.98	50.421
		218.385	54.822	77.673	591.314	1406.125	2063.79	
	4ft	32.550	147.300	1140.000	0.220	1.810	3355.20	43.481
		30.430	79.200	596.000	0.220	5.940	2971.20	
	5ft	1.540	34.600	2.680	4.500	13.700	1035.20	59.957
		19.363	54.822	1.884	0.220	18.371	1117.68	
	8ft	34.630	54.700	1.880	66.100	135.300	907.20	63.539
		38.897	54.458	1.872	56.449	120.365	855.40	
	10ft	37.132	53.862	1.851	71.980	141.794	530.94	55.512
		40.099	54.822	1.884	64.343	129.388	444.19	

Table 19 Chemical analysis of US 79 soil

	Extracted at pH 12 (mg/kg)						
Location	**Mg**	**K**	**Ca**	**Fe**	**Al**	**SO4**	**Si**
A1	33.300	65.900	2.680	151.000	200.900	459.20	147.350
	70.615	54.099	36.020	184.945	322.516	485.80	
A2	2.060	5.618	0.265	13.025	17.149	485.80	155.649
	49.049	54.822	1.884	111.949	189.120	380.04	
A3	0.732	4.059	0.266	9.377	12.083	328.28	124.041
	42.555	54.579	1.876	96.286	168.525	282.57	
A4	1.543	36.190	2.686	80.078	102.728	267.80	129.012
	39.179	54.338	1.868	87.119	152.881	249.54	
B1	0.947	4.672	0.269	9.301	11.676	428.15	149.114
	44.373	54.458	1.872	97.069	164.867	425.31	
B2	0.426	3.957	0.263	8.607	11.034	419.74	110.289
	39.340	54.700	1.880	85.900	151.000	347.20	
B3	1.537	33.735	2.674	65.255	83.614	234.68	125.581
	35.790	54.700	1.880	75.300	131.500	251.20	
B4	1.540	29.010	2.680	49.880	66.000	219.20	110.100
	28.906	54.579	1.876	54.878	101.075	218.71	
C1	0.379	4.167	0.264	7.993	10.115	405.79	149.652
	41.228	54.579	1.876	91.896	157.849	442.22	
C2	0.153	3.080	0.267	5.157	7.009	297.88	83.939
	26.483	54.338	1.868	48.944	96.358	329.01	
C3	1.513	29.574	2.633	56.004	73.395	199.65	78.617
	28.210	54.700	1.880	52.600	97.600	187.20	
C4	1.520	31.194	2.645	61.382	77.961	216.32	128.445
	32.075	54.218	1.863	59.570	107.445	201.4097	

Table 20 Initial "Act" model parameters

	Water Activity	pH	Temperature (^oC)	Pressure (bar)	Log Activity			
					$Al(OH)_4^-$	SiO_2	Ca^{2+}	SO_4^{2-}
Frisco Soil SO_4 = 3,000 ppm	1	12	25	1.013	-3.864	-5.887	-1.663	-1.6603
Parmer US 290 Intersection Taylor Formation SO_4 = 3,000 ppm	1	12	25	1.013	-3.267	-6.514	-3.154	-1.8784
Frisco Soil SO_4 = 10,000 ppm	1	12	25	1.013	-3.871	-5.706	-1.847	-1.2139
Parmer US 290 Intersection Taylor Formation SO_4 = 10,000 ppm	1	12	25	1.013	-4.578	-7.305	-2.64	-1.4283
Natural Silica activity of Soil	1	12	25	1.013	-4.553	-7.46	-2.467	-1.6363
Influence of Silica Indicating Decrease in Ettringite Precipitation Potential	1	12	25	1.013	-4.553	-5.46	-2.467	-1.6363

$$\log \gamma_i = \frac{Az_i^2 \sqrt{I}}{1 + \overset{o}{a}_i B\sqrt{I}}$$

The basic assumption of Debye-Hückel in calculating the activity coefficients is that ions behave as spheres and charges are at the center of the ions, interacting with each other by coulombic forces. The Debye-Hückel equation indicates that the activity coefficient is directly proportional to the square of electrical charge (z_i) and inversely proportional to ion size perimeter ($å_i$). The constants A and B are functions of temperature, and I represent the ionic strength of solution. Ettringite constitutes of calcium, alumina, sulfate, and water. So the total activity of all these ions will dictate the stability field of ettringite. The total activity of calcium, alumina, and sulfate is obtained from the output results of the react program. In order to calculate the total activity of an ion, the activity coefficients are multiplied by molar concentrations. Then the activities of all the calcium bearing species are added to get the total activity of calcium. The total activities of aluminum, sulfate, and silica are calculated in the same fashion. Log activities are calculated to plot the phase diagrams. Finally, the stability diagrams are plotted using "Act2" program [*50*]. The input values for this program is got from output results of "React" program [*50*]. The flexibility of plotting the diagram species of any ions is provided in the program. Some of the phase diagrams are shown below for the soils along US 290.

Figure 22, Figure 23, Figure 24, and Figure 25 represents the phase diagrams for the soil along US 290. The concentration of elements used in the initial system was that of pH 12 extract values. The phase diagrams indicate the aluminum species that are stable

in the system. It is imperative from the phase diagrams that ettringite is not a favored species.

Figure 25 implies that ettringite is stable in the system. But the quantity of ettringite saturated in the system is insignificant. The soil samples obtained from the site are added with 5% lime and cured for different periods to validate the stability model. The procedure is explained in detail in chapter IV.

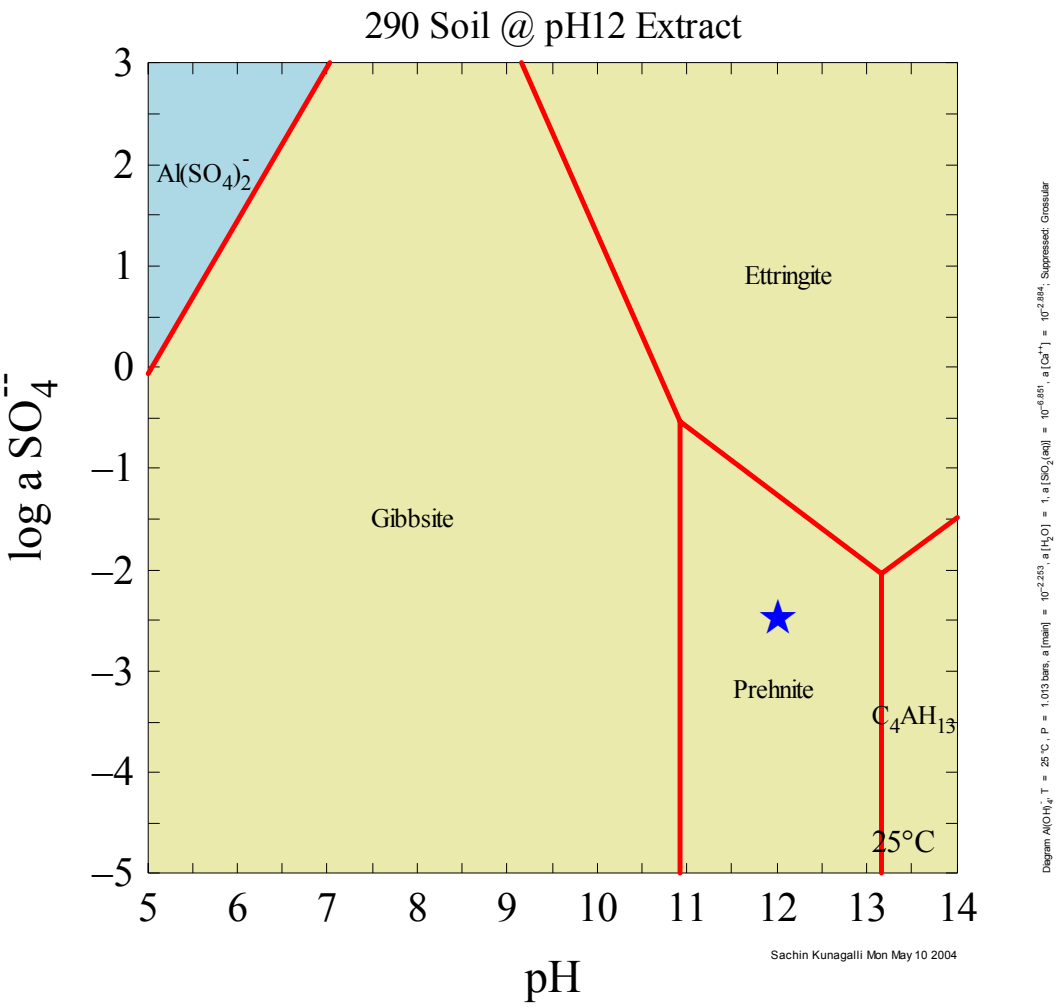

Figure 22 Phase diagram of soil along US 290 (B1 6in @ pH 12 extract)

Note: Star represents the locus of pH and log activity of Sulfate for the condition being considered.

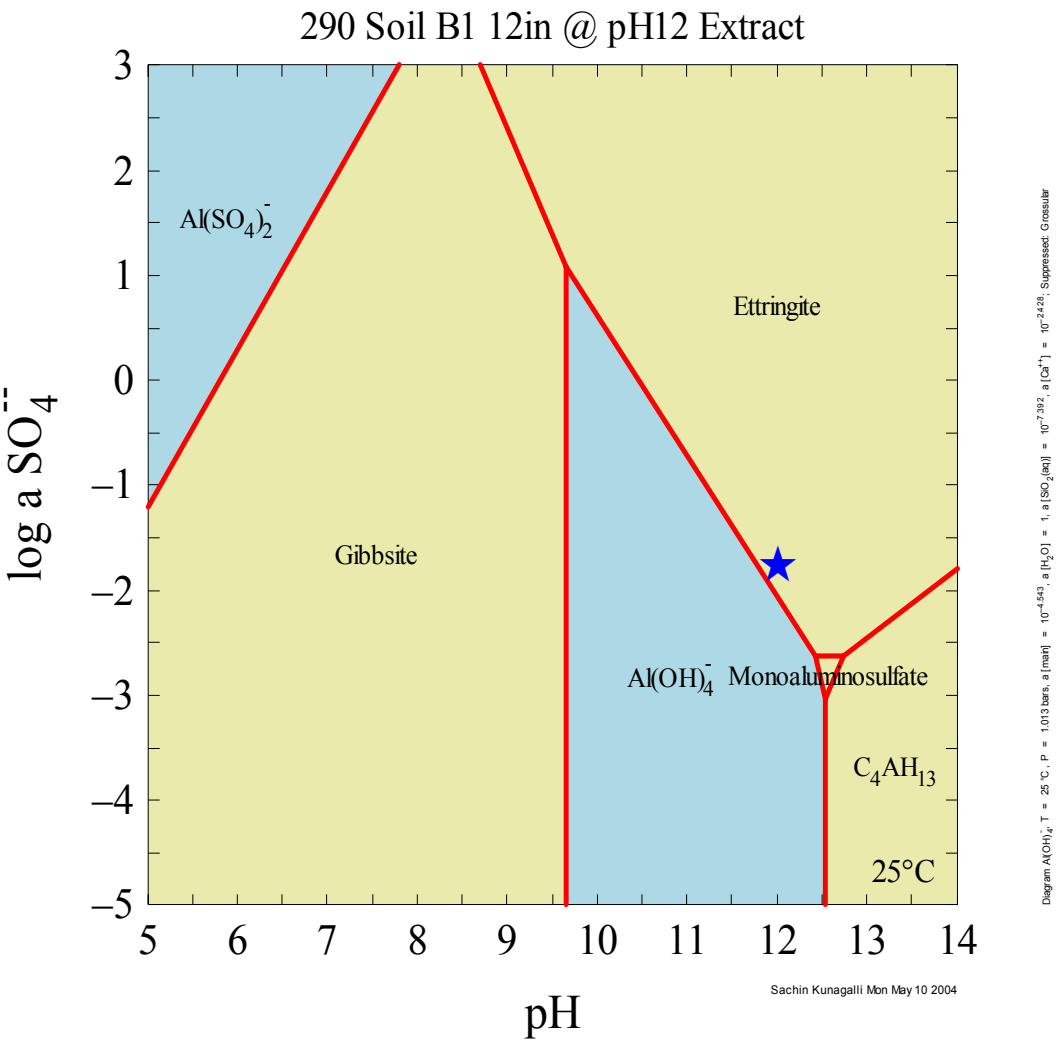

Figure 23 Phase diagram of soil along US 290 (B1 12in @ pH 12 extract)

Note: Star represents the locus of pH and log activity of Sulfate for the condition being considered.

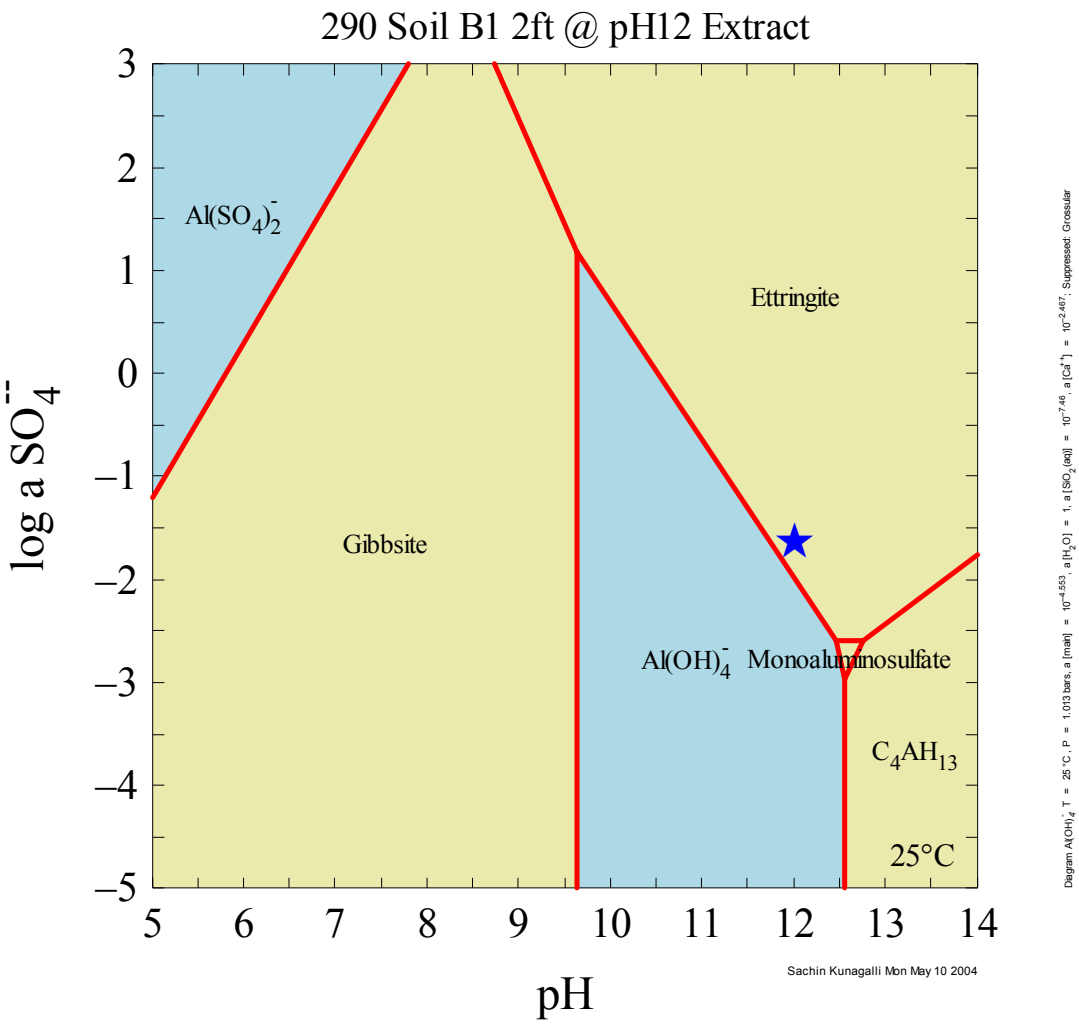

Figure 24 Phase diagram of soil along US 290 (B1 2ft @ pH 12 extract)

Note: Star represents the locus of pH and log activity of Sulfate for the condition being considered.

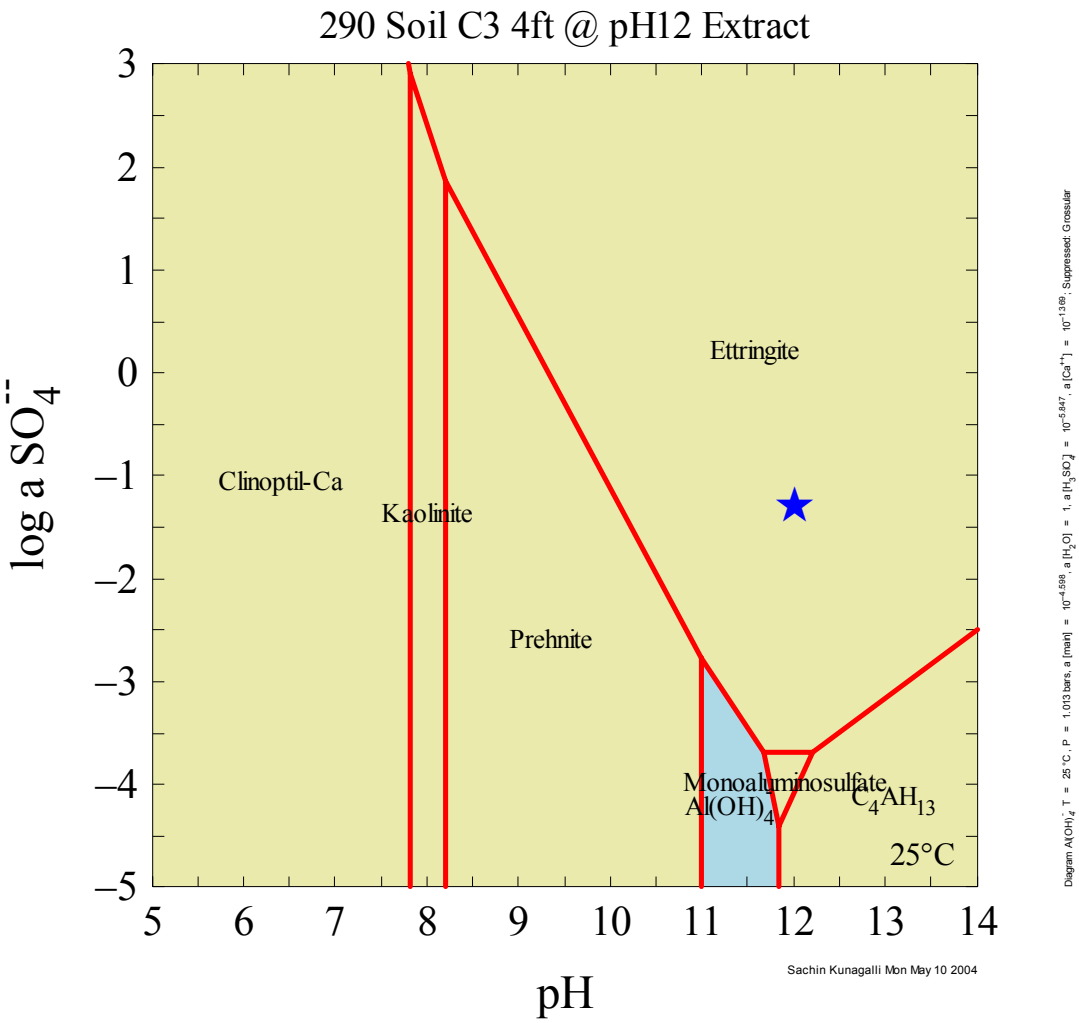

Figure 25 Phase diagram of soil along US 290 (C3 4ft @ pH 12 extract)

Note: Star represents the locus of pH and log activity of Sulfate for the condition being considered.

CHAPTER VI

ETTRINGITE SYNTHESIS

6.1 BACKGROUND

The magnetometer readings (both EM31 and EM38) were taken at the surface and at various depths at selected locations. Three replicate samples were collected at these locations. One replicate was used for sulfate extraction, the second was used for mineralogical analysis, and the third was used to quantify the amount of ettringite present. The process of sulfate extraction and mineralogical analysis was carried out as discussed earlier.

6.2 TESTING PROCEDURE

The bulk soil samples obtained from the site are crushed to pass through No. 4 sieve. Crushed soil was mixed with 5% hydrated lime at 3 to 4% over optimum moisture content. The soil lime mix was then cured for 24 hours at uniform moisture. Samples were prepared using the Harvard Miniature Mold. Samples were cured at three temperatures, 4^0 C, 25^0 C and 30^0 C. The curing temperature of 4^0 C was adopted for accelerated curing. The 4^0 C samples were cured for 7 days.

The 25^0 C and 30^0 C samples were cured for 28 days (Figure 26 and Figure 27). Care was taken to see that enough water was available for ettringite formation. The soil specimens were kept between two porous plates and the plates were always saturated with distilled water. After curing, the samples were taken out of the environmental chamber and dried in an oven for 3 to 4 hours at 65^0 C. Weights were taken at one hour intervals. The drying process was stopped when constant weight was reached. Dried samples were then initially crushed to pass through No. 4 sieve and finally crushed using

Figure 26 Soil molds cured for 28 days at 25^0 C

Figure 27 Soil molds cured for 28 days at 30^0 C

a ring and puck mill apparatus to pass the No. 200 sieve. Measures were taken to ensure that no sample was lost and that all the soil passed the No. 200 sieve.

6.3 DIFFERENTIAL SCANNING CALORIMETRY (DSC)

After processing the soil samples by crushing to pass through the No 200 sieve, the soil was tested for the presence of ettringite. Differential Scanning Calorimetry (DSC) has the capability of not only identifying a mineral but also quantifying it. The sample preparation procedure and analysis is explained in detail as below.

Sample Preparation:

1. Samples were quartered to obtain a 100 g representative sub-sample.
2. Sub-samples were dried at 45 °C until a constant weight was reached.
3. Dried samples were ground using a Tungsten-Carbide ring and puck mill and sieved on a No. 200 U. S. Standard sieve before testing.

DSC Analysis:

All experiments were performed on a Mettler TA8000 system. This system combines a DSC 822e measuring cell and analytical unit. The DSC 822e cell measures the difference between the heat that flows to a sample and to the reference crucible. The unit has a high signal resolution and detects even small changes in the heat flow. The cell obtains measurements according to set conditions, and continuously sends data to the control unit. Software helps evaluate experimental curves within selected integration limits.

A 100 μL aluminum crucible, containing the sample, and a reference crucible were placed on a censor plate of the DSC measuring cell. The cell was heated at a constant rate of 10°C/min from 50°C to 350°C. The experiment was performed in

flowing nitrogen. The sample demonstrated an endothermic profile. To assess the heat of this endothermic reaction the area under the peaks was integrated and ex-pressed in Joules per gram; this heat corresponds to the specific content of the compound in question (ettringite in this case). All obtained DSC thermograms are enclosed in appendix B.

CHAPTER VII

SUMMARY

Based on the results of this research, it can be concluded that GIS can be used to screen a construction corridor for problematic level of soluble sulfates and successive use of an electrical conductivity device (magnetometer) can be effectively adopted to identify areas where threshold levels of sulfates capable of forming ettringite exist. This research demonstrates that:

1. GIS can be used to fairly eliminate the areas where ettringite forming potential is insignificant.
2. If GIS predicts ettringite potential areas, then magnetometers can be used to further eliminate the areas where sulfates concentrations are below threshold level to form ettringite.
3. If magnetometer also predicts sulfate concentration above the threshold level based on the conductivity readings, the soil is tested for natural chemistry. Based on the chemistry of the soil, stability models are developed to identify the favored mineral precipitating.

The use of GIS to identify areas with potential to form ettringite is a "novel and innovative" method. Researchers have historically studied the geology of the bedrock to identify the areas prone for ettringite formation. Researchers have recognized that the geology of the bedrock, soils, and topography can be effectively used in analyzing areas susceptible to ettringite formation. Burkart and others [*23*] clearly pointed out the role of gypsum in sulfate induced heave. They concluded that:

"Gypsum is a common sulfate mineral in sedimentary rocks and soils developed on Eagle Ford Group shales. The pyrite bearing Eagle Ford shale contains gypsum ($CaSO_4 \cdot 2H_2O$) produced by reaction of calcium carbonate in the shale with acid sulfate from oxidation weathering of pyrite (FeS_2). Acid sulfate from pyrite oxidation can furnish sulfate directly to non buffered soils" [*23*].

The soils formed from the Eagle Ford formation bedrocks have high concentrations of sulfate in the form of gypsum. Gypsum is reported in the AC and C horizons of some of the soils formed on the Eagle Ford group and oxidation of pyrite occurs at the base of the transitional C-zone of soil profile [*23*]. "High alkalinity of Eagle Ford shale soils is the result of high levels of calcium carbonate, and typically these soils effervesce with dilute hydrochloric acid" [*23*]. When pyrites oxidize to dissolve in water, both Fe and S ions oxidize. Fe^{3+} reacts with water to form $Fe(OH)_3$ later on converting to hematite and goethite [*25*]. But calcium carbonate in the soils of the Eagle ford shale buffers the formation of jarosite, and leads to the formation of gypsum [*23*]. Also solutions containing gypsum rise from the water table by capillary action and during infiltration events that are incomplete, it moves to lower levels and is deposited [*52*]. This is quite a remarkable discovery in the sense that low lying areas have greater potential for sulfates.

The GIS maps predict heaving due to ettringite based on the information about the bedrock, the soils formed from the bed rock, and the topography which is a key factor in determining the concentration of sulfates. Eagle Ford soils do not produce sulfate induced heave everywhere that road base has been lime stabilized, but the problem is observed frequently where roads follow streams or run across low-lying areas or hillside slopes

[*23*]. Burkart and others clearly point out that clay rich soils can be important reservoirs of gypsum and that gypsum has complex dynamics in soils [*23*]. Figure 28 represents the origin and migration of gypsum in Eagle Ford soils [*23*].

The location along US 290 as determined by GIS predicts that the geology of the bedrock is The Taylor Group which contains pyrite and the soils formed on these bedrocks also contain sulfates varying from 0% to 5%. Analyzing the aerial photographs and the digital elevation models of the area reveals that it is a low lying area. The analysis leads to the conclusion that the area has the potential to form ettringite after lime stabilization. Therefore further testing of the area using magnetometer and chemical analysis of the soil is necessary as determined by GIS.

The geology of the area along the proposed corridor close to US 79 is also The Taylor group. However, the topography of the area is very flat indicating that gypsum will not be transported from higher elevations and sulfate concentration will not be very high. This area should be less prone for ettringite formation after lime stabilization. Therefore, only limited testing (using the magnetometer) is necessary to validate the hypothesis.

Based on GIS analysis results, the magnetometer should be used selectively to determine conductivity. The results of the EM 38 conductivity meter indicate that a conductivity reading of approximately 300 ms/m corresponds to sulfate level of more than 3300 ppm. The threshold level of sulfates to form ettringite is in the range of 3300 ppm. Therefore, the value of the conductivity reading was reduced to 230 ms/m to indicate the threshold level of sulfates. In the field, any conductivity value nearing 200 ms/m should be considered problematic to make the measurements more conservative.

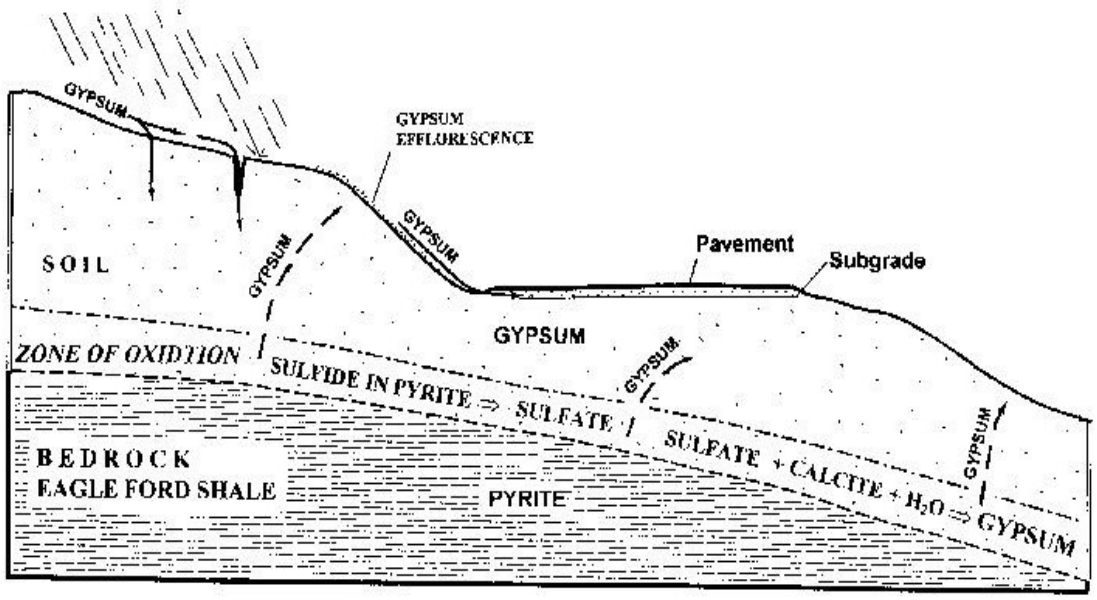

Figure 28 Origin and migration of gypsum in Eagle Ford shale [*23*]

The ranges for the EM 38 conductivity meter to measure conductivity in the horizontal and vertical dipole positions are 0.75m and 1.5m respectively. The EM 38 conductivity meter should never be used in a trench less than a meter wide to avoid interference between dipoles. Nevertheless, magnetometer, even when used in a 0.5 m wide trench, did not produced a false peak, that is the magnetometer never showed a reading of less than 300 ms/m where the concentration of sulfates were greater than the threshold level of sulfates to form ettringite.

Figure 18, Figure 19, Figure 20, and Figure 21 indicate a trend for the variation of sulfates with depth. The sulfate concentration increases with depth and after a certain maximum value, decreases again. This is attributed to the deposition of sulfates near the surface with rise in the water table and a subsequent drying effect. The water would have transported soluble sulfates and upon drying would have deposited sulfates near the surface. Analyzing the concentration of sulfates in low lying areas compared to higher

elevation areas, it is apparent that the concentration increases with a decrease in elevation as discussed by Jaffarzadeh and Burnham [*52*]. This validates the GIS maps ability to predict sulfate heaving potential areas based on bedrock, soils, and topography. The conductivity readings close to US 79 along the proposed corridor is close to 100 ms/m which is far less than 230 ms/m. Chemical analysis revealed that no sulfates were found in soil where the conductivity was less than 230 ms/m.

The chemical analysis conducted on soils reveal that sulfate along US 79 is zero. But the soil obtained along US 290 is rich in sulfates ranging up to 30,000 ppm. The result of sulfate analysis of the soils agrees with the GIS maps clearly indicating the utility of multi-layered spatial maps in predicting sulfate rich areas.

Figure 29, Figure 30, Figure 31, and Figure 32 compare two different soils: soil form the SH-130 corridor that lies in the Taylor geological formation, and soil from near Frisco, Texas, that lies in the Eagle Ford formation. These two soils have different mineralogies as reflected in Table 15. Based on the previous description of thermodynamic modeling, one would expect these two soils to react differently when treated with CaO.

The initial condition for each soil was based on chemical speciation calculations, which are in turn based on measured ion concentrations. Total activities of calcium, aluminum, sulfate, and silica were calculated by the computer program REACT [*50*]. These parameters are shown in Table 20. The soluble sulfate level was held constant for each soil at 3,000 ppm, Figure 29 and Figure 30, and at 10,000 ppm, Figure 31 and Figure 32, during the development of the thermodynamic phase diagrams.

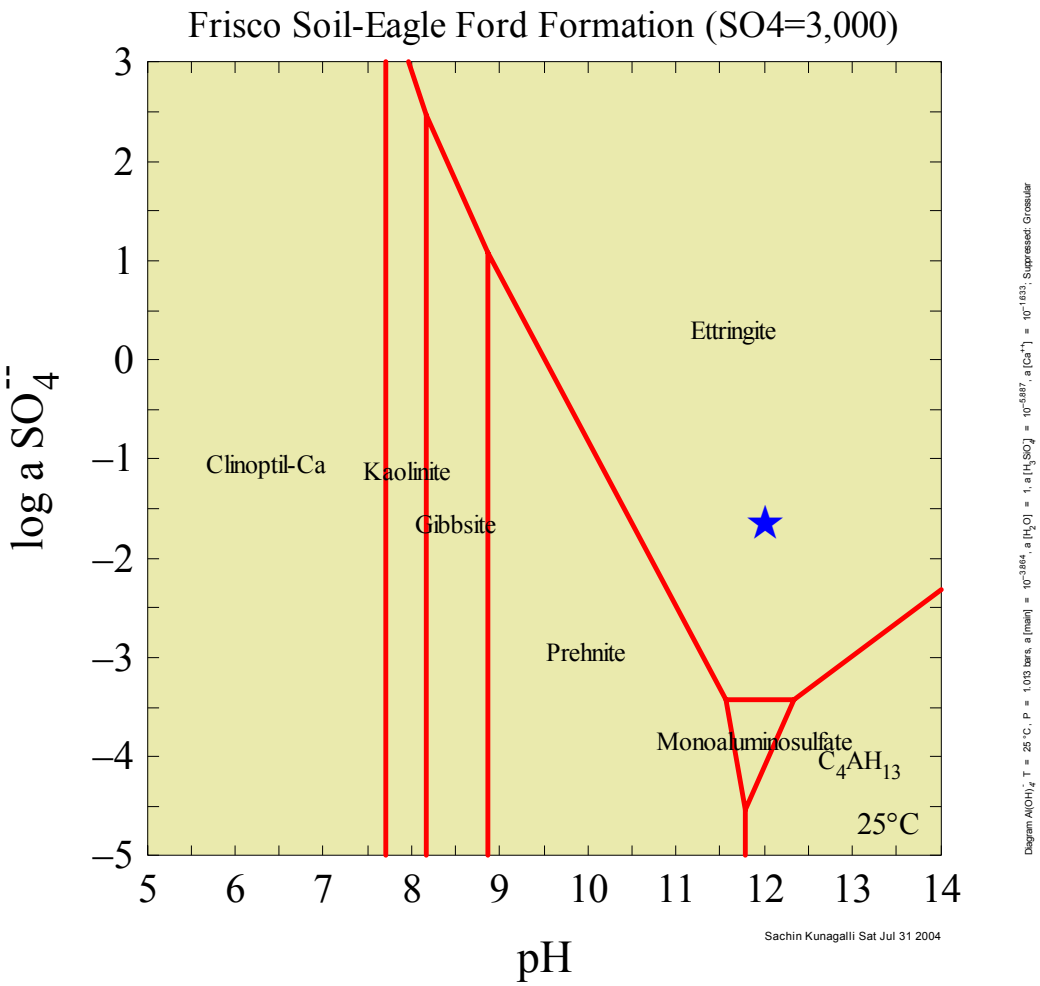

Figure 29 Phase diagram for Frisco soil (Eagle Ford Formation) with soluble sulfate concentration of 3,000 ppm

Note: Star represents the locus of pH and log activity of Sulfate for the condition being considered.

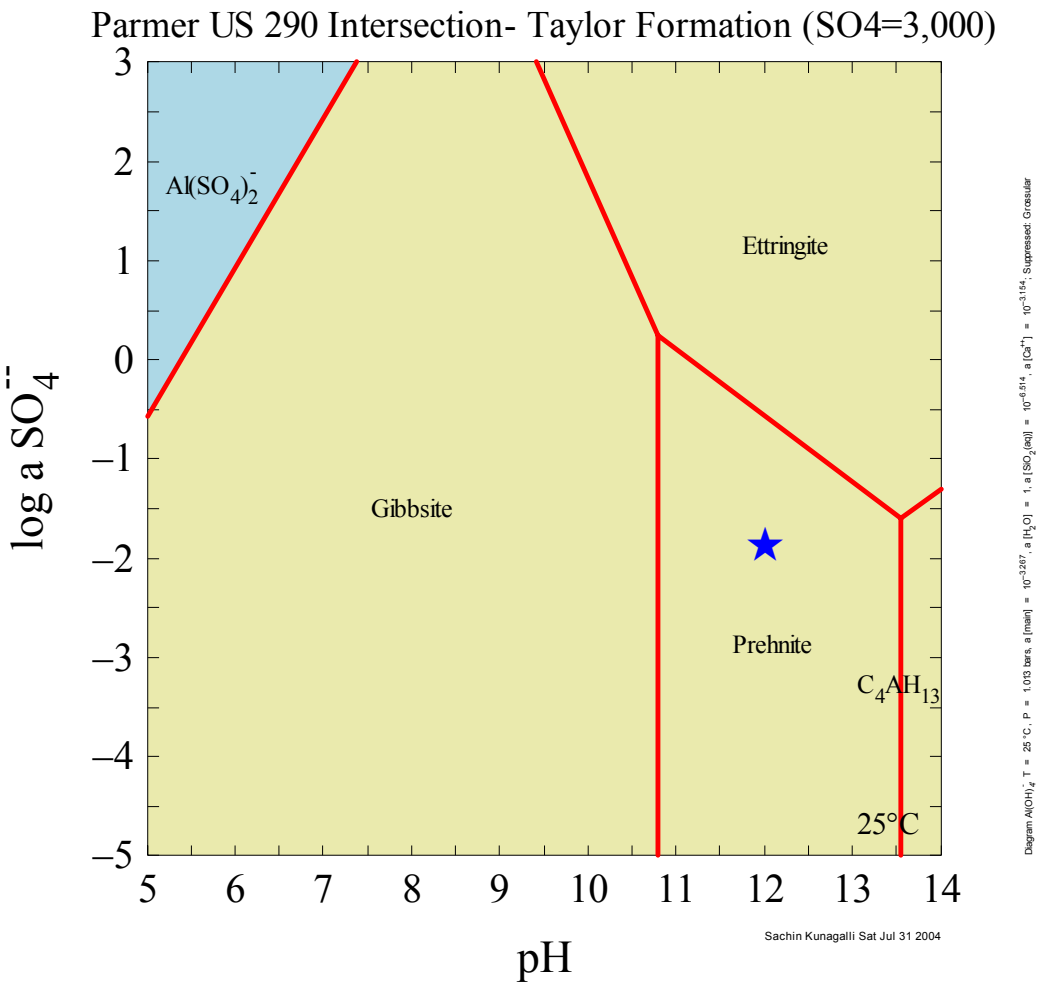

Figure 30 Phase diagram for Parmer US 290 intersection (Taylor Formation) with soluble sulfate concentration of 3,000 ppm

Note: Star represents the locus of pH and log activity of Sulfate for the condition being considered.

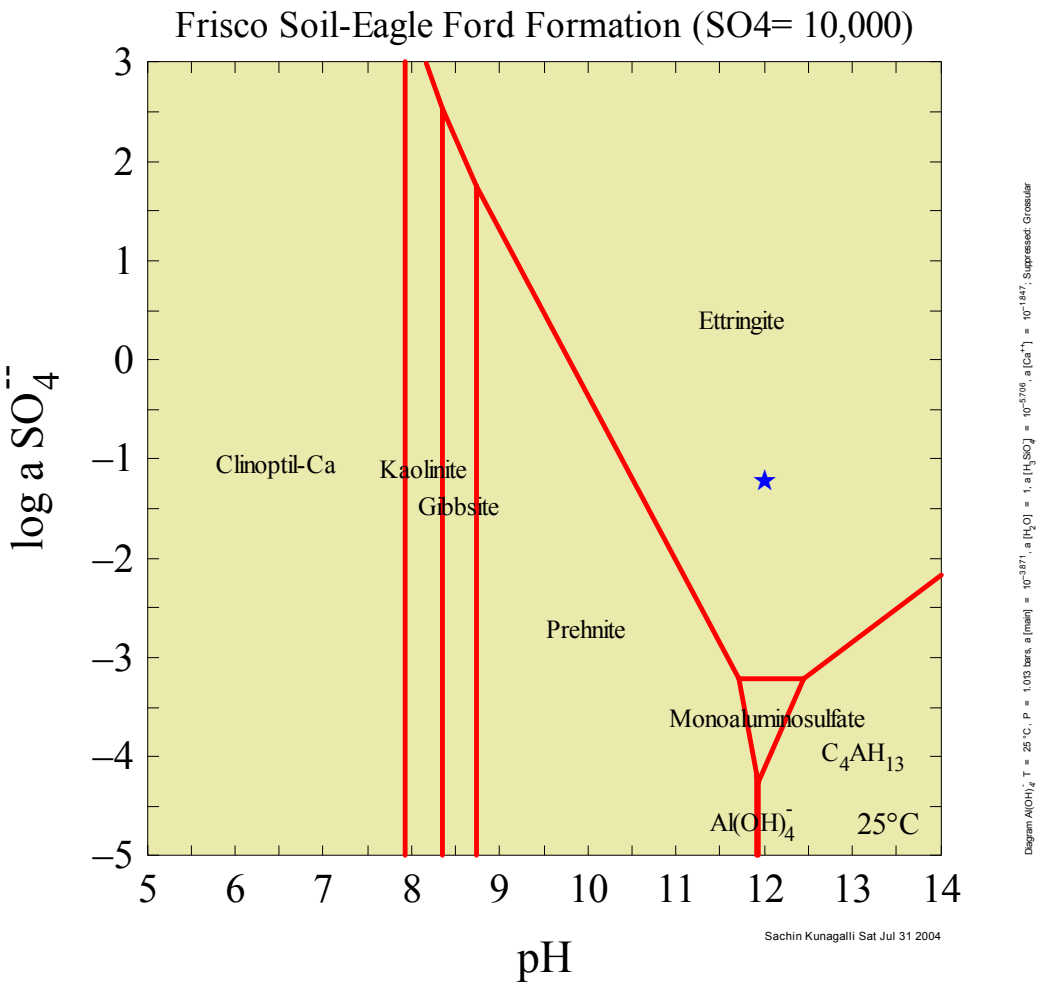

Figure 31 Phase diagram for Frisco soil (Eagle Ford Formation) with soluble sulfate concentration of 10,000 ppm

Note: Star represents the locus of pH and log activity of Sulfate for the condition being considered.

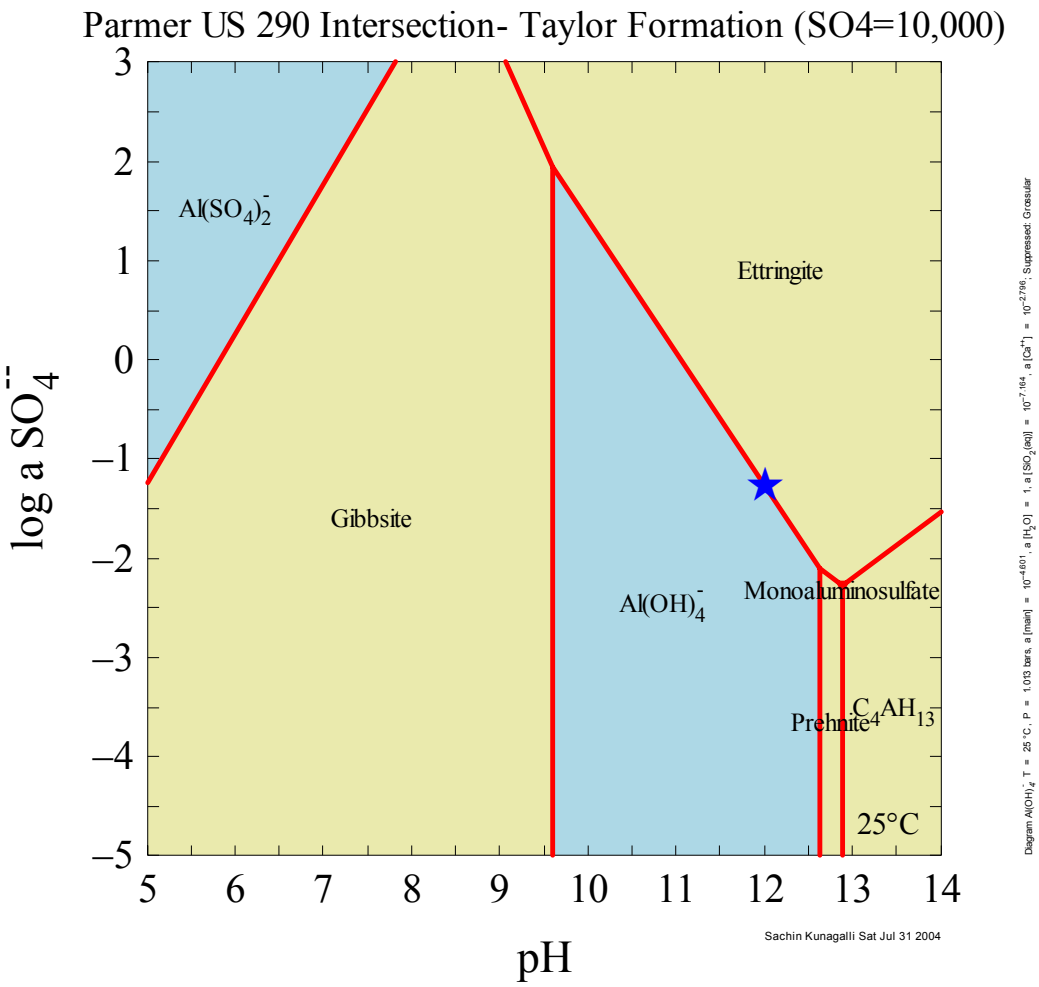

Figure 32 Phase diagram for Parmer US 290 intersection (Taylor Formation) with soluble sulfate concentration of 10,000 ppm

Note: Star represents the locus of pH and log activity of Sulfate for the condition being considered.

The important trend shown in these figures is that at a soluble sulfate concentration of 3,000 ppm the locus of pH and log activity of sulfate is positioned well below the ettringite stability field for the (US 290) Taylor Formation soil, but the locus is well within the ettringite stability field for the (Frisco) Eagle Ford formation soil. This demonstrates the utility of the phase diagram in the engineering application of soil treatment with CaO (lime). Geotechnical and pavement engineers responsible for soil treatment and stabilization have relied on experience to establish "rules of thumb" regarding threshold levels of sulfates leading to significant damage. The stability of phase diagram offers the beginning of a scientifically sound and unbiased approach to establishing a reasonable sulfate threshold level for a given soil.

Figure 33 and Figure 34 show the results of mass-balance calculations. In the development of these figures, the same ion concentrations measured and used in the thermodynamic model development were again used in a simulated mass-balance reaction with kaolinite, smectite, muscovite, goethite, and CaO. Kaolinite, smectite, muscovite, and goethite were quantified using x-ray diffraction (XRD).

The practical implication of Figure 33 and Figure 34 are in line with those of Figure 29 through Figure 32, which is that ettringite begins to form at a much lower level of soluble sulfates in the Eagle Ford Formation soil (approximately 3,000 ppm) than in the Taylor Formation soil (approximately 10,000 ppm). This once again substantiates the very important impact of mineralogy on the potential for ettringite to form and the threshold levels of sulfate that trigger its growth.

Silica-rich additives such as granulated blast furnace slag (GBFS) and fly ash have been successfully used [*42*] to stop the development of ettringite or to at least alter

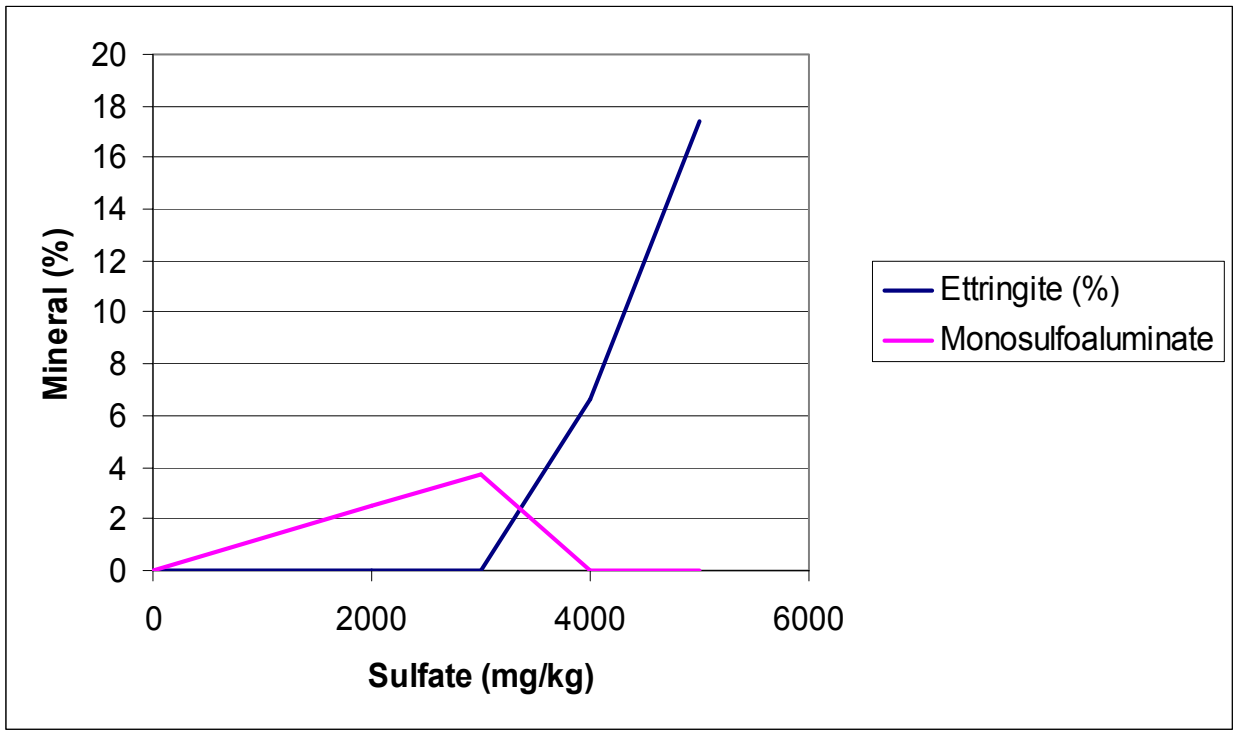

Figure 33 Minerals precipitation threshold in Frisco soil (Eagle Ford Formation)

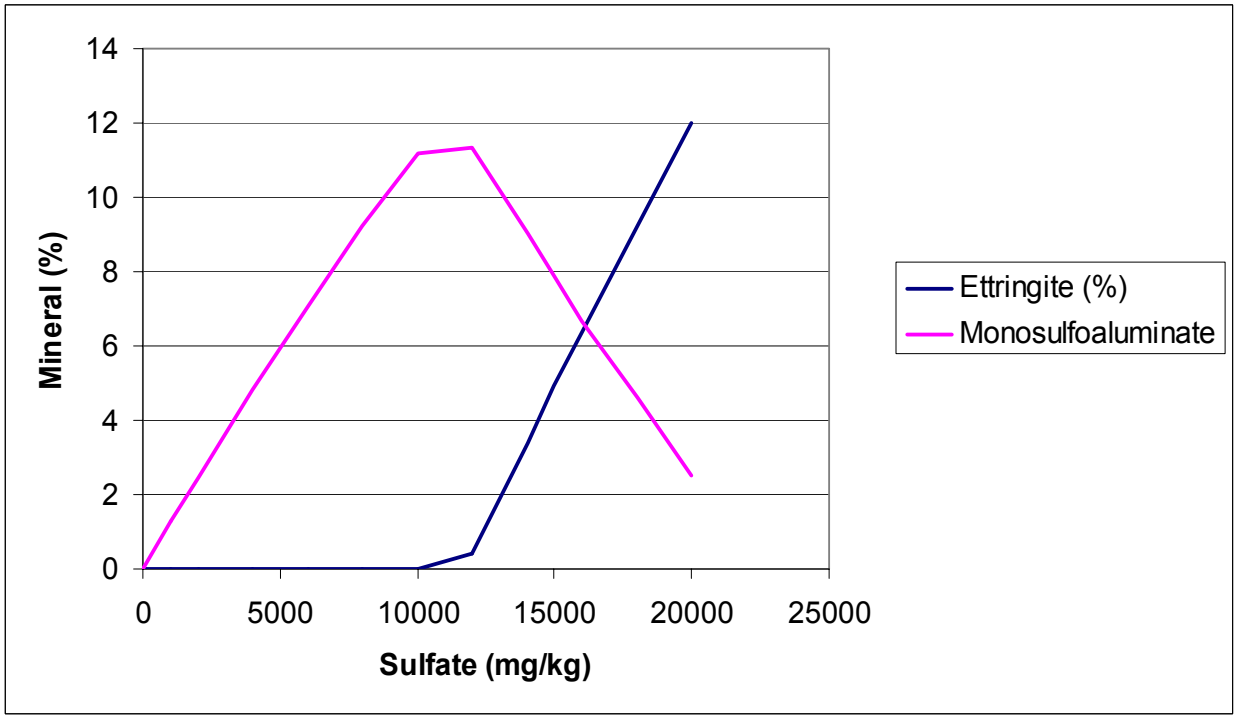

Figure 34 Minerals precipitation threshold in Parmer-US 290 intersection (Taylor Formation)

the form of the ettringite crystal in order to arrest expansion. Figure 35 and Figure 36 compare two soils from the SH 130 corridor (Taylor formation). Each soil contains 20,000 ppm soluble sulfates. In Figure 35, 5 percent calcium oxide was added to increase the pH to approximately 12.4. This pushes the locus of pH and log activity of sulfate ions into the ettringite equilibrium polygon. Figure 36 represents the identical soil system with the same level of soluble sulfates and the same lime addition. However, in Figure 36 the activity of soluble silica is changed from –7.46 (Figure 35) to –5.46 in Figure 36. The result is that the locus of pH and log activity of sulfate ions resides in the Prehnite mineral equilibrium polygon due to the higher soluble silica content. This demonstrates how the stability model can be used to assess the effect of using additives to change energetics and prevent the formation of ettringite.

The stability models were validated in two ways: by comparing solution extracts with predictions from the stability models and by preparing specimens representative of the models and monitoring ettringite growth in these samples. In the latter approach, actual soil samples of the exact type modeled were allowed to react with lime for 60-days in a controlled and moist environment. The lime-soil mixtures were monitored for swell and tested using differential scanning calorimetry (DSC) to assess whether or not ettringite developed. The phase diagrams predicted that ettringite would not form even at low to moderate soluble sulfate contents, below about 10,000 ppm, and this was validated by DSC analysis. High soluble sulfate contents, above about 10,000 ppm plotted on the stability boundary line, and DSC analysis failed to confirm ettringite development. On the other hand, phase diagrams predicted ettringite formation in the Frisco soils, and this was validated by the DSC scans.

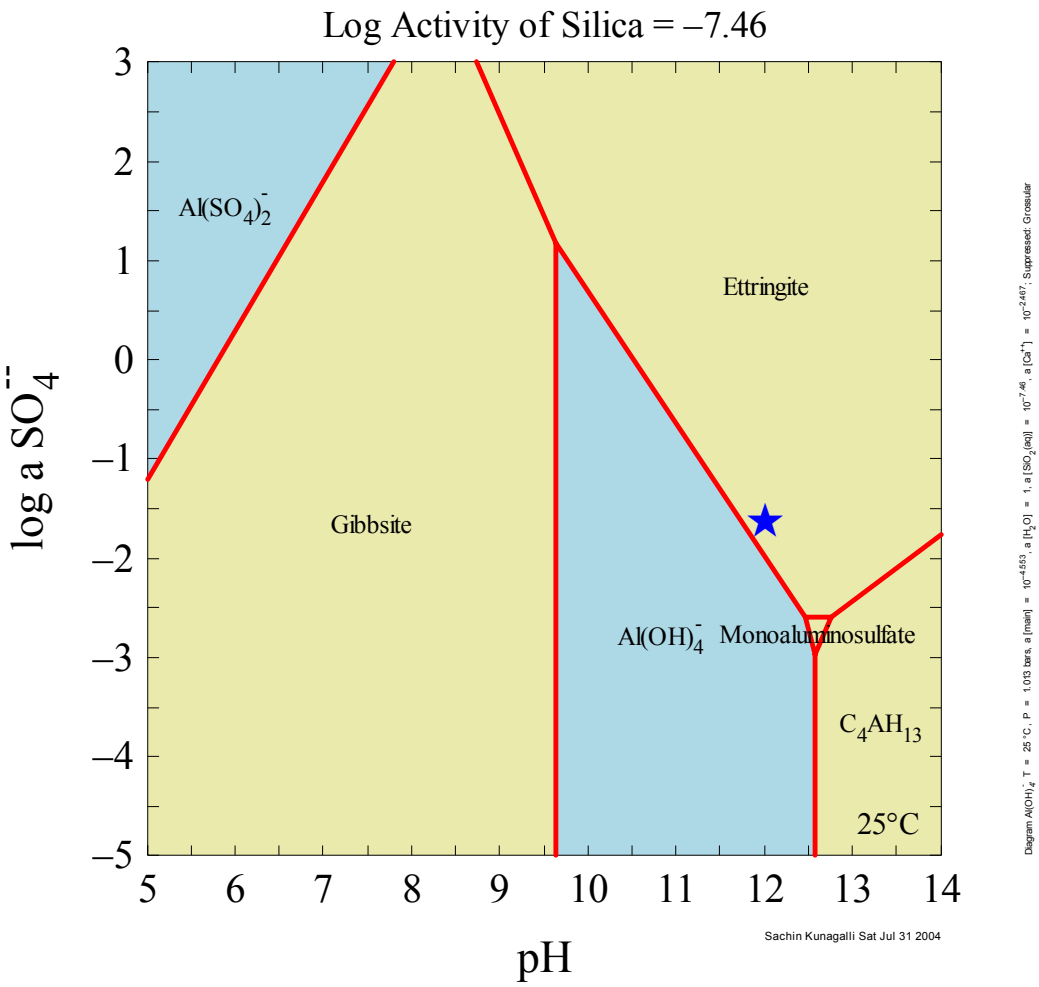

Figure 35 Impact of silica activity on US 290 (Taylor Formation Soil) – Lower silica activity

Note: Star represents the locus of pH and log activity of Sulfate for the condition being considered.

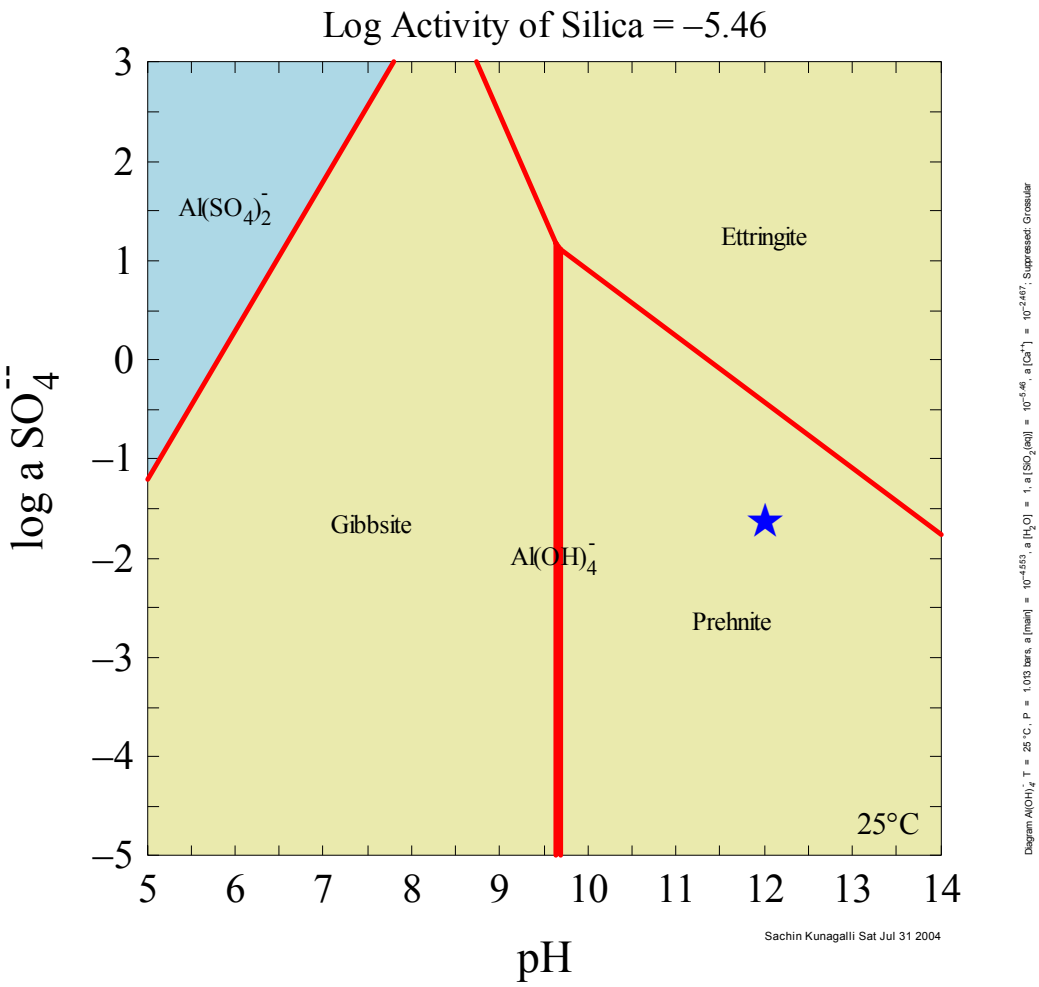

Figure 36 Impact of silica activity on US 290 (Taylor Formation soil) – High silica activity

Note: Star represents the locus of pH and log activity of Sulfate for the condition being considered.

Experience alone is not sufficient to determine a threshold level of soluble sulfates that leads to destructive expansion due to the formation of ettringite. Many factors influence the manifestation of distress as discussed. However, one of the most important is the thermodynamic favorability of ettringite precipitation in a specific soil. The thermodynamic stability model or phase diagram provides a first step toward establishing threshold levels of soluble sulfates for specific soils. The model is highly sensitive to chemical composition and ion activities and provides the additional capability of being able to assess the impact of additives used to shift the reaction from ettringite to some other innocuous mineral. An example of this is the popular solution to add a source of soluble silica, such as fly ash or ground, granulated blast furnace slag.

REFERENCES

1. Soil Stabilization Products Inc. Lime Treatment Tradeoffs. 2001. http://www.sspco.com/8392.pdf. Accessed April 29, 2004
2. Little, D. *Stabilization of Pavement Subgrades and Base Courses with Lime*. Kendall/Hunt Publishing Company, Dubuque, IA, 1995
3. Fahoum, K. and Aggour, M. S. Range of Properties for Lime Stabilized Clay Soils, *Transportation Research Board*, 74th annual meeting, Paper No. 950285 Washington, DC, January, 1995.
4. Jallad, K. N., Santhanam, M, and Cohen, M. D. Stability and Reactivity of Thaumasite at Different pH Levels. *Cement and Concrete Research*, Vol. 33, No. 3, March 2003, pp. 433-437.
5. Warren, C. J., and Reardon, E. J. The Solubility of Ettringite at 25°C, *Cement and Concrete Research*, Vol. 24, April 1994, pp. 1515-1524.
6. Crammond, N. J. The Occurrence of Thaumasite in Modern Construction--A Review, *Cement and Concrete Composites*, Vol. 24, August 2002, pp. 393-402.
7. Barthelmy, D. Mineralogy Database. http://webmineral.com/data/ettringite.shtml. Accessed April 29, 2004.
8. Perkins, R. B, and Palmer, C. D. Solubility of Ettringite ($Ca_6[Al(OH)_6]_2(SO_4)_3 \cdot 26\ H_2O$) at 5-75$^oC$, *Geochimica et Cosmochimica Acta*, Vol. 63, No. 13/14, July 1999, pp. 1969-1980.
9. Mitchell, J. K. Practical Problems from Surprising Soil Behavior. *Journal of Geotechnical Engineering Division, ASCE*, Vol. 112, No. 3, 1986, pp. 259-289.

10. Petry, T. M., and Little, D. N. Update on Sulfate-Induced Heave in Treated Clays: Problematic Sulfate Levels. In *Transportation Research Record 1362*, TRB, National Research Council, Washington, DC, 1992, pp. 51.
11. Petry, T. M. Studies of Factors Causing and Influencing Localized Heave of Lime Treated Clay Soils (Sulfate Induced Heave). U.S. Army Corps of Engineers, Waterways Experiment Station, Vicksburg, MS, 1994.
12. Harris, P., Scullion, T., Sebesta, S., and Claros, G. Measuring Sulfate in Subgrade Soils: Difficulties and Triumphs. In *Transportation Research Board 1837*, TRB, National Research Council, Washington, DC, 2003, pp. 3-11.
13. Moore, A. E., and Taylor, H. F. W. Crystal Structure of Ettringite. *Acta Crystallographica*, *Section B: Structural Science*, Vol. 26, No. 4, 1970, pp. 386-393.
14. Edge, R. A., and Taylor, H. F. W. Crystal Structure of Thaumasite, A Mineral Containing $Si(OH)_6$ Groups. Nature, Vol. 224, 1969, pp. 363-364.
15. Arnett, S. J., Macphee, D. E., and Crammond, N. J. Solid Solutions Between Thaumasite and Ettringite and Their Role in Sulfate Attack, *Concrete Science and Engineering*, Vol. 3, No. 12, December 2001, pp. 209-215.
16. Thaumasite Expert Group, T. The Thaumasite Form of Sulfate Attack: Risks, Diagnosis, Remedial Works and Guidance on New Construction, Department of the Environment, Transport and the Regions: London, 1999.
17. Myneni, S. C. B., Traina, S. J., and Logan, T. J. Ettringite Solubility and Geochemistry of the $Ca(OH)_2$ Al_2 $(SO_4)_3$ H_2O System at 1 atm Pressure and 298 K, *Chemical Geology*, Vol. 148, June 1998, pp. 1-19.

18. Hunter, D. Geochemistry of Lime Induced Heave in Sulfate Bearing Clay Soils. Ph.D. Dissertation, University of Reno, NV, 1989.

19. Damidot, D., and Glasser, F. P. Thermodynamic Investigation of the CaO-Al2O3-CaSO4-K2O-H2O System at 25ºC, *Cement and Concrete Research*, Vol. 23, No. 5, September 1993, pp. 1195-1204.

20. Mohamed, A. M. O., Boily, J. F., Hossein, M., and Hassani, F. P. Ettringite Formation in Lime-Remediated Mine Tailings; I, Thermodynamic Modeling. *CIM Bulletin*, Vol. 88, No. 995, 1974, pp. 69-75.

21. Bredenkemp, S., and Lytton, R. L. Reduction of Sulfate Swell in Expansive Clay Subgrdes in Dallas District, *Texas Transportation Institute Research Report*, TTI: 7-1994, May 1995.

22. Thompson, M. R. Suggested Method of Mixture Design Procedures for Lime Treated Soils, *American Society of Testing and Materials*, Special Technical Publication No. 479, 1970.

23. Burkart, B., Goss, G., Kern, J. The Role of Gypsum in Production of Sulfate-Induced Deformation of Lime-Stabilized Soils, *Environmental & Engineering Geoscience*, Vol. 5, No. 2, Summer 1999, 173.

24. Klein, C., and C. S. Hurlbut Jr. *Manual of Mineralogy*, 21st ed. John Wiley and Sons, New York, 1985.

25. Krauskopf, K. B. *Introduction to Geochemistry*, 2nd ed., McGraw-Hill Book Co., New York, 1979.

26. Taylor, H. F. W. *The Chemistry of Cements*, Vol. 1, Academic Press, New York, 1964.

27. Lambe, T. W., Michaels, A. S., and Moh, Z. C. Improvement of Soil Cement with Alkali Metal Compounds. *Highway Research Record*, Vol. 241, 1960, pp 67-103.

28. Ladd, C. C., Moh, Z. C., and Lambe, T. W. Recent Soil-Lime Research at the Massachusetts Institute of Technology, *Highway Research Record*, Vol. 262, 1960, pp.64-84.

29. Hollis, B. G., and Fawcett, N. D. Laboratory Investigation of the Use of Mixtures of Lime and Pulverized Fuel Ash for Soil Stabilization: *Road Construction*, Vol. 44, No. 517, 1966, pp.3-6.

30. Texas Natural Resources Information Systems. Digital Data. http://www.tnris.state.tx.us/ Accessed May 3, 2004

31. Earth Information Technologies Corporation. Electromagnetic Induction. http://www.earthit.com/services/electromagnetic.html. Accessed May 4, 2004

32. McNeill, J. D. Electromagnetic Terrain Conductivity Measurement at Low Induction Numbers, *Technical Note* TN-6, Geonics Limited, Mississauga, Ontario, 1980, pp 5.

33. Bennett, D., George, R., and Ryder, A. Soil Salinity Assessment Using the EM38: Field Operating Instructions and Data Interpretation. Dept of Agriculture *Miscellaneous Publication* 4/95, Perth, WA, Australia. 1995.

34. Little, D., and Graves, R. Investigation of Sulfate Levels and Expansive Properties of Subgrade Soils along Route 86 Project, Imperial County, California, 1993.

35. Petry, T. Studies of Factors Causing and Influencing Localized Heave of Lime-Treated Clay Soils (Sulfate-Induced Heave), Technical Report for U.S. Army Corps of Engineers, Waterways Experiment Station, Vicksburg, MS, 1994.

36. Damidot, D., and Glasser, F.P. Thermodynamic Investigation of the CaO-Al2O3-CaSO4-H2O System at 50ºC and 85ºC, *Cement and Concrete Composites*, Vol. 22, No. 6, November 1992, pp. 1179-1191.

37. Skopp, J. Analysis of Time-Dependent Chemical Processes in Soils. Journal of *Environmental Quality*, Vol. 15, 1986, pp. 205-213.

38. Tsang, C. F. Comments on Model Validation. *Trans. Porous Media*, Vol. 2, No. 6, 1987, pp. 623-630.

39. Oreskes, N., K. Shrader-Frechette, and Belitz, K. Verification, Validation, and Confirmation of Numerical Models in the Earth Sciences. *Science,* Vol. 263, No. 4, 1994, pp. 641-646.

40. James, R. V., and Rubin, J. Applicability of the Local Equilibrium Assumption to Transport Through Soils of Solutes Affected by Ion Exchange, in *Chemical Modeling in Aqueous Systems,* American Chemical Society, Washington, DC, 1979, pp. 225-235.

41. Rubin, J. and James, R. V. Transport of Reactive Solutes in Porous Media: Relation Between Mathematical Nature of Problem Formulation and Chemical Nature of Reactions, *Water Resources Research*, Vol. 19, No. 5, 1983, pp. 1231-1252.

42. Miller, F. M., and Conway, T. Use of Granulated Blast Furnace Slag for Reduction of Expansion due to Delayed Ettringite Formation, *Cement, Concrete, & Aggregates*, Vol. 25, No.2, West Conshohocken, PA, 2003, pp. 59-68.

43. Mitchell, J. K., and Dermatas, D. Clay Soil Heave Caused By Lime-Sulfate Reactions. *ASTM Special Publication 1135,* June, 1990, pp.41-64.

44. Perrin, L. Expansion of Lime-Treated Clays Containing Sulfates*. Proceedings of 7th International Conference on Expansive Soils*, Vol. 1, ASCE Expansive Soils Research Council, New York, 1992, pp. 409-414.

45. McCallister, L. D, and Tidwell, L. Double Lime Treatment to Minimize Sulfate-Lime Induced Heave in Expansive Clays. US Army Engineers, Waterways Experiment Station, Vicksburg, MS, 1997.

46. Little, D. N, and Graves, R. E. Guidelines for Use of Lime in Sulfate Bearing Soils. Unpublished report, 1995.

47. Rollings, R. S., Burkes, J. P., and Rollings, M. P. Sulfate Attack on Cement-Stabilized Sand. *Geotechnical and Geoenvironmental Engineering*, Vol. 125, No. 5, May 1999, pp. 364-372.

48. Berger, E., Little, D. N., Smith, K., Marvin, S., Atkinson, D., Estrada, M., Williams, T., Coover, R., Nguyen, P., and Zaremba, T. South Orange County Sulfate Study, September 2002.

49. Holmquist, D. Supplementary Evaluation of Risk of Adverse Lime/Sulfate Reaction. Unpublished Report to CTL Thompson, 1991.

50. Betke, C. M. *Geochemical Reaction Modeling*. Oxford University Press. 1996.

51. Roinson, R. A. and Stokes, R. H. *Electrolyte Solutions*, Butterworths, London, 1968.

52. Jaffarzadeh, A. A. and Burnham, C. P. Gypsum Crystals in Soils, *Soil Science*, Vol. 43, 1992, pp. 409-420.

53. Soil Survey of Williamson County, Texas. United States Department of Agriculture Soil Conservation Service in cooperation with Texas Agricultural Experimentation Station, Washington, DC, January 1983, pp 15-52.

54. Soil Survey of Travis County, Texas. United States Department of Agriculture Soil Conservation Service in cooperation with Texas Agricultural Experimentation Station, Washington, DC, June 1974, pp 11-47.

55. Soil Survey of Caldwell County, Texas. United States Department of Agriculture Soil Conservation Service in cooperation with Texas Agricultural Experimentation Station, Washington, DC, July 1978, pp 7-31.

56. Soil Survey of Guadalupe County, Texas. United States Department of Agriculture Soil Conservation Service in cooperation with Texas Agricultural Experimentation Station, Washington, DC, March 1977, pp 6-34.

APPENDIX A

CALIBRATION OF EM38

Calibration Method for Phasing and Instrument Zero

This calibration should be carried out at least 3 to 4 times per day unless the ground is very resistive in which case you would repeat it more often.

IMPORTANT! Because of the high sensitivity of the EM38 it is advisable to remove all metal objects from wrists, fingers, neck and pockets during the calibration procedure. Sensitivity to metal objects, which is discussed in Section 2 is greatest near the coils at either end of the instrument. Turn instrument on by setting the ON/OFF/BATT switch to "ON" and follow proceeding steps.

Step 1

With the EM38 on the ground, mode switch set to Q/P, and the instrument in the vertical dipole mode of operation (see Fig. 1) set the Quad phase (Q/P) reading to zero using the Q/P zero control knob.

Step 2

Set the mode switch to Inphase (I/P) and set the Inphase reading to zero using the I/P coarse and fine controls. Go back and make sure that the Q/P still reads zero.

Step 3

With the mode switch in Q/P, set Q/P to 50 mS/m, using the Q/P zero control knob.

Step 4

Set the mode switch back to I/P and raise the I/P reading to 50 mS/m by using the coarse and fine I/P controls.

Step 5

Return mode switch back to Q/P and make sure it reads 50 mS/m. If the Q/P reading is not 50 mS/m then adjust the Phase control so that the Q/P reading is 50 mS/m (+/-1 mS/m).

Step 6

Bring both readings of Q/P and I/P to zero once again, as described in steps 1 and 2. Now lift the EM38 to a height of about 1.5 Meters (5 feet).

Step 7

With the instrument in the air and in the horizontal dipole mode of operation (Fig. 1), set the Q/P and I/P readings to zero as was done in steps 1 and 2.

Step 8

Now with the mode switch in the Q/P position adjust the Q/P zero control so that an arbitrary value (i.e. H=10 mS/m) appears on the display. Rotate the EM38 to the vertical dipole mode and note the reading (hypothetically V=16 mS/m). Subtract the horizontal dipole reading from the vertical (V-H=6mS/m).

Step 9

Finally, with the mode switch still in the Q/P position and instrument still in the horizontal dipole mode, rotate the Q/P zero control until the display reads the value calculated in step 8. In this example it would be 6 mS/m. Now when you rotate the EM38 to the vertical dipole mode the reading should be 12 mS/m. With instrument at least 1.5 meters above ground or higher, the Q/P reading or conductivity should always satisfy the following equation:

V=2H

Where V = vertical dipole mode reading

and

H = horizontal dipole mode reading

Source; This calibration procedure has been taken from the EM38 Ground Conductivity Meter Operating Manual, GEONICS LIMITED (http://www.geonics.com)

APPENDIX B

THERMOGRAMS OF

DIFFERENTIAL SCANNING CALORIMETRY

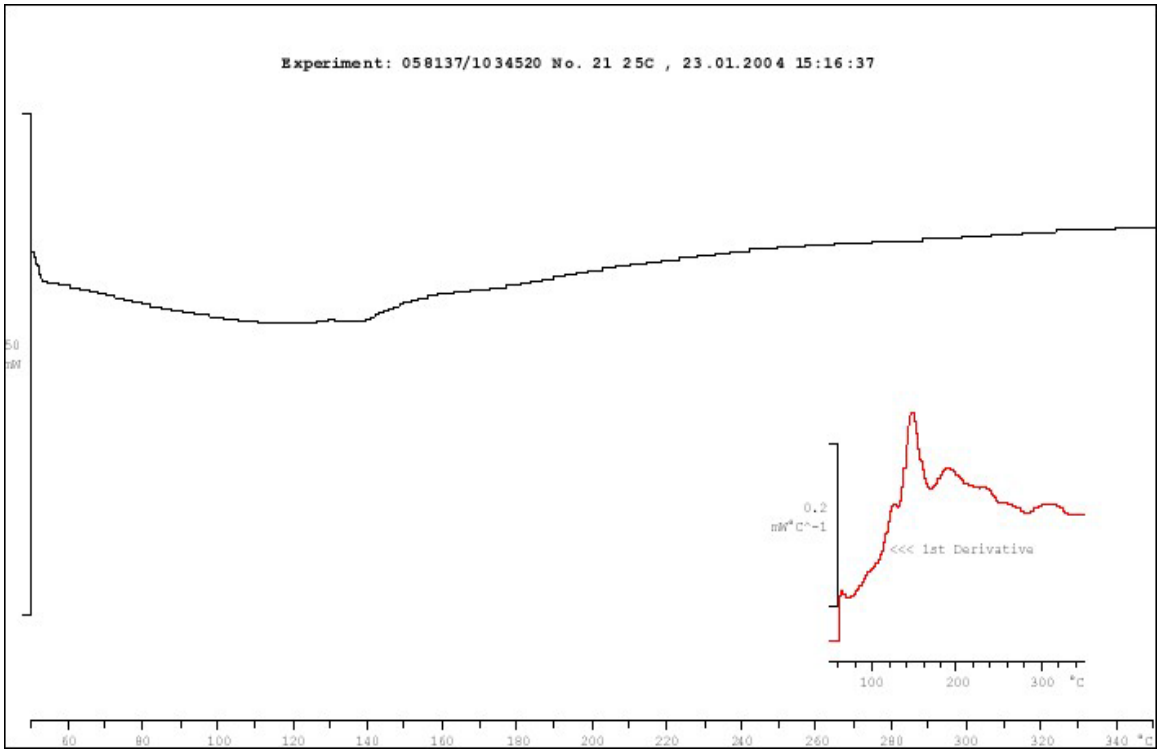
Experiment: 058137/1034520 No. 21 25C , 23.01.2004 15:16:37
50
mW
0.2
mW*C^-1
<<< 1st Derivative
100
200
300 °C
60
80
100
120
140
160
180
200
220
240
260
280
300
320
340 °C

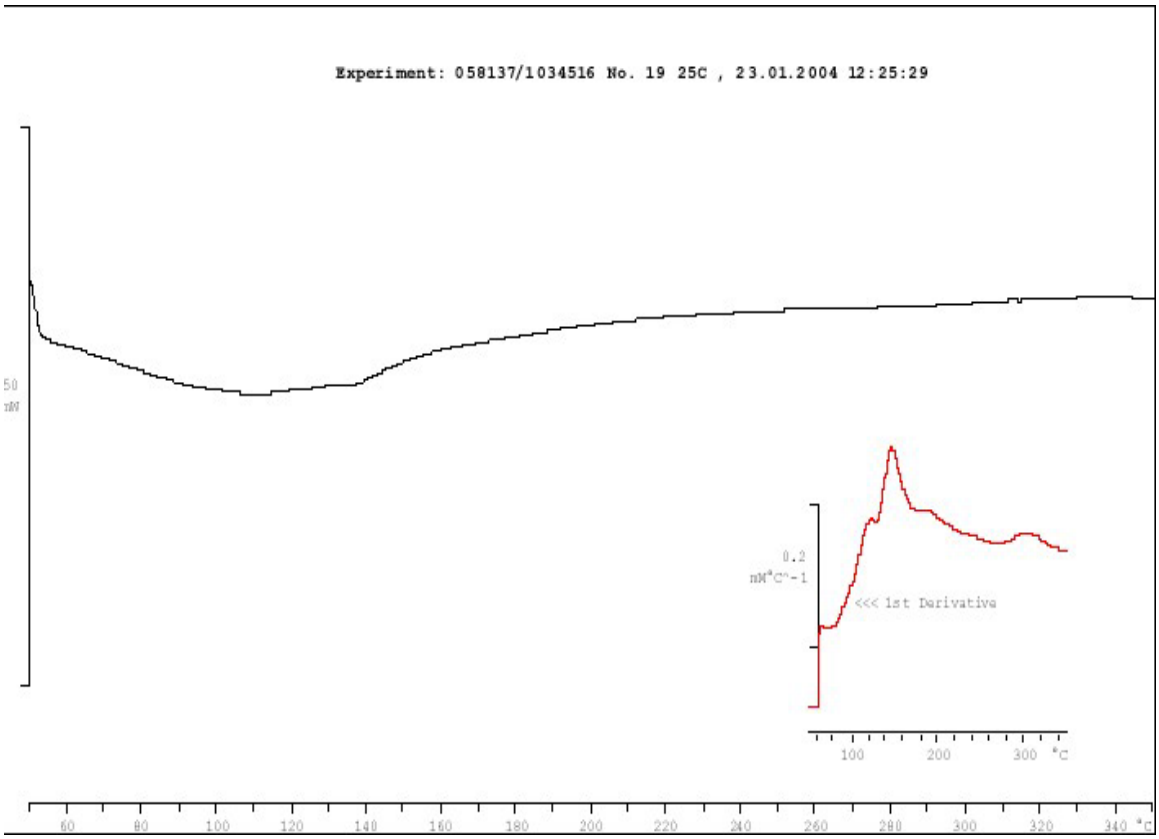
Experiment: 058137/1034516 No. 19 25C , 23.01.2004 12:25:29
50
mW
0.2
mW*C^-1
<<< 1st Derivative
100
200
300 °C
60
80
100
120
140
160
180
200
220
240
260
280
300
320
340 °C

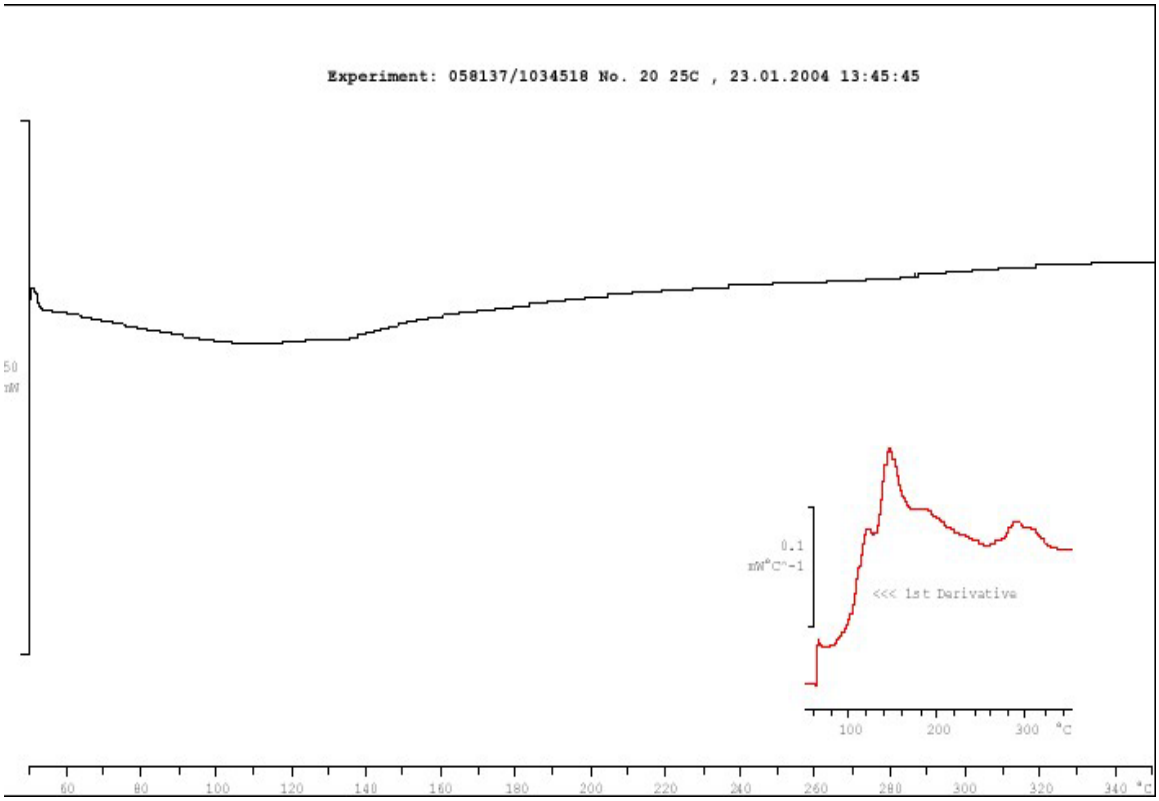
Experiment: 058137/1034518 No. 20 25C , 23.01.2004 13:45:45
50
mW
0.1
mW°C^-1
<<< 1st Derivative
100
200
300
°C
60
80
100
120
140
160
180
200
220
240
260
280
300
320
340
°C

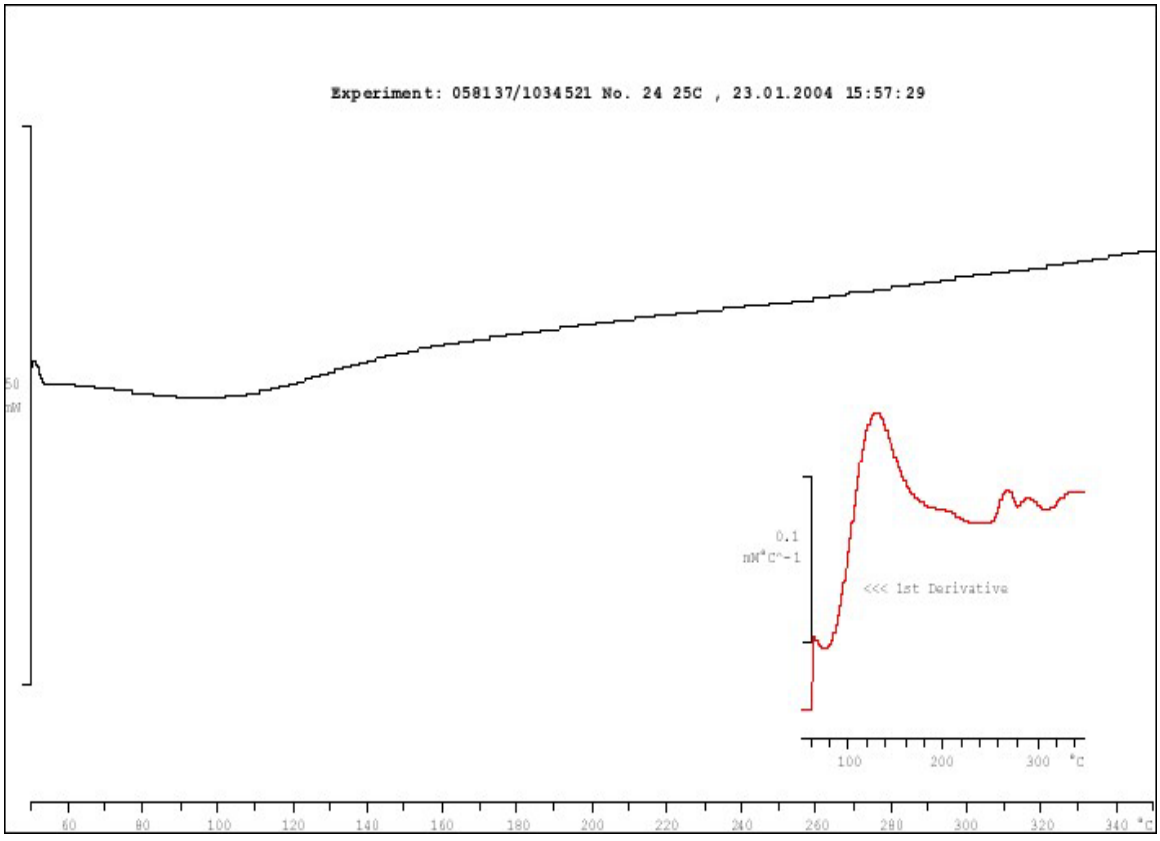
Experiment: 058137/1034521 No. 24 25C , 23.01.2004 15:57:29
50
mW
0.1
mW°C^-1
<<< 1st Derivative
100
200
300
°C
60
80
100
120
140
160
180
200
220
240
260
280
300
320
340
°C

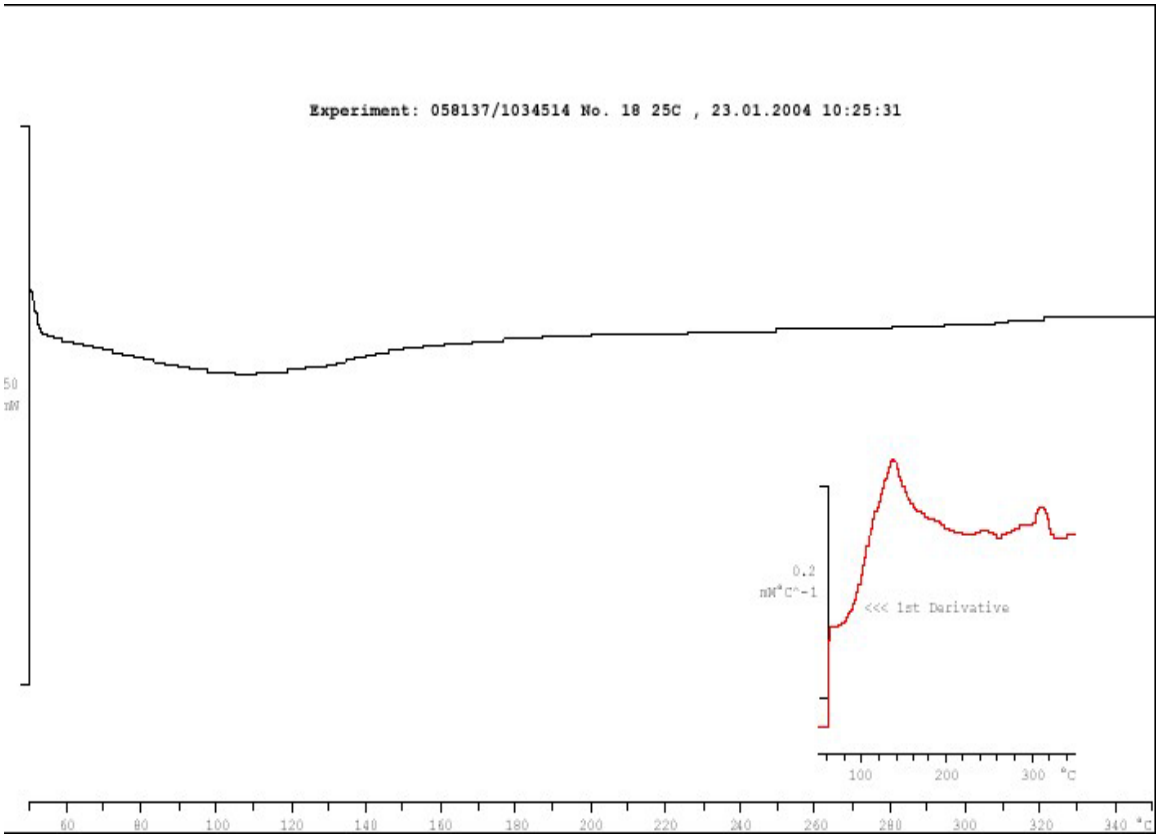
Experiment: 058137/1034514 No. 18 25C , 23.01.2004 10:25:31
50
mW
0.2
mW°C^-1
<<< 1st Derivative
100
200
300
°C
60
80
100
120
140
160
180
200
220
240
260
280
300
320
340
°C

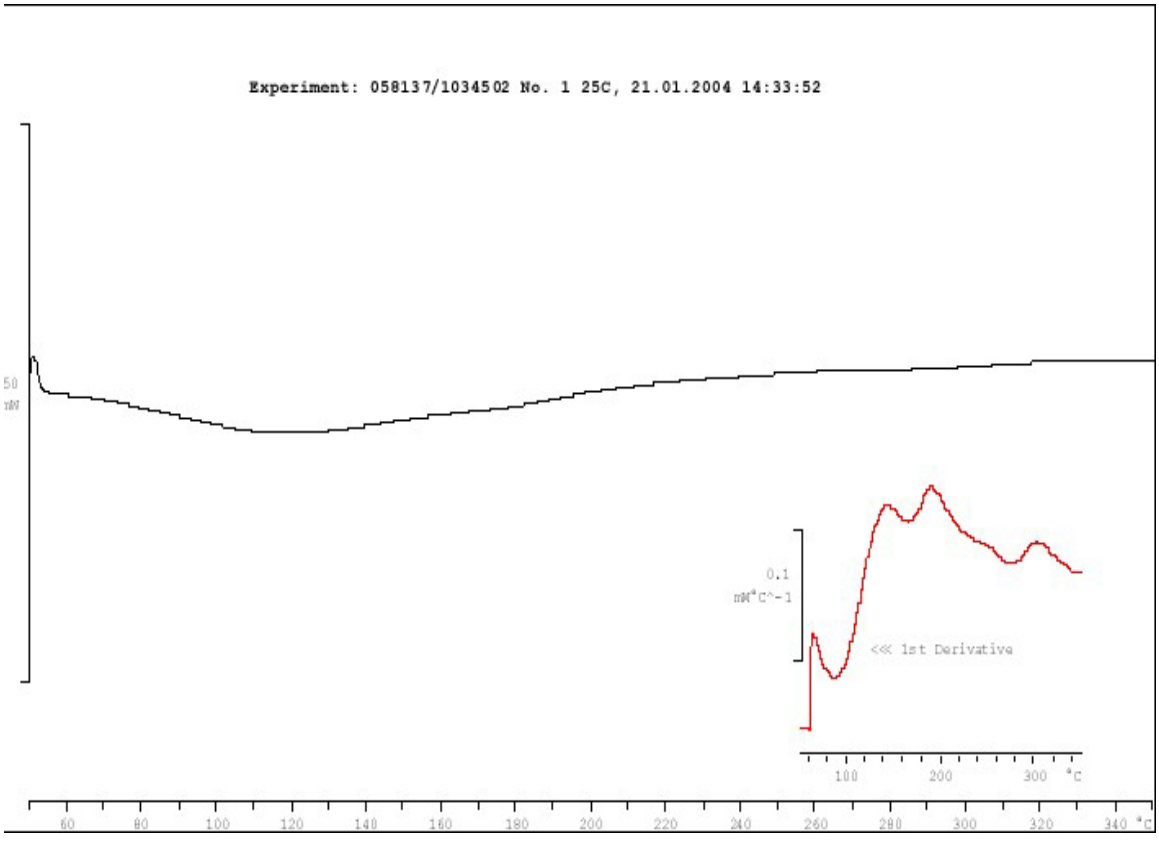
Experiment: 058137/1034502 No. 1 25C, 21.01.2004 14:33:52
50
mW
0.1
mW°C^-1
<<< 1st Derivative
100
200
300
°C
60
80
100
120
140
160
180
200
220
240
260
280
300
320
340
°C

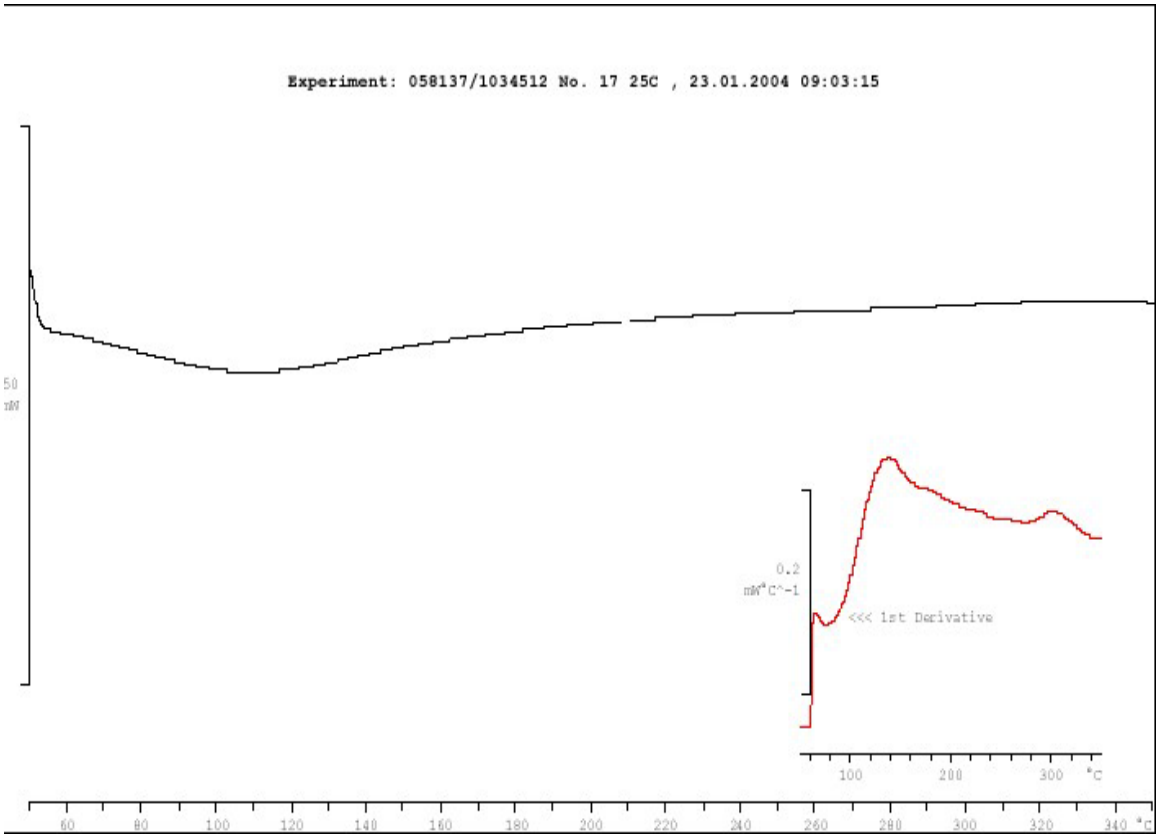
Experiment: 058137/1034512 No. 17 25C , 23.01.2004 09:03:15
50
mW
0.2
mW°C^-1
<<< 1st Derivative
100
200
300
°C
60
80
100
120
140
160
180
200
220
240
260
280
300
320
340 °C

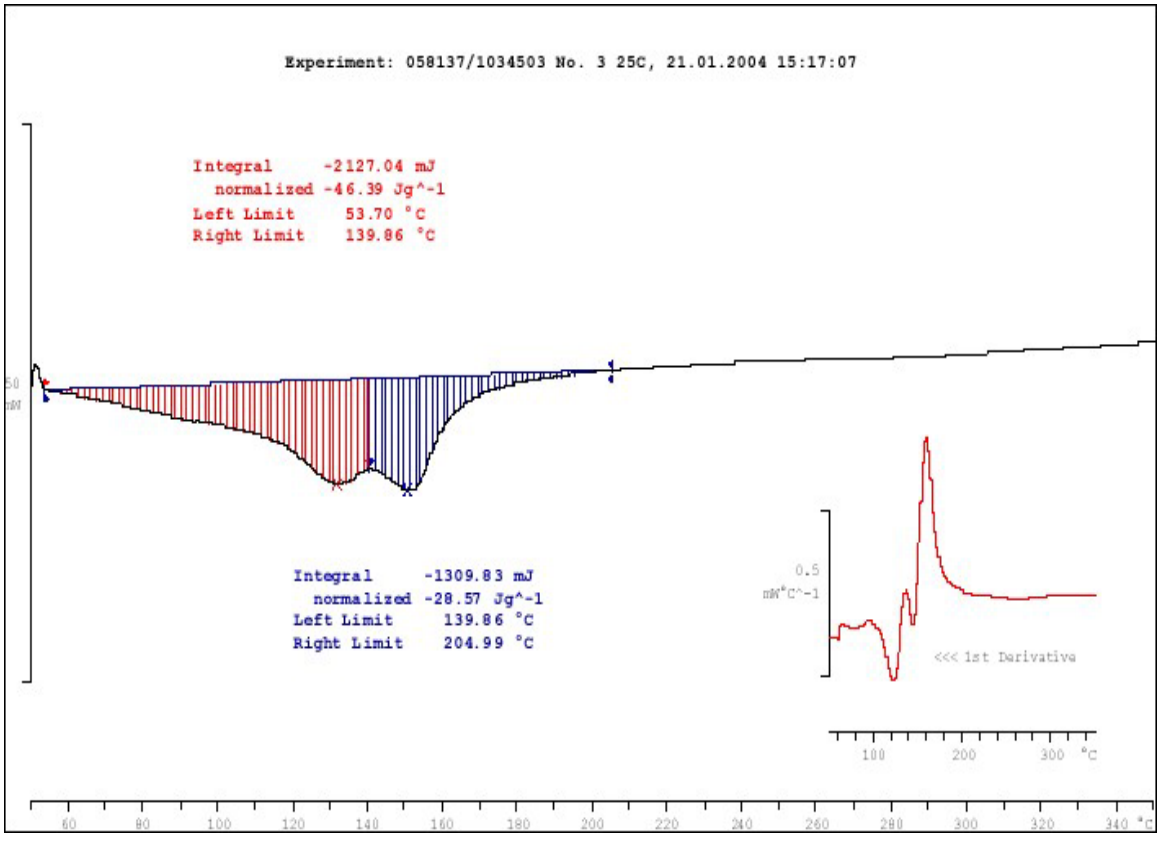
Experiment: 058137/1034503 No. 3 25C, 21.01.2004 15:17:07
Integral -2127.04 mJ
normalized -46.39 Jg^-1
Left Limit 53.70 °C
Right Limit 139.86 °C
50
mW
Integral -1309.83 mJ
normalized -28.57 Jg^-1
Left Limit 139.86 °C
Right Limit 204.99 °C
0.5
mW°C^-1
<<< 1st Derivative
100
200
300
°C
60
80
100
120
140
160
180
200
220
240
260
280
300
320
340 °C

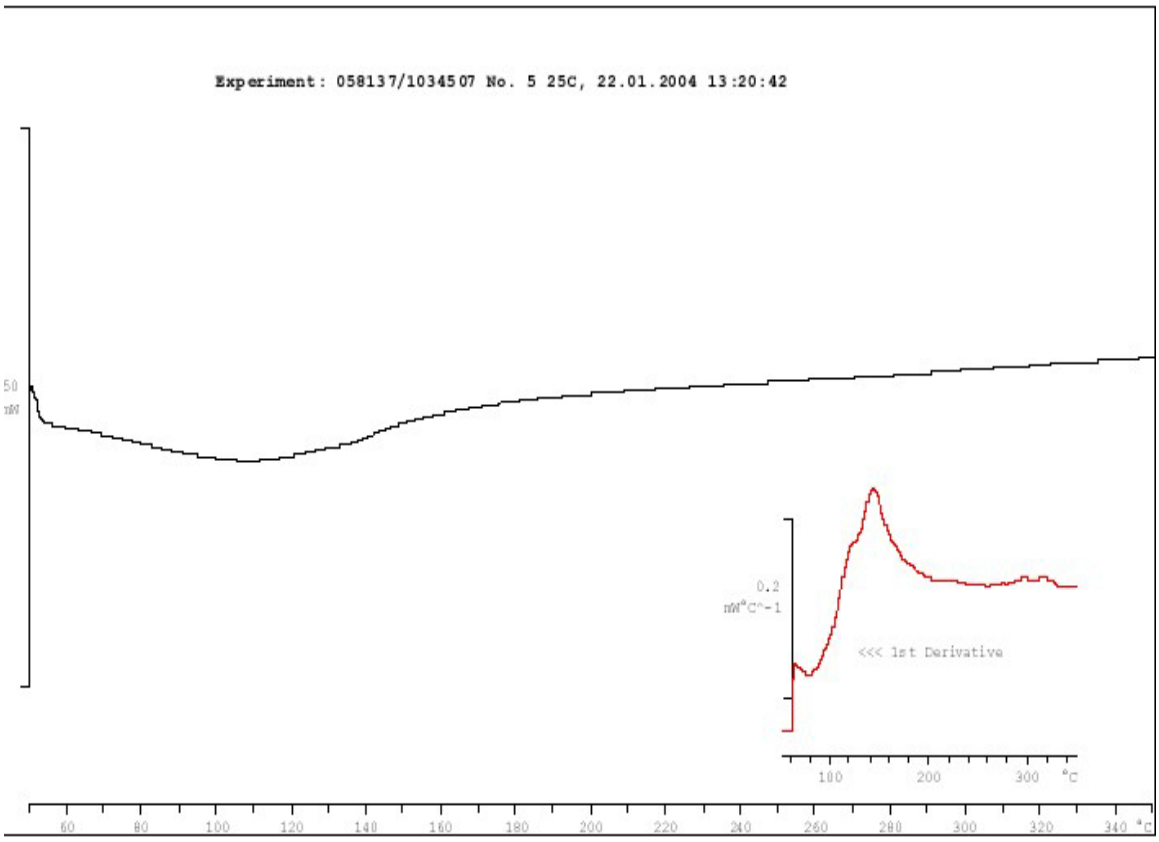
Experiment: 058137/1034507 No. 5 25C, 22.01.2004 13:20:42
50
mW
0.2
mW°C^-1
<<< 1st Derivative
100
200
300
°C
60
80
100
120
140
160
180
200
220
240
260
280
300
320
340 °C

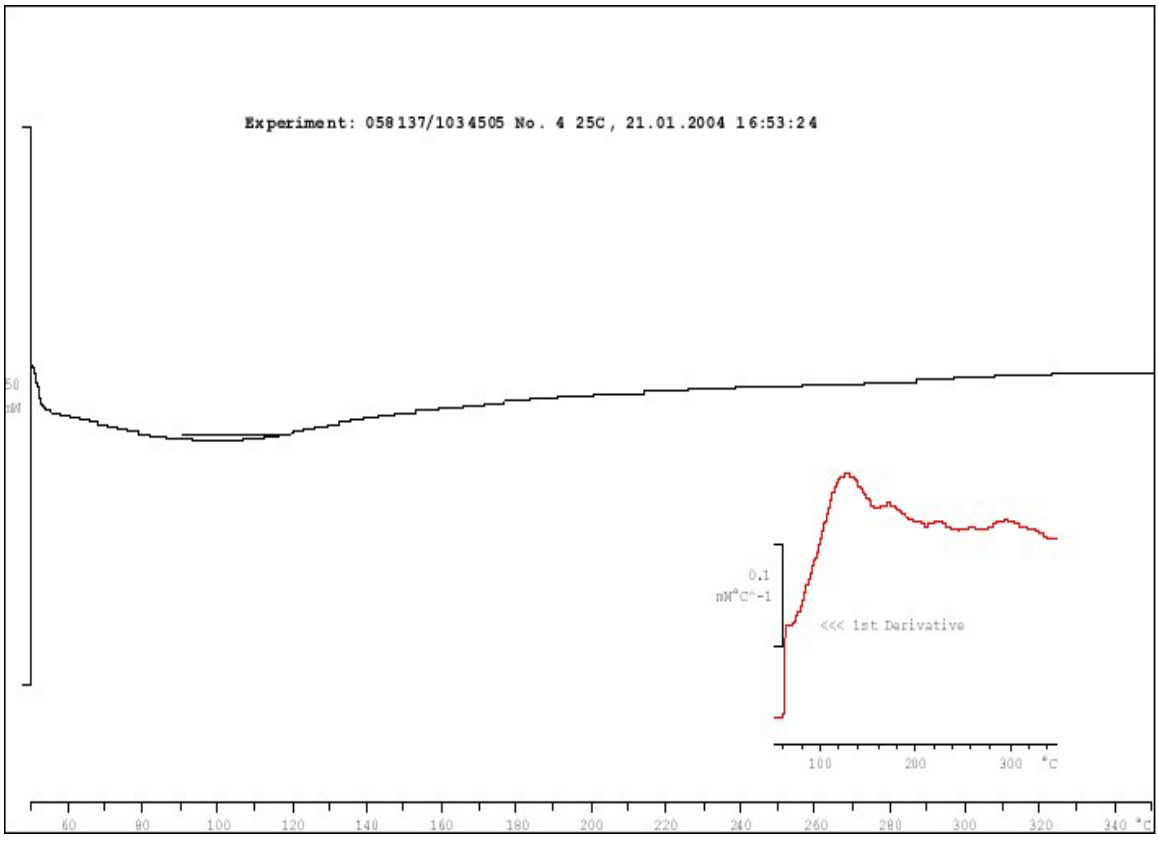
Experiment: 058137/1034505 No. 4 25C, 21.01.2004 16:53:24
50
mW
0.1
mW°C^-1
<<< 1st Derivative
100
200
300
°C
60
80
100
120
140
160
180
200
220
240
260
280
300
320
340 °C

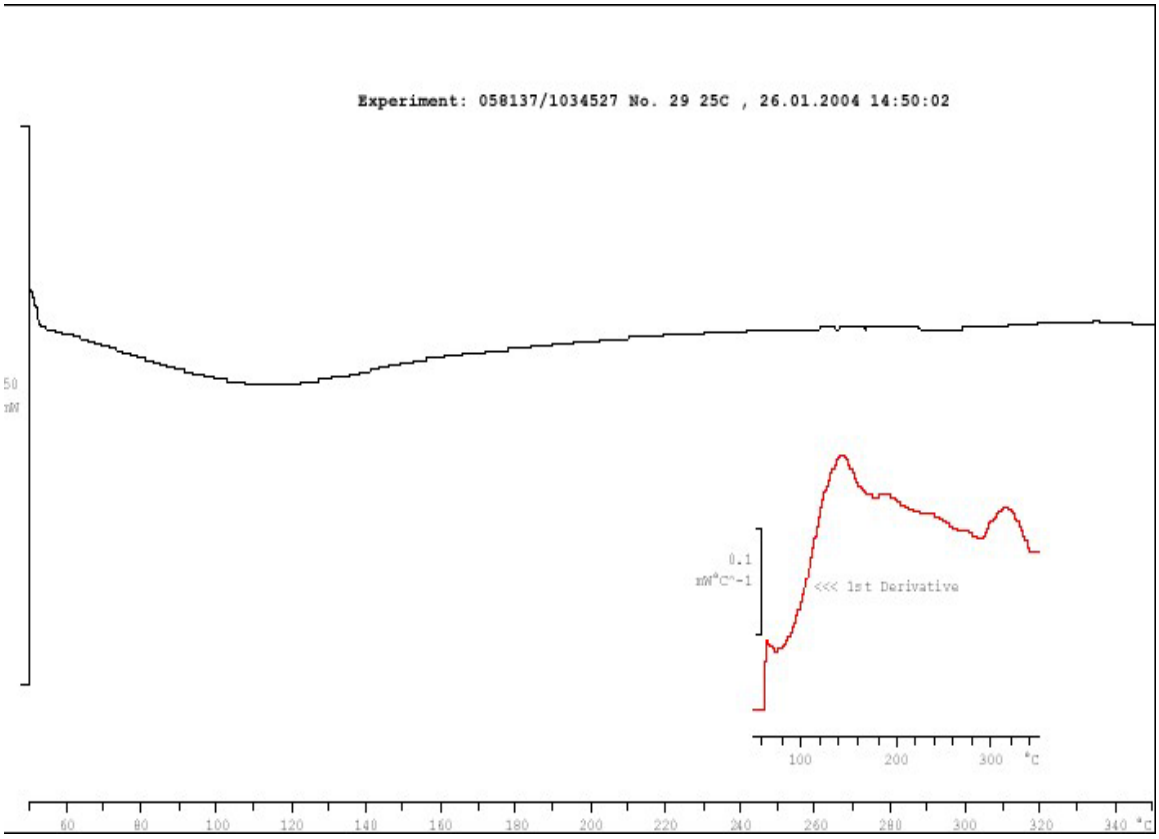
Experiment: 058137/1034527 No. 29 25C , 26.01.2004 14:50:02
50
mW
0.1
mW°C^-1
<<< 1st Derivative
100
200
300
°C
60
80
100
120
140
160
180
200
220
240
260
280
300
320
340 °C

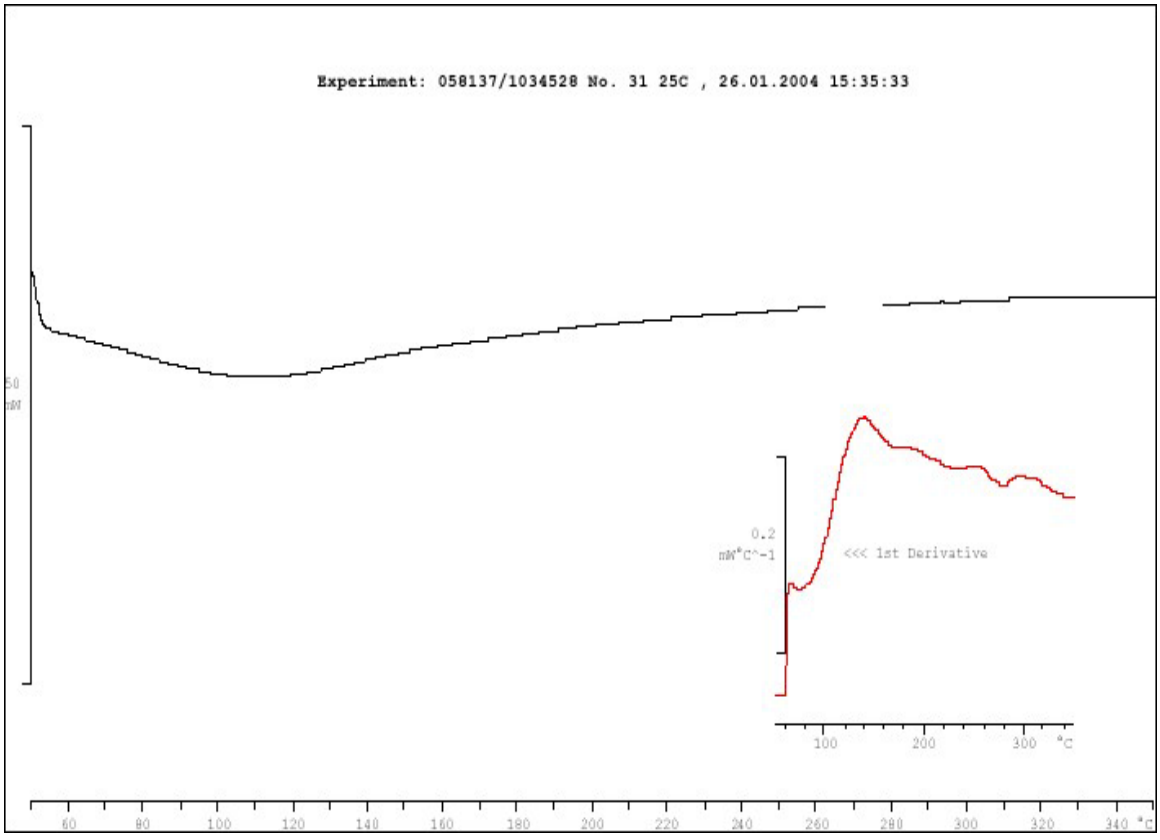
Experiment: 058137/1034528 No. 31 25C , 26.01.2004 15:35:33
50
mW
0.2
mW°C^-1
<<< 1st Derivative
100
200
300
°C
60
80
100
120
140
160
180
200
220
240
260
280
300
320
340 °C

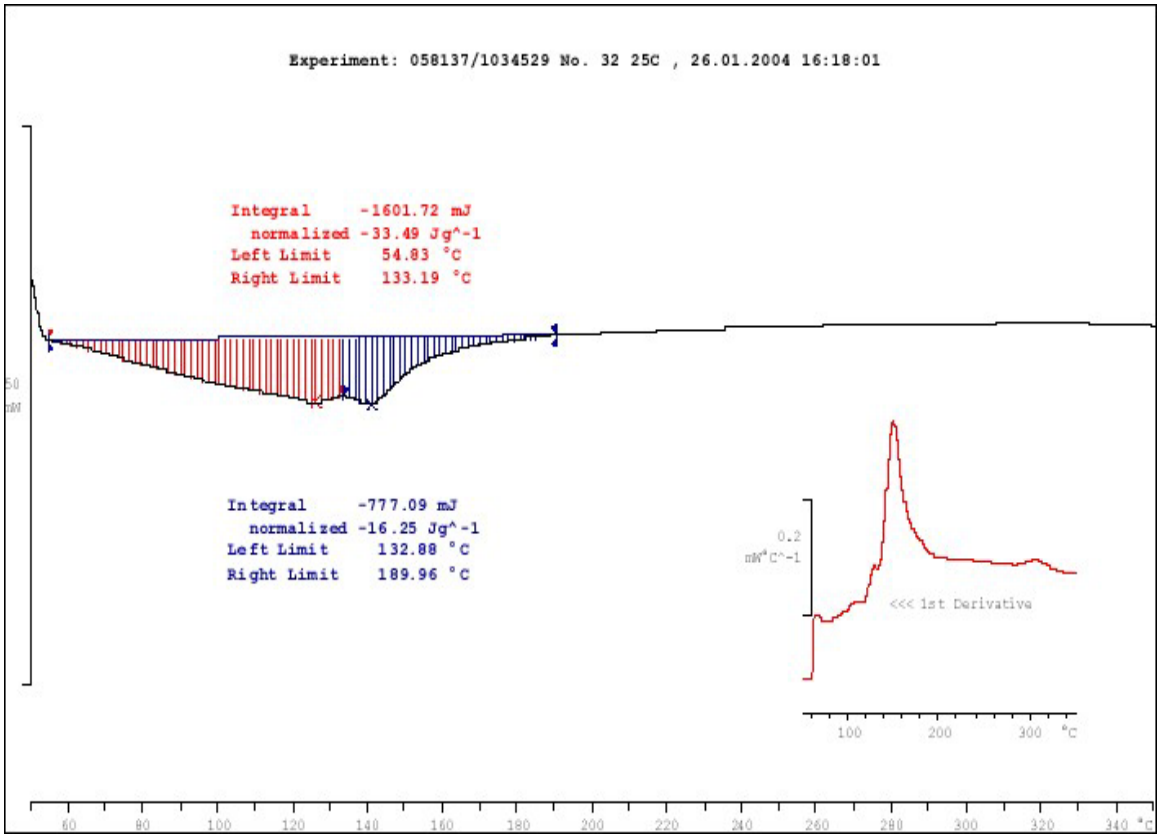
Experiment: 058137/1034529 No. 32 25C , 26.01.2004 16:18:01
Integral -1601.72 mJ
normalized -33.49 Jg^-1
Left Limit 54.83 °C
Right Limit 133.19 °C
Integral -777.09 mJ
normalized -16.25 Jg^-1
Left Limit 132.88 °C
Right Limit 189.96 °C
0.2
mW°C^-1
<<< 1st Derivative
100
200
300
°C
60
80
100
120
140
160
180
200
220
240
260
280
300
320
340 °C

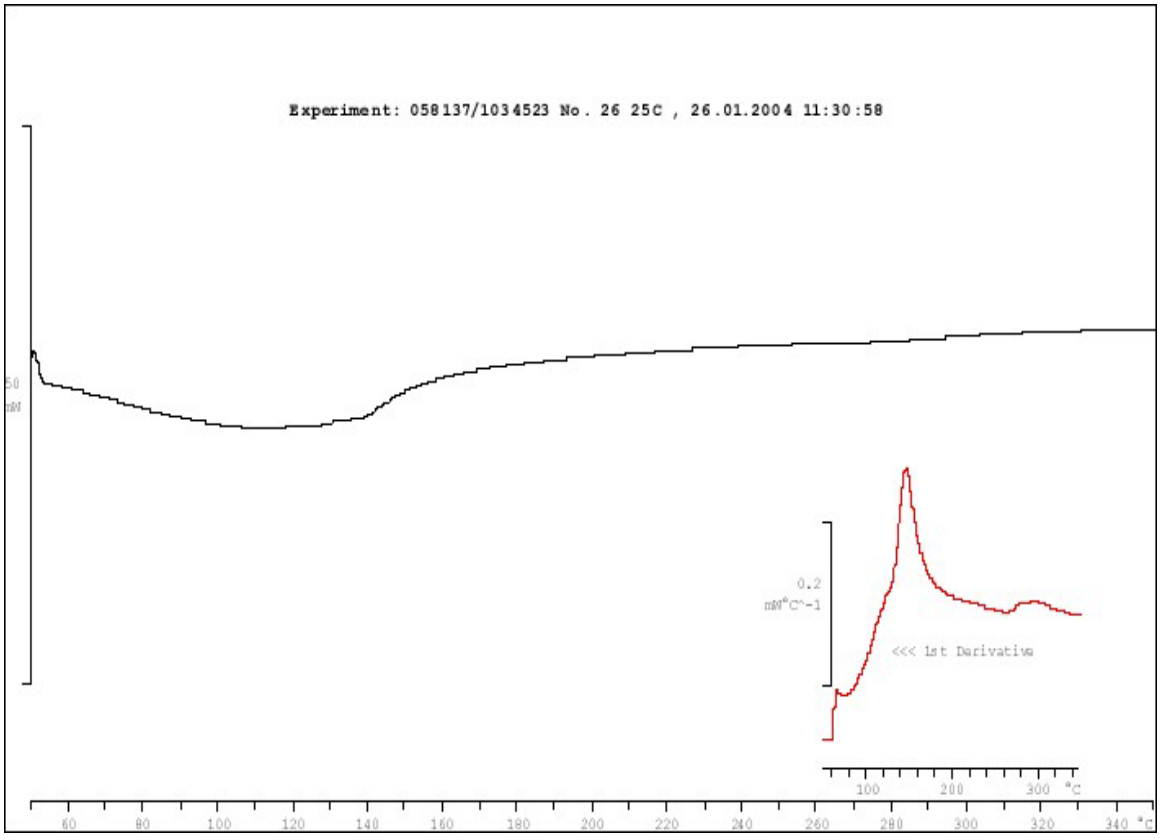
Experiment: 058137/1034523 No. 26 25C , 26.01.2004 11:30:58
0.2
mW°C^-1
<<< 1st Derivative
100
200
300
°C
60
80
100
120
140
160
180
200
220
240
260
280
300
320
340 °C

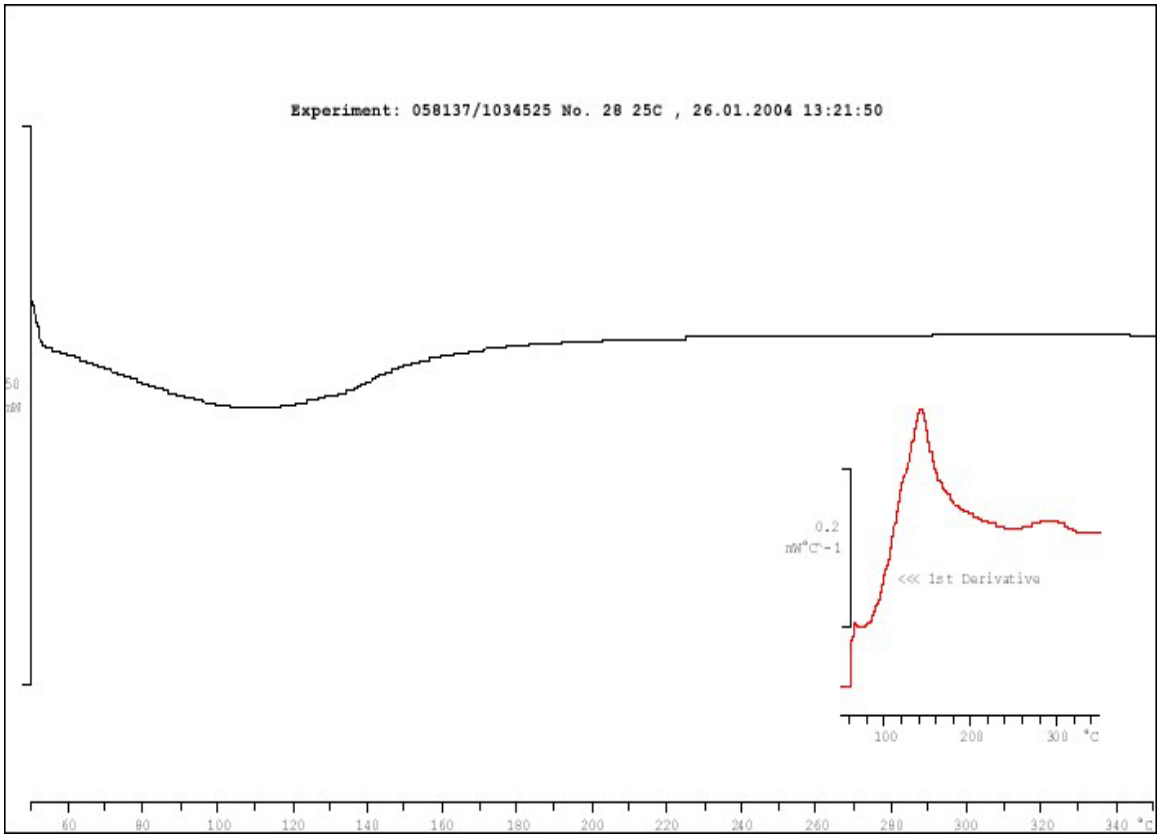
Experiment: 058137/1034525 No. 28 25C , 26.01.2004 13:21:50
50
mW
0.2
mW°C^-1
<<< 1st Derivative
100
200
300 °C
60
80
100
120
140
160
180
200
220
240
260
280
300
320
340 °C

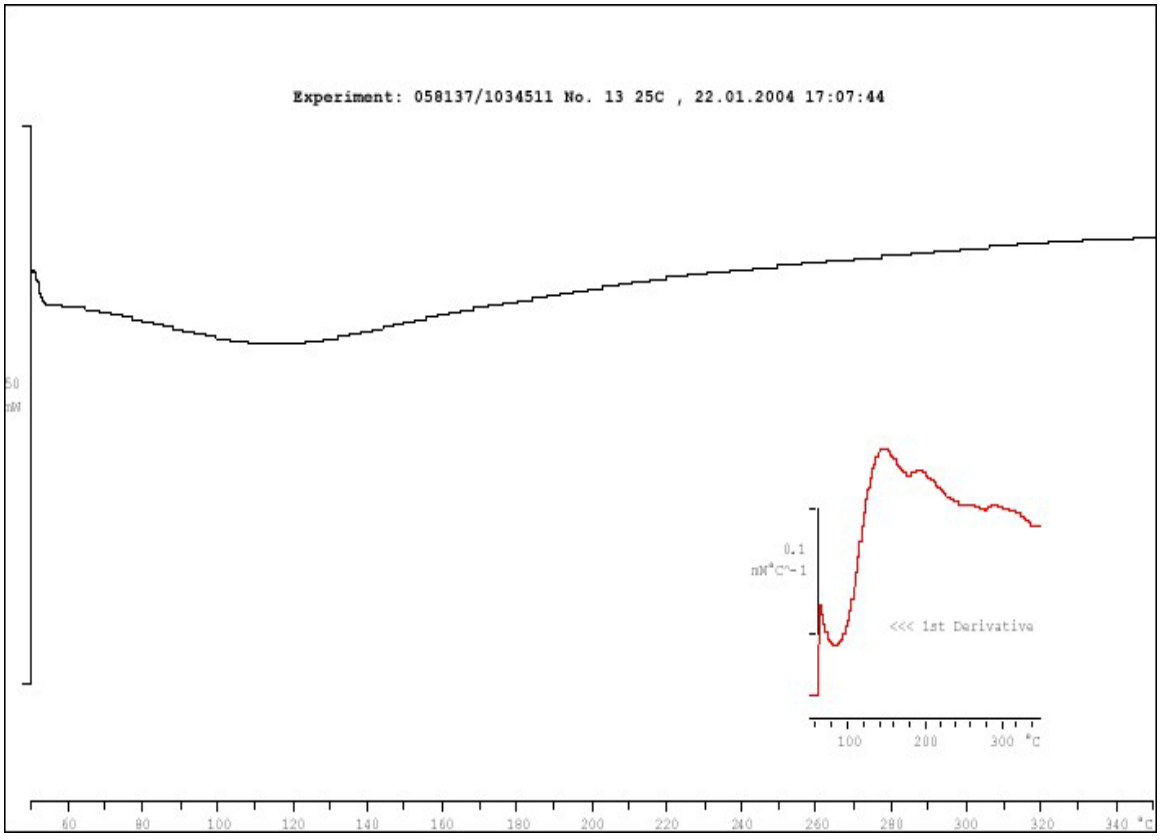
Experiment: 058137/1034511 No. 13 25C , 22.01.2004 17:07:44
50
mW
0.1
mW°C^-1
<<< 1st Derivative
100
200
300 °C
60
80
100
120
140
160
180
200
220
240
260
280
300
320
340 °C

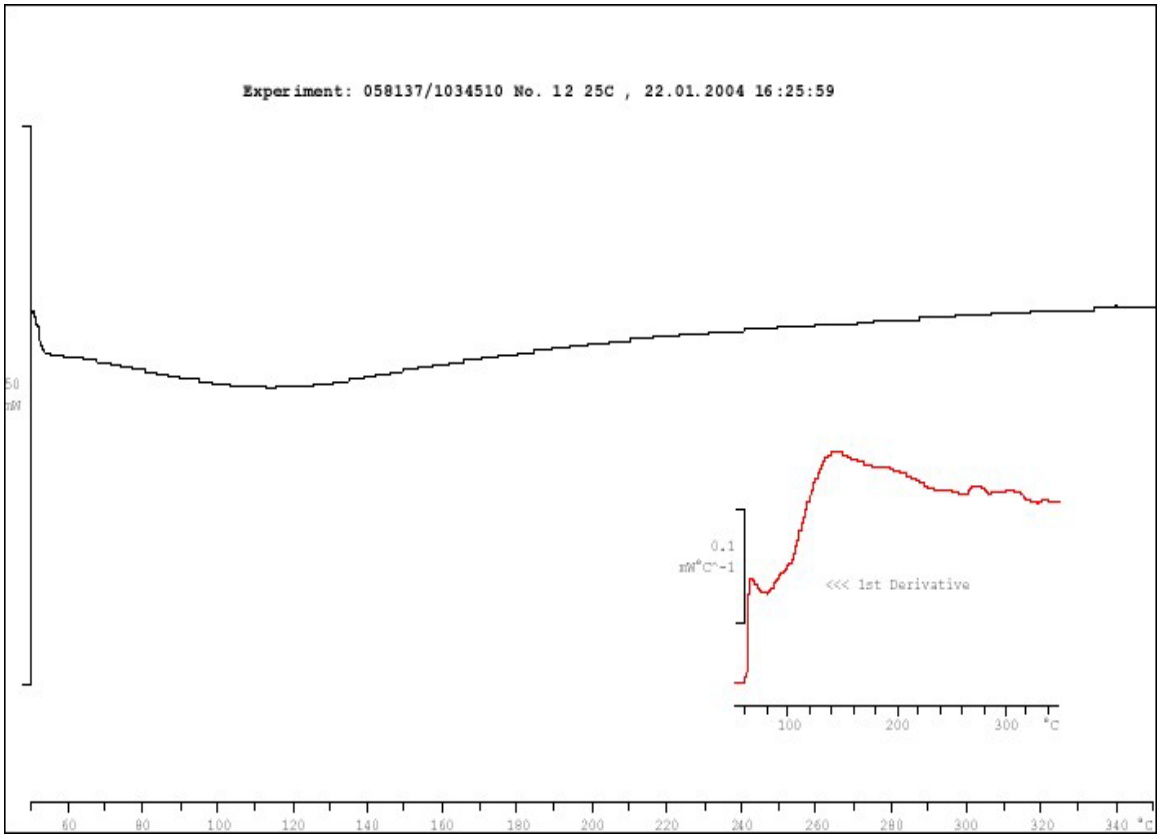
Experiment: 058137/1034510 No. 12 25C , 22.01.2004 16:25:59
50
mW
0.1
mW°C^-1
<<< 1st Derivative
100
200
300
°C
60
80
100
120
140
160
180
200
220
240
260
280
300
320
340 °C

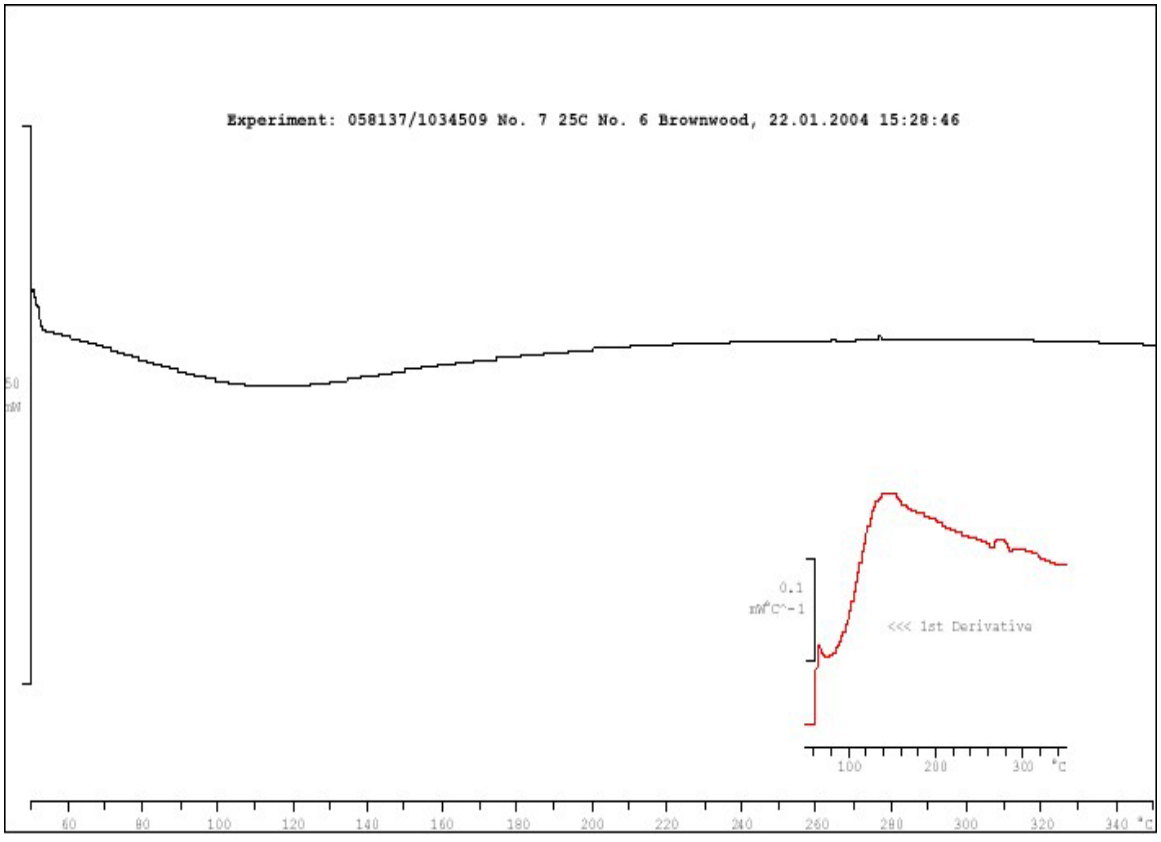
Experiment: 058137/1034509 No. 7 25C No. 6 Brownwood, 22.01.2004 15:28:46
50
mW
0.1
mW°C^-1
<<< 1st Derivative
100
200
300
°C
60
80
100
120
140
160
180
200
220
240
260
280
300
320
340 °C

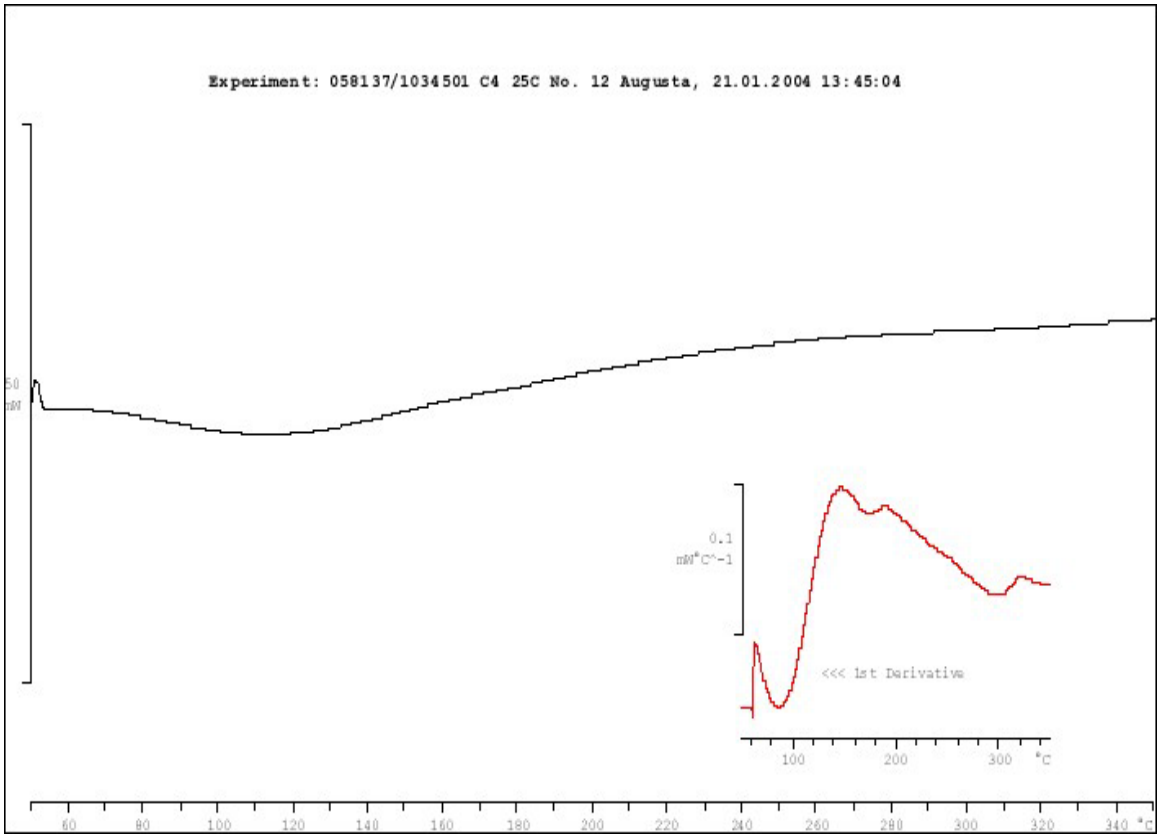
Experiment: 058137/1034501 C4 25C No. 12 Augusta, 21.01.2004 13:45:04
50
mW
0.1
mW°C^-1
<<< 1st Derivative
100
200
300
°C
60
80
100
120
140
160
180
200
220
240
260
280
300
320
340 °C

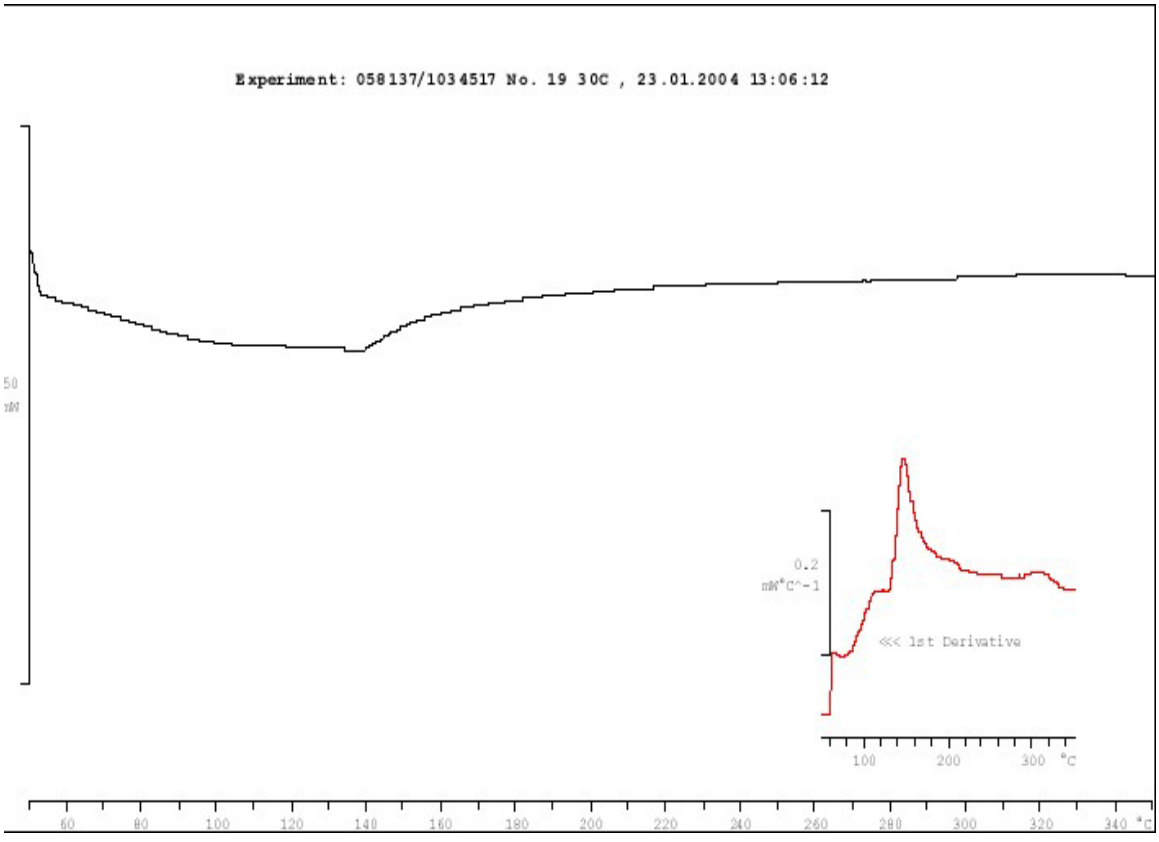
Experiment: 058137/1034517 No. 19 30C , 23.01.2004 13:06:12
50
mW
0.2
mW°C^-1
<<< 1st Derivative
100
200
300
°C
60
80
100
120
140
160
180
200
220
240
260
280
300
320
340 °C

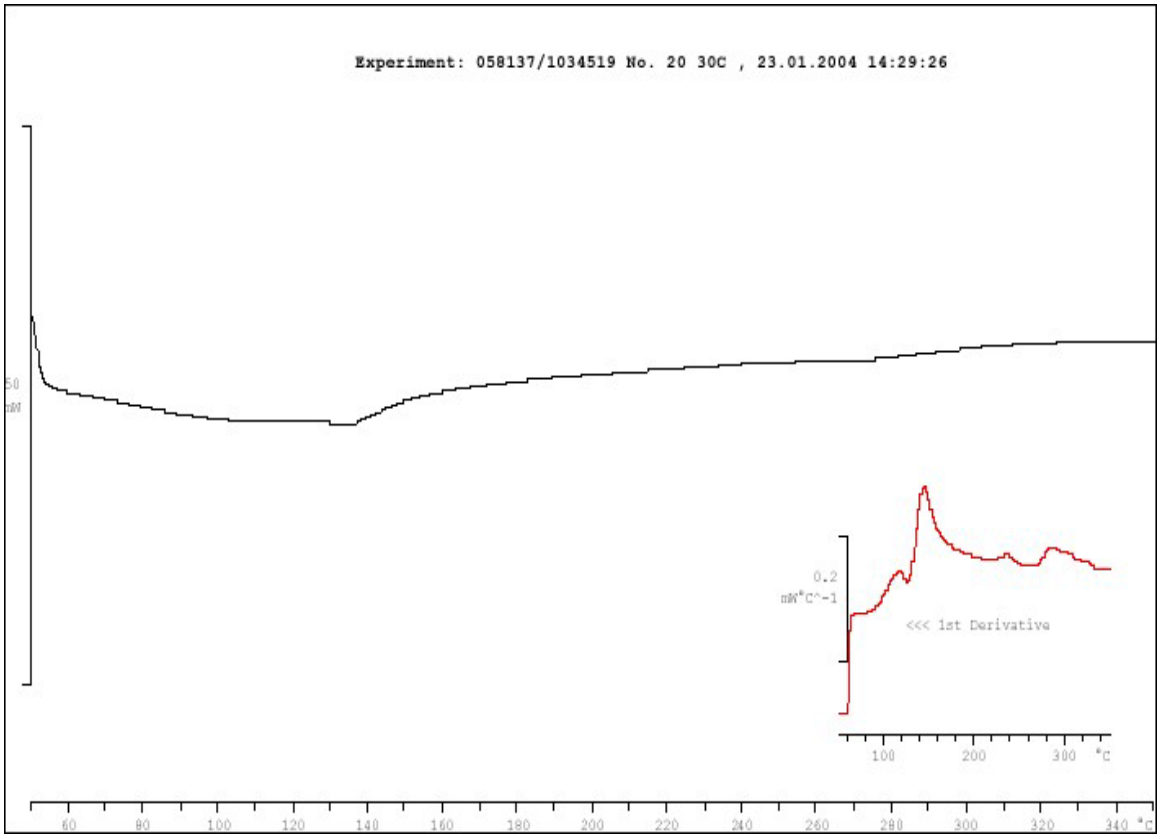
Experiment: 058137/1034519 No. 20 30C , 23.01.2004 14:29:26
50
mW
0.2
mW°C^-1
<<< 1st Derivative
100
200
300
°C
60
80
100
120
140
160
180
200
220
240
260
280
300
320
340 °C

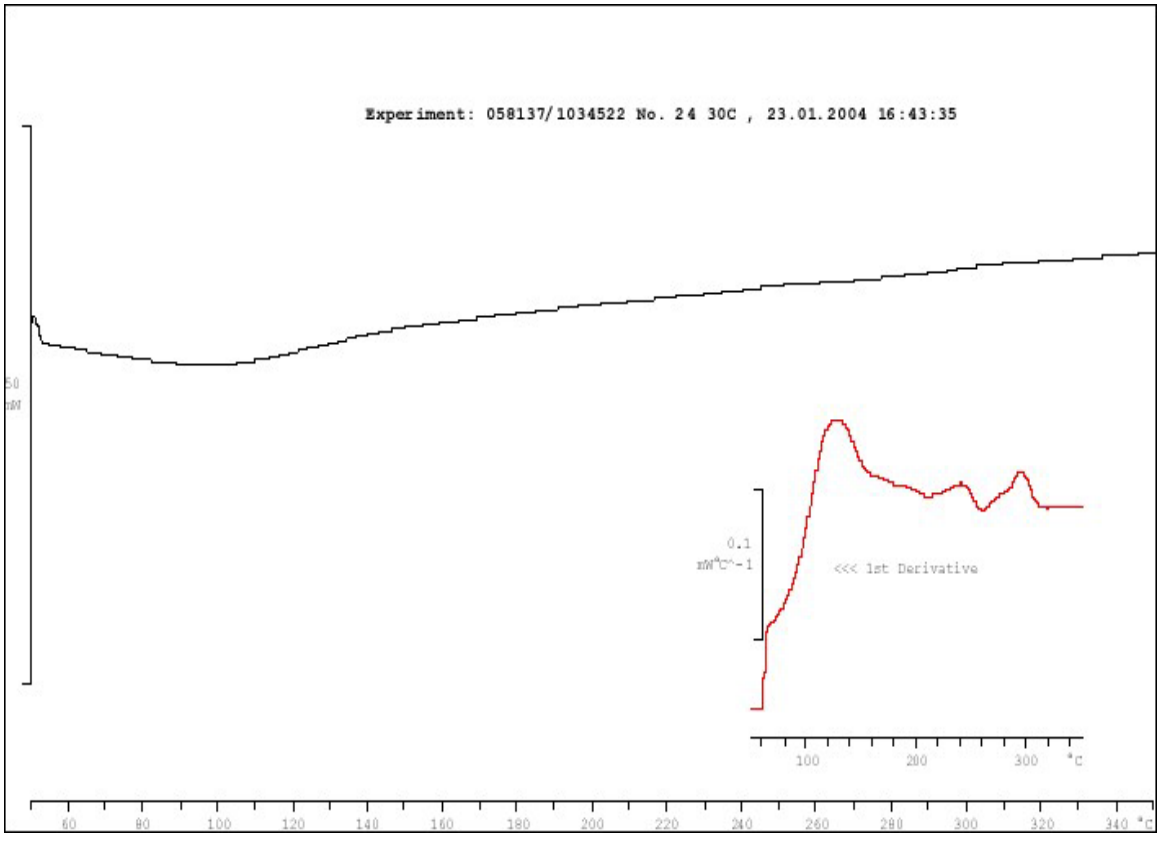
Experiment: 058137/1034522 No. 24 30C , 23.01.2004 16:43:35
50
mW
0.1
mW°C^-1
<<< 1st Derivative
100
200
300
°C
60
80
100
120
140
160
180
200
220
240
260
280
300
320
340 °C

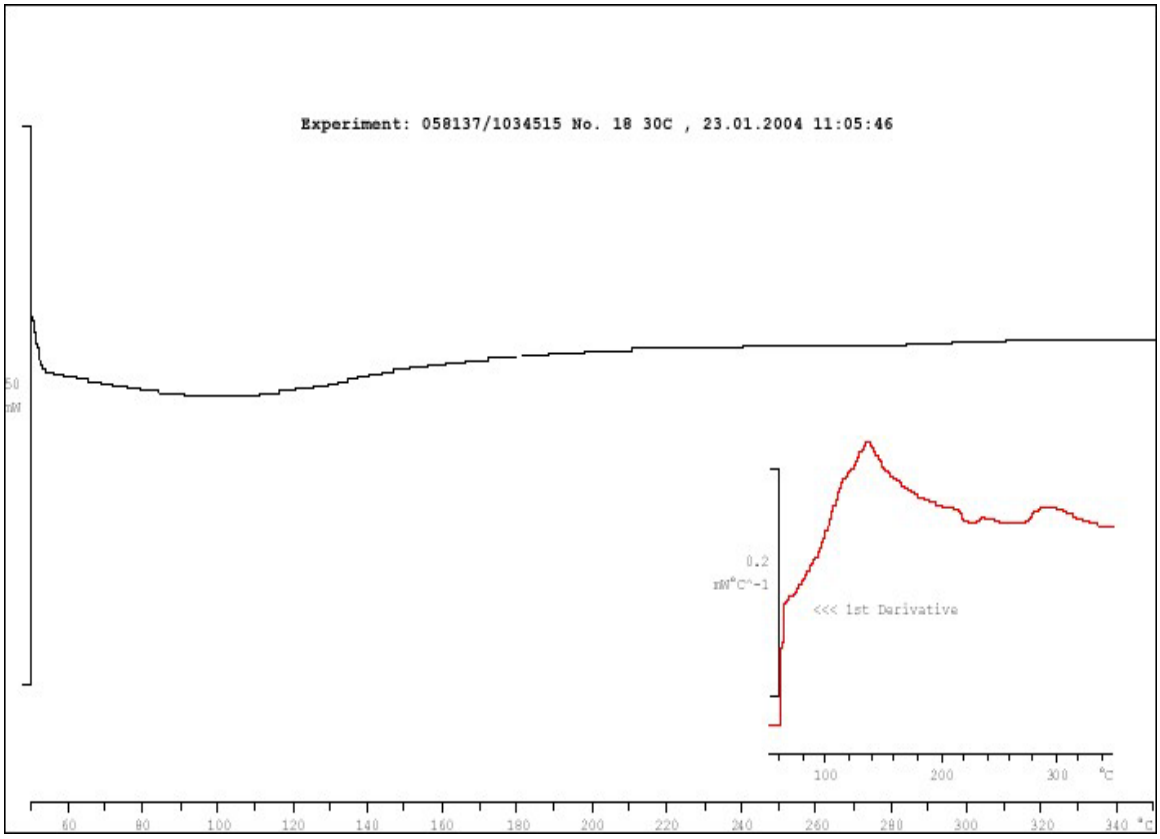
Experiment: 058137/1034515 No. 18 30C , 23.01.2004 11:05:46
50
mW
0.2
mW°C^-1
<<< 1st Derivative
100
200
300
°C
60
80
100
120
140
160
180
200
220
240
260
280
300
320
340 °C

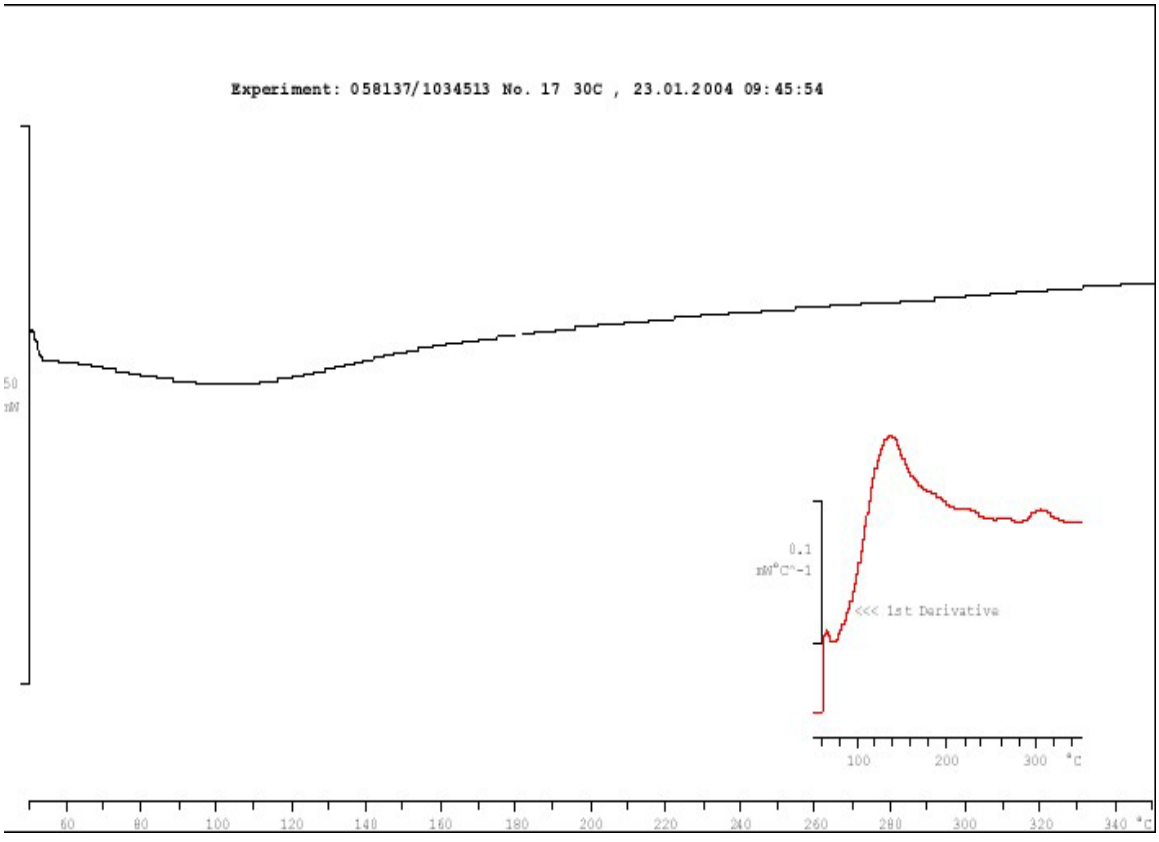
Experiment: 058137/1034513 No. 17 30C , 23.01.2004 09:45:54
50
mW
0.1
mW°C^-1
<<< 1st Derivative
100
200
300
°C
60
80
100
120
140
160
180
200
220
240
260
280
300
320
340 °C

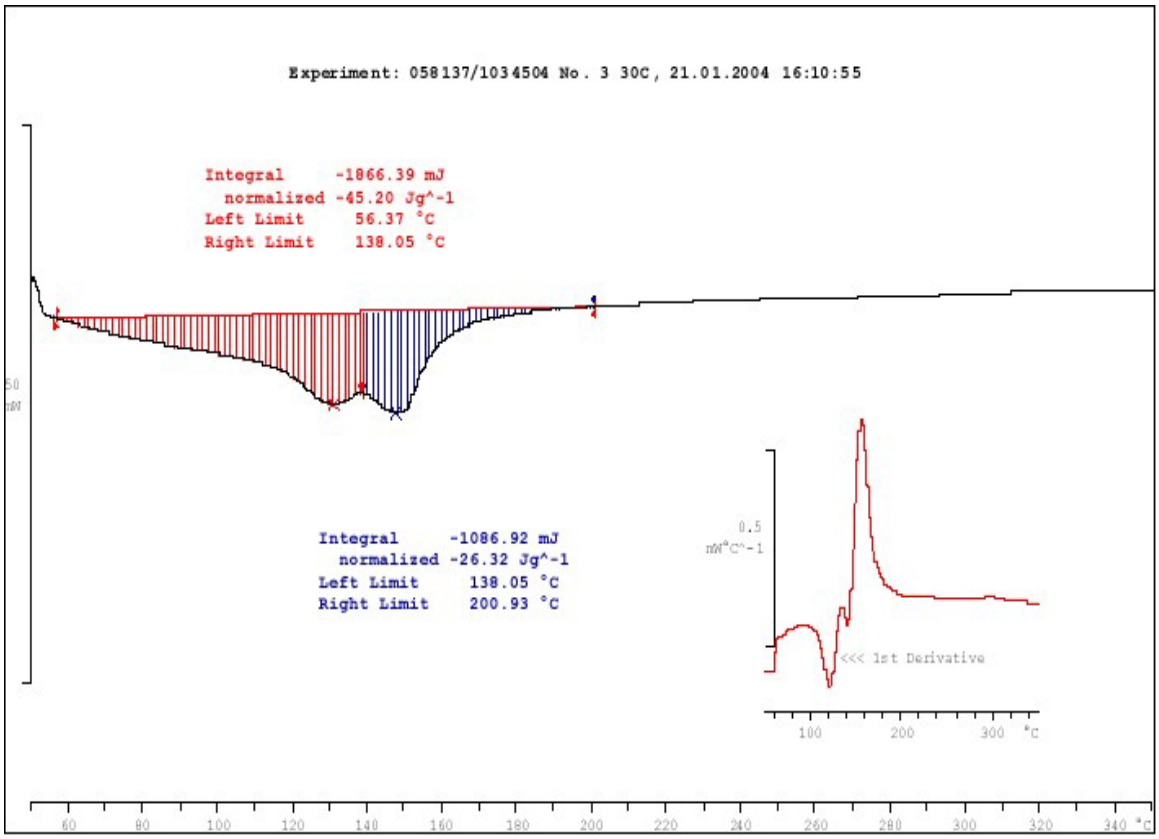
Experiment: 058137/1034504 No. 3 30C, 21.01.2004 16:10:55
Integral -1866.39 mJ
normalized -45.20 Jg^-1
Left Limit 56.37 °C
Right Limit 138.05 °C
Integral -1086.92 mJ
normalized -26.32 Jg^-1
Left Limit 138.05 °C
Right Limit 200.93 °C
0.5
mW°C^-1
<<< 1st Derivative
100
200
300
°C
50
mW
60
80
100
120
140
160
180
200
220
240
260
280
300
320
340 °C

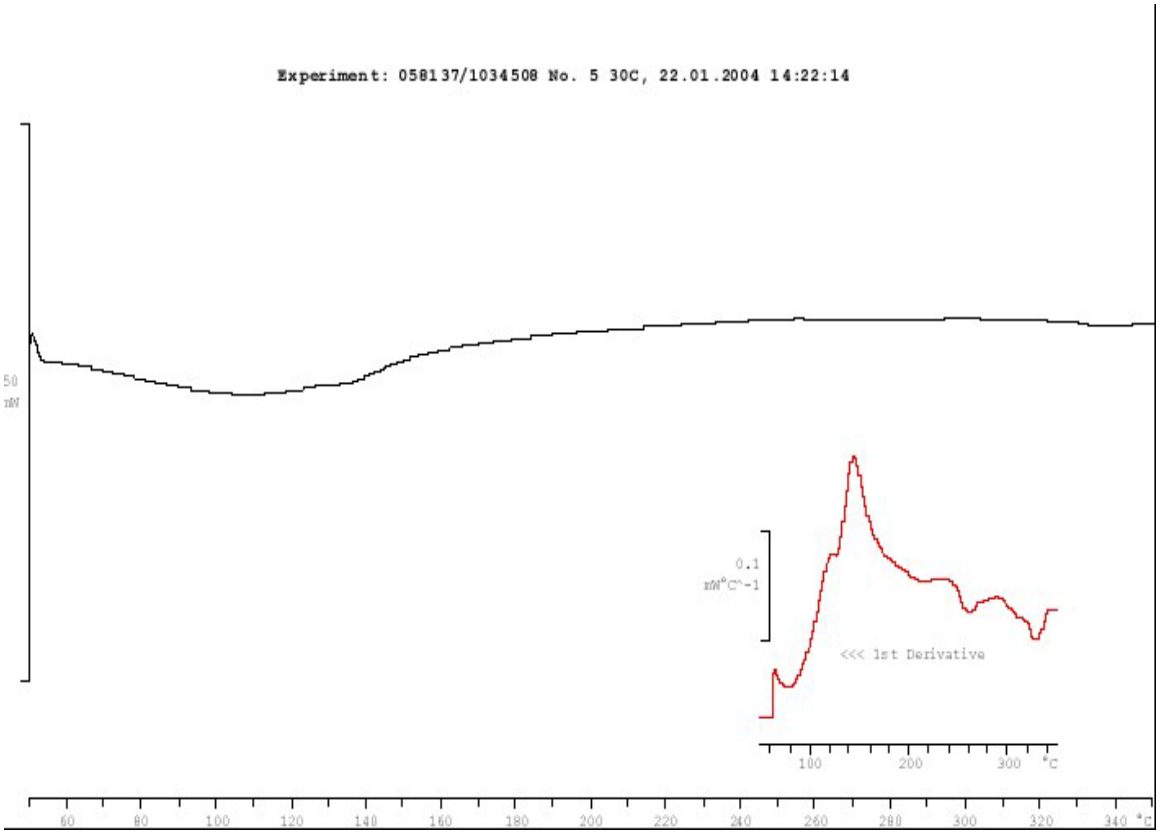
Experiment: 058137/1034508 No. 5 30C, 22.01.2004 14:22:14
0.1
mW°C^-1
<<< 1st Derivative
100
200
300
°C
50
mW
60
80
100
120
140
160
180
200
220
240
260
280
300
320
340 °C

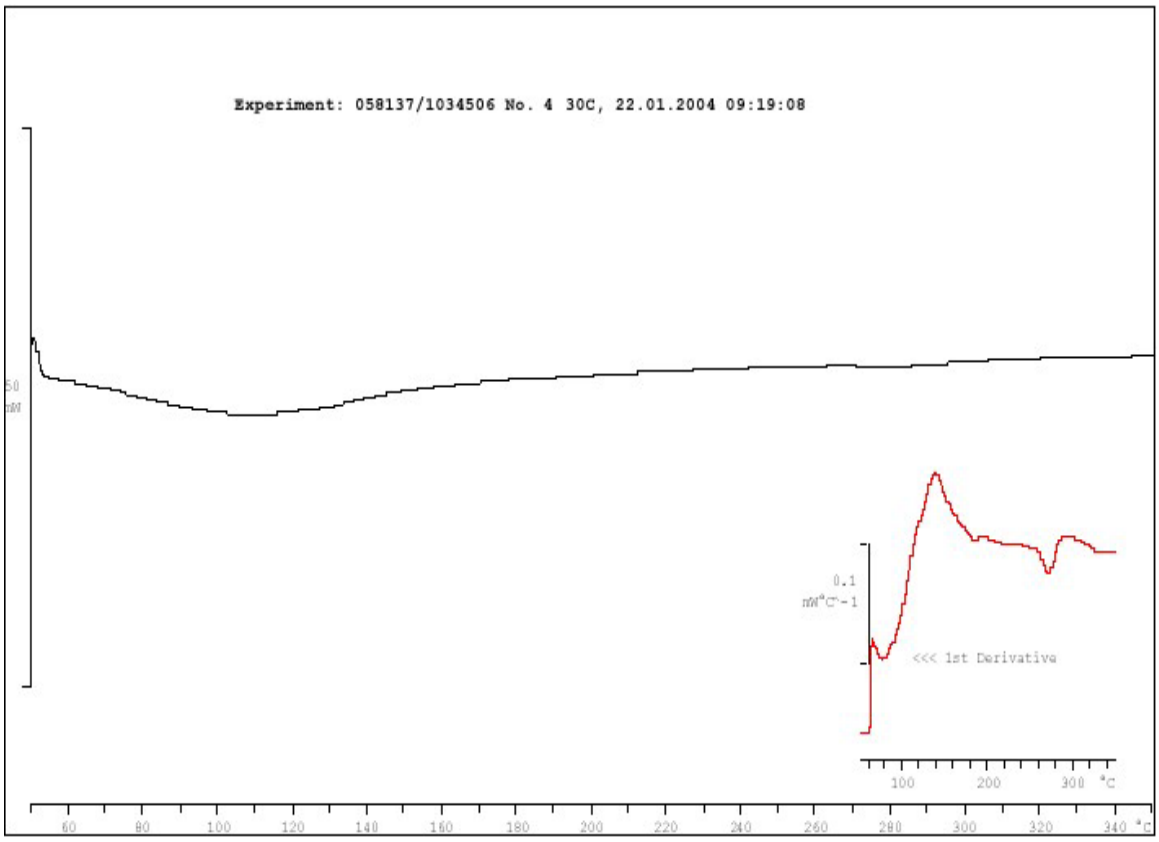
Experiment: 058137/1034506 No. 4 30C, 22.01.2004 09:19:08
50
mW
0.1
mW°C^-1
<<< 1st Derivative
100
200
300 °C
60
80
100
120
140
160
180
200
220
240
260
280
300
320
340 °C

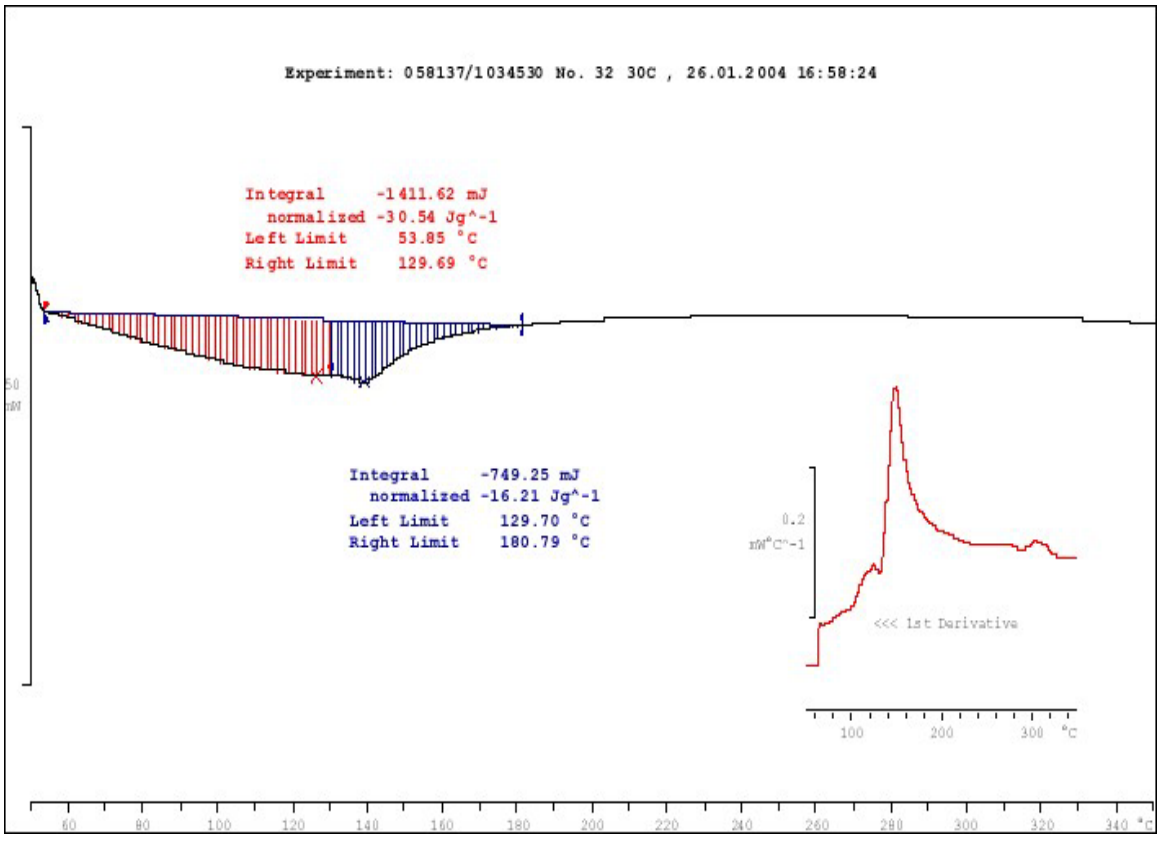
Experiment: 058137/1034530 No. 32 30C , 26.01.2004 16:58:24
Integral -1411.62 mJ
normalized -30.54 Jg^-1
Left Limit 53.85 °C
Right Limit 129.69 °C
50
mW
Integral -749.25 mJ
normalized -16.21 Jg^-1
Left Limit 129.70 °C
Right Limit 180.79 °C
0.2
mW°C^-1
<<< 1st Derivative
100
200
300 °C
60
80
100
120
140
160
180
200
220
240
260
280
300
320
340 °C

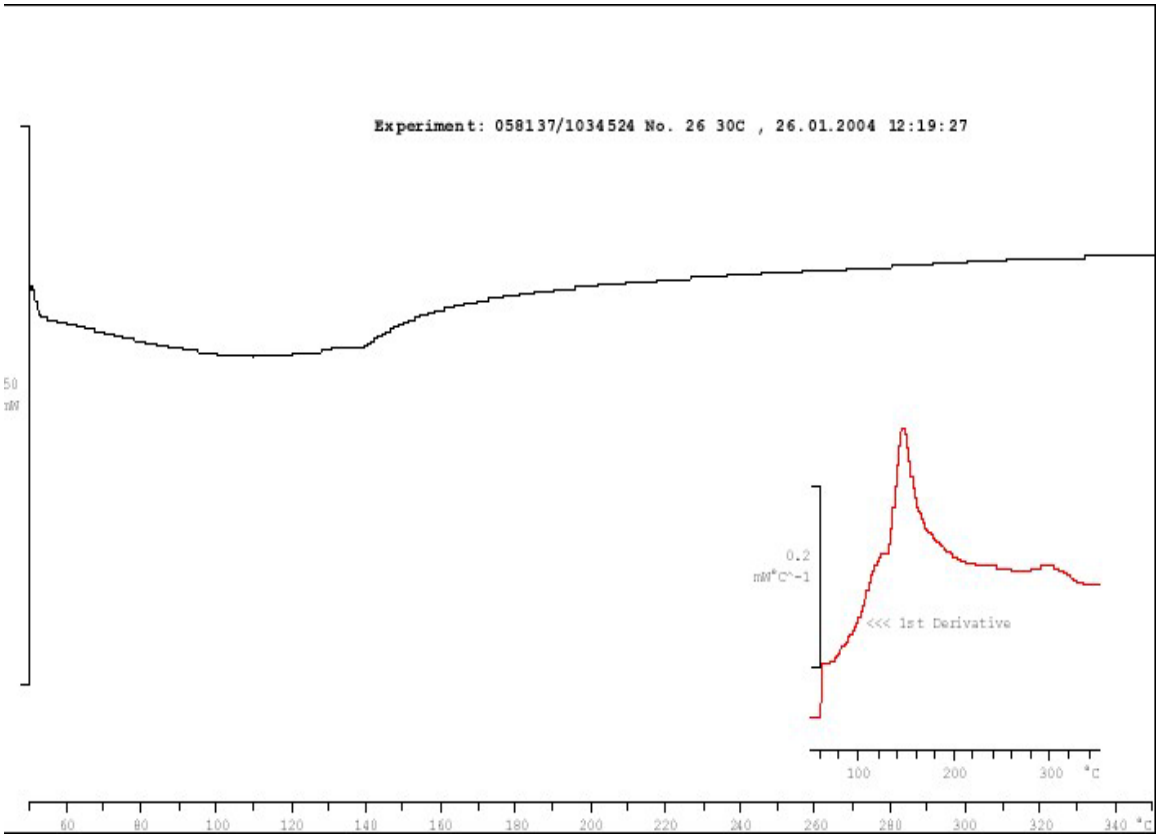
Experiment: 058137/1034524 No. 26 30C , 26.01.2004 12:19:27
50
mW
0.2
mW°C^-1
<<< 1st Derivative
100
200
300
°C
60
80
100
120
140
160
180
200
220
240
260
280
300
320
340 °C

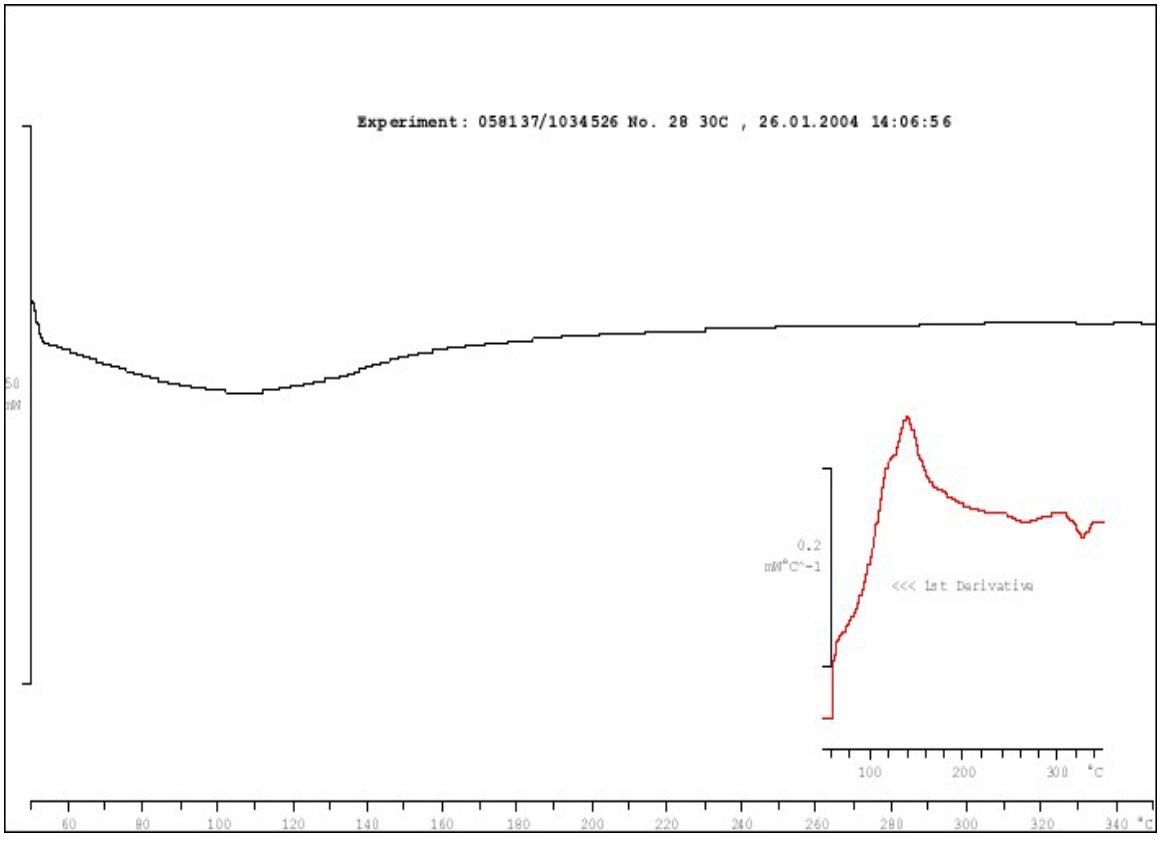
Experiment: 058137/1034526 No. 28 30C , 26.01.2004 14:06:56
50
mW
0.2
mW°C^-1
<<< 1st Derivative
100
200
300
°C
60
80
100
120
140
160
180
200
220
240
260
280
300
320
340 °C

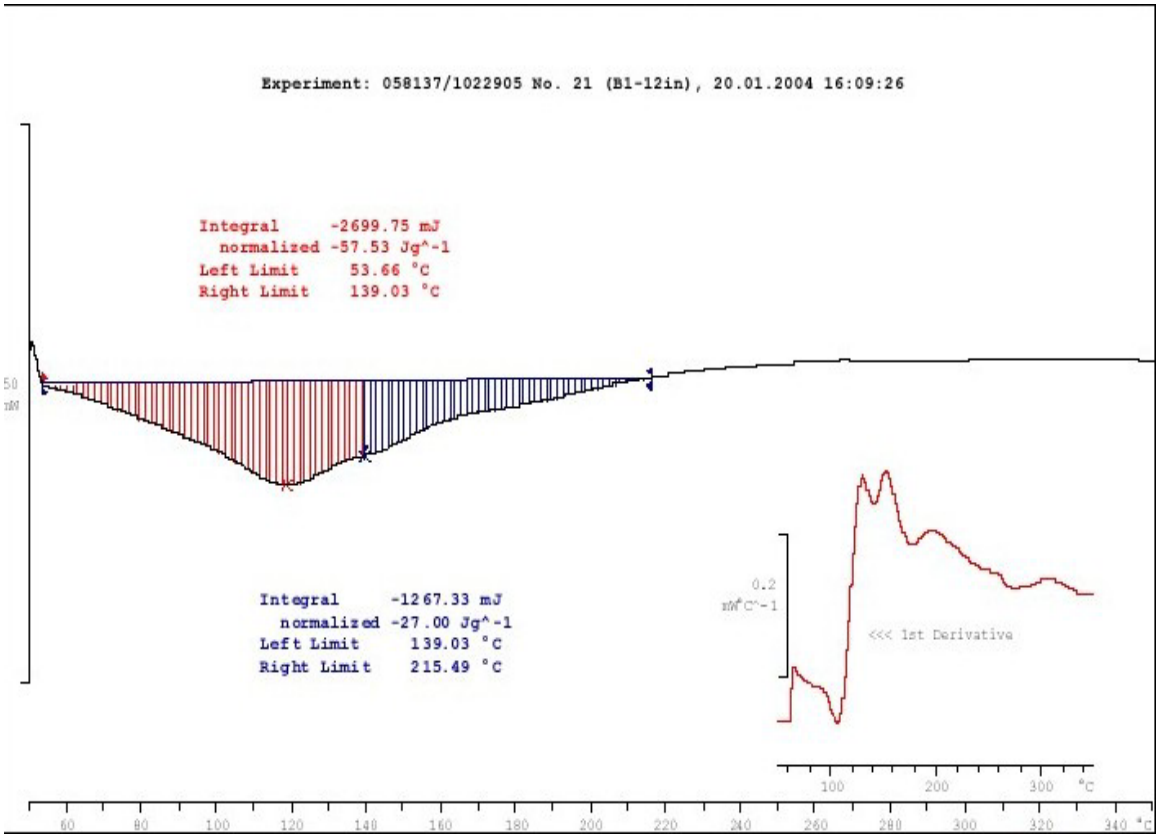
Experiment: 058137/1022905 No. 21 (B1-12in), 20.01.2004 16:09:26
Integral -2699.75 mJ
normalized -57.53 Jg^-1
Left Limit 53.66 °C
Right Limit 139.03 °C
Integral -1267.33 mJ
normalized -27.00 Jg^-1
Left Limit 139.03 °C
Right Limit 215.49 °C
0.2
mW°C^-1
<<< 1st Derivative
100
200
300
°C
60
80
100
120
140
160
180
200
220
240
260
280
300
320
340 °C

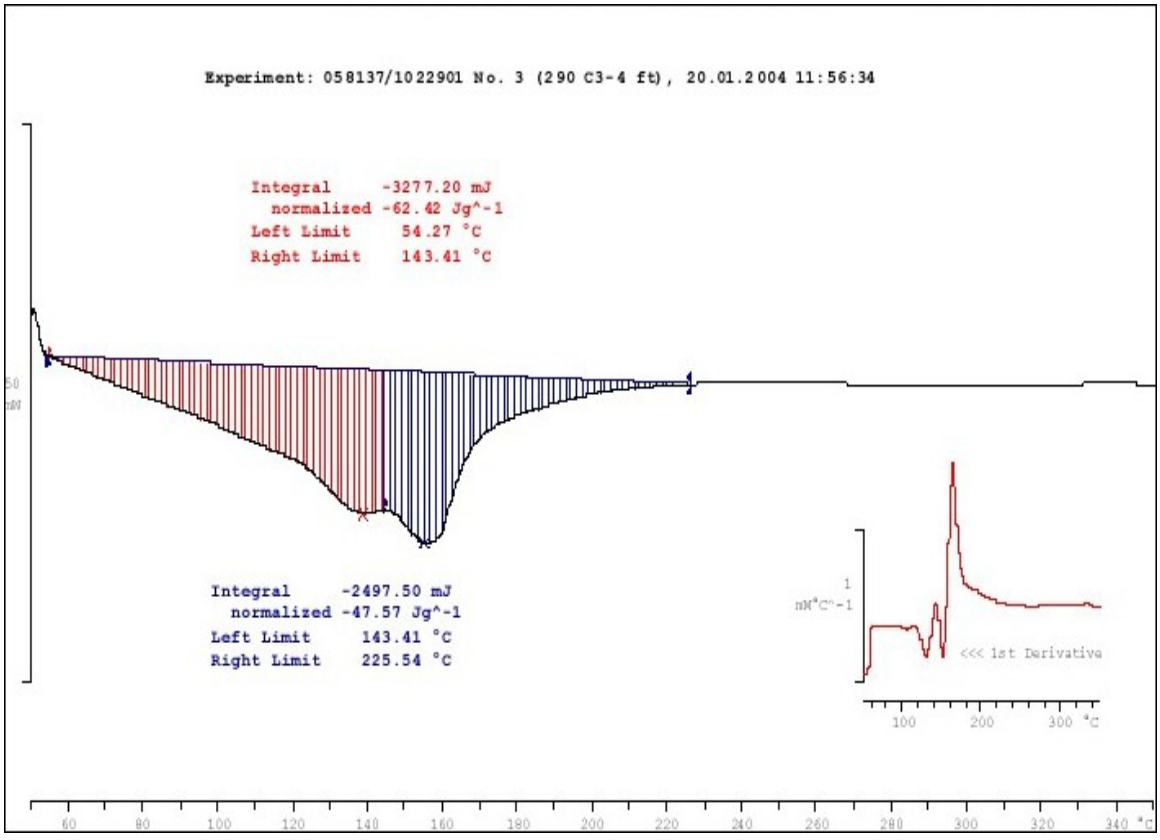
Experiment: 058137/1022901 No. 3 (290 C3-4 ft), 20.01.2004 11:56:34
Integral -3277.20 mJ
normalized -62.42 Jg^-1
Left Limit 54.27 °C
Right Limit 143.41 °C
Integral -2497.50 mJ
normalized -47.57 Jg^-1
Left Limit 143.41 °C
Right Limit 225.54 °C
1
mW°C^-1
<<< 1st Derivative
100
200
300 °C
60
80
100
120
140
160
180
200
220
240
260
280
300
320
340 °C

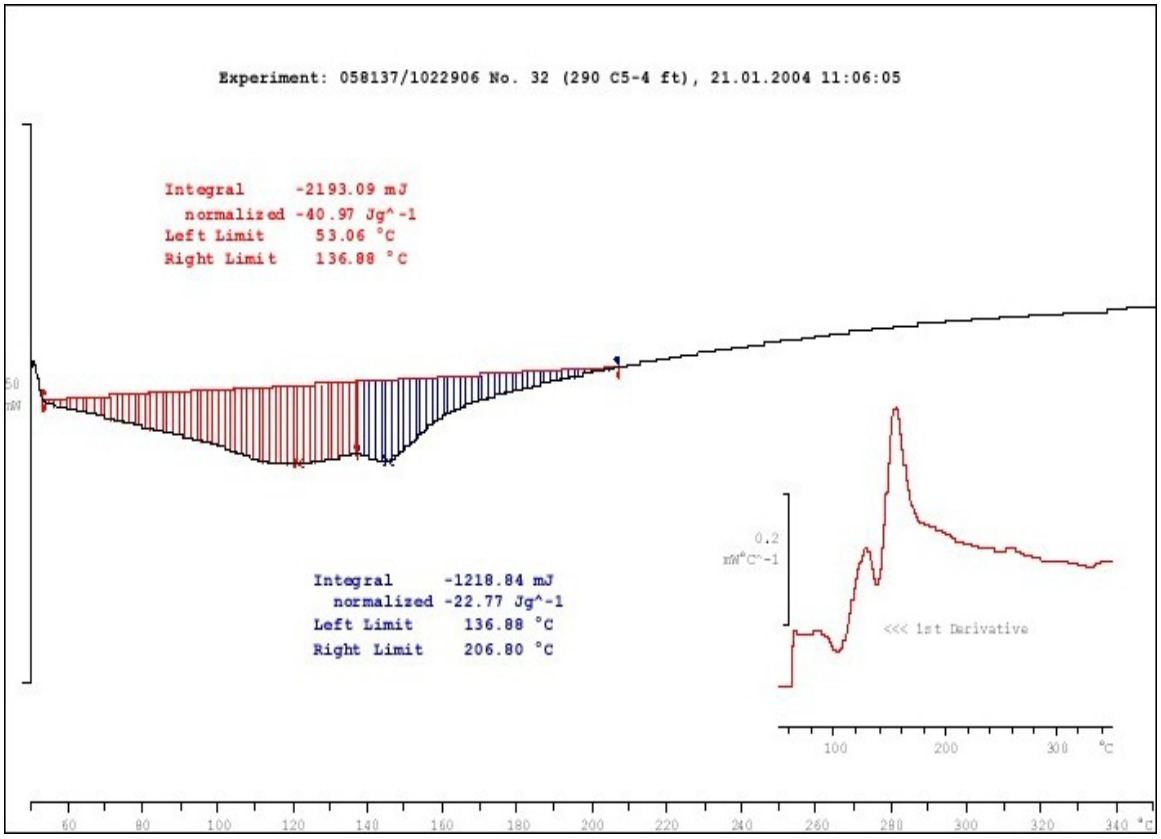
Experiment: 058137/1022906 No. 32 (290 C5-4 ft), 21.01.2004 11:06:05
Integral -2193.09 mJ
normalized -40.97 Jg^-1
Left Limit 53.06 °C
Right Limit 136.88 °C
Integral -1218.84 mJ
normalized -22.77 Jg^-1
Left Limit 136.88 °C
Right Limit 206.80 °C
0.2
mW°C^-1
<<< 1st Derivative
100
200
300
°C
60
80
100
120
140
160
180
200
220
240
260
280
300
320
340 °C

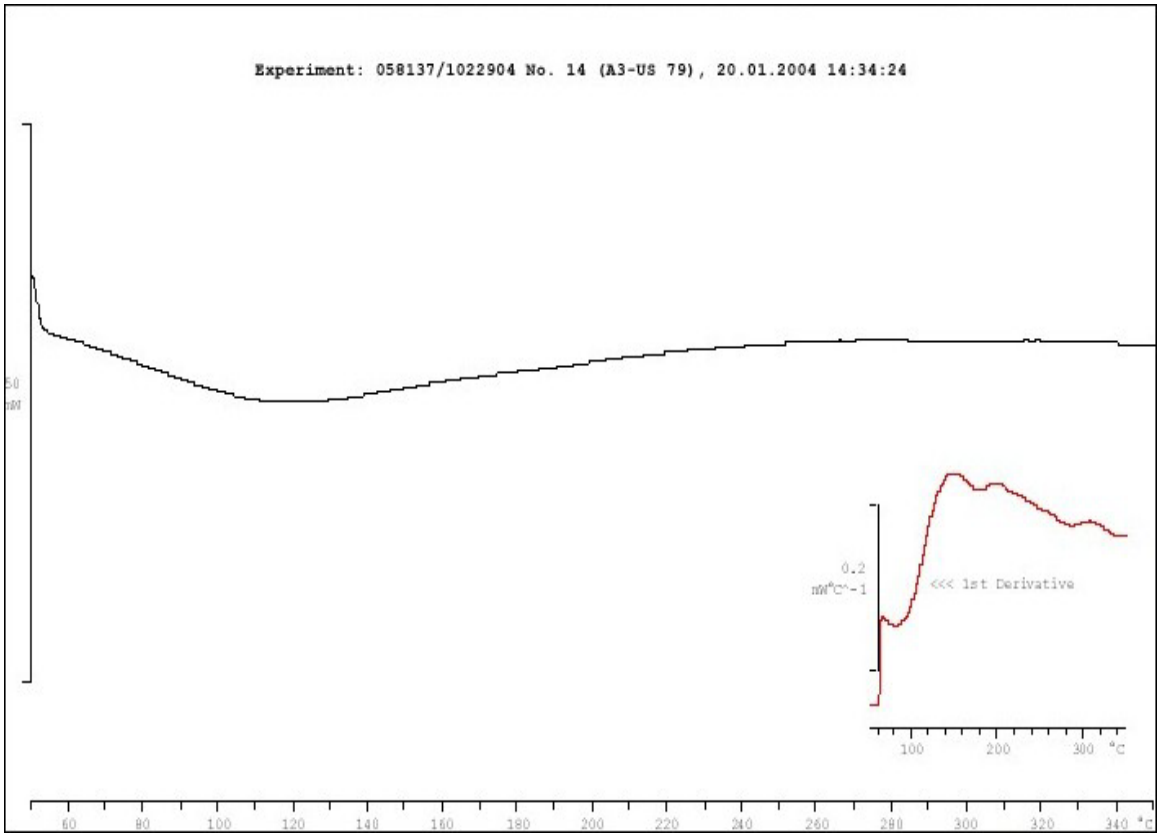
Experiment: 058137/1022904 No. 14 (A3-US 79), 20.01.2004 14:34:24
0.2
mW°C^-1
<<< 1st Derivative
100
200
300
°C
60
80
100
120
140
160
180
200
220
240
260
280
300
320
340 °C

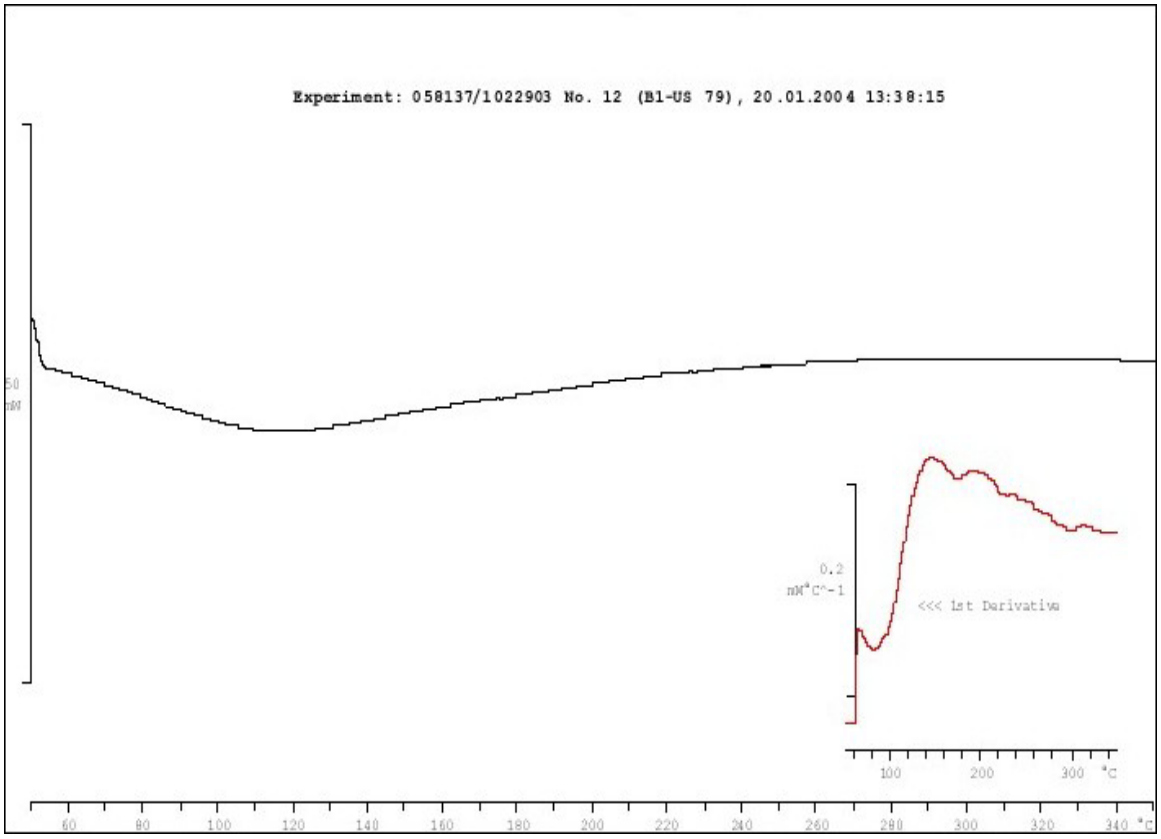
Experiment: 058137/1022903 No. 12 (B1-US 79), 20.01.2004 13:38:15
0.2
mW°C^-1
<<< 1st Derivative
100
200
300 °C
60
80
100
120
140
160
180
200
220
240
260
280
300
320
340 °C

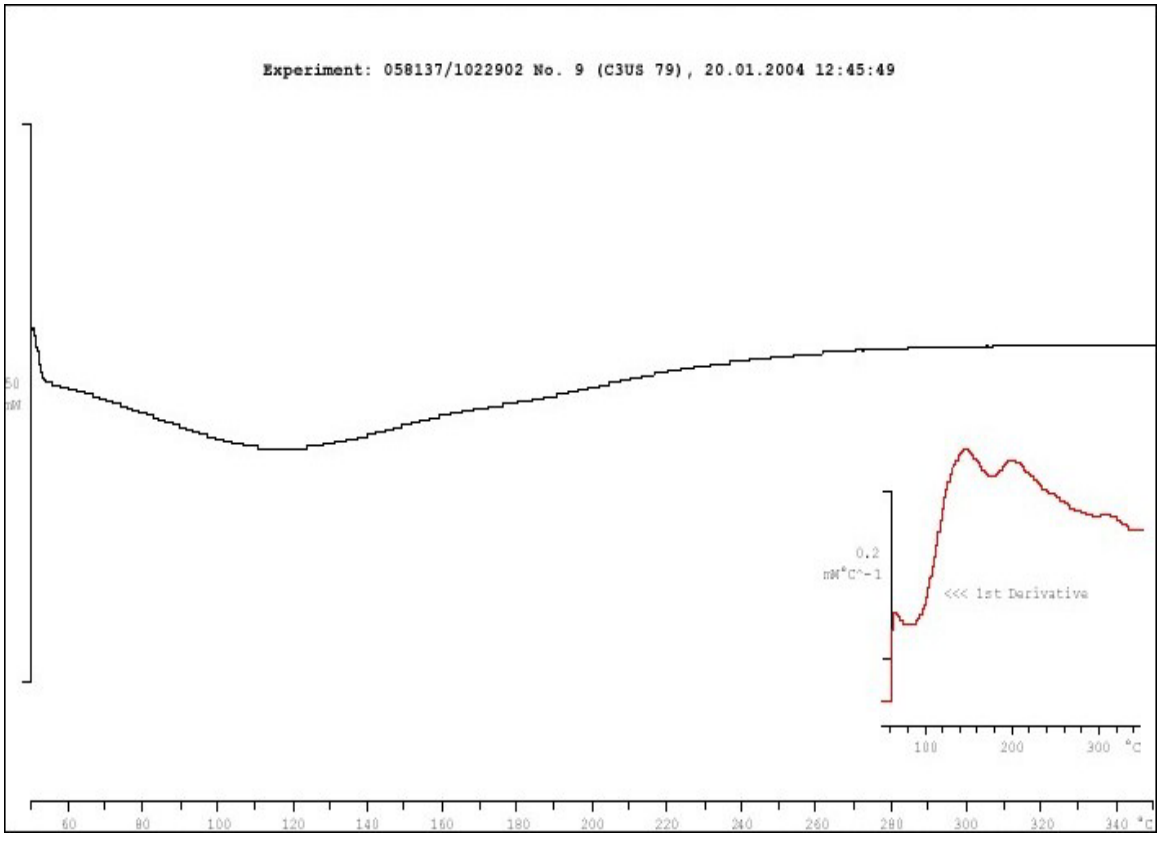
Experiment: 058137/1022902 No. 9 (C3US 79), 20.01.2004 12:45:49
0.2
mW°C^-1
<<< 1st Derivative
100
200
300 °C
60
80
100
120
140
160
180
200
220
240
260
280
300
320
340 °C

APPENDIX C

STABILITY MODELS

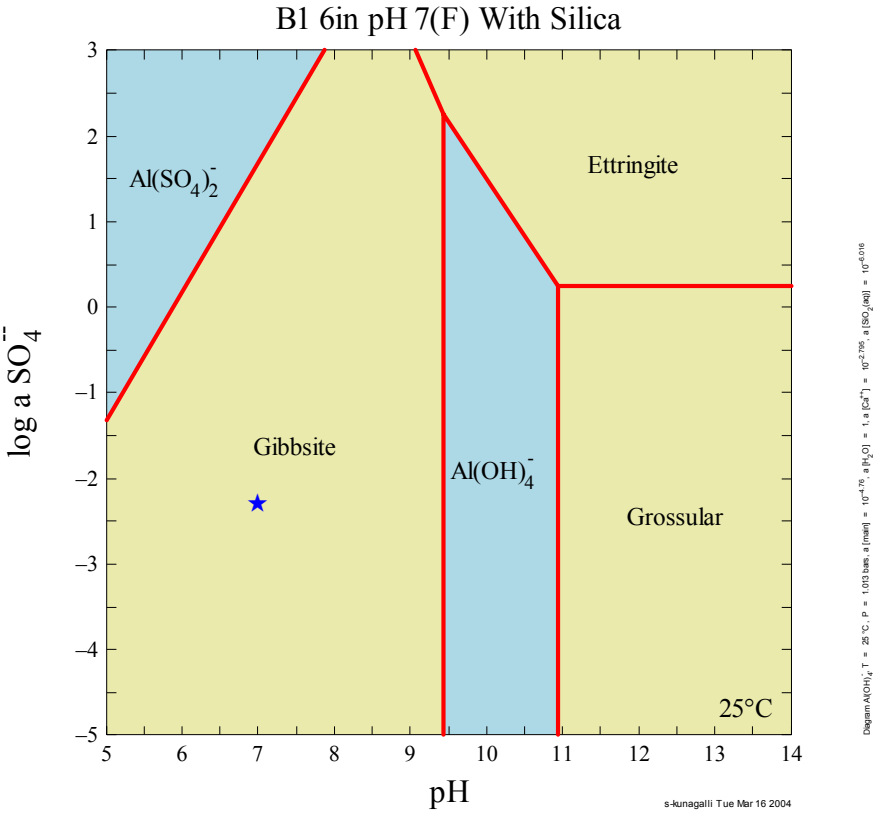
B1 6in pH 7(F) With Silica
log a SO_4^{--}
pH
$Al(SO_4)_2^-$
Gibbsite
$Al(OH)_4^-$
Ettringite
Grossular
25°C
s-kunagalli Tue Mar 16 2004

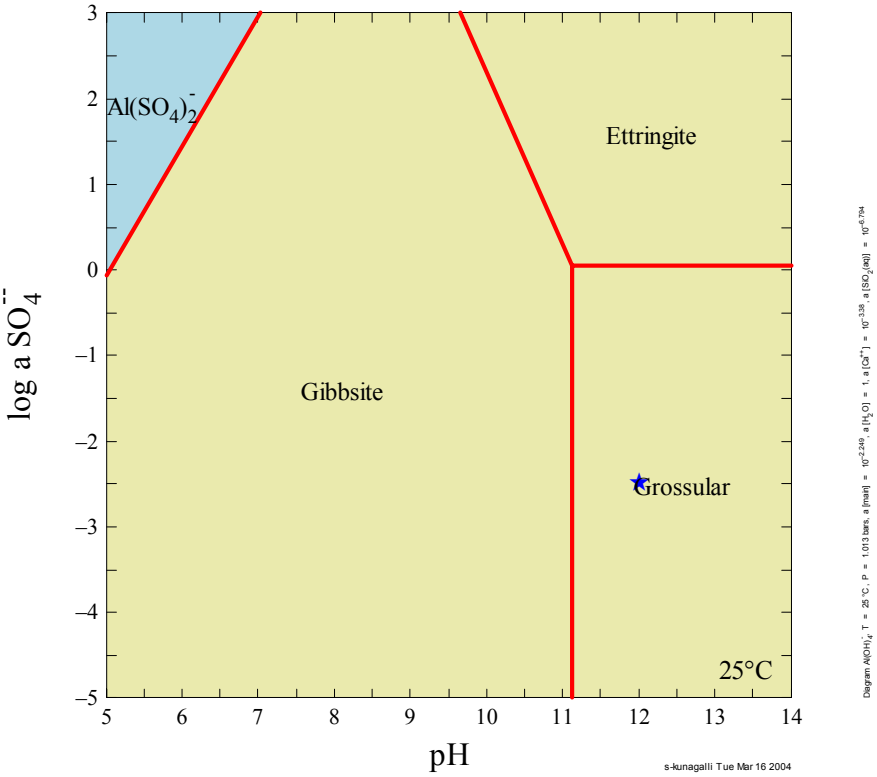
B1 6in pH 12(F) With Silica
log a SO_4^{--}
pH
$Al(SO_4)_2^-$
Gibbsite
Ettringite
Grossular
25°C
s-kunagalli Tue Mar 16 2004

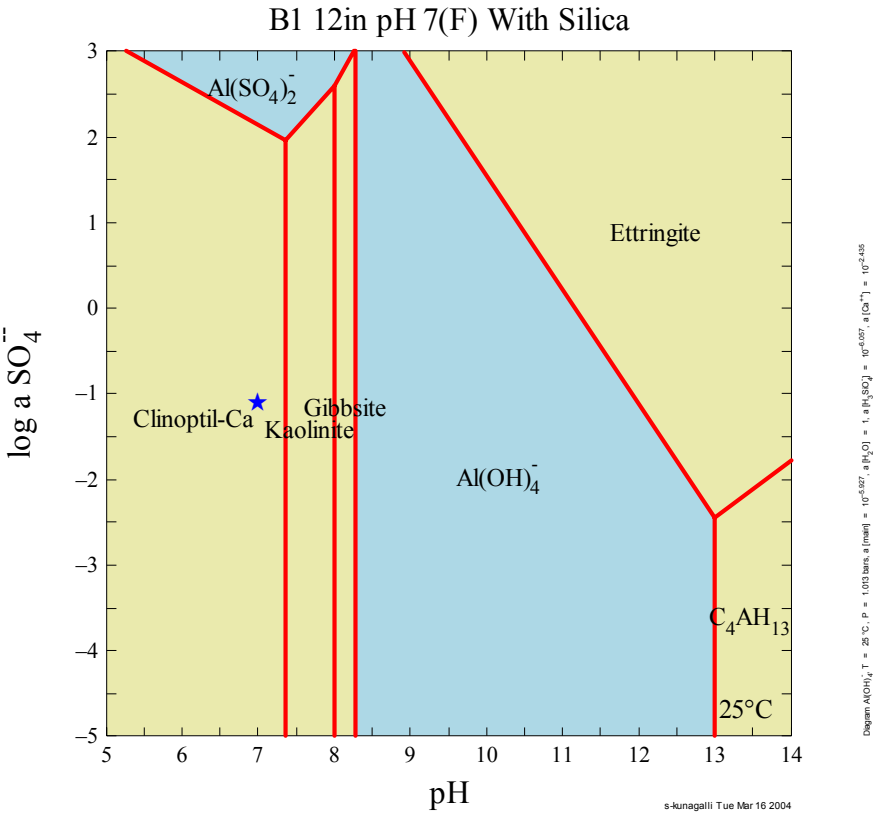
B1 12in pH 7(F) With Silica
Al(SO4)2-
Ettringite
Clinoptil-Ca
Gibbsite
Kaolinite
Al(OH)4-
C4AH13
25°C
log a SO4--
pH
s-kunagalli Tue Mar 16 2004

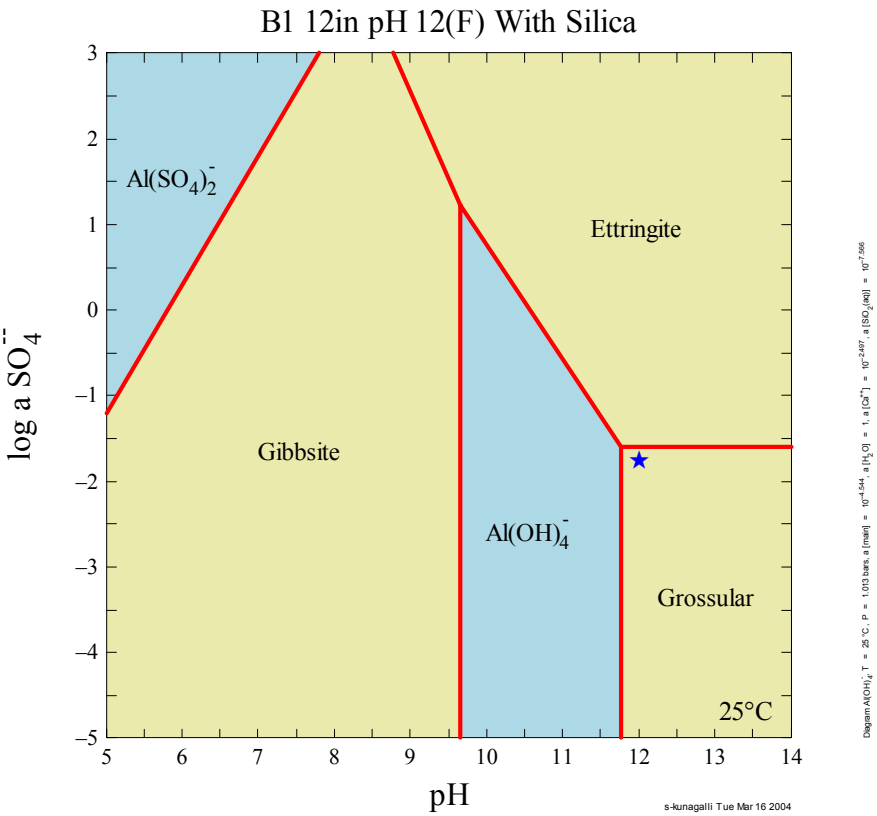
B1 12in pH 12(F) With Silica
Al(SO4)2-
Ettringite
Gibbsite
Al(OH)4-
Grossular
25°C
log a SO4--
pH
s-kunagalli Tue Mar 16 2004

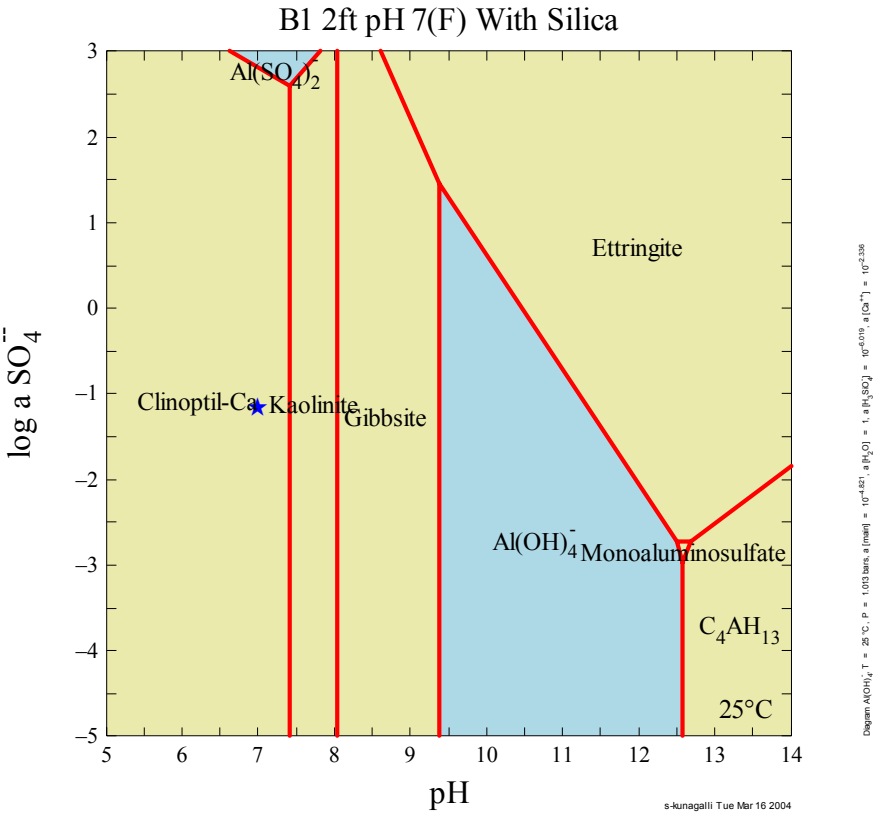
B1 2ft pH 7(F) With Silica
Al(SO4)2
Ettringite
Clinoptil-Ca
Kaolinite
Gibbsite
Al(OH)4
Monoaluminosulfate
C4AH13
25°C
log a SO4
pH
s-kunagalli Tue Mar 16 2004

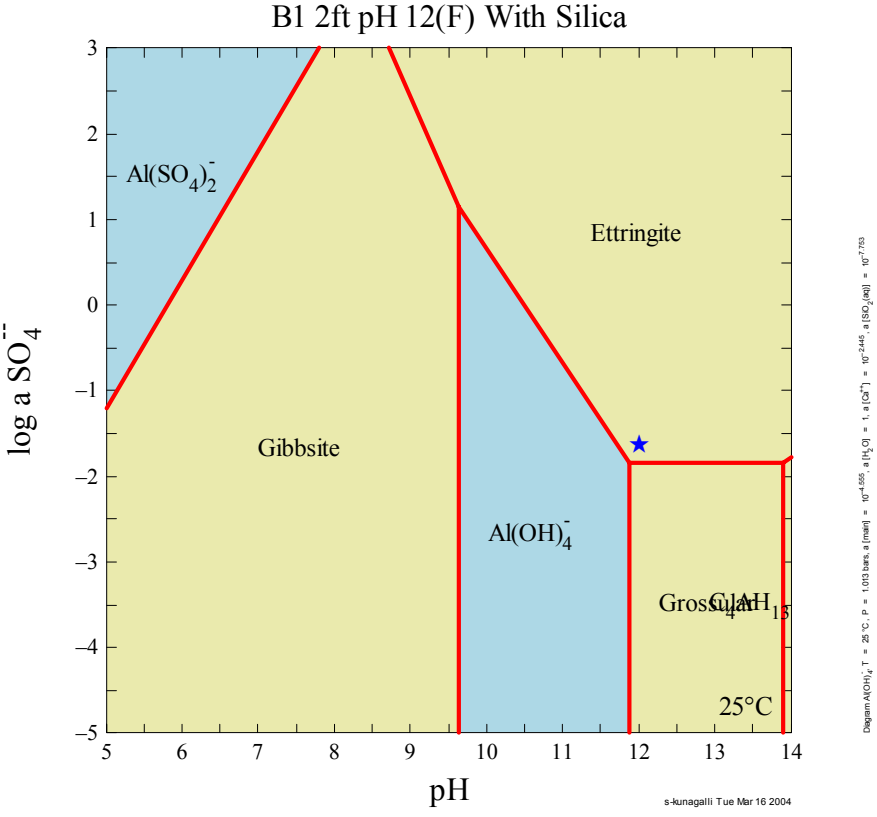
B1 2ft pH 12(F) With Silica
Al(SO4)2
Ettringite
Gibbsite
Al(OH)4
Grossular
C4AH13
25°C
log a SO4
pH
s-kunagalli Tue Mar 16 2004

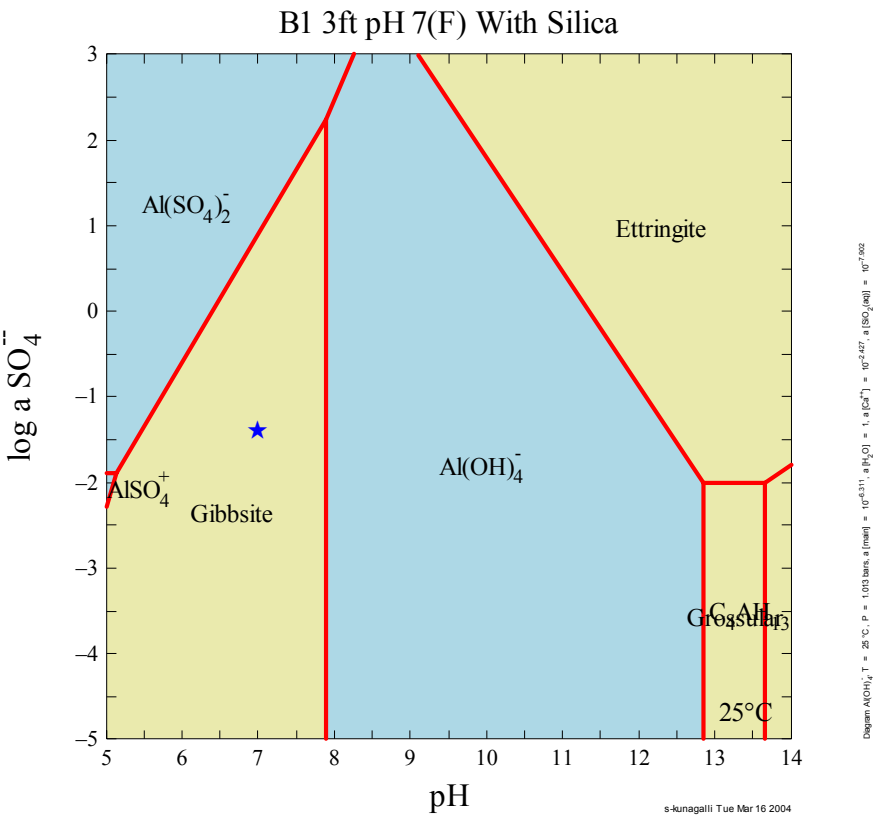
B1 3ft pH 7(F) With Silica
log a SO_4^{--}
pH
$Al(SO_4)_2^-$
$AlSO_4^+$
Gibbsite
$Al(OH)_4^-$
Ettringite
C_3AH_{13}
Grossular
25°C
s-kunagalli Tue Mar 16 2004

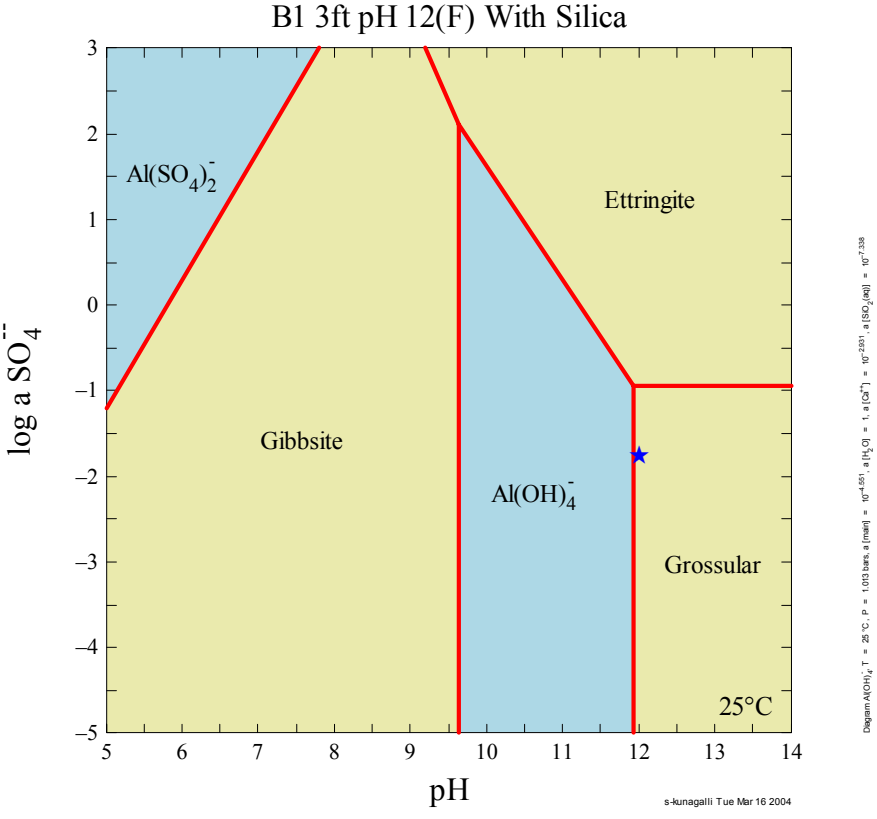
B1 3ft pH 12(F) With Silica
log a SO_4^{--}
pH
$Al(SO_4)_2^-$
Gibbsite
$Al(OH)_4^-$
Ettringite
Grossular
25°C
s-kunagalli Tue Mar 16 2004

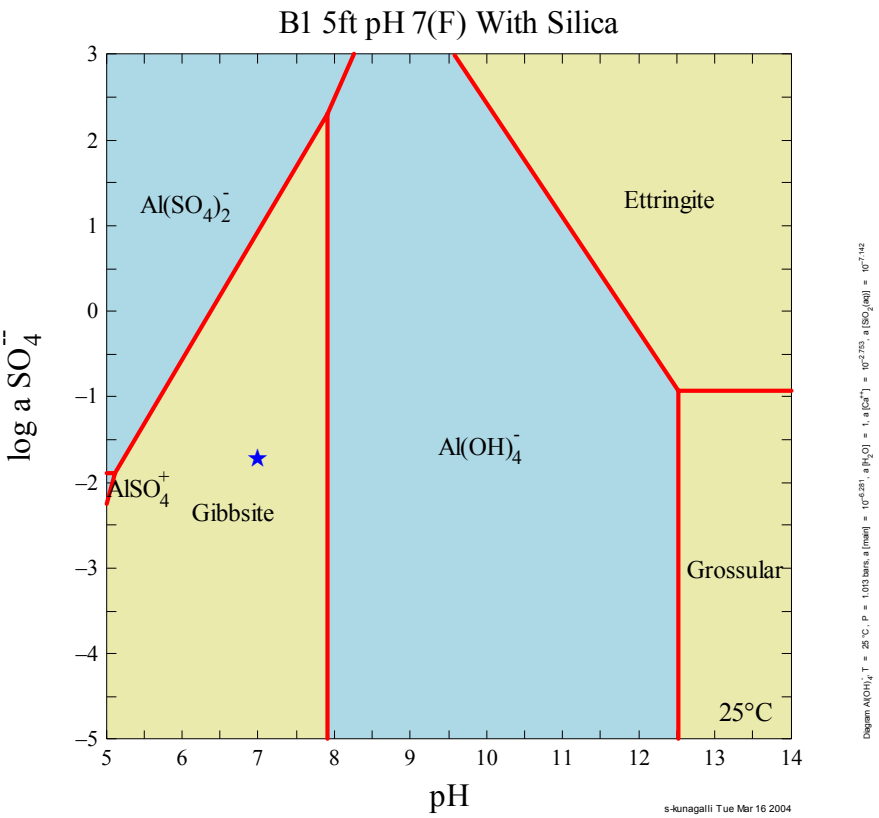
B1 5ft pH 7(F) With Silica
log a SO_4^{--}
pH
$Al(SO_4)_2^-$
$AlSO_4^+$
Gibbsite
$Al(OH)_4^-$
Ettringite
Grossular
25°C
s-kunagalli Tue Mar 16 2004

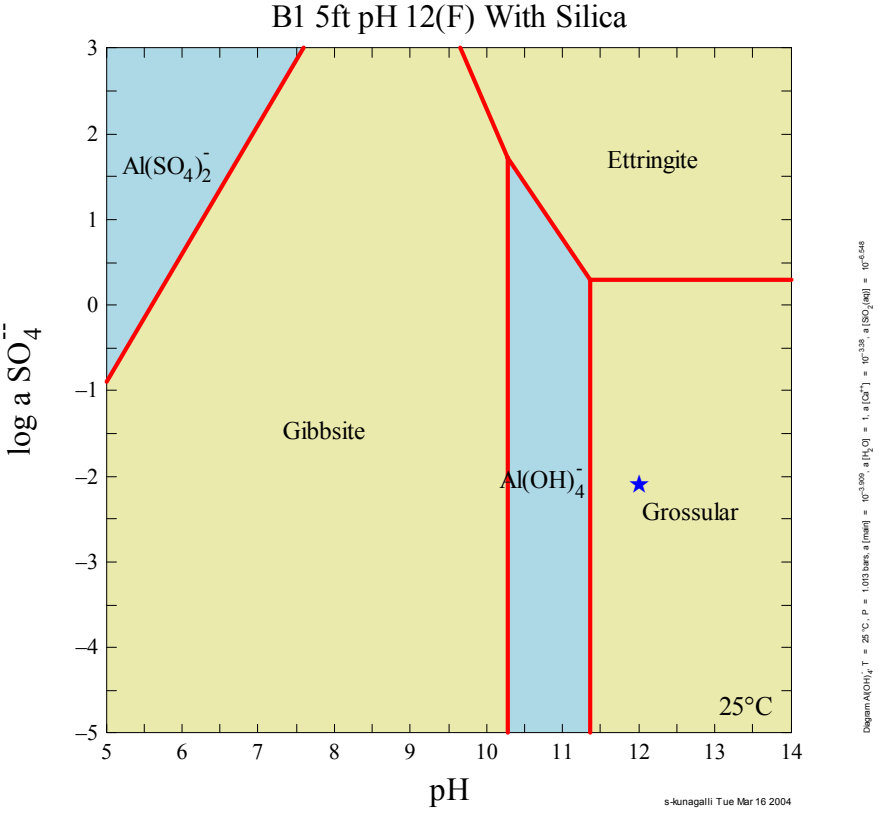
B1 5ft pH 12(F) With Silica
log a SO_4^{--}
pH
$Al(SO_4)_2^-$
Gibbsite
$Al(OH)_4^-$
Ettringite
Grossular
25°C
s-kunagalli Tue Mar 16 2004

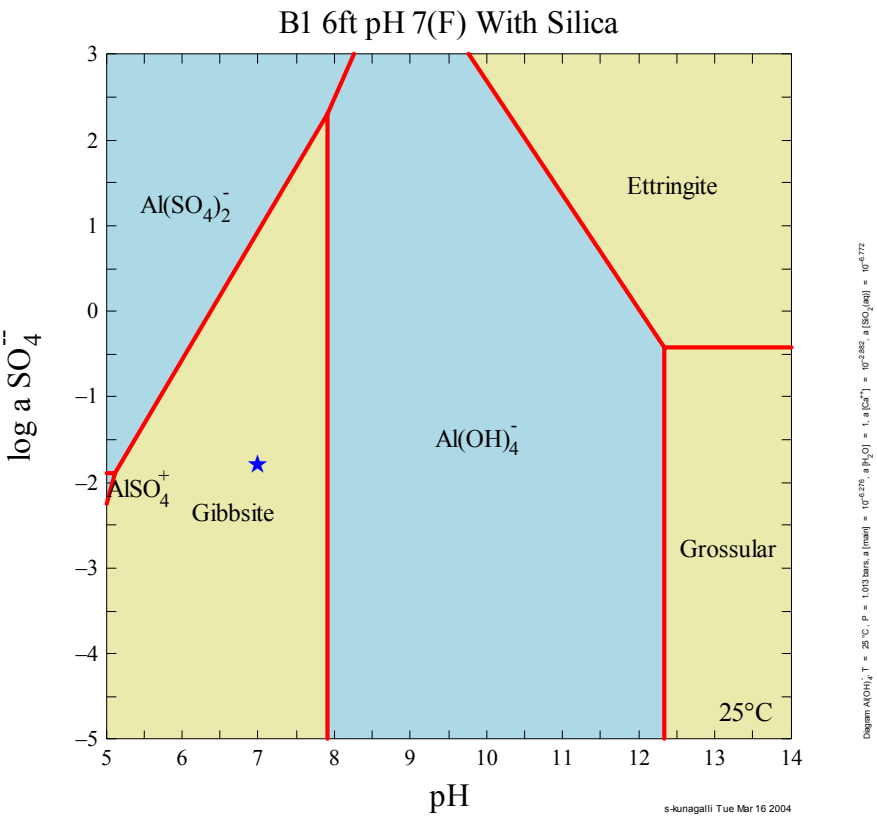
B1 6ft pH 7(F) With Silica
log a SO_4^{--}
pH
$Al(SO_4)_2^-$
Ettringite
$Al(OH)_4^-$
$AlSO_4^+$
Gibbsite
Grossular
25°C
s-kunagalli Tue Mar 16 2004

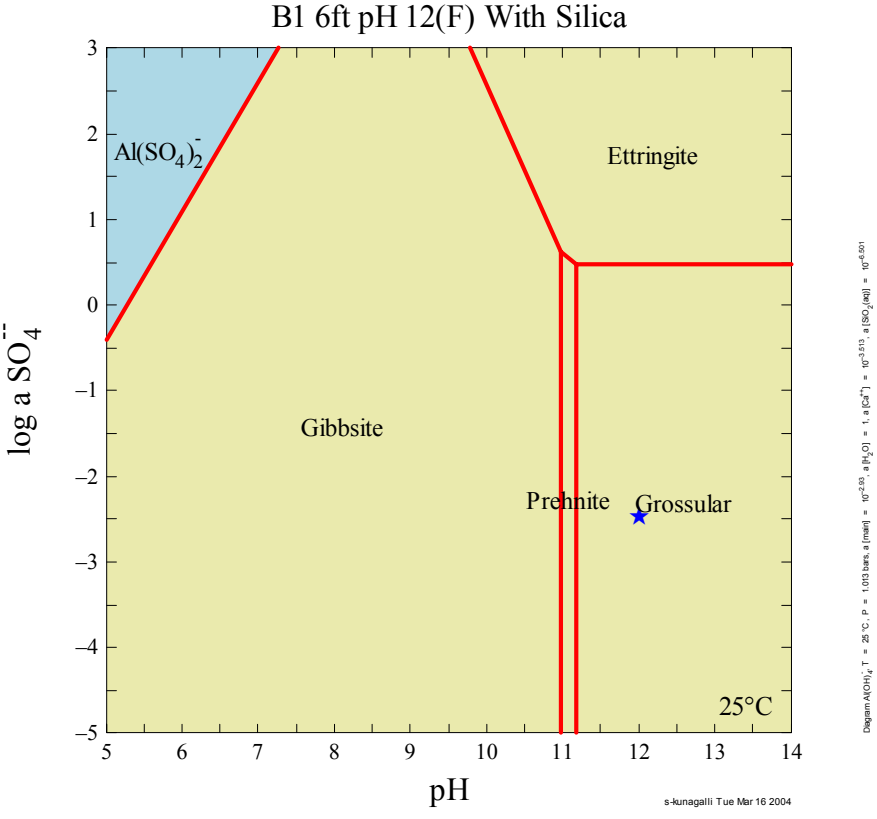
B1 6ft pH 12(F) With Silica
log a SO_4^{--}
pH
$Al(SO_4)_2^-$
Ettringite
Gibbsite
Prehnite
Grossular
25°C
s-kunagalli Tue Mar 16 2004

B1 7.5ft pH 7(F) With Silica

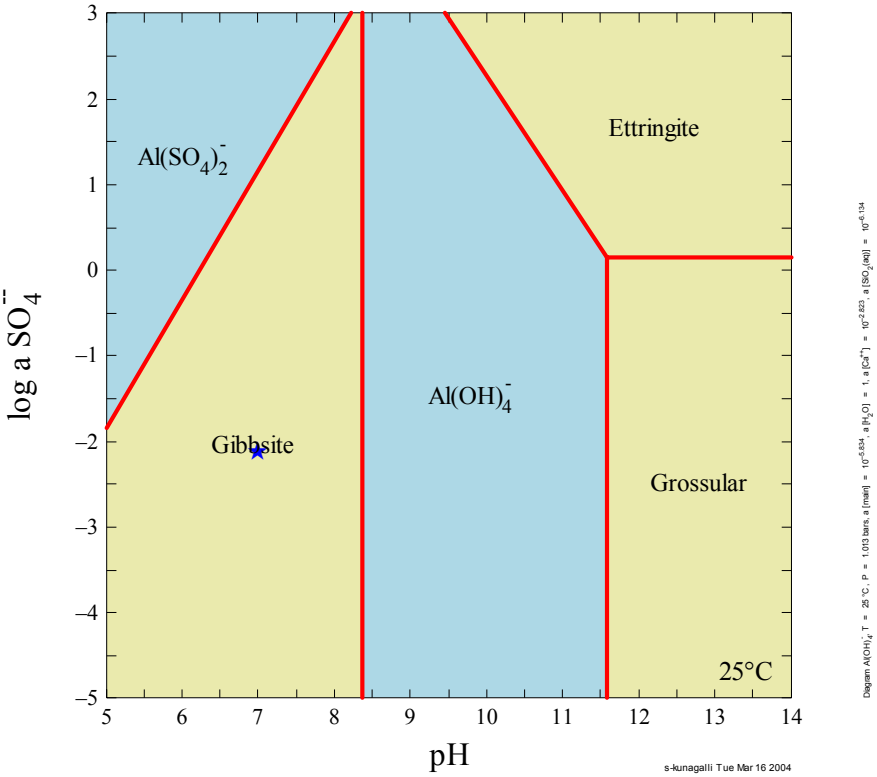

B1 7.5ft pH 12(F) With Silica

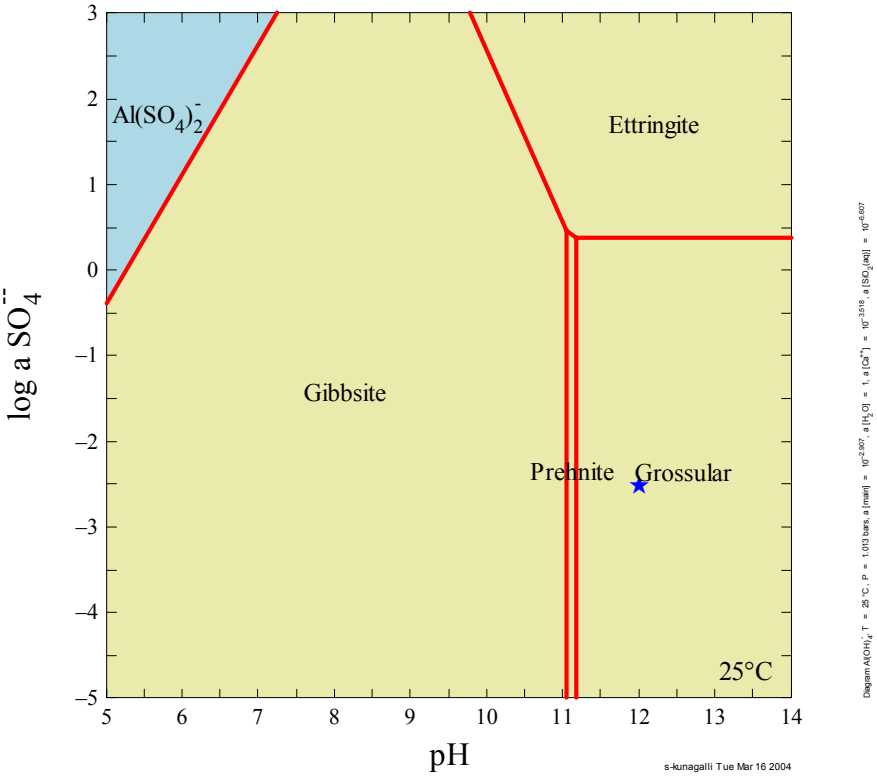

B1 10ft pH 7(F) With Silica

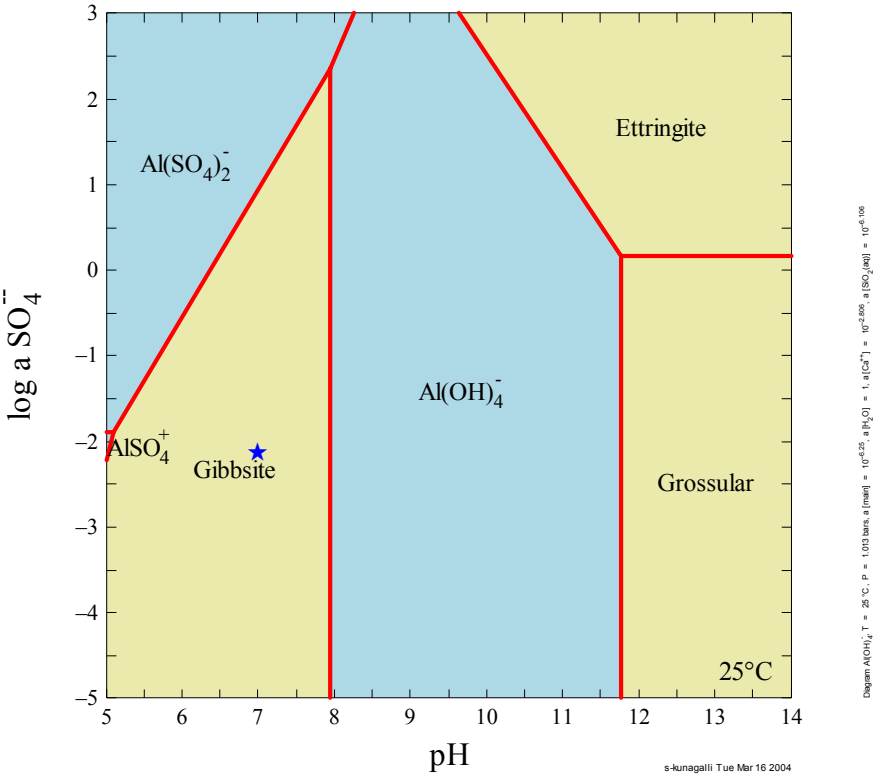

B1 10ft pH 12(F) With Silica

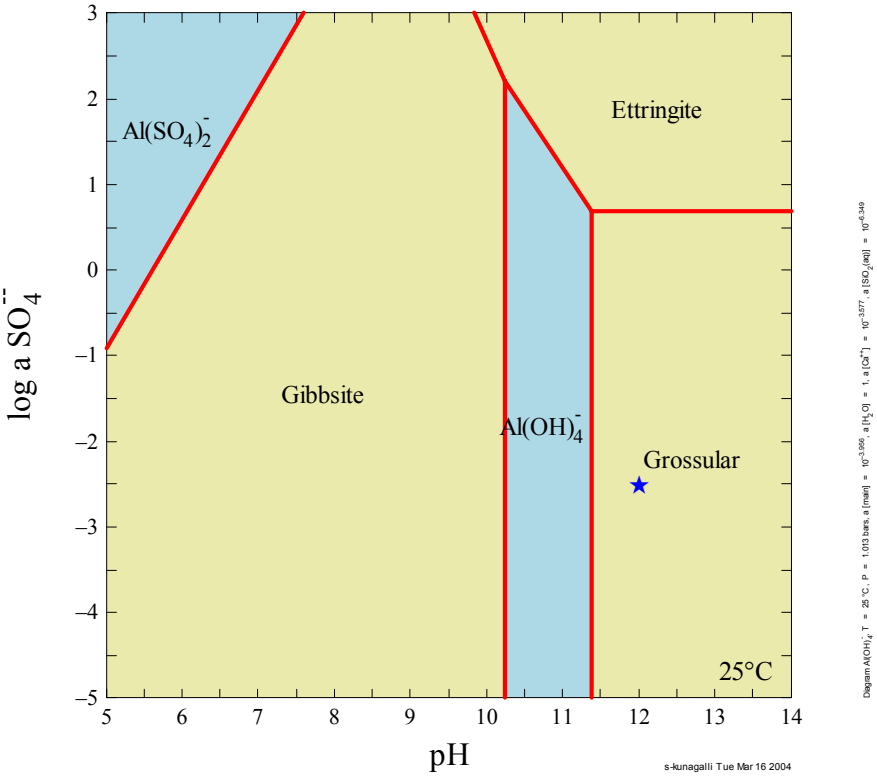

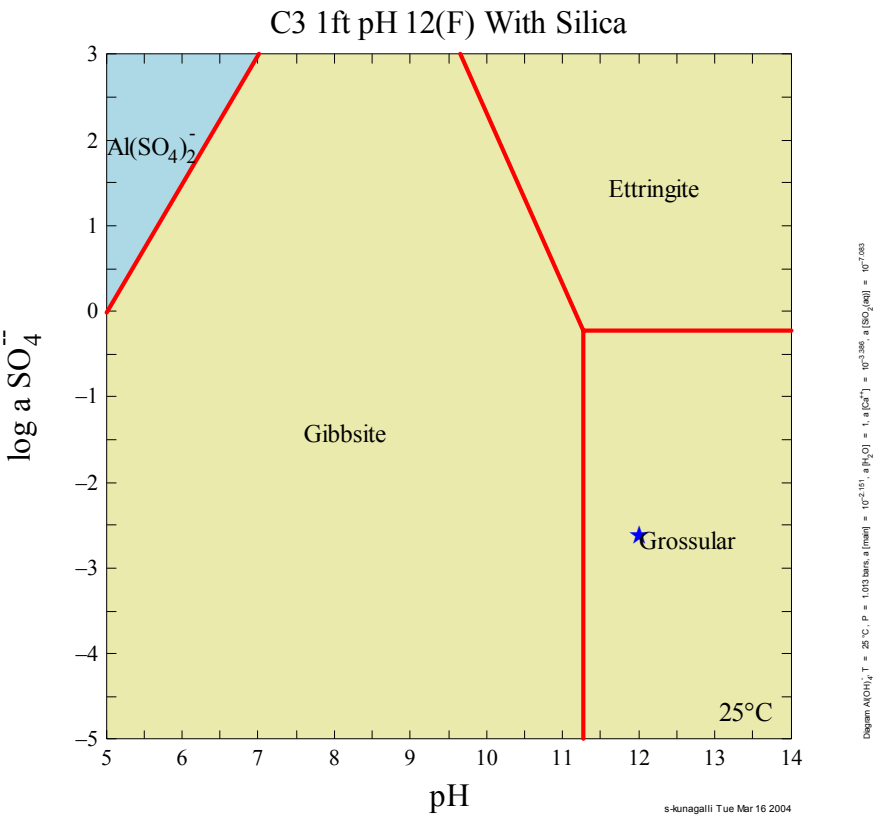
C3 1ft pH 12(F) With Silica
Al(SO4)2-
Ettringite
Gibbsite
Grossular
25°C
log a SO4--
pH
s-kunagalli Tue Mar 16 2004

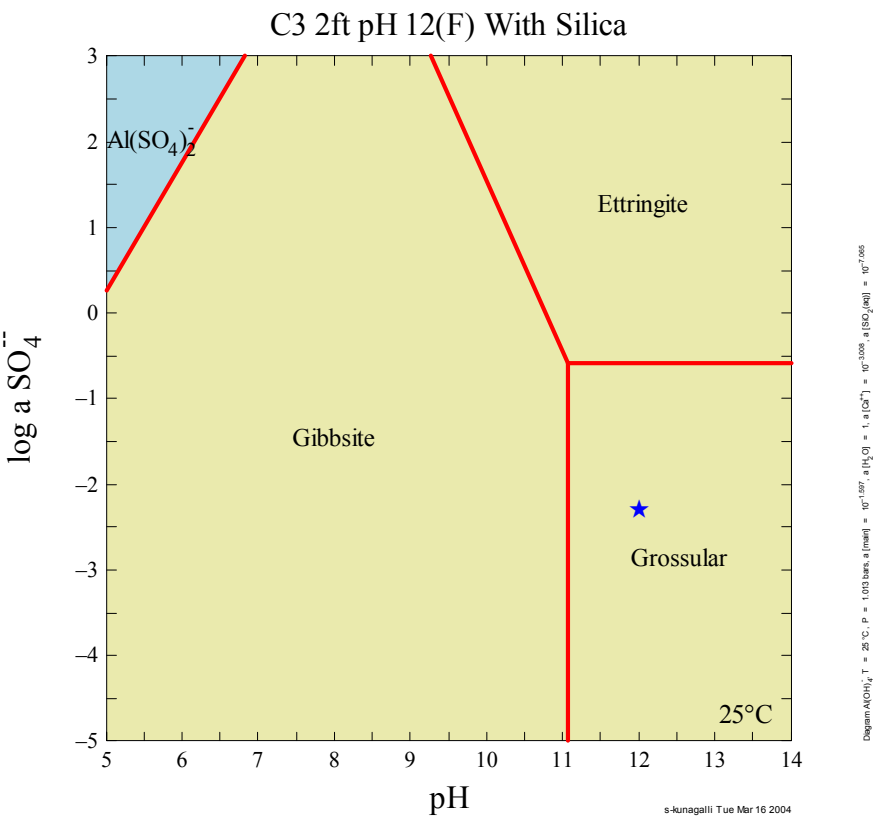
C3 2ft pH 12(F) With Silica
Al(SO4)2-
Ettringite
Gibbsite
Grossular
25°C
log a SO4--
pH
s-kunagalli Tue Mar 16 2004

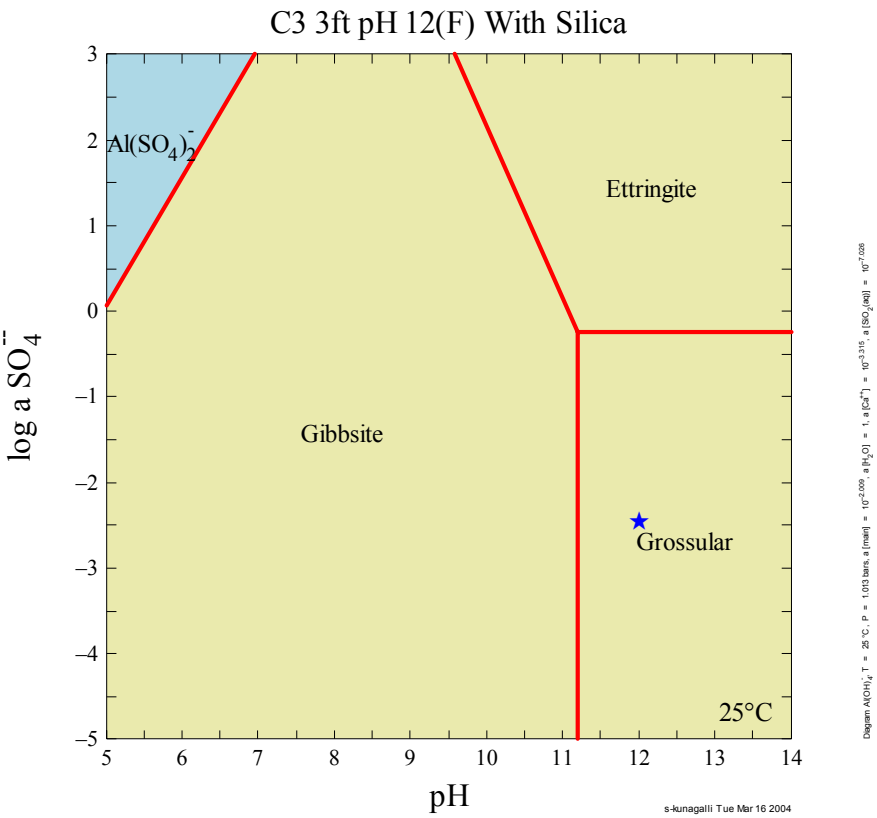
C3 3ft pH 12(F) With Silica
log a SO_4^{--}
pH
$Al(SO_4)_2^-$
Ettringite
Gibbsite
Grossular
25°C
s-kunagalli Tue Mar 16 2004

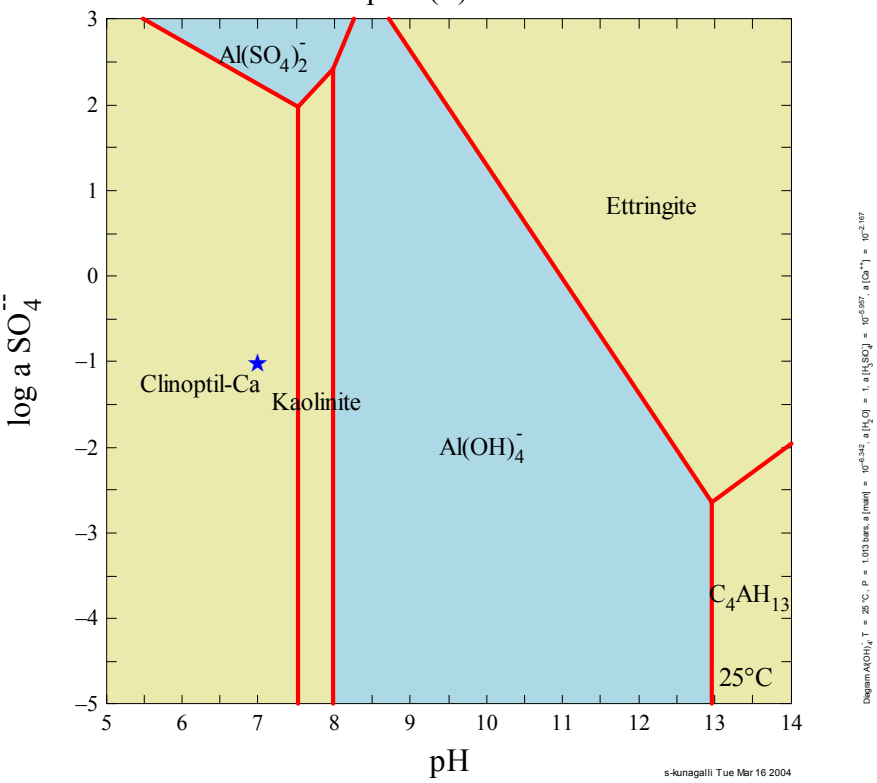
C3 4ft pH 7(F) With Silica
log a SO_4^{--}
pH
$Al(SO_4)_2^-$
Ettringite
Clinoptil-Ca
Kaolinite
$Al(OH)_4^-$
C_4AH_{13}
25°C
s-kunagalli Tue Mar 16 2004

C3 4ft pH 12(F) With Silica

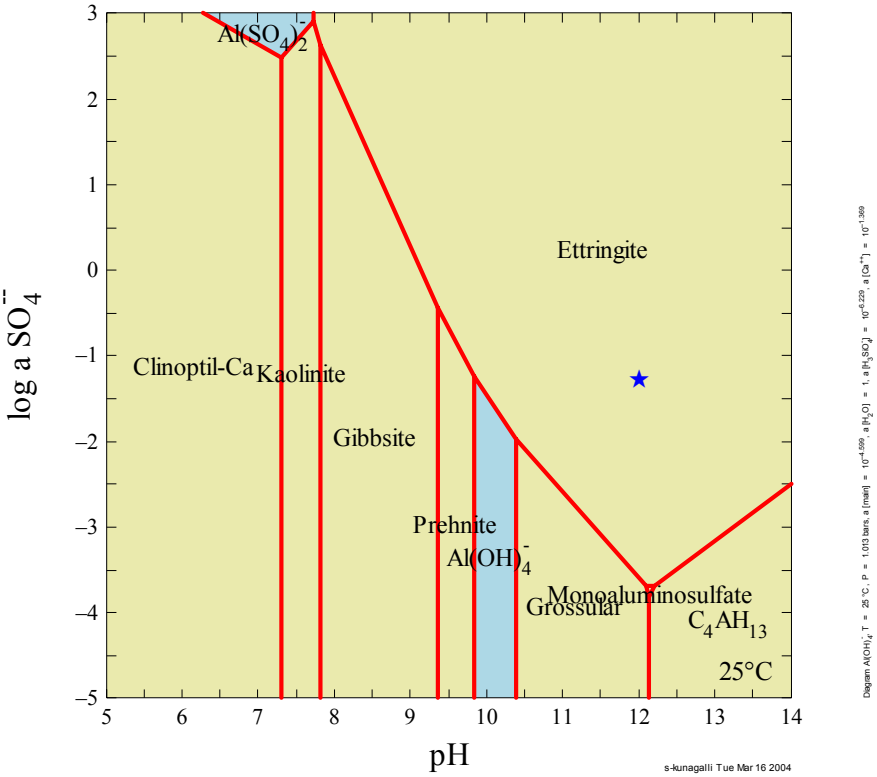

C3 5ft pH 7(F) With Silica

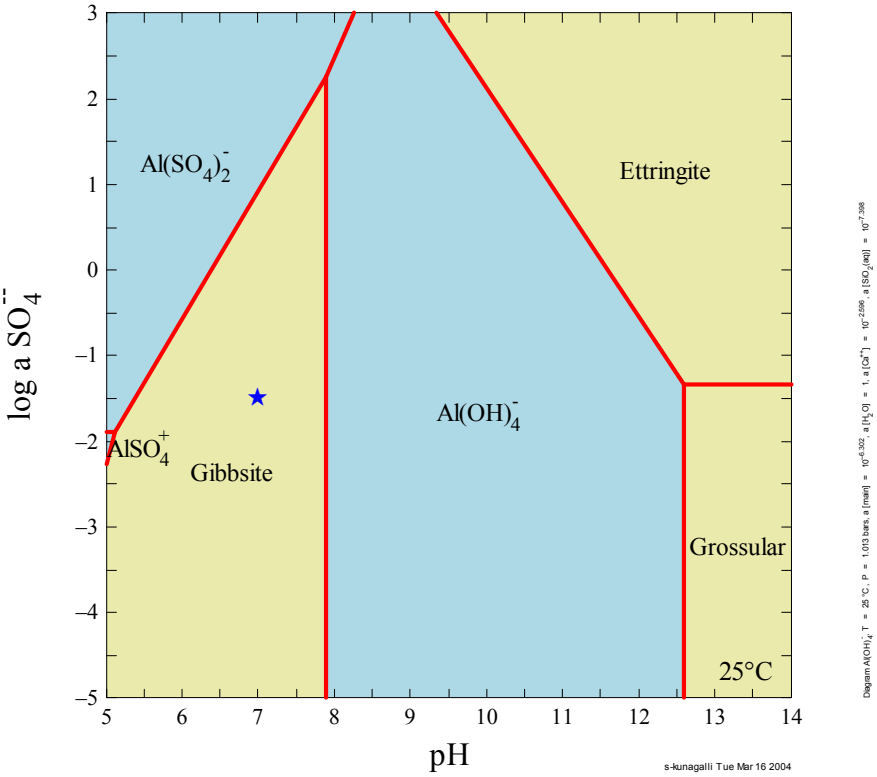

C3 5ft pH 12(F) With Silica

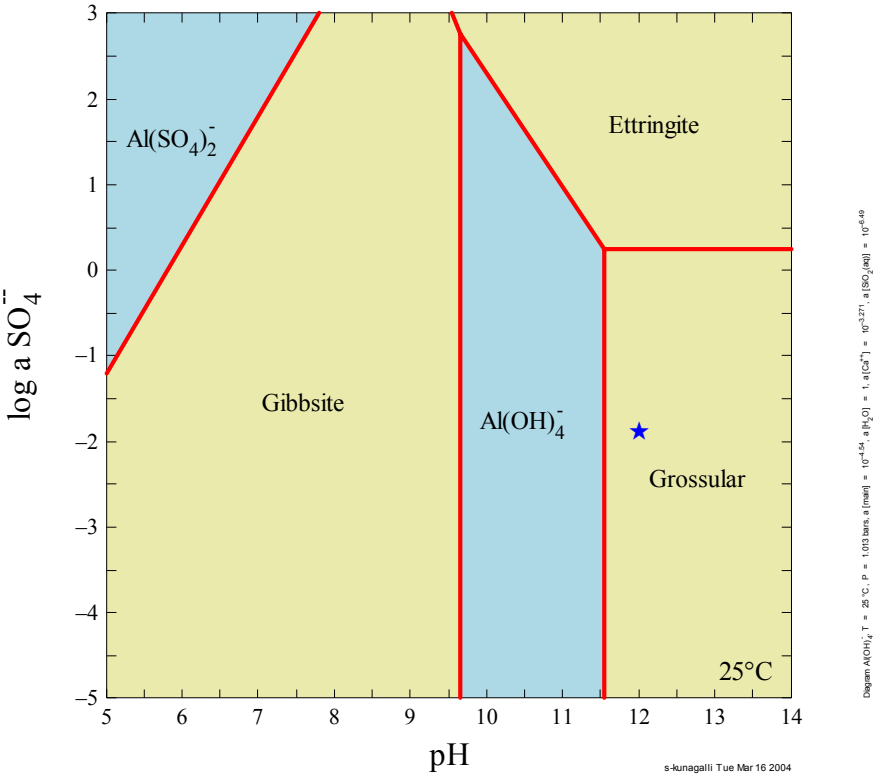

C3 7ft pH 7(F) With Silica

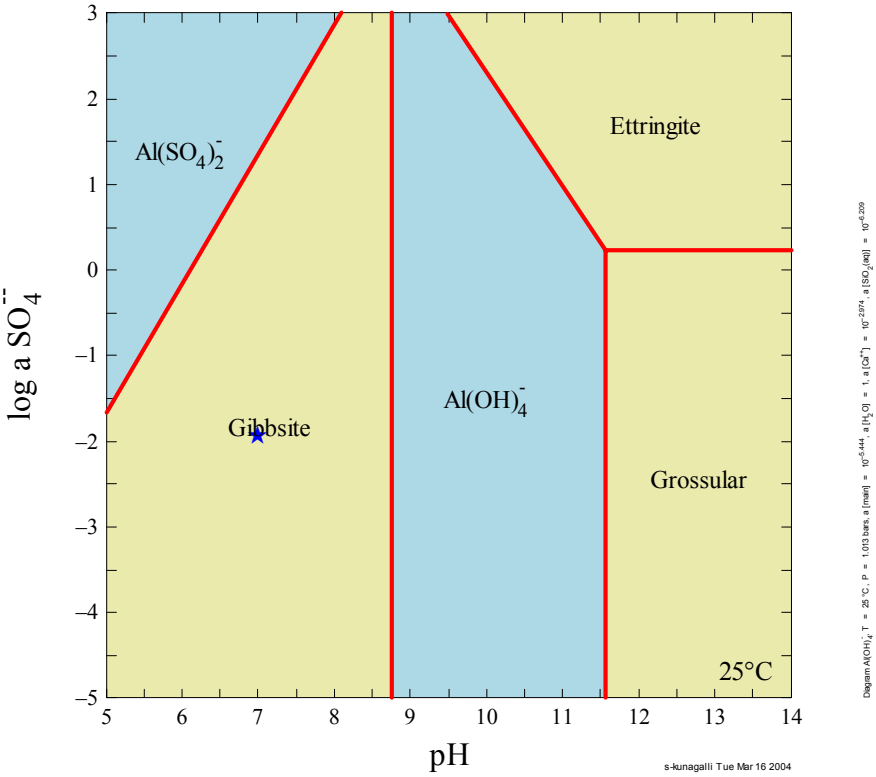

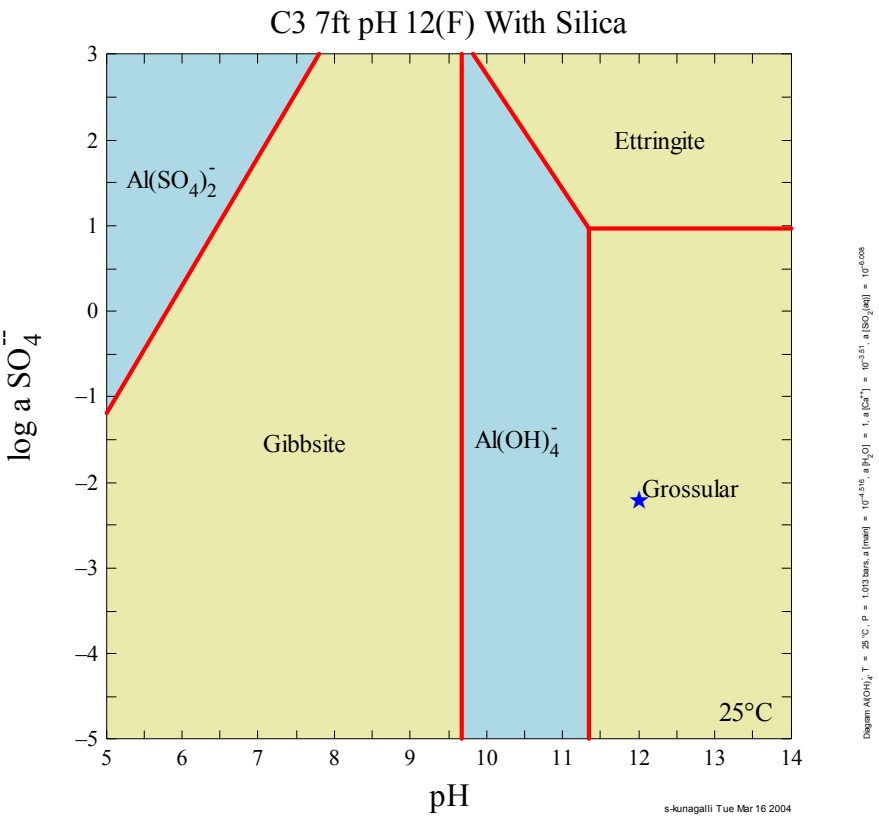
C3 7ft pH 12(F) With Silica
log a SO_4^{--}
pH
$Al(SO_4)_2^-$
Gibbsite
$Al(OH)_4^-$
Ettringite
Grossular
25°C
s-kunagalli Tue Mar 16 2004

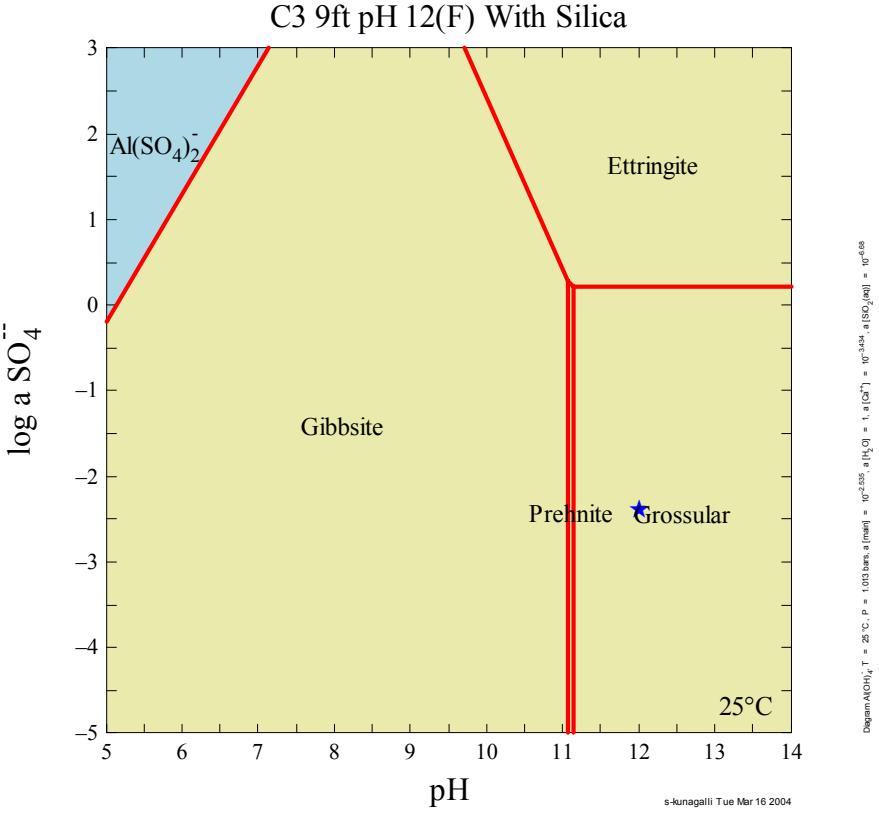
C3 9ft pH 12(F) With Silica
log a SO_4^{--}
pH
$Al(SO_4)_2^-$
Gibbsite
Ettringite
Prehnite
Grossular
25°C
s-kunagalli Tue Mar 16 2004

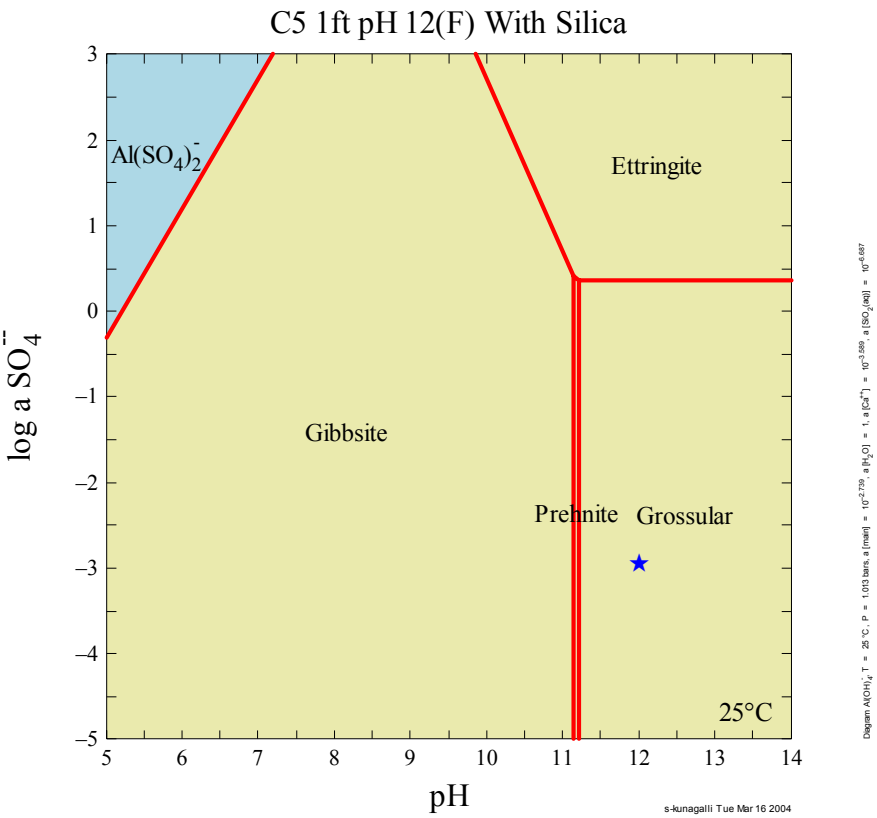
C5 1ft pH 12(F) With Silica
log a SO_4^{--}
pH
$Al(SO_4)_2^-$
Ettringite
Gibbsite
Prehnite
Grossular
25°C
s-kunagalli Tue Mar 16 2004

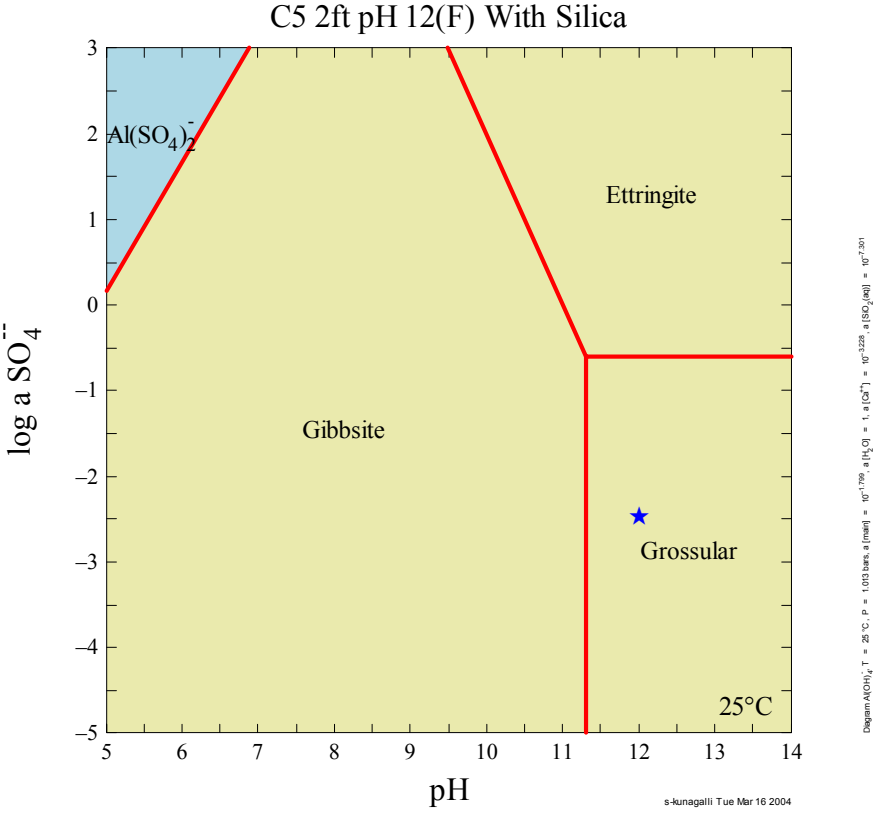
C5 2ft pH 12(F) With Silica
log a SO_4^{--}
pH
$Al(SO_4)_2^-$
Ettringite
Gibbsite
Grossular
25°C
s-kunagalli Tue Mar 16 2004

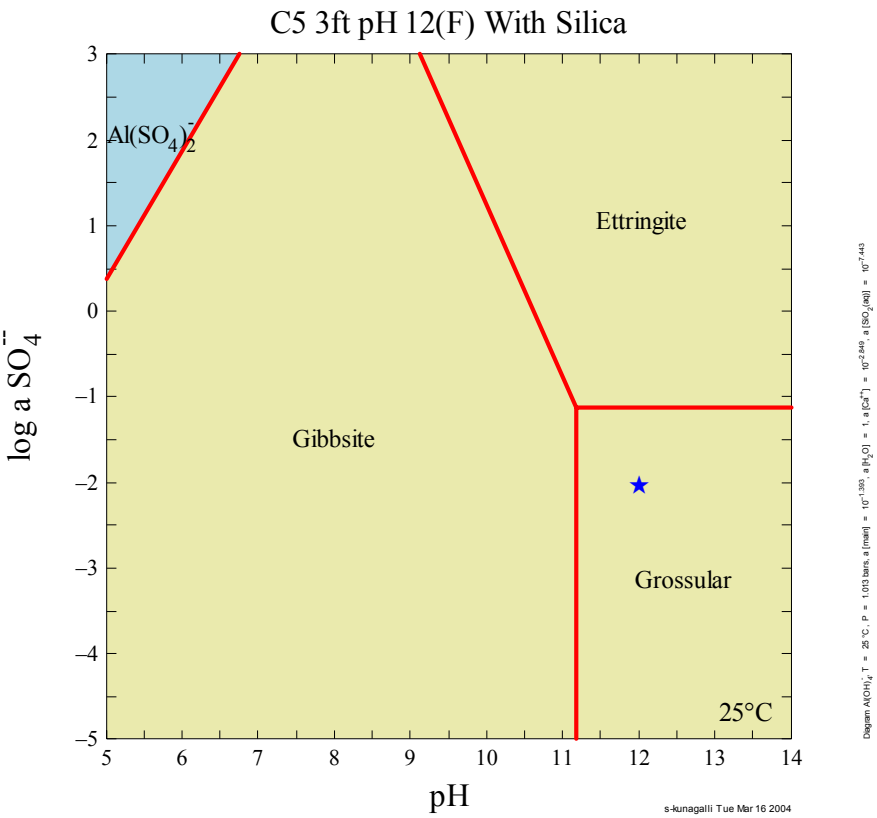
C5 3ft pH 12(F) With Silica
log a SO_4^{--}
pH
$Al(SO_4)_2^-$
Ettringite
Gibbsite
Grossular
25°C
s-kunagalli Tue Mar 16 2004

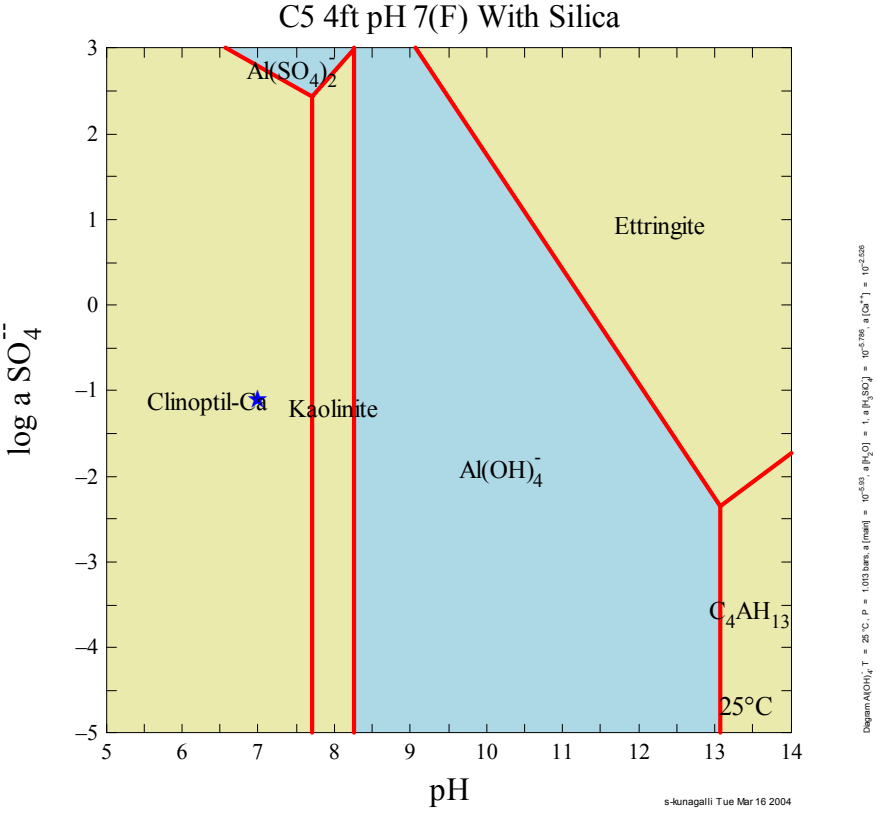
C5 4ft pH 7(F) With Silica
log a SO_4^{--}
pH
$Al(SO_4)_2^-$
Ettringite
Clinoptil-Ca
Kaolinite
$Al(OH)_4^-$
C_4AH_{13}
25°C
s-kunagalli Tue Mar 16 2004

C5 4ft pH 12(F) With Silica

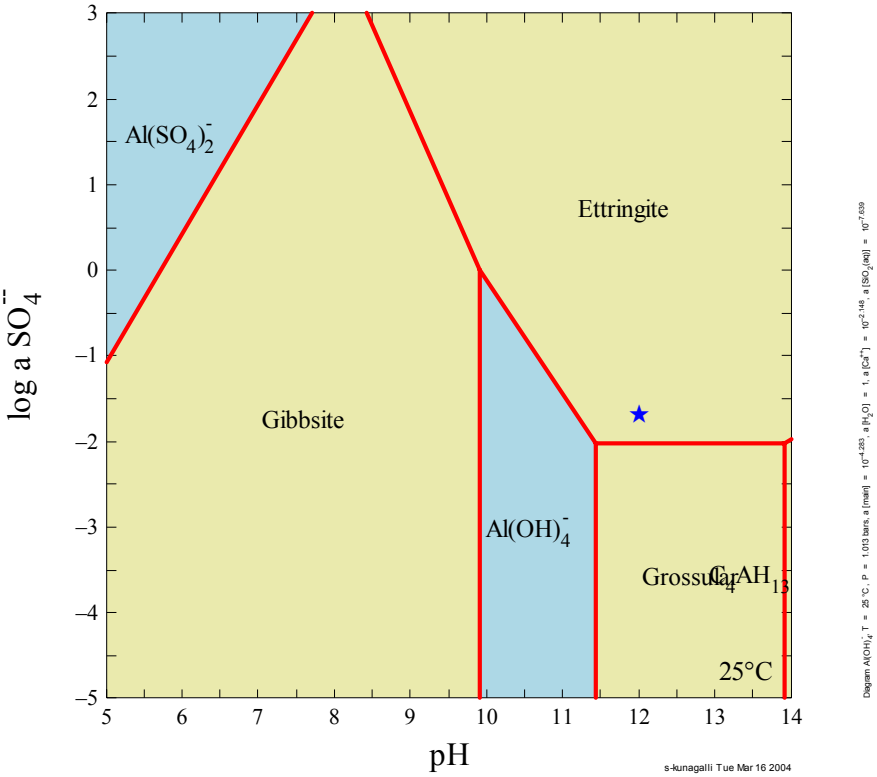

C5 5ft pH 7(F) With Silica

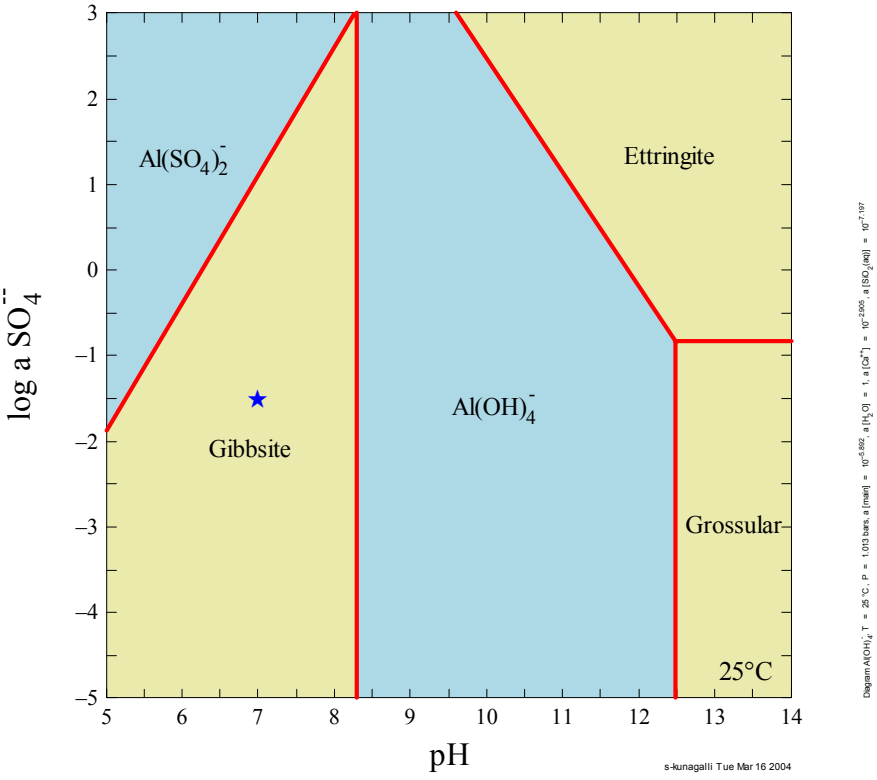

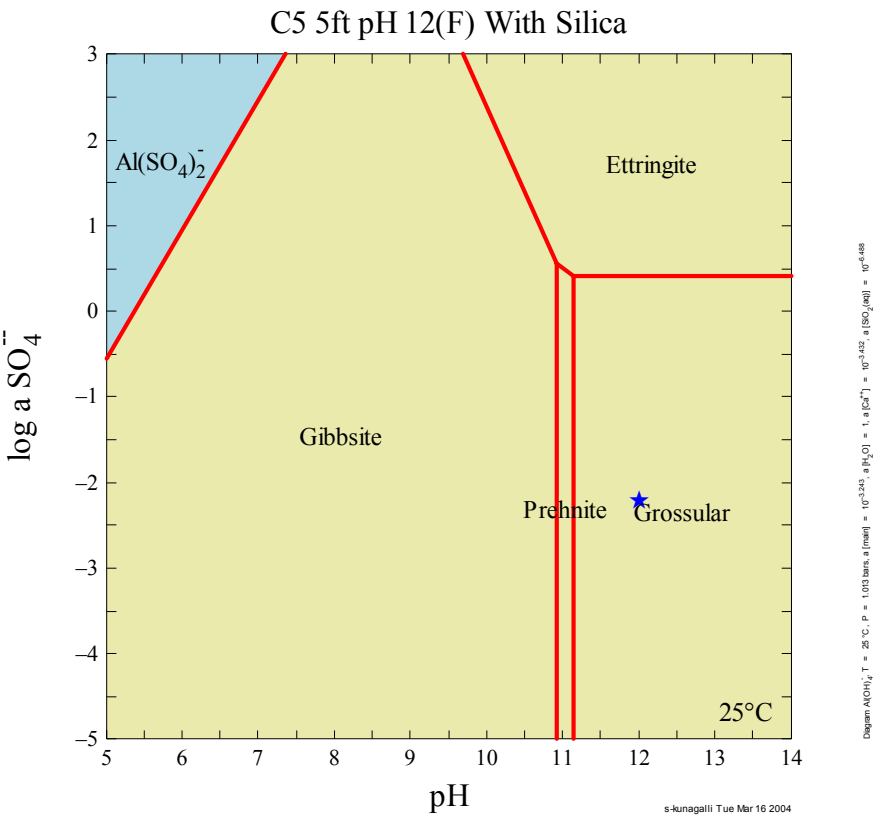
C5 5ft pH 12(F) With Silica
log a SO_4^{--}
pH
$Al(SO_4)_2^-$
Ettringite
Gibbsite
Prehnite
Grossular
25°C
s-kunagalli Tue Mar 16 2004

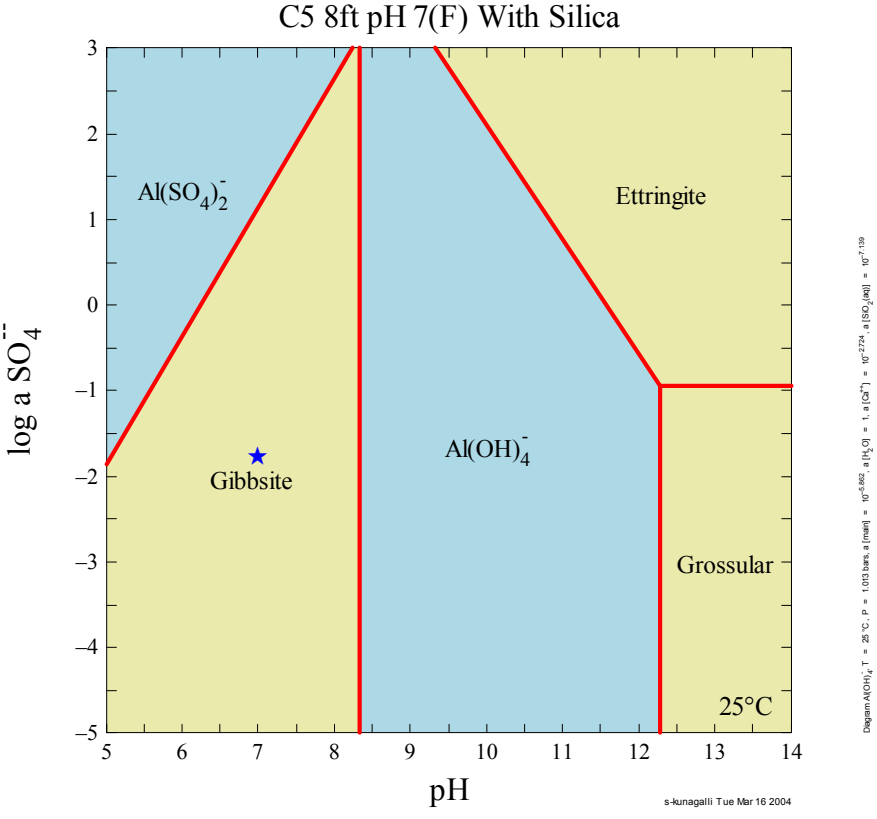
C5 8ft pH 7(F) With Silica
log a SO_4^{--}
pH
$Al(SO_4)_2^-$
Ettringite
Gibbsite
$Al(OH)_4^-$
Grossular
25°C
s-kunagalli Tue Mar 16 2004

C5 8ft pH 12(F) With Silica

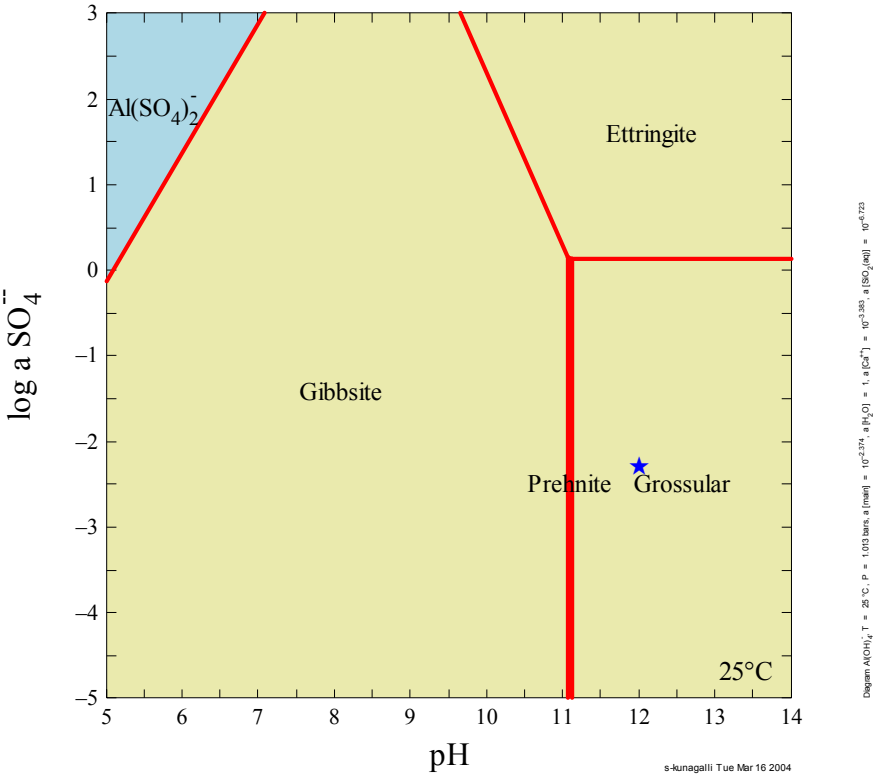

C5 10ft pH 12(F) With Silica

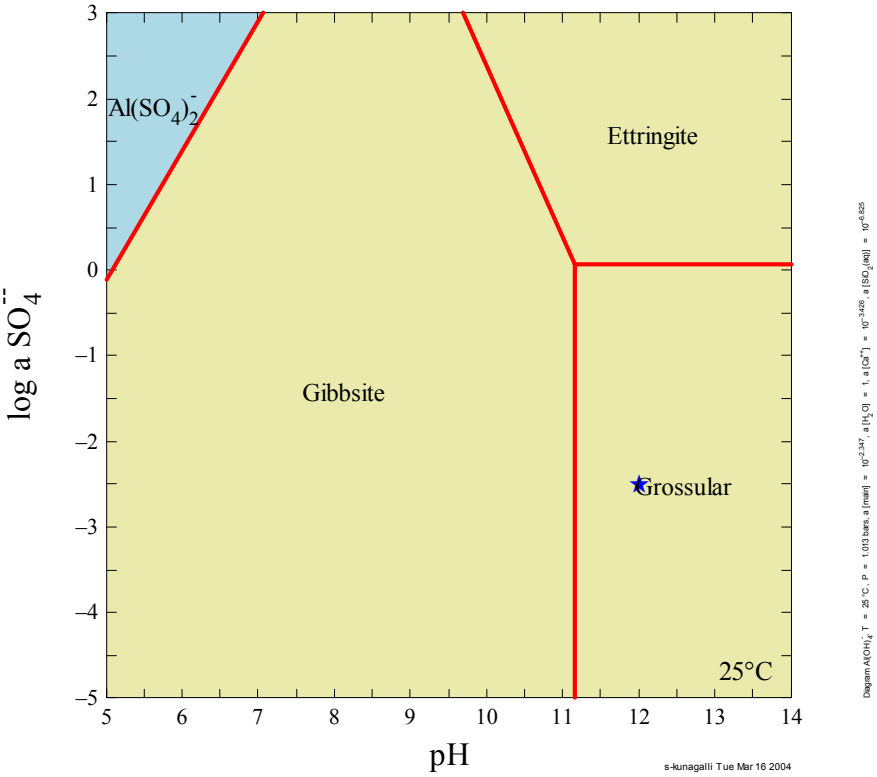

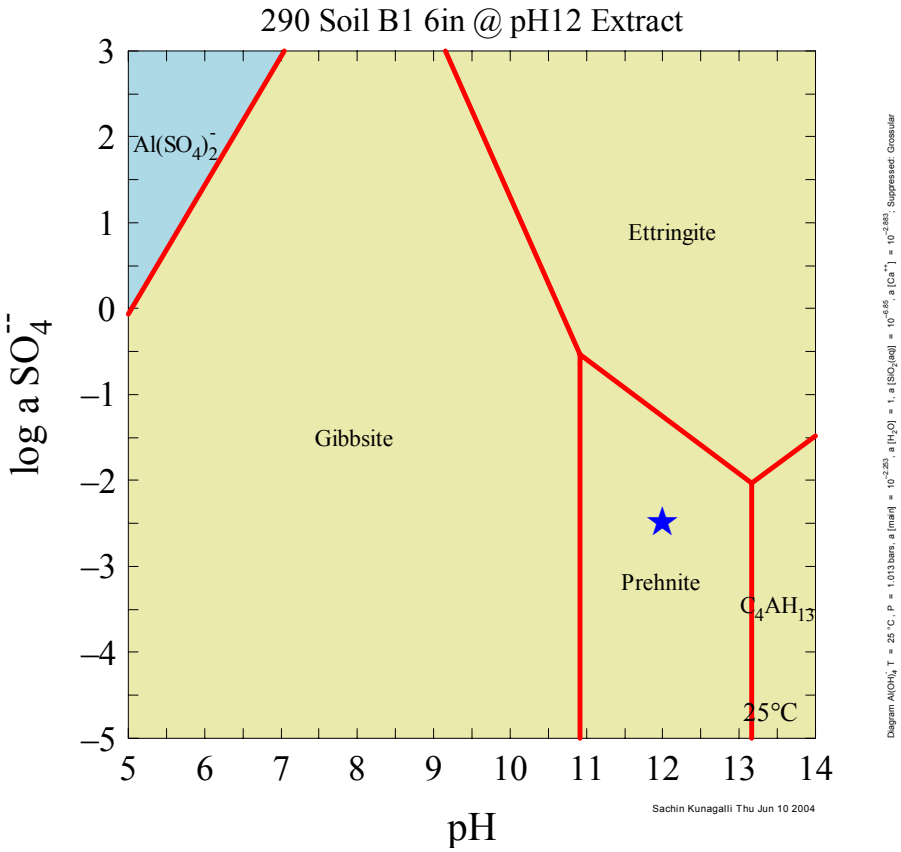
290 Soil B1 6in @ pH12 Extract
log a SO_4^{--}
pH
$Al(SO_4)_2^-$
Gibbsite
Ettringite
Prehnite
C_4AH_{13}
25°C
Sachin Kunagalli Thu Jun 10 2004

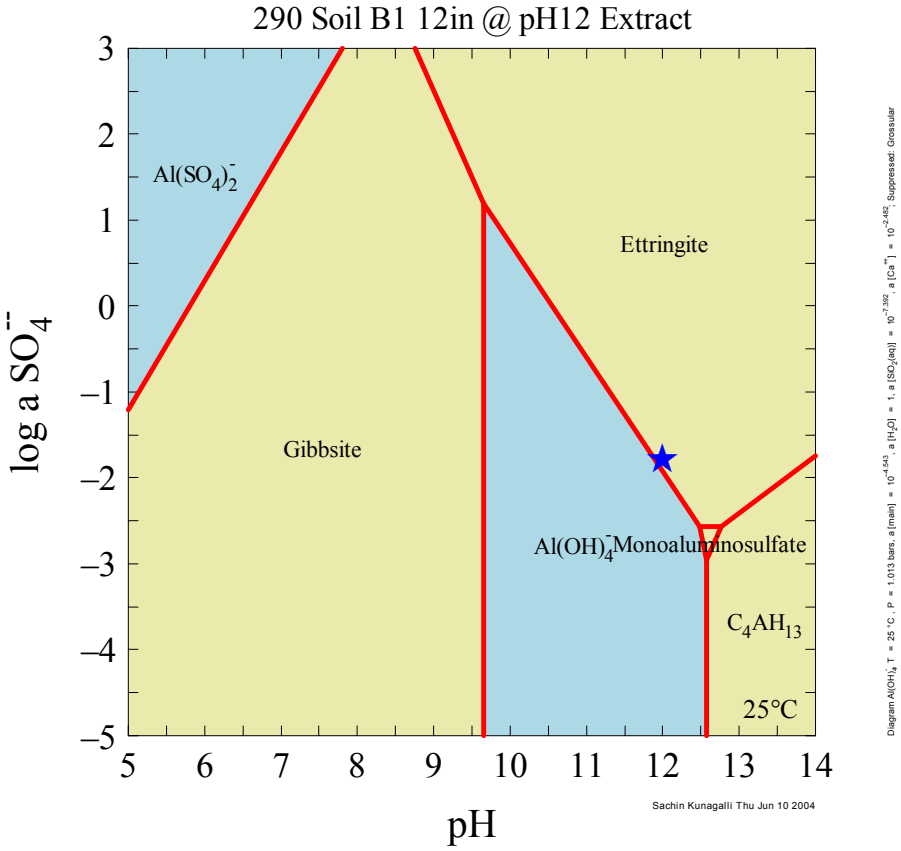
290 Soil B1 12in @ pH12 Extract
log a SO_4^{--}
pH
$Al(SO_4)_2^-$
Gibbsite
Ettringite
$Al(OH)_4^-$Monoaluminosulfate
C_4AH_{13}
25°C
Sachin Kunagalli Thu Jun 10 2004

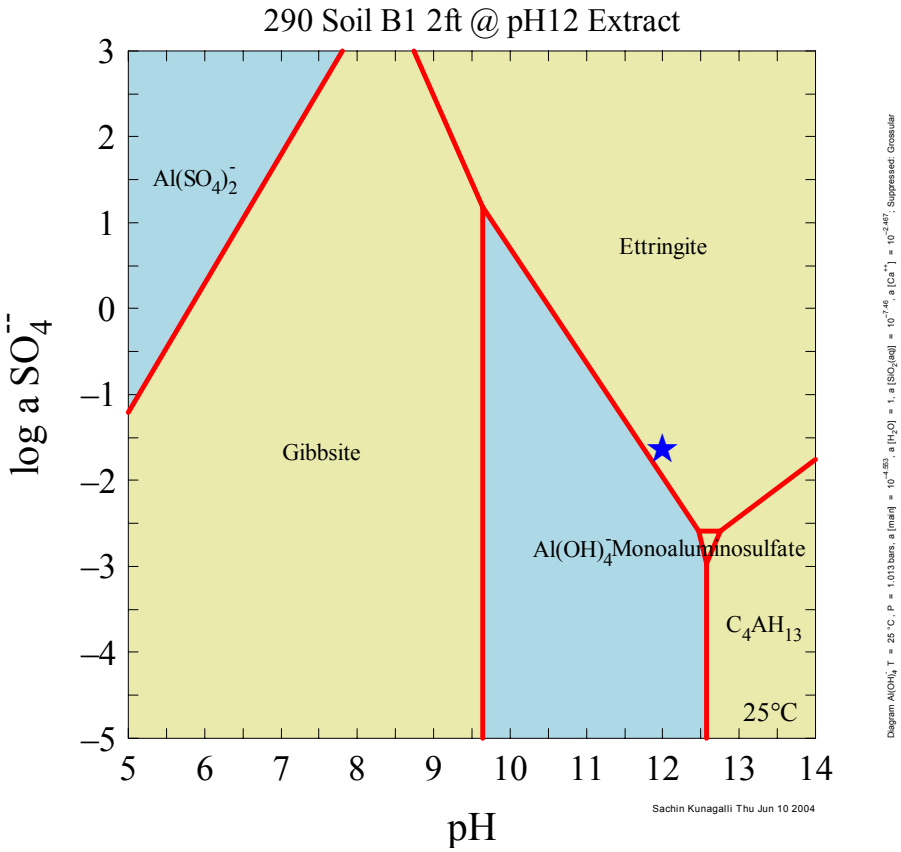
290 Soil B1 2ft @ pH12 Extract
log a SO_4^{--}
pH
$Al(SO_4)_2^-$
Gibbsite
Ettringite
$Al(OH)_4^-$
Monoaluminosulfate
C_4AH_{13}
25°C
Sachin Kunagalli Thu Jun 10 2004

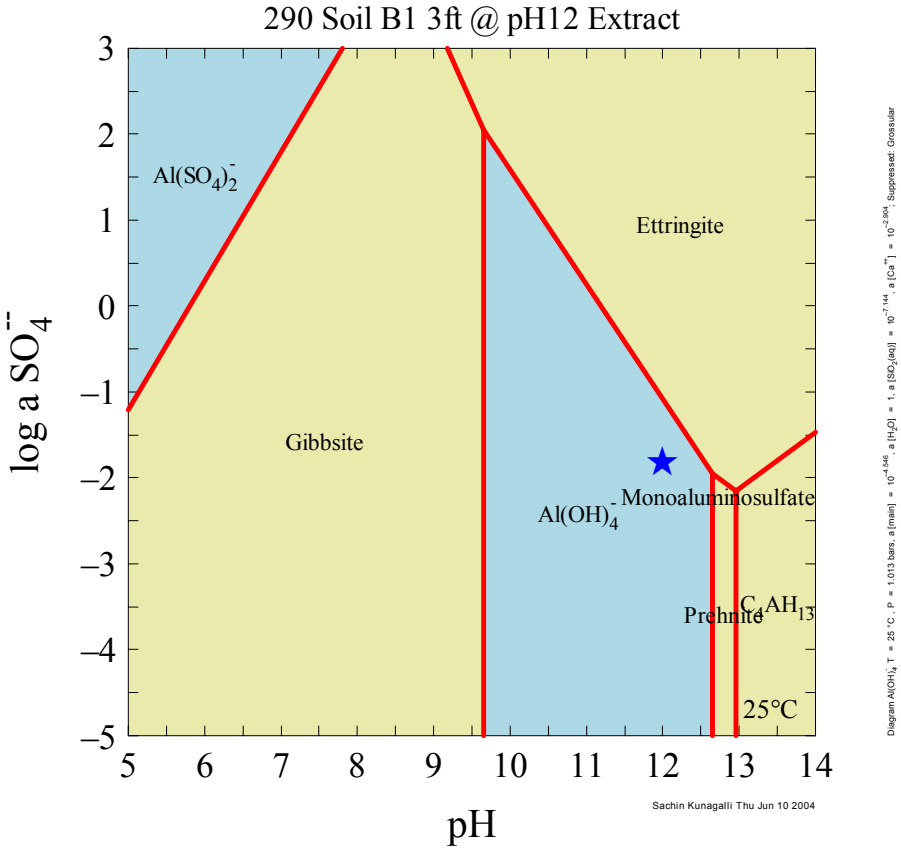
290 Soil B1 3ft @ pH12 Extract
log a SO_4^{--}
pH
$Al(SO_4)_2^-$
Gibbsite
Ettringite
$Al(OH)_4^-$
Monoaluminosulfate
Prehnite
C_4AH_{13}
25°C
Sachin Kunagalli Thu Jun 10 2004

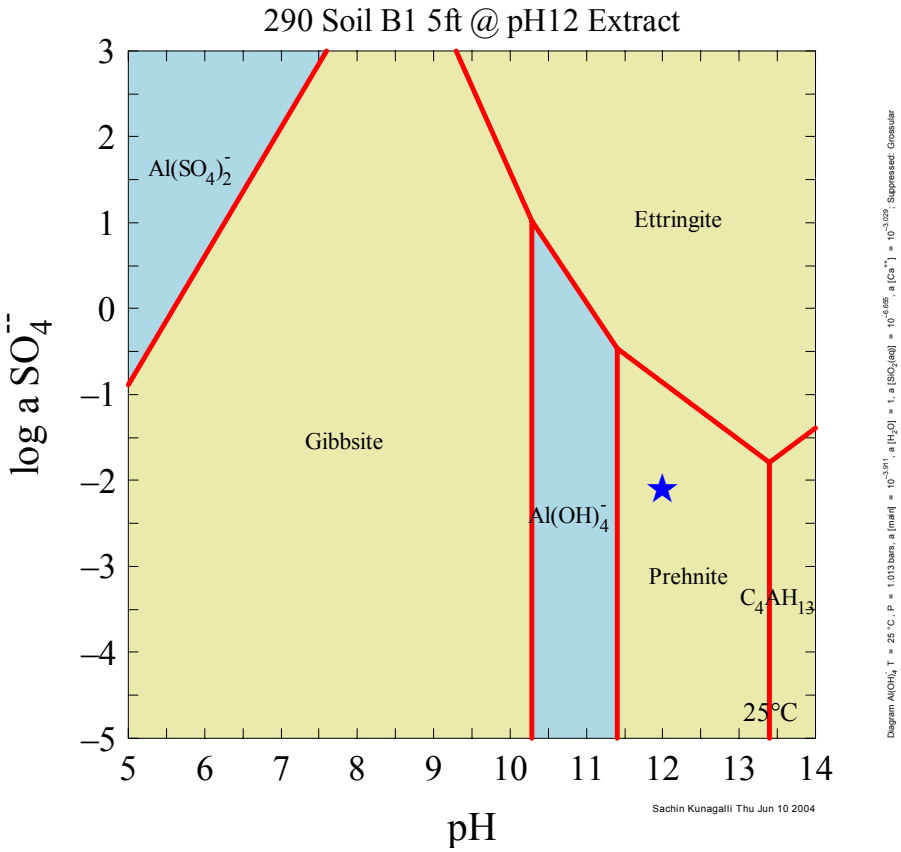
290 Soil B1 5ft @ pH12 Extract
log a SO_4^{--}
pH
$Al(SO_4)_2^-$
Gibbsite
$Al(OH)_4^-$
Ettringite
Prehnite
C_4AH_{13}
25°C
Sachin Kunagalli Thu Jun 10 2004

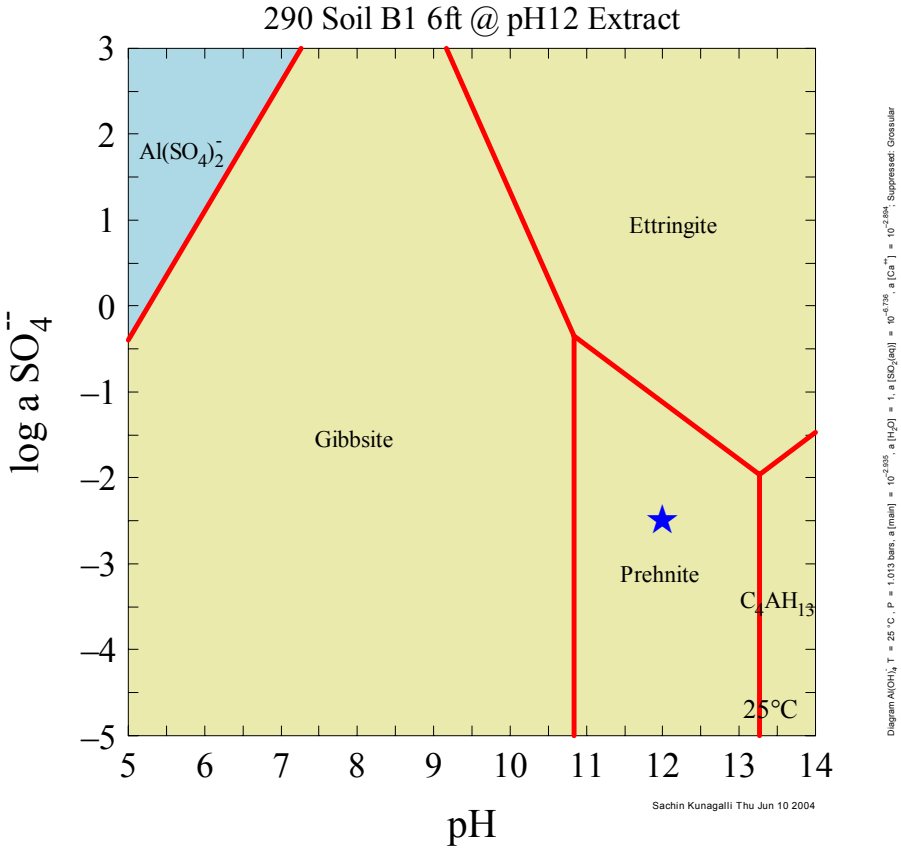
290 Soil B1 6ft @ pH12 Extract
log a SO_4^{--}
pH
$Al(SO_4)_2^-$
Gibbsite
Ettringite
Prehnite
C_4AH_{13}
25°C
Sachin Kunagalli Thu Jun 10 2004

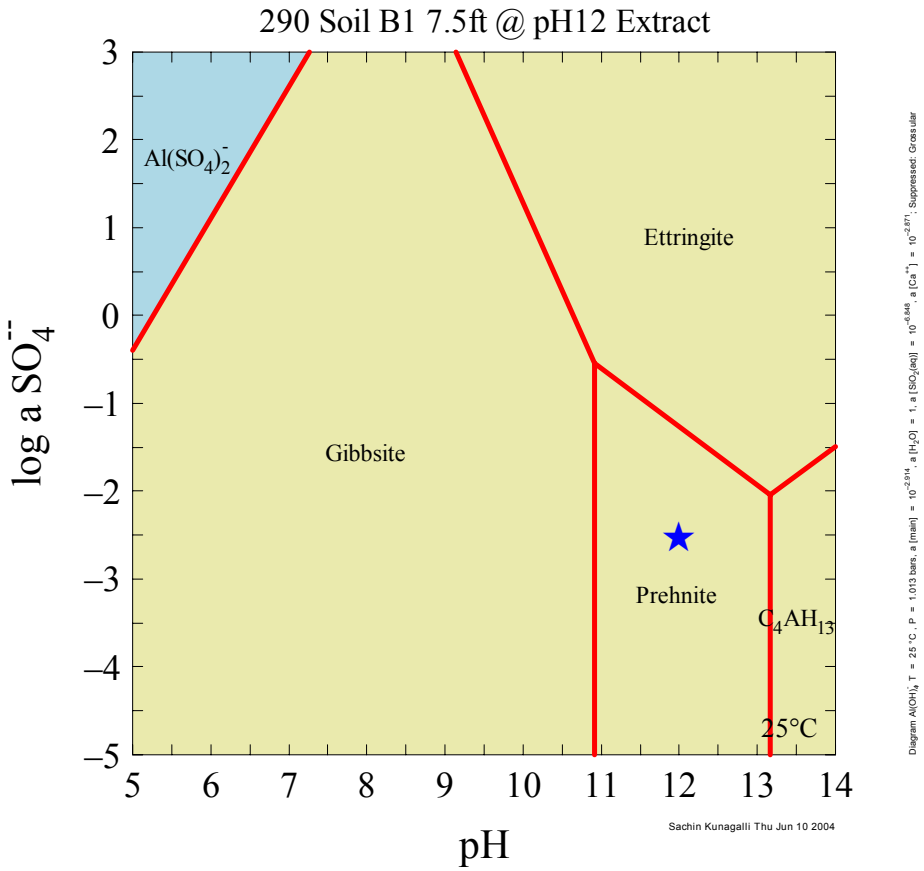
290 Soil B1 7.5ft @ pH12 Extract
log a SO_4^{--}
pH
$Al(SO_4)_2^-$
Gibbsite
Ettringite
Prehnite
C_4AH_{13}
25°C
Sachin Kunagalli Thu Jun 10 2004

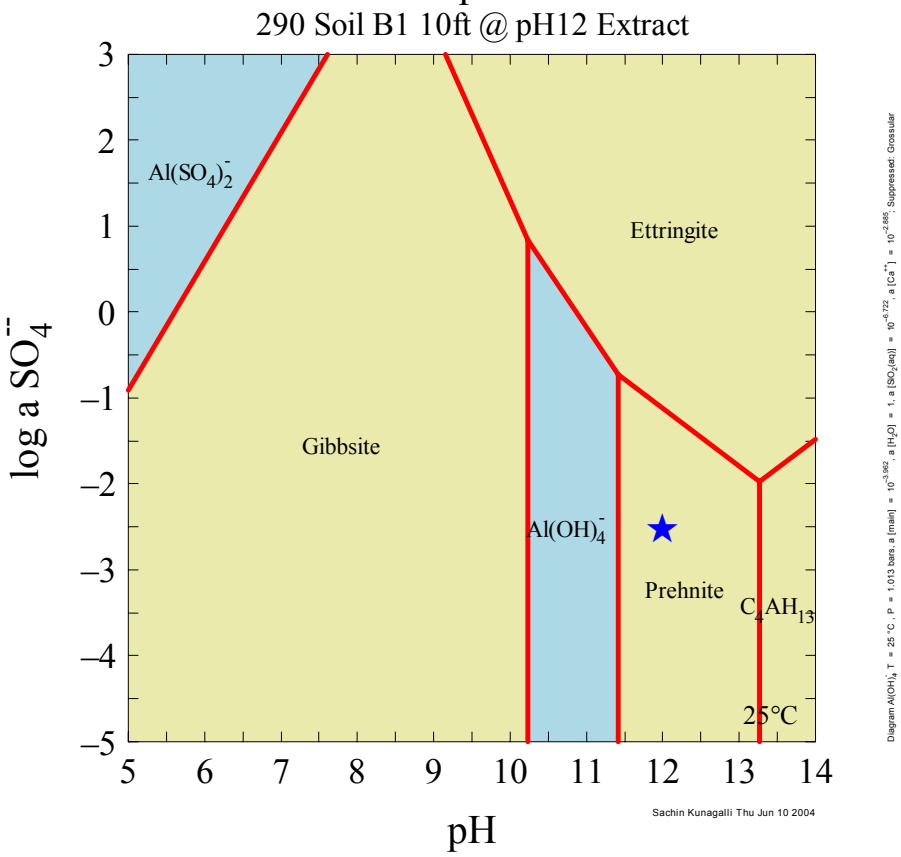
290 Soil B1 10ft @ pH12 Extract
log a SO_4^{--}
pH
$Al(SO_4)_2^-$
Gibbsite
$Al(OH)_4^-$
Ettringite
Prehnite
C_4AH_{13}
25°C
Sachin Kunagalli Thu Jun 10 2004

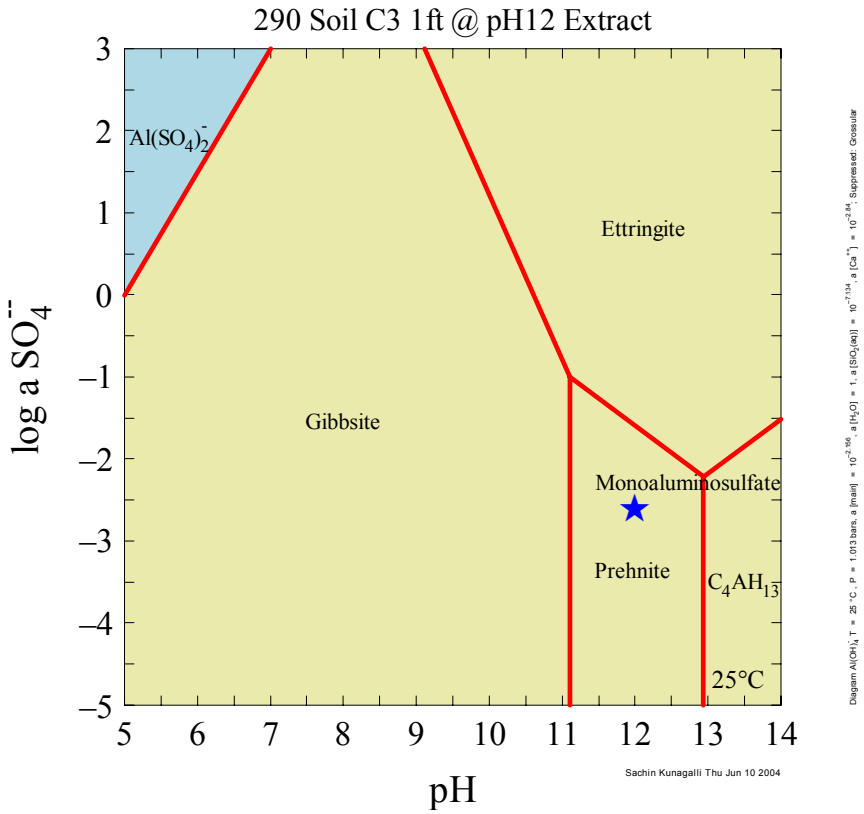
290 Soil C3 1ft @ pH12 Extract
log a SO_4^{--}
pH
$Al(SO_4)_2^-$
Ettringite
Gibbsite
Monoaluminosulfate
Prehnite
C_4AH_{13}
25°C
Sachin Kunagalli Thu Jun 10 2004

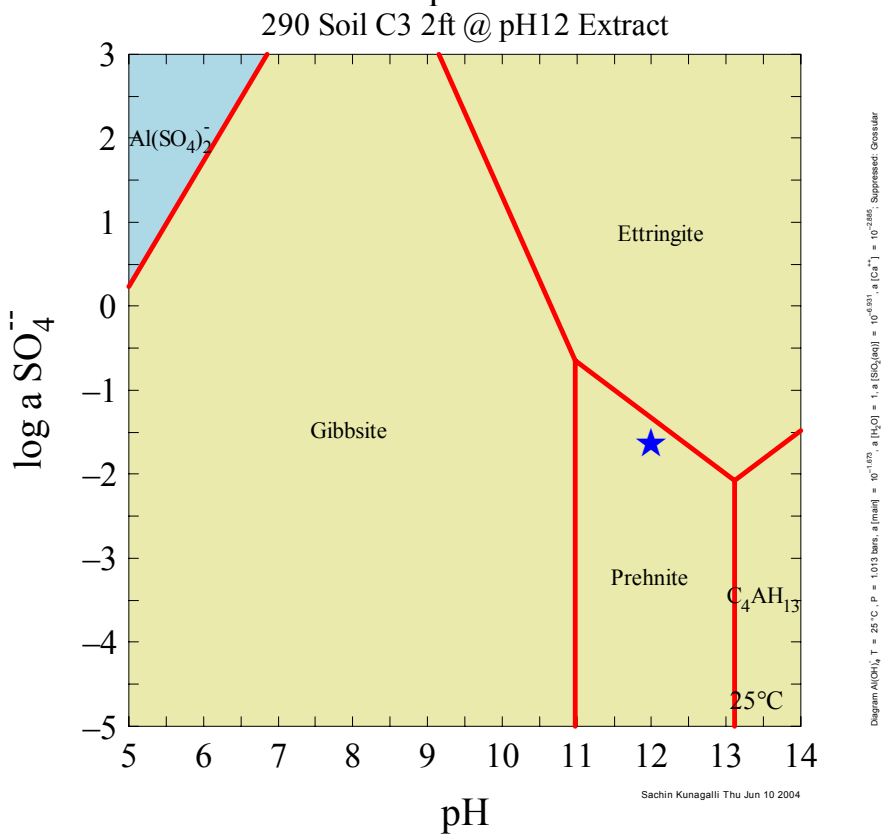
290 Soil C3 2ft @ pH12 Extract
log a SO_4^{--}
pH
$Al(SO_4)_2^-$
Ettringite
Gibbsite
Prehnite
C_4AH_{13}
25°C
Sachin Kunagalli Thu Jun 10 2004

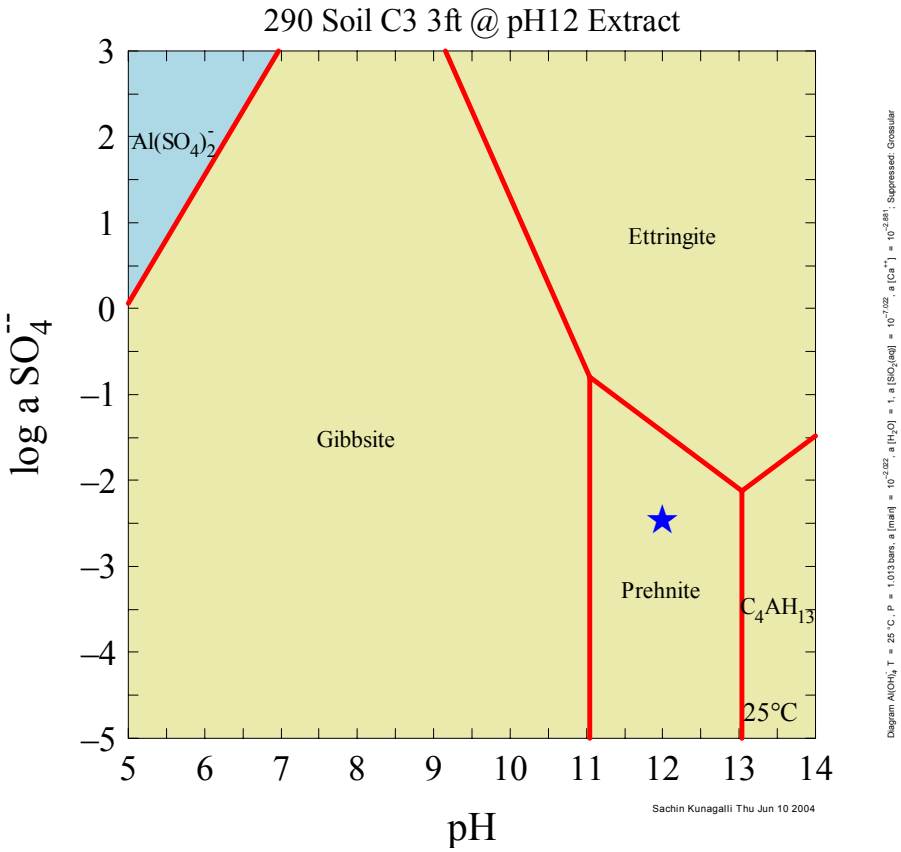
290 Soil C3 3ft @ pH12 Extract
log a SO_4^{--}
pH
$Al(SO_4)_2^-$
Gibbsite
Ettringite
Prehnite
C_4AH_{13}
25°C
Sachin Kunagalli Thu Jun 10 2004

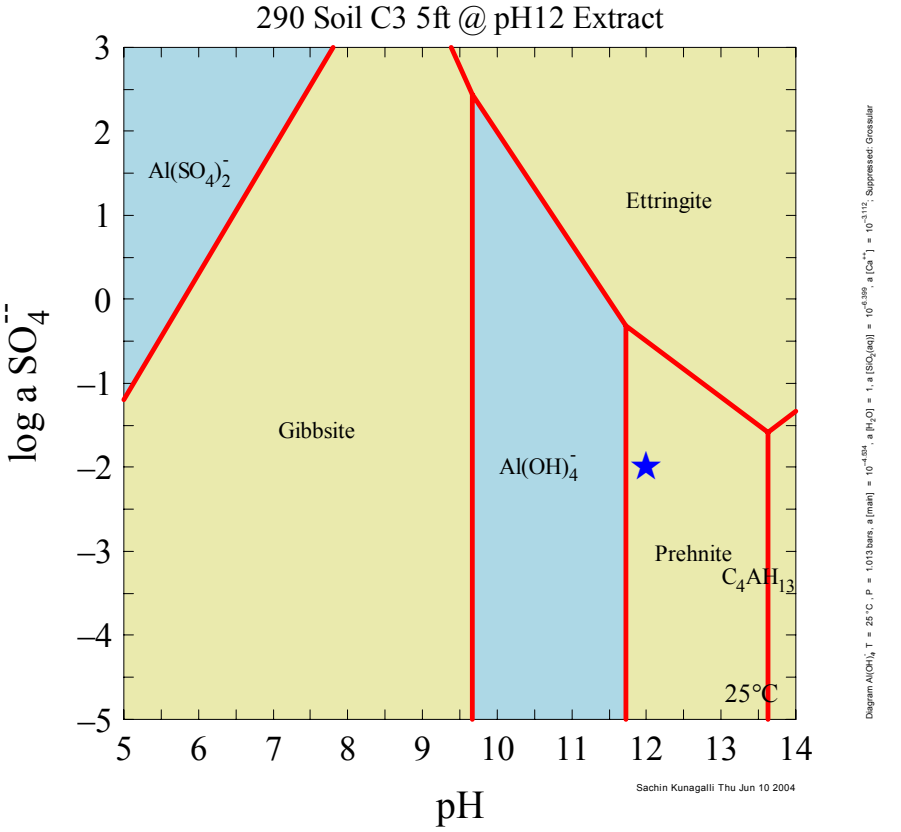
290 Soil C3 5ft @ pH12 Extract
log a SO_4^{--}
pH
$Al(SO_4)_2^-$
Gibbsite
$Al(OH)_4^-$
Ettringite
Prehnite
C_4AH_{13}
25°C
Sachin Kunagalli Thu Jun 10 2004

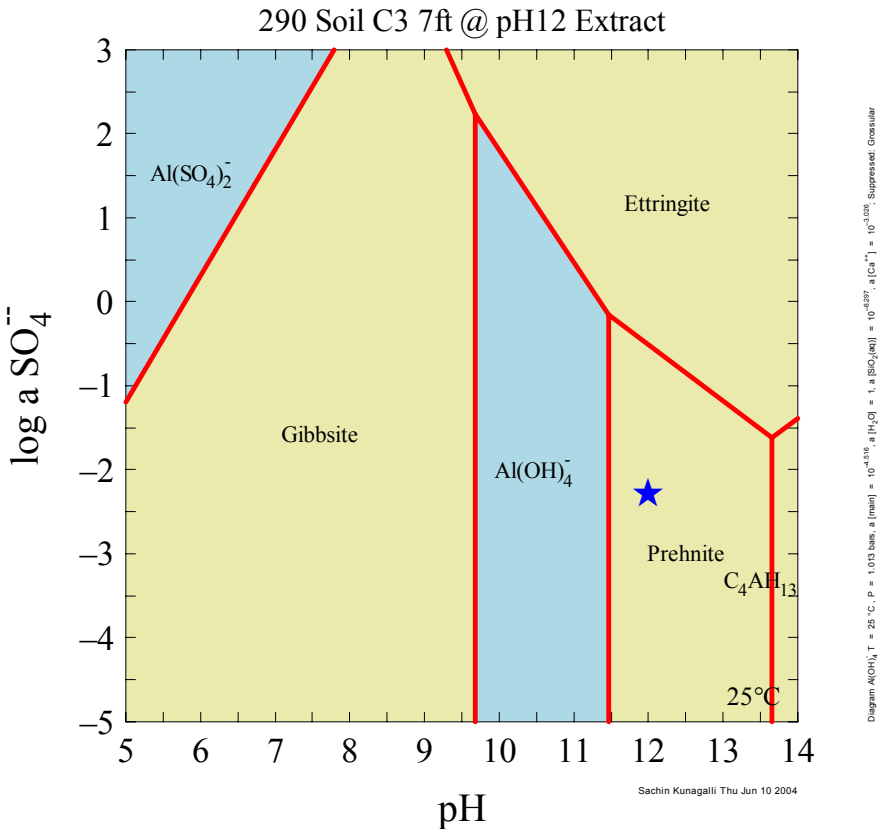
290 Soil C3 7ft @ pH12 Extract
log a SO_4^{--}
pH
$Al(SO_4)_2^-$
Gibbsite
$Al(OH)_4^-$
Ettringite
Prehnite
C_4AH_{13}
25°C
Sachin Kunagalli Thu Jun 10 2004

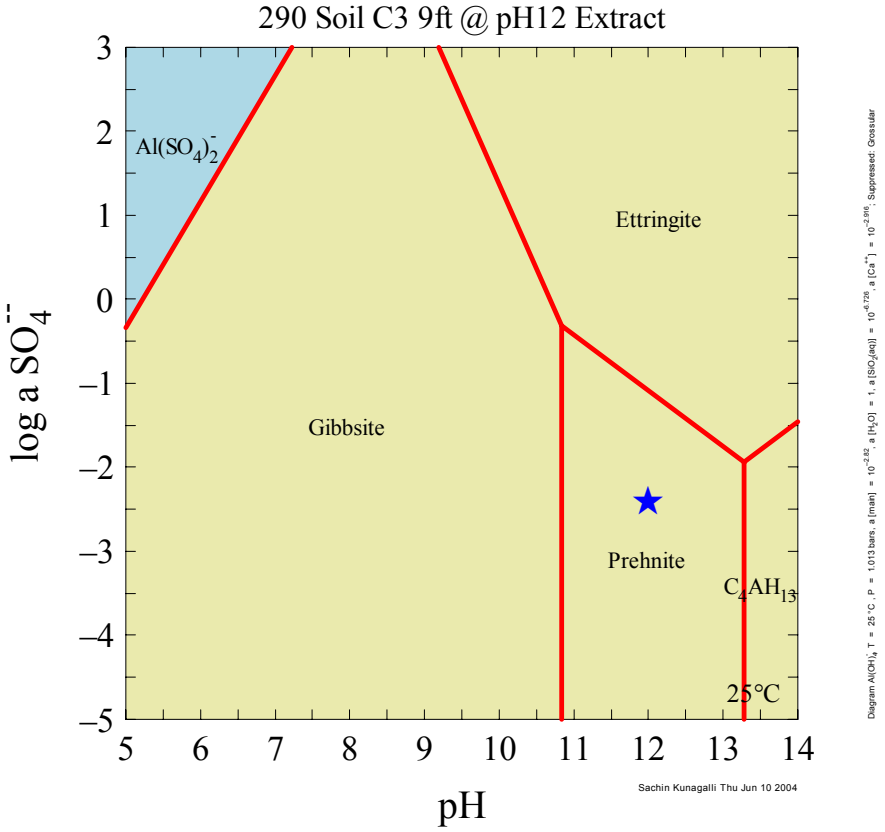
290 Soil C3 9ft @ pH12 Extract
log a SO_4^{--}
pH
$Al(SO_4)_2^-$
Gibbsite
Ettringite
Prehnite
C_4AH_{13}
25°C
Sachin Kunagalli Thu Jun 10 2004

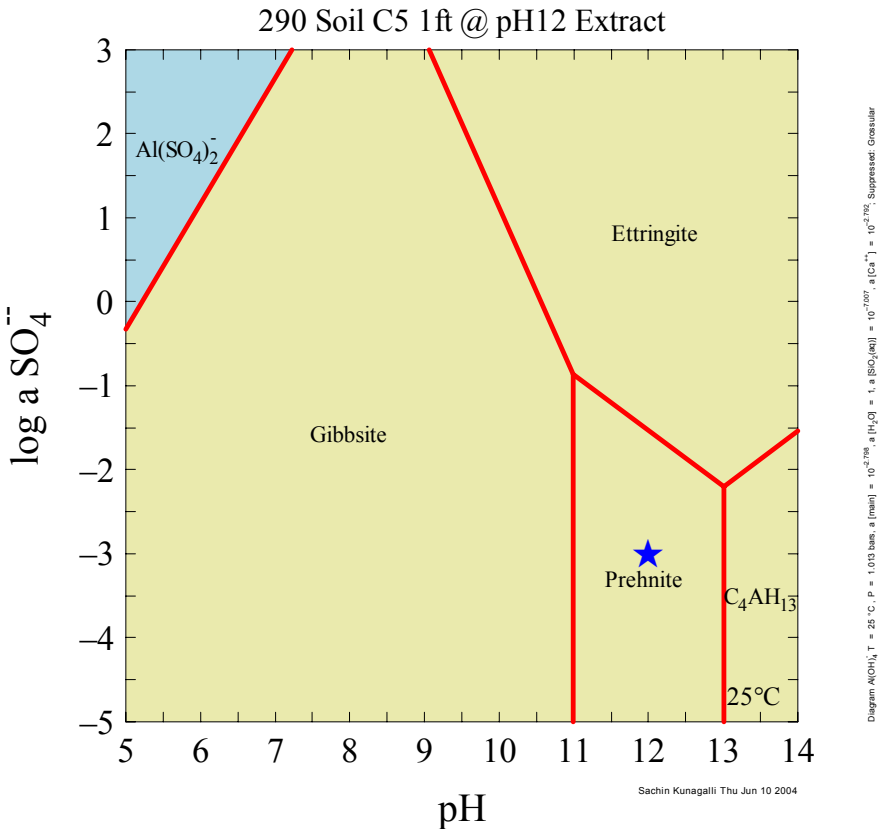
290 Soil C5 1ft @ pH12 Extract
log a SO_4^{--}
pH
$Al(SO_4)_2^-$
Gibbsite
Ettringite
Prehnite
C_4AH_{13}
25°C
Sachin Kunagalli Thu Jun 10 2004

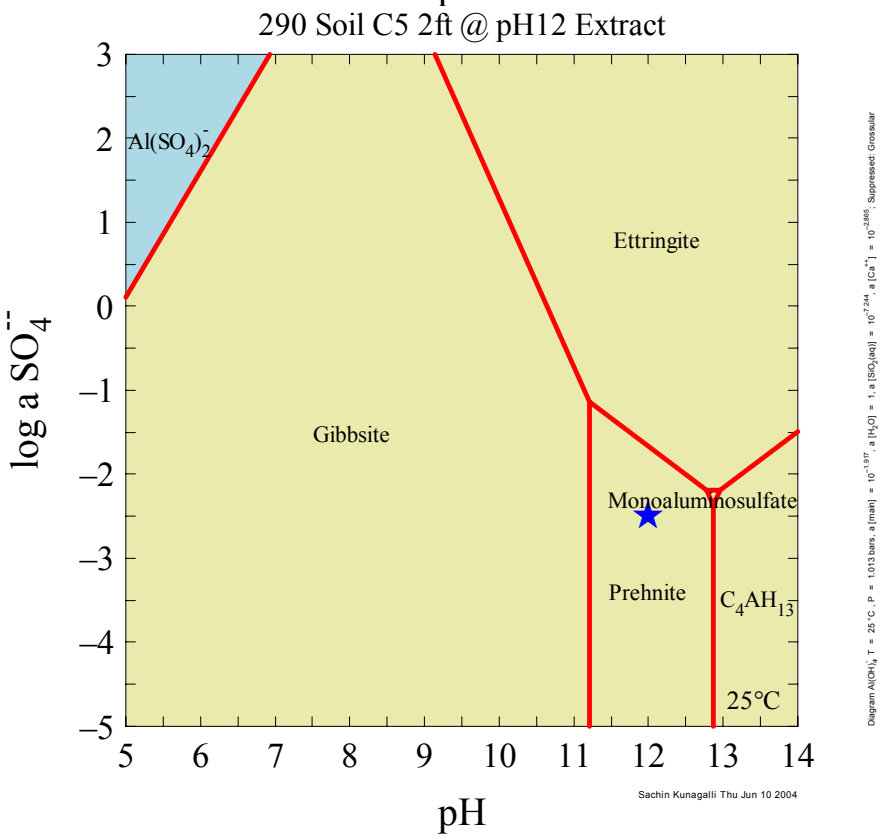
290 Soil C5 2ft @ pH12 Extract
log a SO_4^{--}
pH
$Al(SO_4)_2^-$
Gibbsite
Ettringite
Monoaluminosulfate
Prehnite
C_4AH_{13}
25°C
Sachin Kunagalli Thu Jun 10 2004

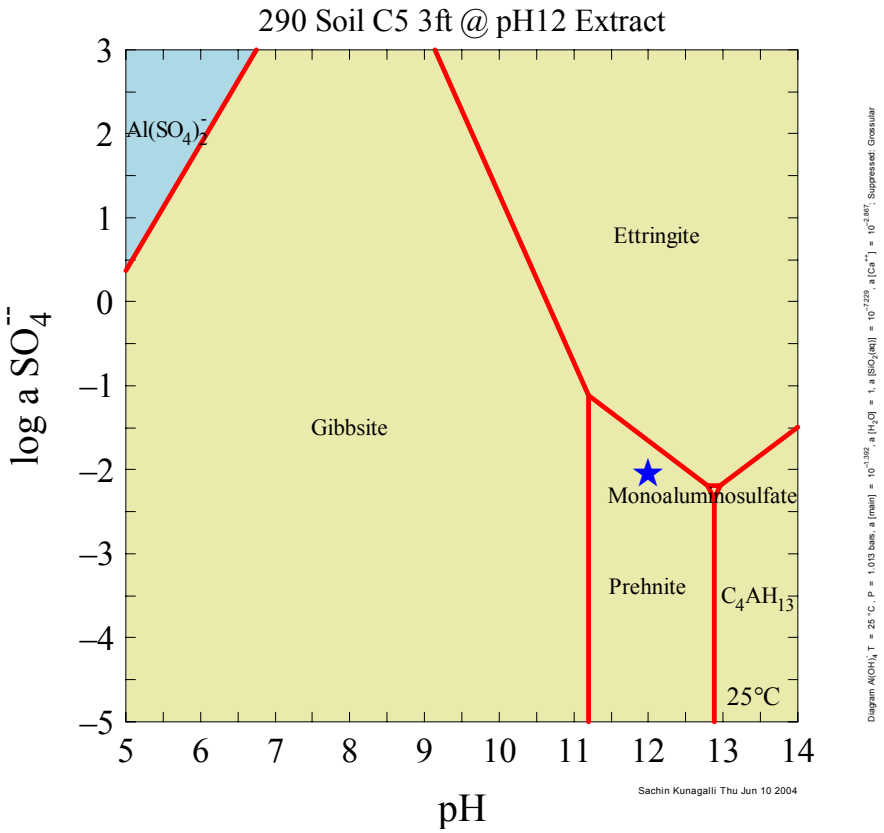
290 Soil C5 3ft @ pH12 Extract
log a SO_4^{--}
pH
$Al(SO_4)_2^-$
Gibbsite
Ettringite
Monoaluminosulfate
Prehnite
C_4AH_{13}
25°C
Sachin Kunagalli Thu Jun 10 2004

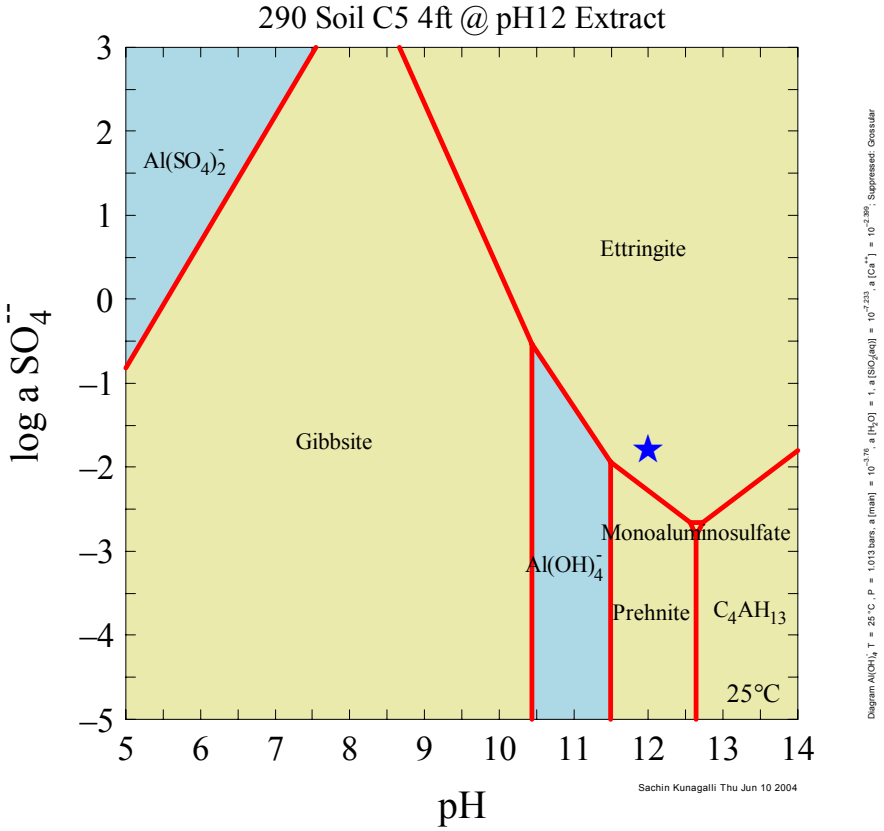
290 Soil C5 4ft @ pH12 Extract
log a SO_4^{--}
pH
$Al(SO_4)_2^-$
Gibbsite
Ettringite
$Al(OH)_4^-$
Monoaluminosulfate
Prehnite
C_4AH_{13}
25°C
Sachin Kunagalli Thu Jun 10 2004

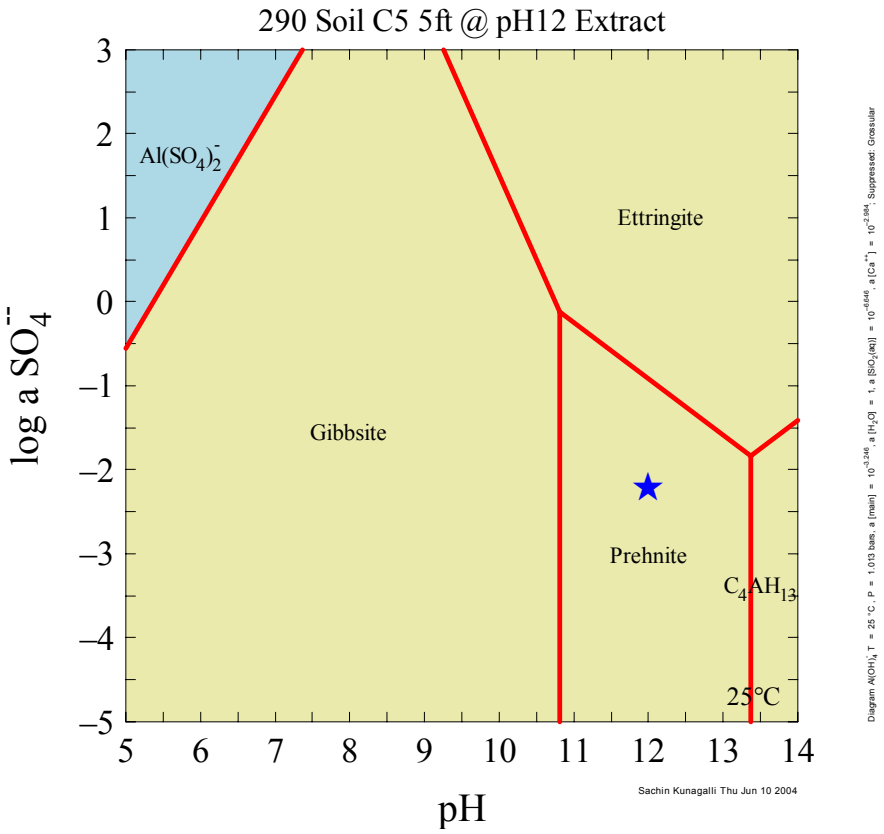
290 Soil C5 5ft @ pH12 Extract
log a SO_4^{--}
pH
$Al(SO_4)_2^-$
Ettringite
Gibbsite
Prehnite
C_4AH_{13}
25°C
Sachin Kunagalli Thu Jun 10 2004

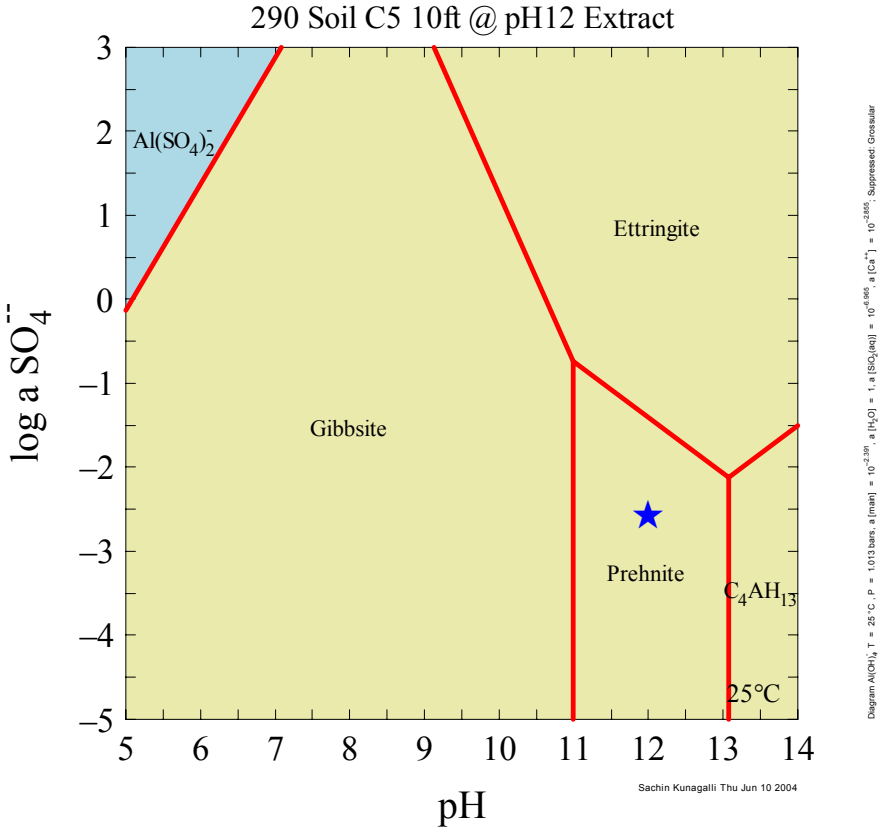
290 Soil C5 10ft @ pH12 Extract
log a SO_4^{--}
pH
$Al(SO_4)_2^-$
Ettringite
Gibbsite
Prehnite
C_4AH_{13}
25°C
Sachin Kunagalli Thu Jun 10 2004

VITA

Sachin Kunagalli Natarajan was born in Mysore, Karnataka, India on August 24, 1978. His entire childhood was spent in Mysore. His B. E. degree was from The National Institute of Engineering, Mysore University. He graduated from Mysore University from the Department of Civil Engineering with honors in 2000. He received an endowment award from the university for scoring highest marks in detailing of R. C. C structures. After his bachelor's degree, he moved to United States to start his master's study in civil engineering at Texas A&M University, College Station, Texas. During his master's study, he worked as a research assistant at the Texas Transportation Institute from January 2002 to August 2004 under the supervision of Dr. Dallas Little. His research was related to soil stabilization, pavement design, and material characterization. He co-authored the TRB paper "Ettringite Formation in Lime-Treated Soils: Establishing Thermodynamic Foundations for Engineering Practice" that is scheduled for publication and presentation at the 85th annual meeting of Transportation Research Board in Washington, DC in January 2005. He graduated from Texas A&M University with his M.S. in December of 2004. He can be reached through his parents, Mr. and Mrs. K.S.Natarajan at:

No 536 'M' Block 2nd Main 3rd Cross
Kuvempunagar, Mysore,
Karnataka, India 570023

He can also be reached through email at: sachinkn@yahoo.com